2017

Application of Multiaxial Cyclic Loading for Constitutive Model and Parameter Determination of Steels

Bassem Felemban
University of Central Florida

APPLICATION OF MULTIAXIAL CYCLIC LOADING FOR CONSTITUTIVE MODEL AND PARAMETER DETERMINATION OF STEELS

by

BASSEM FAREED FELEMBAN
M.S. University of Central Florida, 2012
B.S. King Abdulaziz University, 2009

A dissertation submitted in partial fulfillment of the requirements
for the degree of Doctor of Philosophy
in the Department of Mechanical and Aerospace Engineering
in the College of Engineering and Computer Science
at the University of Central Florida
Orlando, Florida

Fall Term
2017

Major Professor: Ali P. Gordon

ABSTRACT

For many candidate materials, constitutive models and their parameters are identified using uniaxial test data. Real components, however, generally operate in a multi-axial loading environments. Consequently, constitutive models deployed by uniaxial conditions may carry over to service conditions with inherit limitations. Research is proposed to determine the constitutive model constants for the creep and plasticity responses of a material via multi-axial fatigue testing which may contain ratcheting. It is conjectured that directly regressing data under conditions that favor those of actual service use will lead to more accurate modeling under these conditions, as well as a reduced consumption of model development resources. Application of observations of multiaxial loading in the determination of constitutive modeling constants and model selection represents a paradigm shift for material characterization. Numerical simulation and experimentation are necessary for material selection for application at high temperature. The candidate material used in this study is primarily applied for structural components in high-temperature environments for steam generating systems – 304 stainless steel. It confers an excellent balance of ductility, corrosion resistance, and creep resistance at moderate temperatures (i.e., up to 550˚C). Under service conditions, both creep and cyclic plasticity can occur under either isothermal or non-isothermal conditions. Accurate deformation modeling and life prediction of these structures only achieved with an accurate understanding of how this and other key alloys behave under complex conditions. This research conveys a proposed methodology that can be used to apply creep and plasticity constitutive models that correlate with experimental data. Several creep and plasticity models are examined to augment the accuracy of the models. These results are presented to illustrate modeling performance. Based on this idea has been determined that novel

methods of measuring the accuracy of modeling be needed, as well as methods for optimizing material response under multiaxial conditions. The models are applied under service-like conditions to gain an understanding of how this and other key alloys behave under complex conditions. This research will study the complex tensile-torsion loading to determine the constitutive constants for material, and thus will decrease the number of uniaxial experiments. Additionally, combined analytical and experimental methods will be used to establish the Bree diagram for elevated temperature tensile-torsion responses. This deformation mechanism map has been useful as a design tool for materials undergoing ratcheting.

KEYWORDS: Multiaxial, Creep, Plasticity, Cyclic, ANSYS, Garofalo, Norton, Ramberg-Osgood, Chaboche, Kinematic hardening

ACKNOWLEDGMENTS

I would like to thank my advisor Dr. Ali P. Gordon for his guidance, encouragement, and understanding during my Ph.D efforts at University of Central Florida. My aptitude as a researcher, writer, and professional has been greatly improved by his indispensable guidance.

Also, I would like to thank my committee members: Dr. Fissal Moslehy, Dr. Yuanli Bay, and Dr. Boohyun Nam have made significant assistance to my work and developed the content of this dissertation.

I would like to thank the the Taif University and Cultural Ministy fellowship for supporting my doctoral studies. Derek Medellin is recognized for his controbution to figures based on metallury.

Finally, the Ph.D. thesis will not done without the support and encouragement of my family. My parents have sent their guidance and love from nearby and far away over many years. I would like to thank my wife for her support, and helped me to reach this level.

TABLE OF CONTENTS

LIST OF FIGURES

LIST OF TABLES

CHAPTER 1 INTRODUCTION

1.1 Background and Motivation

Many machine components are subjected to complex cyclic loading and subsequent deformation. For example, power generation equipment, turbine engine blades, and throttle valve bodies experience multiaxial loading at elevated temperature. Conventionally, design engineers develop methods for either deformation or lifing via uniaxial test data; however, to have the most confidence in models, lifing simulation tools must be exercised under conditions that components might be expected to experience in the field. Additionally, multiaxial behavior can reveal more insight into the rate-dependence, hardening, softening, and other behavior compared to uniaxial loading alone. The main purpose of this study is to demonstrate a method of constitutive modeling that can carry over to axial-torsional conditions with high accuracy.

Key attributes of material behavior are the dependence on rate, temperature, and history when they utilized for components subjected to extreme environments. Low alloy 2.25Cr–1Mo steel is a key material that is used primarily for structural components in high-temperature conditions (i.e., 500˚C to 650˚C). For example, steam chests, boilers, and turbine components (Pineda-León et al., 2015), are devices that subjected to both steady and cyclic loading multiple axes. Engines subjected to stress and high temperature. Under these circumstances, elastic conditions give rise to creep and plasticity once the mechanical load is substantial enough. The characteristics of the candidate material include an excellent balance in ductility, corrosion resistance, and creep resistance at moderate temperatures (Cheruvu, 1989; Jonsson et al., 2011).

A variety of plasticity models have been developed to approximate the deformation behavior of ductile materials. Assuming cyclic conditions, there are two different evolution models behavior types are highly relevant: isotropic and kinematic hardening. Isotropic hardening controls the size of the yield surface, and kinematic hardening corresponds to a shift in the yield surface. Some approaches to plasticity modeling use one or both of these hardening approaches. Additionally, several plasticity models that are native to general-propose finite element software packages such as ABAQUS, ANSYS, etc. use either of these approaches.

Creep is time-dependent deformation induced by stress typically at high heats exceeding 30% of the melting temperature T_m. Stress relaxation can occur under constant strain. Although there are three regimes of creep (i.e., primary, secondary, tertiary), this study focuses on steady state stage, which has a constant strain rate. Two common creep models are the Norton model and Garofalo model for secondary creep (Geist, 1998). These two models are also typically built into FEA software. Regression determines the constitutive models parameters with uniaxial creep data.

This paper begins with a discussion of 2.25Cr-1Mo steel and 304 stainless steel. Next, the constitutive modeling framework provided. Both plasticity and creep models are presented and exercised against uniaxial data at various temperature. After the models established, the model is exercised in a finite element mesh subjected to multiaxial loading key observations are provided.

1.2 Research Objective

This study develops a framework that allows for the determination of the constitutive models and their constants by using complex loading conditions, such as cyclic tension-torsion, similar to service conditions. The previous study found the constitutive model constants under

axial loading, but the tension-torsion will be more representative of service like multiaxial loads to which components subjected. This research focus on 2.25Cr-1Mo steel and 304 stainless steel under axial-torsional loading in a high-temperature environment and several axial only and torsion only experiments will be required for verification. The experiments are designed to draw out plasticity and creep, which are compared with the numerical results. Additionally, the Bree diagram is developed under tension and thermal loading, but this research will find the Bree diagram under tension-torsion loading. This study includes some digitized data from the previously mentioned research to compare with the simulation data. Some effort geared towards not only the discovery and quantification of ratcheting and relaxation but also the application of this response towards constant determination. Demonstrate a new way to find the ratcheting or optimize it. The following are objectives to investigate:

1. **Direct model constant determination via multiaxial fatigue experiments**: Axial-torsion experiments can be used to acquire the data needed to determine the constitutive model and constants for a material at a given temperature for 2.25Cr-1Mo steel or similar steels. This objective which proposes to determine the plasticity and creep constants from multiaxial test data. The most important step in this research is the experimental test and simulations for tensile-torsion testing, tensile testing, and creep testing. A new technique will be developed to obtain the plasticity and creep parameter. One plausible numerical approach is to use data generated by way of ANSYS, and the other one will make use of theoretical mechanics (e.g., multiaxial Ramberg-Osgood). The first approach will be the simulation the multiaxial load. From the simulation will have the axial strain and shear strain. Also, from the simulation will have the equivalent stress-strain curve, and that curve

will help to obtain the plasticity and creep constants. The second approach is to find the constants analytically. Both the initial loading (i.e., Ramberg-Osgood) and hysteretic responses (i.e., Massing) will consider. The main objective for this is finding the plasticity and creep parameter from a small batch of multiaxial tests. The effectiveness of approaches will be verified with axial and torsional data. Several multiaxial plasticity and creep models have presented in literature, but researchers have get to attempt to leverage multi-axial data to identify the modeling Parameters. This process will be repeated at various temperatures. The constants of Ramberg-Osgood will be shear constants. After that, the experiments will be one of the most important to compare the analytical results and the real experiments data. The framework will be verified with experiments controlled on 304 stainless steel.

2. **Axial-torsional Bree diagram**: A minimal number of axial-torsion experiments/simulations can be used to develop the Bree diagram. Building the axial-torsion version of the Bree diagram from tensile-torsion loading, and reducing the number of tests to find the different regions. The literature review found that most researchers were using the Bree diagram for material under cyclic temperature and pressure, for example, the pressure vessel with thermal loading. This research will find the Bree diagram for axial stress and shear stress under a number of conditions. The main objective from the Bree diagram is to determine the stress regimes. The researchers used this test for pressure vessel tanks because it has constant pressure and variable temperatures. In this case, an axial load is constant, and torsion is cyclic. The first step will run some simulation for multi-axial loading to build the Bree diagram. Afterward, analysis and observation be used to identify the transitions between adjacent regions. It expected that constitutive modeling constants would be useful. The research will study the combination of the tensile load and the torque.

Consequently, the main goal of this study is to determine if the Bree diagram can predict via plasticity constants. The most important points for this study to prove or disprove are if the Bree diagram can determine the constant axial stress and cyclic shear stress. In the axial stress, there are limitations, so the maximum axial stress divided by axial yield strength is equal to one. The highest ratio of shear stress divided by shear yield strength is equal to six. Also, this research will study the Bree diagram for 304 stainless steel.

3. **Steady-state creep model and constant determination via stress relaxation**: A limited number of tensile-torsion experiments can be used to determine the creep and stress relaxation properties of the material. The data needed to simulate the multiaxial loading came from a tensile test, creep test, and fatigue test. One methodology of this research is to find the tensile constants, creep constants, and fatigue constants from the stress-strain curve, which come from multiaxial loading. This study will obtain a new method to find the data needed to determine the constitutive model constants for material from a complex axial-torsion experiment. Some experiments will be performed to study the material behavior for 304 stainless steel (304 SS).

CHAPTER 2 LITERATURE REVIEW

2.1 Low Alloy Steel (2.25Cr-1Mo)

2.1.1 Application

The material of the present study is 2.25Cr-1Mo; this low alloy steel has great importance in high-temperature applications based on its excellent strength under fatigue and creep loading. This particular steel is used in steam pipes, pressure vessels, boilers, rotor forgings, power plants, and turbine engines, and therefore has been studied widely (Song et al., 2010; Tsai and Yang, 2003; Wang et al., 2013; Yang and Kim, 2001). The low alloy steel commonly used in high-temperature environments (i.e., 500°C to 650°C). The melting temperature, T_m, of the material is 1500°C. This material is used in high-temperature environments for long durations, and it subjected to the long-term, sustained loading; for example, the service time for this material is approximately 150,000 hours in high temperature in some applications.

2.1.2 Chemical Composition

The main factor influencing the microstructure and stability of carbide particles is chemical composition. The composition of 2.25Cr-1Mo steel shown in Table 2-1 (Wang et al., 2013). High amounts of Cr content elevate the ultimate tensile strength, cyclic hardening, and the elongation of the material. Adding Mo improves heat resistance, thereby increasing the strength of the low alloy steel at high temperatures. A SEM image of the microstructure of 2.25Cr-1Mo steel shown in Figure 2.1. The figure shows that the average grain size of this material is approximately four μm (Vicente Braz et al., 2005), and the random grain orientation gives rise to isotropic properties.

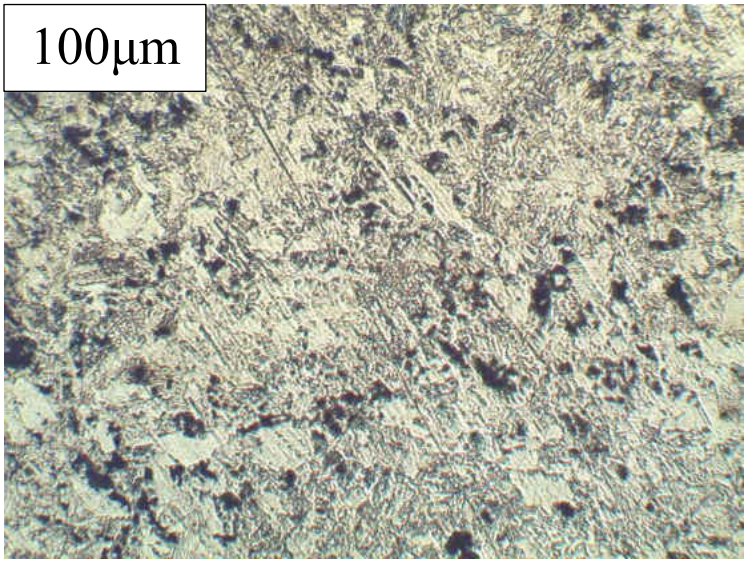

Figure 2.1: Microstructure of 2.25Cr–1Mo steel.

Table 2-1: Chemical composition of 2.25Cr-1Mo Steel

Element	C	Mn	P	S	Si	Cr	Mo	Cu	Ni	V	Fe
Min-Weight (%)	0.18	0.25	0.025	0.025	0.50	1.88	0.85	0.43	0.43	0.04	Bal.
Max-Weight (%)	0.18	0.66	0.025	0.025	0.50	2.62	1.15	0.43	0.43	0.04	Bal.

2.1.3 Mechanical Properties

Steel 2.25Cr-1Mo is sensitive to post-processing route. The mechanical properties of 2.25Cr-1Mo have been given by some sources (Bynum et al., 1976; Metals, 1989a; Parker, 1985; Polák et al., 1988; Science, 2004). Figure 2.2 shows elongation, elastic modulus, monotonic yield, ultimate strength, and cyclic yield strength of different of temperature. The elastic modulus and monotonic and cyclic strengths decreased with increasing temperature. Alternately, the elongation increases with increasing temperature (Bouchenot et al., 2016a). From this data, the Ramberg-Osgood and Chaboche constants have found and

developed. The mechanical properties for 2.25Cr-1Mo are shown Table *2-2* (Wang et al., 2013). Steel 2.25Cr-1Mo is commonly subjected to a variety of post-processing routes. There are three different popular post-processing steps: (1) normalized and tempering (NT), (2) post-welding heat treatment (PWHT), and (3) step cooling (SC) (Wang et al., 2013). In most situation, the material utilized in the NT condition; consequently, the variant of 2.25Cr-1Mo presented here is NT to have relevance to the service environment.

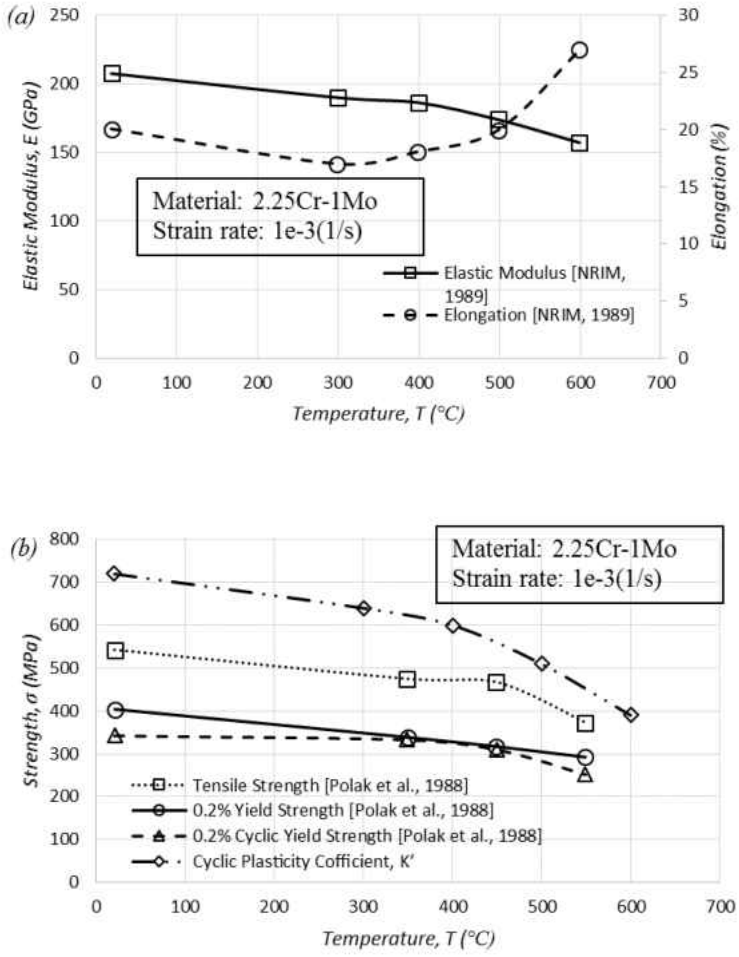

Figure 2.2: Temperature-dependence of a) Young's modulus and elongation and b) yield strength, ultimate tensile strength, and cyclic yield strength with different temperature for 2.25Cr-1Mo steel.

Table 2-2: Monotonic tensile properties of Normalized and Tempered 2.25Cr-1Mo

Temperature, T (°C)	**Model of Elasticity, E** (GPa)	**0.2% Yield Strength, $\sigma_{0.2\%Y}$** (MPa)	**Ultimate Tensile Strength, σ_{UTS}** (MPa)	**Fracture Strain, ε_f** (mm/mm)
21	234	414	516	0.0668
302	224	373	532	0.0636
399	197	348	516	0.0635
482	176	327	475	0.0655
566	166	298	362	0.0726
649	111	232	247	0.0787

2.1.4 Plasticity

A variety of studies have presented the plasticity response of 2.25Cr-1Mo (Bynum et al., 1976; Metals, 1989a; Polák et al., 1988; Science, 2004). The tensile curves presented by NRIM (Metals, 1989a; Science, 2004) in Figure 2.3 a. and Bynum (Bynum et al., 1976) in Figure 2.3 b. are a representation of its behavior across a range of temperatures. The monotonic tensile responses of 2.25Cr-1Mo shown at different temperatures. Despite various data sources, the behavior of the material is very similar. The material is more compliant at elevated temperature. Based on the tensile curve, offset yield strength, $\sigma_{0.2\%Y}$, ultimate tensile strength, σ_{UTS}, and

fracture strain, ε_f, for 2.25Cr-1Mo steel were acquired for several temperatures, as shown in Table 2-3. Generally, the modulus decreases with increasing temperature, while the elongation increases slightly.

Under cyclic conditions, 2.25Cr-1Mo steel exhibits isotropic softening over a range of temperatures. Material data provided by the National Institute for Material Science (Japan) show the midlife stress and strain amplitude for low-cycle fatigue (LCF) at temperatures from 20°C to 600°C Strain rates from 1×10^{-5} s^{-1} to 5×10^{-3} s^{-1} are used (Metals, 1989a; Science, 2004). Fatigue test data for 2.25Cr-1Mo have also been presented by other researchers (Metals, 1989a; Polák et al., 1988; Science, 2004). The trend of cyclic softening and temperature-dependence are consistent across studies. The Ramberg-Osgood model can be used to interpolate both the monotonic and cyclically-stable stress-strain curves of the material.

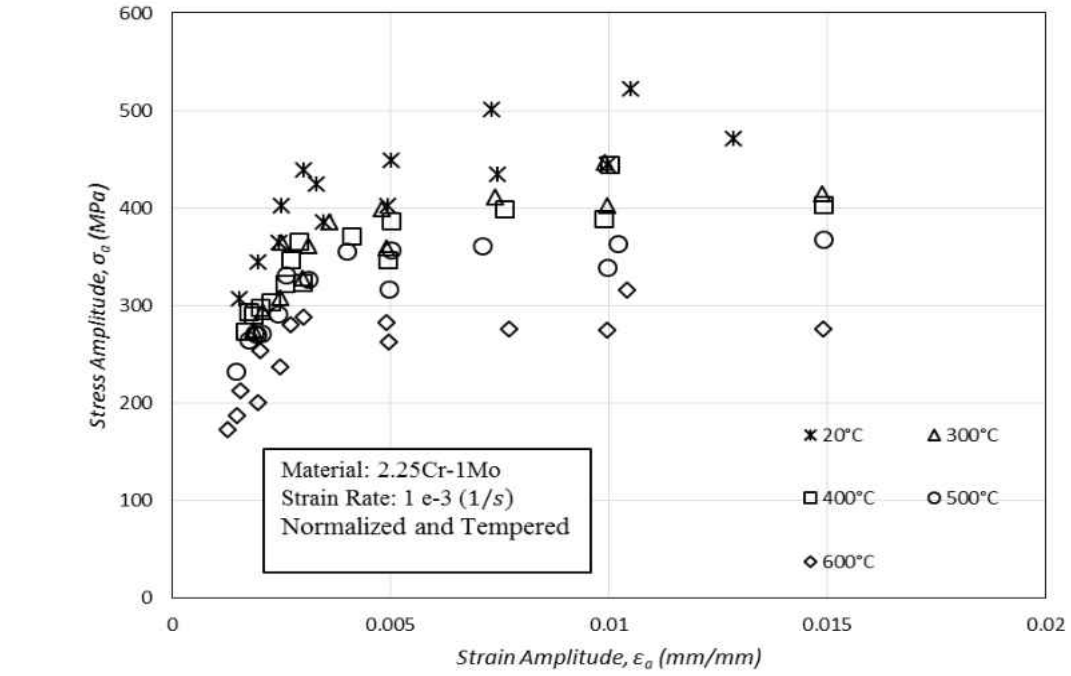

(b)

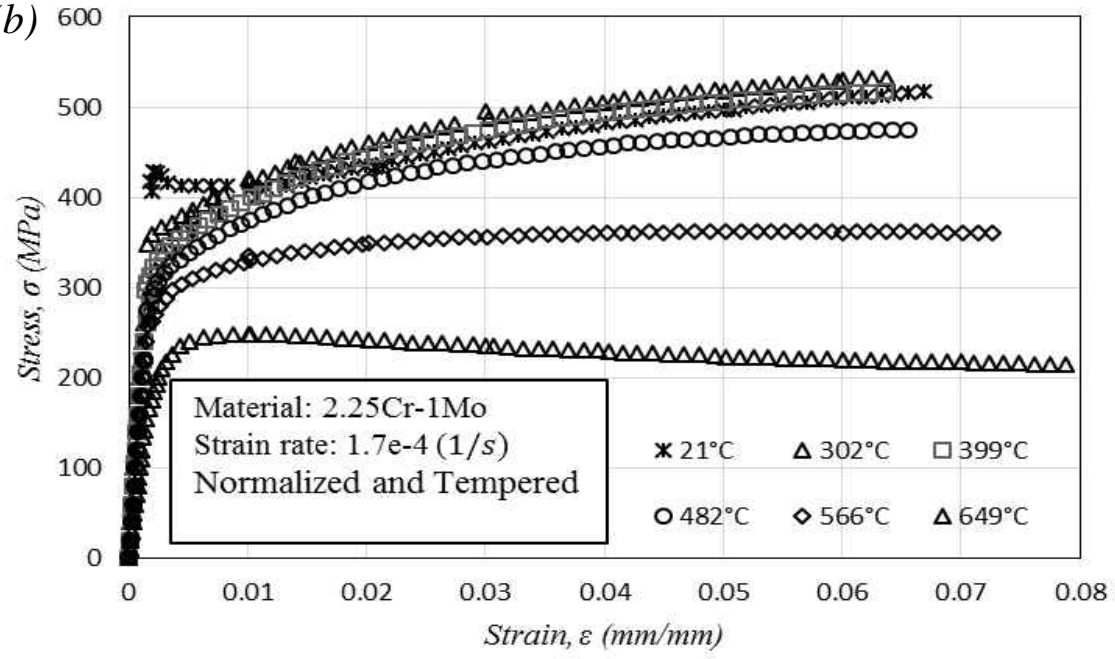

Figure 2.3: Monotonic tensile response of 2.25Cr-1Mo steel at different temperatures: (a) from NRIM/NIMS (Metals, 1989a; Science, 2004) and (b) from Bynum et al. (Bynum et al.).

Table 2-3: Monotonic and cyclic Ramberg-Osgood plasticity parameters for 2.25Cr-1Mo Steel

Temperature, *T* (°C)	**Monotonic Plasticity Coefficient, *K*** (MPa)	**Monotonic Plasticity Exponent, *n*** (Unitless)
	Monotonic	
21	720	0.1249
302	747	0.1199
399	729	0.1223
482	680	0.1253
566	426	0.5500
649	295	0.0350
Temperature, *T* (°C)	**Cyclic Plasticity Coefficient, *K'*** (MPa) $\varepsilon = \frac{\sigma}{E} + \left(\frac{\sigma}{K'}\right)^{\frac{1}{n'}}$	**Cyclic Plasticity Exponent, *n'*** (Unitless)
	Cyclic	
20	720	0.100
300	640	0.100
400	600	0.085
500	510	0.075
600	390	0.070

2.1.5 Creep

Creep deformation occurs in 2.25 Cr-1Mo when it is subjected to temperatures above 450°C. Creep deformation data was established by a variety of sources by Parker and co-workers. Results from Parker and co-authors (Parker, 1985) and NIMS (Metals, 1989a) were selected and presented as shown in Figure 2.4. The steady creep state creep behavior (i.e., stress versus strain rate) of 2.25Cr-1Mo shown for temperatures between 450°C to 650°C. The creep rate of the material near and above 100MPa is strongly dependent on the temperature. At 100 MPa with temperatures between 450°C and 650°C, the resulting strain rates range from 1e-5 to 1e-3 1/hr; however, as stress increases the range in strain rate exhibited reaches four or along of magnitude. For a narrow range of strain rate, the data appear to follow a linear trend; however, over wide strain rate ranges, the data are nonlinear. Both Norton and Garofalo models constants found to fit the data. In Table 2-4 shows the creep models constants for both constitutive modeling approaches.

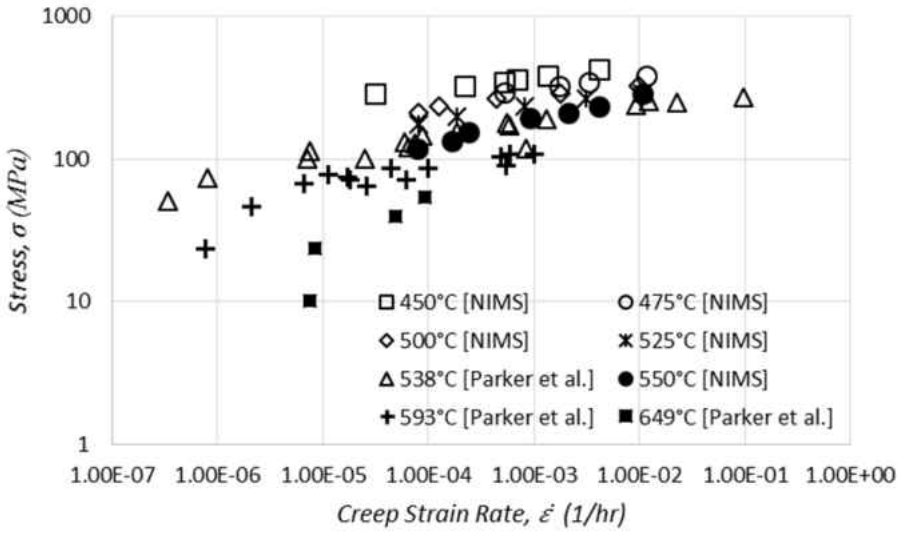

Figure 2.4: Minimum creep rate behavior of Normalized and tempered 2.25Cr-1Mo steel at various temperatures (Metals, 1989a; Parker, 1985).

Table 2-4: Norton and Garofalo creep constants for 2.25Cr-1Mo steel

Norton Constants				
Temperature, *T* (°C)	***A'*** ($\mathrm{MPa} - \mathrm{hr}^{1/\mathrm{n}}$)	***n'*** (Unitless)	***A*** ($\mathrm{MPa}^{-\mathrm{n}} - hr^{-1}$)	***n*** (Unitless)
		$\dot{\varepsilon} = A\sigma^n$		
450	640.9	0.0782	3.975E-36	12.59
475	579.8	0.0903	2.592E-31	11.07
500	495.0	0.0860	2.320E-31	11.34
525	468.4	0.1021	1.276E-26	9.683
538	393.4	0.1175	1.750E-21	7.902
550	629.4	0.1741	1.117E-16	5.689
593	240.7	0.1195	1.980E-17	6.663
649	160.7	0.1704	1.011E-11	4.643

Garofalo Constants			
Temperature, *T* (°C)	***A*** (hr^{-1})	***α*** (MPa^{-1})	***n*** (Unitless)
		$\dot{\varepsilon} = A\ sinh(\alpha\sigma)^n$	
450	1.695E-9	0.947	0.037
475	3.852E-8	0.925	0.035
500	7.036E-9	0.999	0.043
525	4.261E-8	1.638	0.026
538	6.808E-8	0.078	0.656
550	2.727E-6	1.628	0.018
593	6.384E-8	0.334	0.255
649	1.229E-6	2.138	0.041

2.1.6 Multiaxial Behavior

Several studies have investigated the multiaxial response of 2.25-Cr-1Mo steel. Inoue and co-workers investigated the response of the material under both proportionally and non-proportionally combined axial-torsion at 600°C. Both Blass (Blass, 1990) and Shang et al. (Shang et al., 2007) investigated the effects of axial-torsional on fatigue life at 538°C and 600°C, respectively. Under proportional loading paths, the axial and torsional components lead to normal and shear stresses that follow histories with identical shape. The principal axes of stress and strain rotate under non-proportional cyclic loading causing more complex hardening of the material. This research has four different cases as shown in Table 2-5. These various cases came from different experimental date, and this experiment data found by Inoue et al., and the table shows the stress or strain controls and stress/strain rate for 2.25Cr-1Mo. Inoue et al., (Inoue et al., 1989, 1994) have different multiaxial loading test, and this study covered four different tests and compared the simulation with experiments results. Test one is using stress control, and the loading path have used in test 1 is linear the test 2 used strain control, and the loading path is Diamond CCW. Test 3 loading path is Cruciform CCW, the control is strain control, and the last test is strain control with Elliptical CCW loading path. The temperature for these four different experiments happen under 600°C. The different simulations used four models, and these models are Chaboche-Garofalo, Chaboche-Norton, Romberg-Osgood-Garofalo, and Ramberg-Osgood-Norton.

Table 2-5: Multiaxial simulations and experiments on 2.25Cr-1Mo steel

Test	Paper	Test Control	Axial	Shear	Rate	Loading Path
M1	Inoue et al., 1994	Stress/Load Control	60MPa	-160 to200 MPa	$\dot{\sigma} = 10\text{MPa/s}$ $\sqrt{3}\,\dot{\tau} = 0.1\text{MPa/s}$	Linear
M2	Inoue et al., 1994	Strain Control	$\pm 0.2\%$	$\pm 0.23\ \%$	$\dot{\varepsilon} = 0.01\%/\text{s}$ $\sqrt{3}\,\dot{\gamma} = 0.01\%/\text{s}$	Diamond CCW
M3	Inoue et al., 1989	Strain Control	$\pm 0.6\%$	$\pm 0.35\ \%$	$\dot{\varepsilon} = 0.1\%/\text{s}$ $\sqrt{3}\,\dot{\gamma} = 0.1\%/\text{s}$	Cruciform CCW
M4	Inoue et al., 1989	Strain Control	$\pm 0.6\%$	$\pm 0.35\ \%$	$\dot{\varepsilon} = 0.1\%/\text{s}$ $\sqrt{3}\,\dot{\gamma} = 0.1\%/\text{s}$	Elliptical CCW

The goal of this study is to explore the response of a constitutive model developed with uniaxial data presented with experiments leading to multiaxial data. In Figure 2.5, several non-proportional waveforms are co-authors (Inoue et al., 1989, 1994). The first test (Figure 2.5 a) displays torsional cycling with a constant axial load. Since this stress-control test shows mean stress and the temperature are at 600°C, some ratcheting is expected. The next three cases (i.e., Figure 2.5 b through Figure 2.5 d) are strain-controlled and display a phase shift between the axial and torsional components. The goal of each test is to induce plasticity or creep in one axes and demonstrating the evolution of hardening as the other axis in loaded.

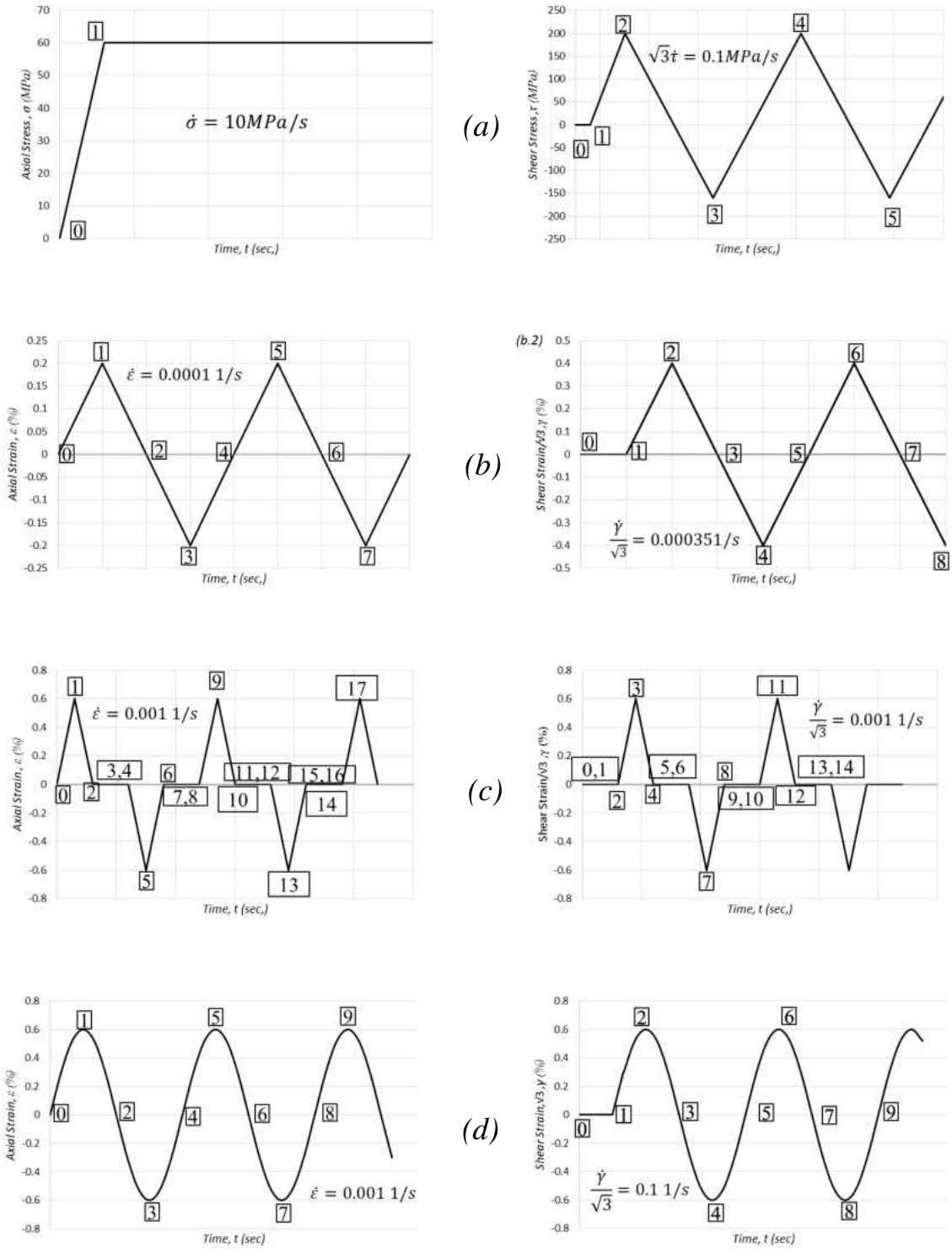

Figure 2.5: Load steps applied in 2.25Cr-1Mo at 600°C: a) Linear, b) Diamond Counter Clock-wise (CCW), c) Cruciform CCW, and d) Elliptical CCW.

2.2 304 Stainless Steel

Types 304 stainless steel is the material of importance for the study. Considered as one of the most commonly used steels worldwide, this specific alloy, and others like it are used in a vast collection of industrial applications. In regards to research, this material is favored over others because it is very accessible, which lowers the performance to cost ratio. In addition, strengthening its overall value, this alloy has been thoroughly researched, including its behavioral properties. The material used in a high-temperature environment. In this research, this material is studied to assess to new methods of plasticity and creep modeling. The experiments here apply the material to wide temperature of 20°C to 600°C.

2.2.1 Application

Stainless steel is a prime candidate for industrial usage because of its resistance to oxidation and its price when compared to other, weaker steels. The products most often used in the food industry that are made with 304SS are cookware, cutlery, processing equipment, and appliances (Smith, 1984). Because this alloy is resistant to corrosion, it is helpful in the construction of buildings and monuments by maintaining their initial appearance. This steel is also the base of internal mechanisms and outer casings of military firearms Petrochemical piping, heat exchangers, and valves are included in the heavy industrial practices of items produced with 304 stainless steel. Within the energy industry, this steel is still utilized in the production of hydraulic turbine wheels (Simoneau and Roberge, 1981; Wert and DiSabella, 2006; Xu and Li, 2012) as well as exhaust recuperates, for gas turbine components (Maziasz et al., 1999).

Because of 304 stainless steel similar properties to industrial parts in nuclear and combined cycle power, it has been used as a repair material for defective steam blades. This steel can be

welded straight on to rotor steels and can serve as a way repairing cracks while maintaining the material performance (Bhaduri et al., 2001). Researchers within these industries are aspiring to determine the specific behavioral characteristics of this material due to the above mentioned applications in thermomechanical cycling.

2.2.2 Chemical Composition

The composition of 304 stainless steel is primarily chromium and nickel. There are various blends in which the steel is comprised of the above two alloying agents; however, the most common is 18-20% chromium and 8-10.5% nickel. This is why it is typically called the "18/8 steel". The favorable oxidation resistance of the steel is due to the existence of the chromium. Nickel, helps to suppress the conversion of austenite (γ-Fe) into cementite (Fe3C) and ferrite (α-Fe) during the cooling, in manufacturing, from a liquid state. While this is accurate, in the most recent years, some of the nickel content in austenite has been replaced with manganese to prevent the above mentioned carbon diffusion and phase change (Di Schino, 2000). The wrought 304SS is dominated by larger austenite pieces with heavy boundaries outlined in thick chromium carbide (Cr3C2) (Di Schino et al., 2000).

While chromium and nickel make up approximately 26% of the weight, there are other elements in the makeup. During the melting process, silicon is added to prevent oxidation, and sulfur and phosphorous are used to improve machinability (Harvey, 1982). Carbon is noted in low quantities to provide the steels advantageous strength over iron. Table 2-6, shows the compositions for 304SS according to the UNS S30400 specification. It shows the trace amount of copper and cobalt as contaminants of other agents (Lampman et al., 2007).

Table 2-6: Chemical composition of 304 stainless steel

Element	C	Mn	Si	Cr	Ni	P	S	N
Min-Weight (%)	0.04	Up to	Up to	18	8	Up to	Up to	Up to
Max-Weight (%)	0.10	2.00	1.00	20	10.5	0.045	0.030	0.10

Since no chemical mixture is exactly the same, the amount of each alloying agent will vary by batch; therefore, different material behaviors will be exhibited. Because of the various mixtures, the noted numbers are the mean values in a scatter band in a statically analysis. When the level of manganese rises, the strength is increased and the nitrogen solubility, but it will affect the diminished fatigue resistance and quicker work-hardening rates. A low percentage of carbon results in sensitivity to intergranular deterioration and a higher level leads to increased strength (Davis, 1994).

2.2.3 Tensile Properties

As wrought, the 304 stainless steel is strong and has an ultimate tensile strength of 520 MPa and with conditioning can rise to 1040 MPa. Another characteristic is the loss of ductility that may be experienced when grains are lengthened through worked 304SS and the tensile strength increases to 1040 MPa. Up to 55% elongation at failure is possible when the steel is wrought. When using a typical annealing process, the metal can reach 630MPa after heating and will not lose any ductility. As well, 304SS has positive elevated temperature attributes where ultimate tensile strength at 600°C decreases to relatively 55% of its room temperature value and elastic modulus gradually softens (Lampman et al., 2007; Peckner and Bernstein, 1977). In the Figure 2.6 shows the mechanical properties for 304 stainless steel with various

temperature(American Iron and Steel Institute, 2012; INCO Databook, 1968; Mills, 1988). The elastic modulus for 304 stainless steel, decreases with increasing the temperature. This material is softening with increase the temperature, and the same behavior occure with yield strength as shown in Figure 2.7. After the yield strenght found from the literature the study will find the equation to find the yield strength for any temperature. In Figure 2.8 shows the ultimate tensile strength for 304 stainless steel, then the ultimate tensile strength found from the literature the study will find the equation to find the ultimate tensile strength for any temperature. Form the previous figure shows the material behaviour are softening with increase the temperature, and the elongation is decrease with increasing the temperature as shown in Figure 2.9. The next step is finding the methematical model for the material behaviour, so from the model, the study found the material properties for any temperature. In Table 2-7 shows the 304 stainless steel tensile properties for the model found.

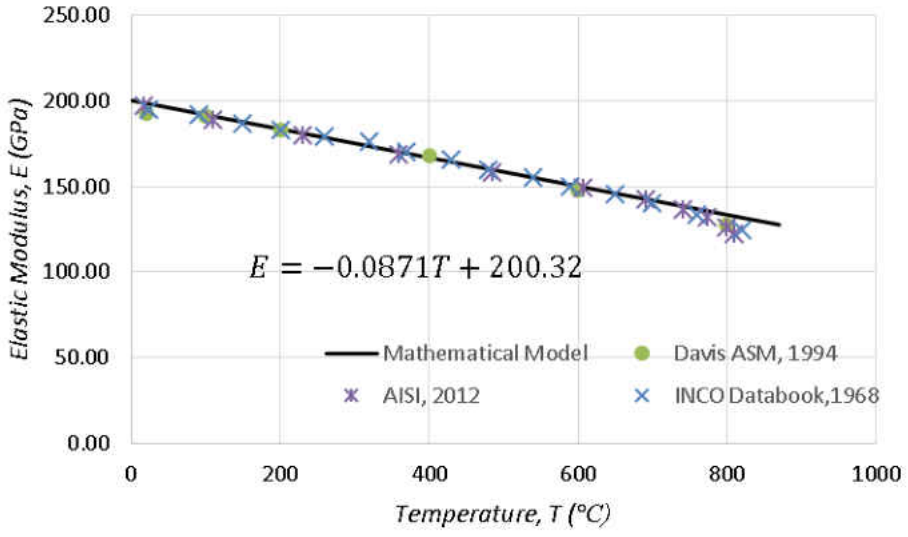

Figure 2.6: Elastic modulus of 304 stainless steel with various temperature (American Iron and Steel Institute, 2012; INCO Databook, 1968; Mills, 1988).

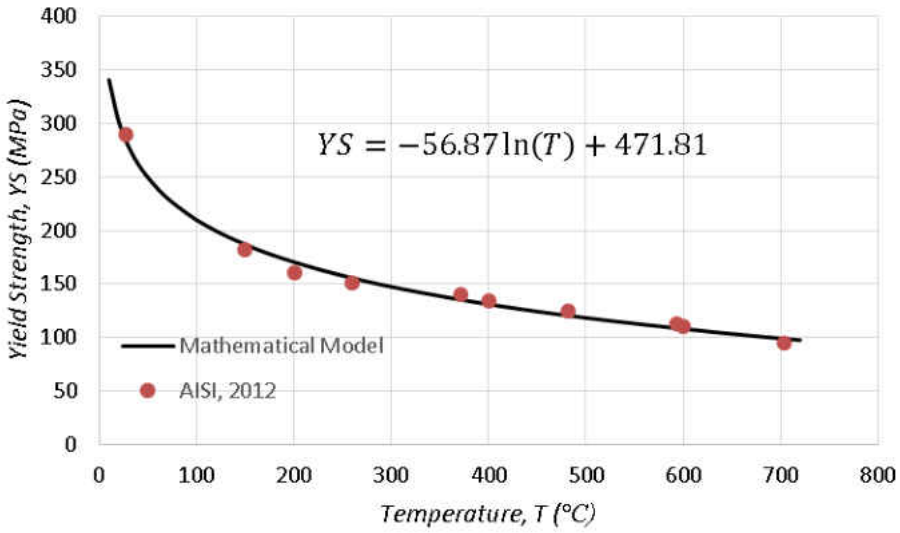

Figure 2.7: Yield strength of 304 stainless steel with various temperature (American Iron and Steel Institute, 2012).

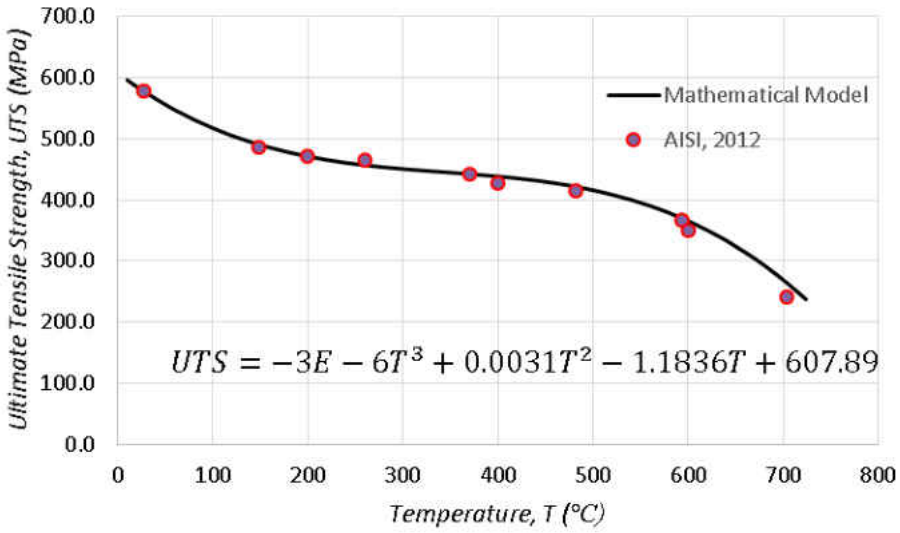

Figure 2.8: Ultimate tensile strength of 304 stainless steel with various temperature (American Iron and Steel Institute, 2012).

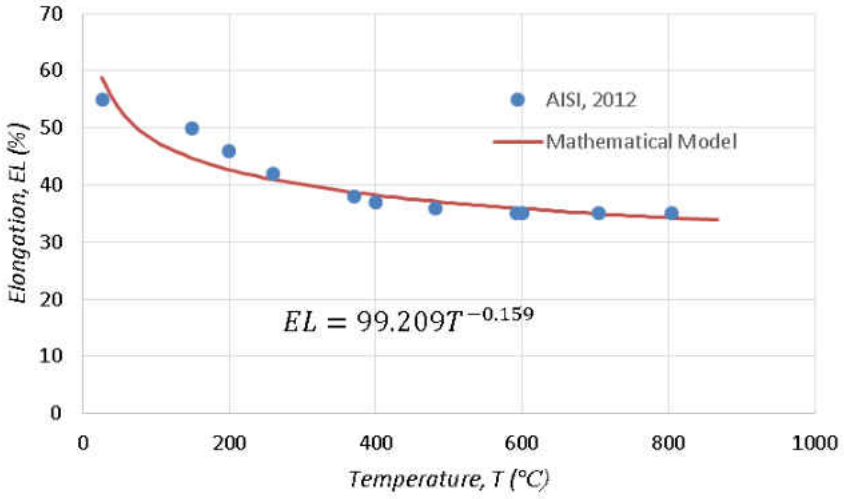

Figure 2.9: Elongation of 304 stainless steel with various temperature (American Iron and Steel Institute, 2012).

Table 2-7: Mechanical properties for 304 stainless steel

Temperature, *T* °C	Elastic Modulus, *E* GPa	Yield Strength, *YS* MPa	Ultimate Tensile Strength, *UTS* MPa	Elongation, *EL* %
20	199	301	585	62
100	192	210	517	48
200	184	170	471	43
300	175	147	451	40
400	167	131	439	38
500	159	118	416	37
600	150	108	366	36
700	142	99	270	35
800	134	92	109	34

This steel is markedly favorable compared to others because it can be applied in many structural operations up to 600ºC. In steam turbine operations, 600ºC is the highest encountered, however, the tensile strength rapidly decreases above 650ºC as opposed to lower temperatures, but can still be used at temperatures up to 1093ºC for low-stress applications (AISI, 2012). As can be predicted, there is a significant decrease in strength with higher temperatures. Thus the tensile reaction of 304SS is graphed as a monotonic, stress-strain curve similar to other metals. By using the Ramberg-Osgood model, the monotonic curve for 304 stainless steel as shown in Figure 2.10(Ramberg and Osgood, 1943). The Ramberg-Osgood parameters found for different temperature by used curve fitting. The parameters are monotonic plasticity coefficient, *K,* and monotonic plasticity exponent, *n* as shown in Table 2-8. Figure 2.10 shows the plasticity behavior of the 304 stainless steel with various temperatures, so for the low temperature has the highest stress. the Ramberg-Osgood parameters are decreases with increasing the temperature.

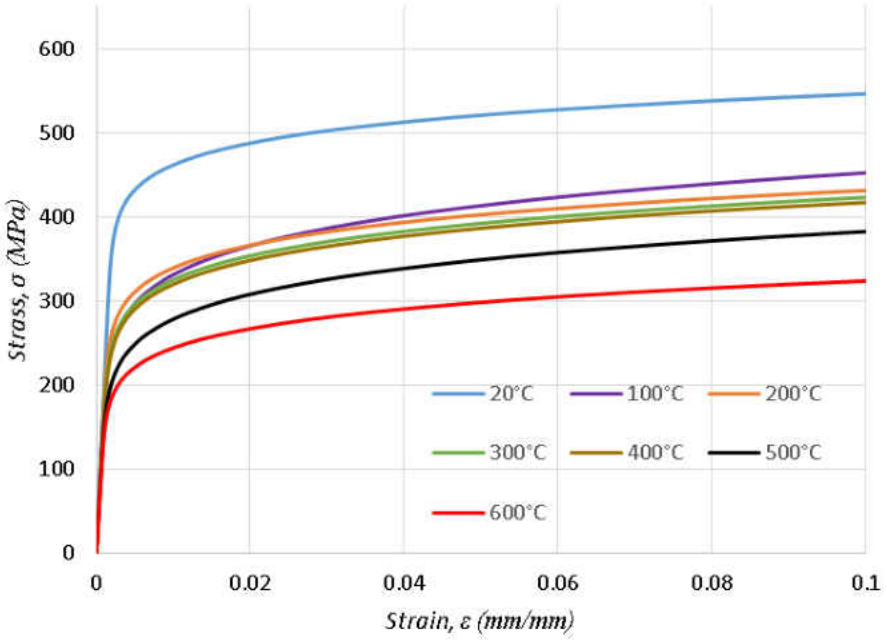

Figure 2.10: Monotonic tensile response of 304 stainless steel at various temperatures.

Table 2-8: Monotonic Ramberg-Osgood plasticity parameters for 304 stainless steel

Temperature, *T* (°C)	**Monotonic Plasticity Coefficient, *K*** (MPa)	**Monotonic Plasticity Exponent, *n*** (Unitless)
20	638	0.066
100	607	0.126
200	540	0.096
300	541	0.106
400	534	0.107
500	516	0.129
600	423	0.115

The reaction of the equation is that of elastic and plastic strains terms where 304SS is at room temperature, the value of *K* is 638MPa and *n* is 0.066. These values produce a good fit at the approximate yield point. This is only optimal when the strain value does not over reach in to the plastic region. This supplies a similar kind of equation representing the stress and strain relationship. The determined parameters have a secondary fit established on the linear relation between flow stress to hardening. The optimal approach used to find these parameters via is curve fitting. The curve fitting used here for excel, and that method by minimize the error value which is almost zero. The curve fitting done by add trend line on Excel, and from the Excel the minimize error value by used the solver on this software.

2.2.4 Creep Behavior

When Type 304 stainless steel is exposed to elevated temperature for long periods, there are two primary considerations in regards to the alloy behavior. Due to the elevated levels of chromium and carbon, it is possible to have a loss of ductility when the previous two elements form chromium carbides at grain boundaries. The second behavior is the eventual result of stress relaxation or conversion to creep.

When exposed to temperatures higher than 475ºC, for extensive lengths of time, 304SS can experience embrittlement (Boyer and Gall, 1985). At the grain boundaries, there are small regions of chromium carbides. These may expand when the temperatures reach between 475ºC and 815ºC and the carbide and chromium extend outward from the austenite lattice. The chromium present in steels like 304SS can lead to multiple metallic carbides with carbon. Specifically in austenitic steels is Cr23C6. The two main elements have a similar ratio to the overall mixture (Rashid et al., 2012). With a hardness and elastic modulus a magnitude higher, the carbide mechanical properties are much different than austenite steels (Freyd and Suprunov, 1970). This mixture leads to a propensity towards voids opening at the interface due to shear stresses or for existing cracks to quickly propagate through the carbide.

Creep deformation occurs in 304 stainless steel when it subjected to temperatures above 475°C. Creep deformation data was established by a variety of sources (Booker, 1978; Chopra and Natesan, 1977). Results from Booker, Natesan, and co-authors were selected, and presented in Figure 2.11. The steady creep state creep behavior (i.e., stress versus strain rate) of 304 stainless steel shown for temperatures between 540°C to 815°C; however, as stress increases, the range in strain rate exhibited reaches along of magnitude. For a narrow range of strain rate, the data appear

to follow a linear trend; however, over wide strain rate ranges, the data are nonlinear. Both Norton and Garofalo models constants found to fit the data.

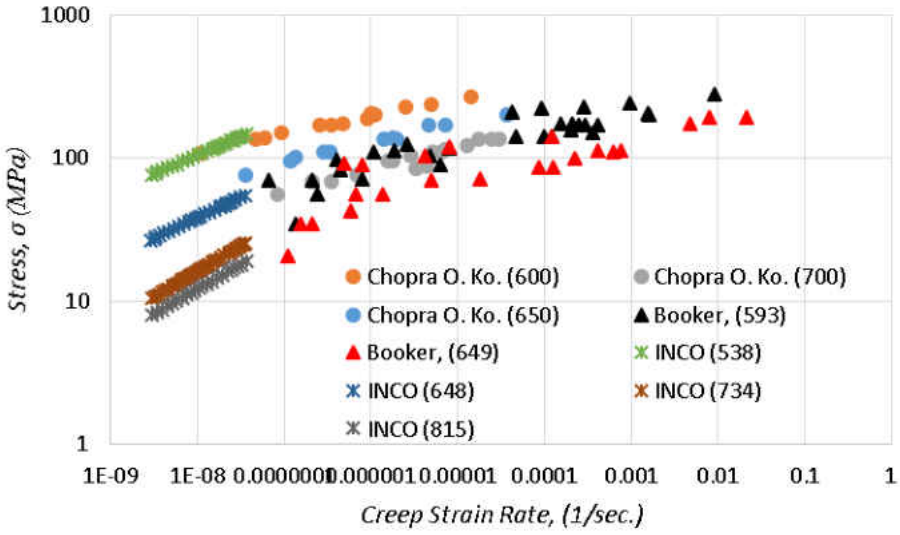

Figure 2.11: Minimum creep rate behavior of 304 stainless steel at various temperatures(Booker, 1978; Chopra and Natesan, 1977; INCO Databook, 1968).

From this data, the creep constants are derived using the models used in this research are Norton and Garofalo creep models. In Table 2-9 shows the Norton and Garofalo constants with various temperature. The reason form that to found the equation for each parameters, and from this equation give the study the availability to find the parameter for any temperature. The model parameters are important to use that parameter in simulation.

Table 2-9: Minimum creep constants for Norton and Garofalo models for 304 stainless steel (Booker, 1978; Chopra and Natesan, 1977; INCO Databook, 1968)

Norton Model		
Temperature, T °C	A ($\mathrm{MPa^{-n} - hr^{-1}}$)	n (Unitless)
600	7.01E-25	7.910
650	1.08E-21	7.100
750	1.94E-18	6.125
538	1.87E-16	3.825
648	2.85E-14	3.501
734	4.29E-12	2.789
815	7.11E-12	2.901
649	5.47E-16	5.514
538	2.39E-18	6.138

Garofalo Model			
Temperature, T °C	A (1/sec.)	α (1/MPa)	n (Unitless)
600	5.00E-9	0.01784	1.80
650	7.09E-7	0.0071	5.57
750	5.22E-6	0.008	4.02
593	4.34E-7	0.013	3.38
649	3.06E-6	0.014	3.83

2.3 Plasticity Models

Plasticity models are applied to describe observed material behavior. There are several constitutive models to account for cyclic plasticity, strain hardening/softening, and strain ratcheting. Each method differs by strengths, weaknesses, and data expected for calibration.

2.3.1 Ramberg-Osgood (RO) Model

Plasticity models are applied to describe time-independent material behavior that deviates from elasticity. There are several constitutive models to account for cyclic plasticity, strain hardening/softening, and strain ratcheting. Each method differs by strengths, weaknesses, and expected data for calibration. The Ramberg-Osgood model was developed in 1943. This model is one of the most popular formulation to describe the tensile behavior of materials for engineering analysis and design. The model is also used to describe the cyclic stress-strain curve data (Tudor Sireteanu et al., 2014), i.e.

$$\varepsilon_a = \frac{\sigma_a}{E} + \left(\frac{\sigma_a}{K'}\right)^{\frac{1}{n'}} \qquad (2.1)$$

Here ε_a and σ_a represent cyclic strain and stress amplitude, respectively. Both the cyclic hardening strength, K', and the cyclic hardening exponent, n', display temperature dependence and are fit to data via regression modeling. Previous research shows how K' and n' can be used to simulate both isotropic and kinematic hardening. The theoretical range of the cyclic strain hardening exponent is from near to zero to 0.6. Figure 2.12 shows that the RO model can be used to fit both monotonic

and cyclically stable stress-strain curves. The stress-strain models using the Ramberg-Osgood fit both carve well once *K'* and *n,'* are found by minimizing the error value by regression analysis. For cyclic conditions, the approach assumes that the material has reached steady state, and it can make capture the hysteresis loop. This method can employ at various temperature levels. Figure 2.13 shows the stress-strain curve for 2.25Cr-1Mo at different temperatures using the curve fitting (Bynum et al., 1976). The cyclic strength coefficient K' and the cyclic strain-hardening n' are dependent on the temperature, as shown in Table 2-10. When the temperature increases, the strain hardening coefficient, and the strain hardening exponent will decrease (Metals, 1989b; Science, 2004).

$$Error = \sum_{i=1}^{m} \left(y_i - y_{i\ exp.}\right)^2$$

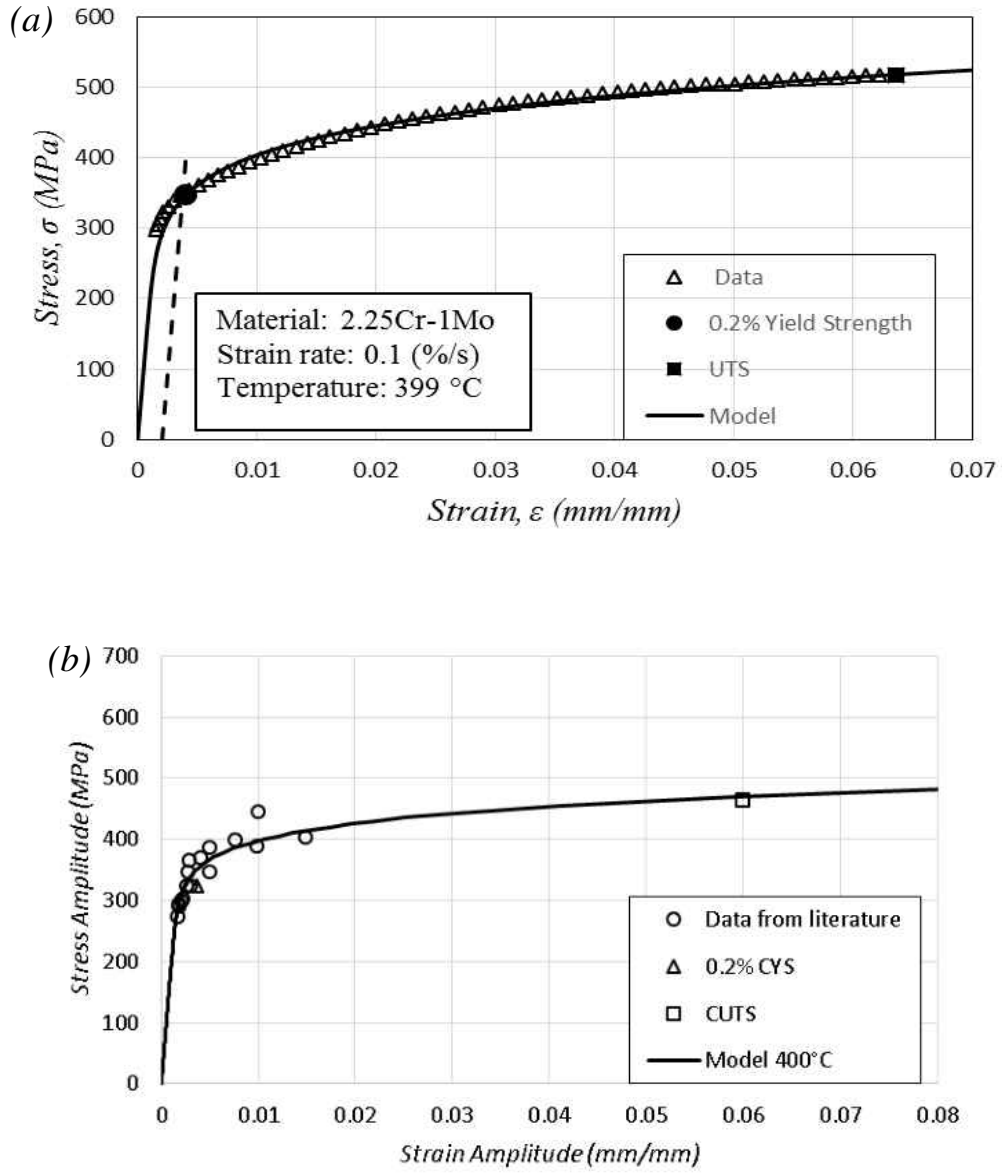

Figure 2.12: Stress-Strain curve fitting of 2.25Cr-1Mo at 399°C and 400°C via Ramberg-Osgood modeling: a) monotonic loading (Bynum et al., 1976)and b) cyclic loading (Bynum et al., 1976).

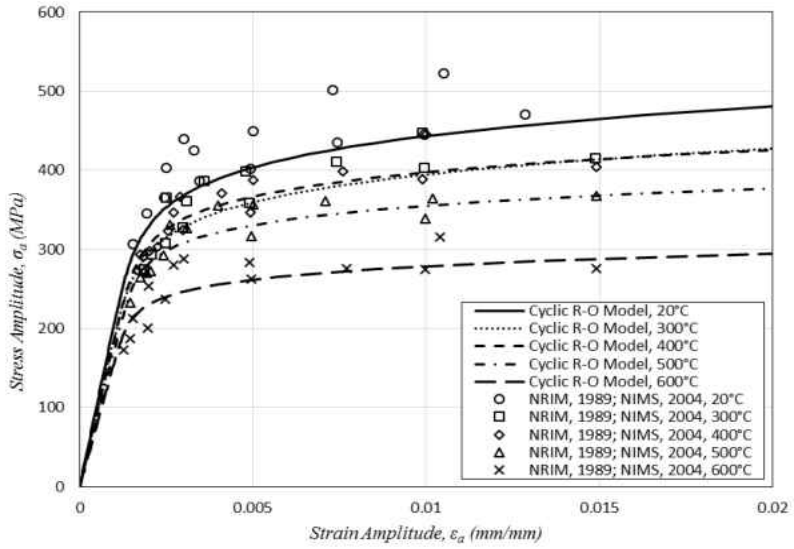

Figure 2.13: Cyclic RO modeling at various temperatures.

Table 2-10: Monotonic Ramberg-Osgood plasticity parameters for 2.25Cr-1Mo

Temperature, *T* (°C)	**Cyclic Plasticity Coefficient, *K'*** (MPa)	**Cyclic Plasticity Exponent, *n'*** (Unitless)
21	720	0.1249
302	747	0.1199
399	729	0.1223
482	680	0.1253
566	426	0.5500
649	295	0.0350

2.3.2 Chaboche Model

The Chaboche plasticity model (Chaboche, 1986) has gained popularity plasticity over the past twenty years because it can be applied to a variety of materials. It exemplifies a dual-surfaced approached which explains the cyclic behavior. The constitutive model is native to several finite element software packages, for example, ANSYS *(Bouchenot et al., 2016a)*. Research shows the Chaboche model has multiple issues with accuracy. One is the estimation of the ratcheting effect which cannot explain the yielding point and cannot explain the hardening memory effect. For that, modifications were made to cyclic hardening and others to hardening memory effect *(Budahazy and Dunai, 2013)*. In 1966, Armstrong and Frederick (Armstrong and Frederick, 1966) proposed the nonlinear kinematic hardening (NLKH) model:

$$\dot{X} = \frac{2}{3} C \dot{\varepsilon}_p - \gamma X \dot{p} + \frac{1}{C} \frac{dC}{d\theta} \dot{\theta} X \qquad (2.2)$$

Where X is the back stress, $\dot{X}$ is the time rate of change of the back stress, $\dot{\varepsilon}_p$ is the plastic strain rate, $\dot{p}$ is the accumulated plastic strain rate, C is the hardening modulus, γ is the hardening modulus rate, θ is the temperature, and $\dot{\theta}$ is the time-based temperature rate (Bouchenot et al., 2016a). In 1986, Chaboche proposed the decomposed nonlinear kinematic hardening rule into multiple back stresses or segments, e.g.

$$X = \sum_{i=1}^{M} X_i \qquad (2.3)$$

here M is typically valued at two, three, or four. This segmenting enhances hysteresis loop modeling (Bari and Hassan, 2000; Bouchenot et al., 2016a; Chaboche, 2008). This kinematic hardening incorporated into the yield surface relation, e.g.

$$\sigma_v = J(\sigma - X) - k \qquad (2.4)$$

where k is the size of the initial yield surface and $J(\sigma - X)$ is a von Mises distance in the deviatoric stress space (Chaboche, 1983, 1989, 1997, 2008). Bouchenet (2016) developed an approach to determine the Chaboche constants as shown in Figure 2.14, and Table 2-11 shows the Chaboche constants (Bouchenot et al., 2016a; Bouchenot et al., 2016b). From Bouchenet et al., 2016 found the way to detriment the Chaboche constants as shown in Figure 2.14 (Bouchenot et al., 2016a; Bouchenot et al., 2016b). The stress-strain curve is divided into three segments based on strain, the first segment is (0.001% to 0.02% plastic strain), the next segment is (0.02% to 0.2% plastic strain), the last segment is (0.2% plastic strain to (twice strain of 0.2% - 0.02% of plastic strain)) as shown in Figure 2.14.

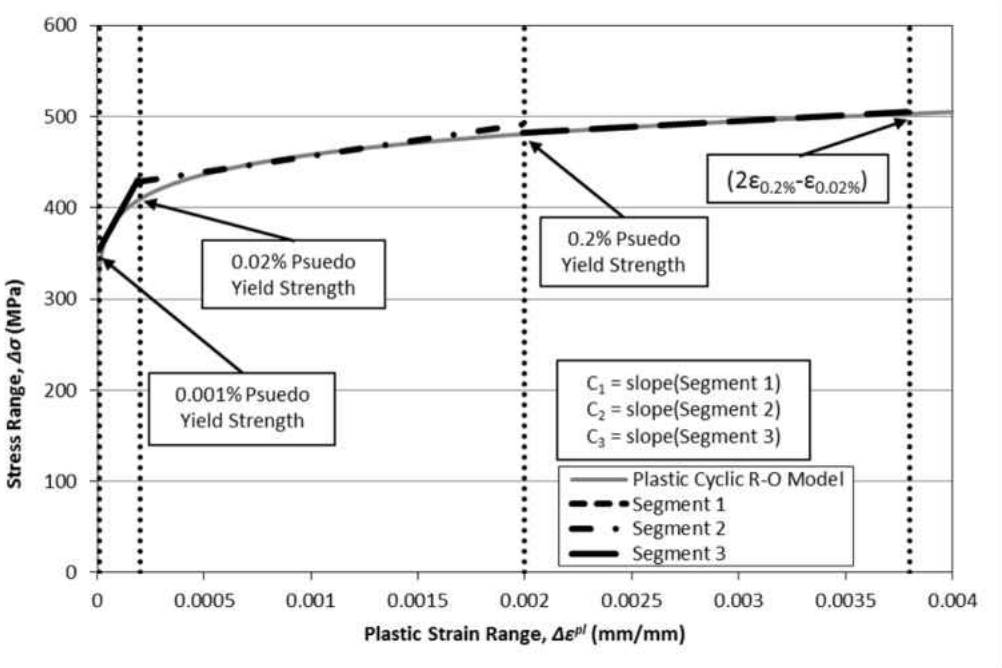

Figure 2.14: Sketch of the fitting and segment bounds on a cyclic RO curve using the proposed determination method.

Table 2-11: Cyclic Chaboche plasticity parameter for 2.25Cr-1Mo Steel

Temperature, *T*	*C1*	*γ1*	*C2*	*γ2*	*C3*	*γ3*
°C	MPa	Unitless	MPa	Unitless	MPa	Unitless
20	783483	12279	83313	1787	27418	280
300	703755	12669	74194	1775	24169	278
400	647907	12140	66156	1776	21354	282
500	545026	12358	54585	1821	17506	290
600	420727	12894	40485	1780	12580	284

2.4 Creep Models

Under consistent loading, the secondary regime of creep dominates the time-dependent response 2.25Cr-1Mo when above 35% of its melting temperature. Parker and co-authors showed creep data for 2.25Cr-1Mo steel in three different temperatures (Parker, 1985). Two key steady states creep models are Garofalo and Norton models. Both laws describe the relation between the minimum creep rate and the applied stress. By using the curve fitting with the data available. Both used for fitting stress versus strain rate data at specific temperature levels. Each has a different fitting procedure.

2.4.1 Norton Model

The Norton Model is the most widely used model for steady state creep of metals (Yoon et al., 2000). The minimum creep rate, behavior primary and tertiary creep correlated with stress for example the slope at the inflection points are not constant on the creep curves (Golan et al., 1996). The Norton power law is used to define at various temperatures, e.g.(Golan et al., 1996; Jin et al., 2014; Tahami et al., 2010; Yoon et al., 2000),

$$\dot{\varepsilon}_{cr} = A\sigma^{n} \qquad (2.5)$$

$$\sigma = A'\dot{\varepsilon}_{cr}{}^{n'} \qquad (2.6)$$

where $\dot{\varepsilon}_{cr}$ is the creep strain rate, A is a material constant, σ is the applied stress during creep test, and n is the power law exponent. Creep data from Figure 2.15 is modeled using Norton. Strong temperature-dependence in the data is captured by the collection of regression lines (Parker, 1985). *Table 2-12* and Figure 2.16 contains the Norton constants at different temperatures for 2.25Cr-1Mo. With increase the temperature, the strain rate is expected to increase if stress is held constant. One limitation of Eq. (2.5) is that it does not capture the full range of stress versus strain rate trend exhibited by that data at very low strain rates near 1e-7 per hour. A model with more parameters model be required.

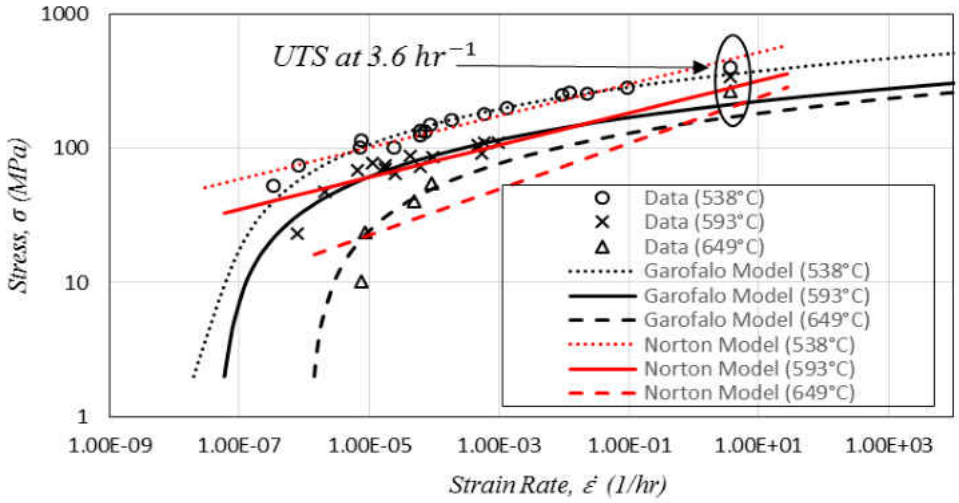

Figure 2.15: Temperature dependence of rate creep for 2.25-1Mo steel (Parker, 1985).

Table 2-12: Norton model constants for 2.25Cr-1Mo

Norton Constants				
Temperature, *T*	***A'***	***n'***	***A***	***n***
(°C)	($\mathrm{MPa} - \mathrm{hr}^{1/\mathrm{n}}$)	(Unitless)	($\mathrm{MPa}^{-\mathrm{n}} - hr^{-1}$)	(Unitless)
538	393.49	0.117517	1.74979E-21	7.90282
593	240.72	0.119509	1.98004E-17	6.66325
649	160.72	0.170416	1.01119E-11	4.64379

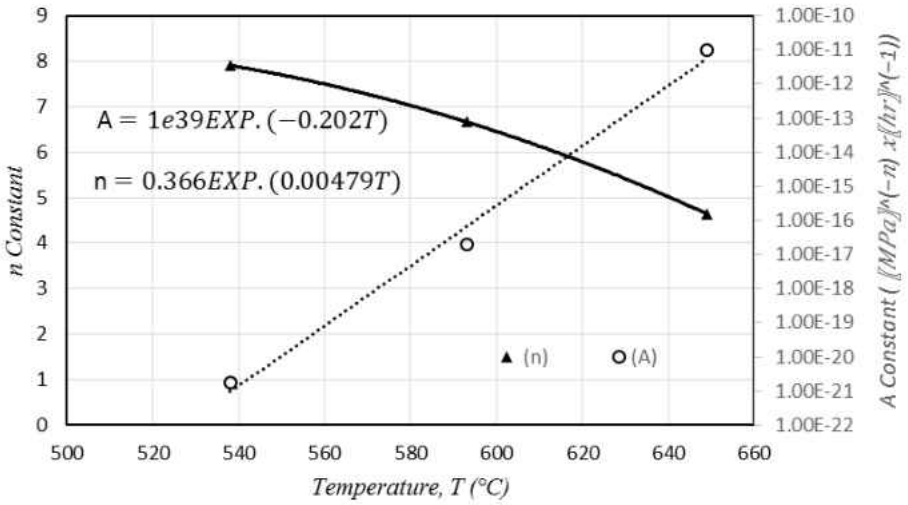

Figure 2.16: Norton model constants for 2.25Cr-1Mo steel with three different temperatures (Parker, 1985).

2.4.2 Garofalo Model

The Garofalo model also simulates the steady state creep response, but it allows for non-negligible rates of creep at reduced stresses. Both Norton and Garofalo models rely on identical steady state creep data. Normally, the experiments creep data plotted for the logarithm of stress, σ, and the logarithm of strain rate $\dot{\varepsilon}_{cr}$ as shown in Figure 2.15. The Garofalo equation is given as.

$$\dot{\varepsilon}_{cr} = A\,[sinh(\alpha\sigma)]^n \qquad (2.7)$$

where A, α, and n are material constants, applied by (Garofalo, 1965; Rieiro et al., 1998) and described by (McQueen et al., 1993; Rieiro et al., 1998). The Garofalo model needs a wider range of creep data compared to Norton based on the additional parameter. A key limitation of the Garofalo model relates to its parameter identification process. The Garofalo equation is hyperbolic, which makes it difficult to solve analytically. Because of the hyperbolic sine, either an analytical approach or least squares formal has been established to identify parameters to fit the data. Riero and co-authors have introduced a method (Rieiro et al., 1996); however, the best technique to identify constants that show smooth transition across temperatures is by way of manual fitting. Garofalo constants presented in Table 2-13 are used to model the data shown in Figure 2.15. A key observation is that the curves based on Garofalo Eq. (2.7) do not overlap for various temperature levels. The constants A increases with temperature regardless of model, and n decreases. For example, they may be out of the range of the simulation when they have a high strain range as described by Rieiro and co-authors (Rieiro et al., 1998). The approach used to identify the creep data for the stress range, so the Garofalo equation used. The theories mentioned

above of Norton and Garofalo study the materials creep behavior under uniaxial loading; however, in practical settings, multiaxial loading is observed. More recent studies have been geared towards identifying creep constants from stress relaxation instead of via creep tests.

Since temperature gradients exist in the service environment interpolation across temperature is needed. The temperature-dependence of the constants determined at various temperature levels as shown Figure 2.17. Framworke are presented for each constant on temperature dependence. Each model has temperature normalized by the melting temperature.

The data shown in Figure 2.15 is being used to the curve fitting by using the Garofalo model. There are two problems with hyperbolic and iterative methods. The first issue is the main one of the method, which is choosing the repeating paths and explaining their appropriateness. The second issue, the assumption of the initial values may result in a decision of the poor-fitting solution, so it can be found using the quadratic of the error function to be more accurate. The challenge is to find A, α, and n with smooth temperature-dependence. This proposal found a new technique to determine these constants by using the toolbar-approach in Excel to find the initial value of constants. The first constant is A, and it is used to move the curve. The way to calculate this unknown is assuming a value for α to find the similar deterioration plans and to calculate the best correspondence with the given experimental data. Now, the initial value of α can set for a range that is from zero to one when using Eq. (2.7).

$$ln\,\dot{\varepsilon} = ln\,A + nln[sinh\,\alpha\sigma] \qquad (2.8)$$

The way to calculate this unknown is assuming a value for α to find the equivalent determination plans and to calculate the best correspondence with the given experimental data. Now, the initial value of α can set for a range that is from zero to one when using Eq. (2.7) (Rieiro et al., 1996; Rieiro et al., 1998). The way to find a solution of nonlinear and iterative methods, the initial value of α must given. The only way to linearize the Eq. (2.8) is by assuming α is constant. The Garofalo equation has four parameters that are A, n, α. The first step is to minimize the Eq. (2.7)to get total error Eq. (2.8).

$$Err = min \sum_{i=1}^{N} ln\, \dot{\varepsilon} - ln\, A - n\, ln[sinh\, \alpha\sigma] \qquad (2.9)$$

When the A is increasing, the curve will move to the right. The second constant is α, and it will control the curvature. By increasing α value, the curvature will increase. The last constant is n, and it will affect the curve angle. The angle will decrease by increasing the n value. Therefore, the study found the Garofalo constants from this technique as shown in Table 2-13. Figure 2.15 has a good curve fitting and minimum error, which means the new technique is appropriate. After finding the initial value for constants by using the Excel toolbar and reducing the error value, the Garofalo constants obtained for each temperature Figure 2.17 show the optimal curve fitting for this data. Also, the curve fitting finds the equation to reach A, α, and n for any temperature. After that, a simulation will be for 2.25Cr-1Mo at the temperatures needs to compare with the experimental data.

Table 2-13: Garofalo model constants for 2.25-1Mo steel

Garofalo Constants			
Temperature, *T* (°C)	***A*** (hr^{-1})	***α*** (MPa^{-1})	***n*** (Unitless)
538	6.808E-8	0.078	0.656
593	6.384E-8	0.334	0.255
649	1.229E-6	2.138	0.041

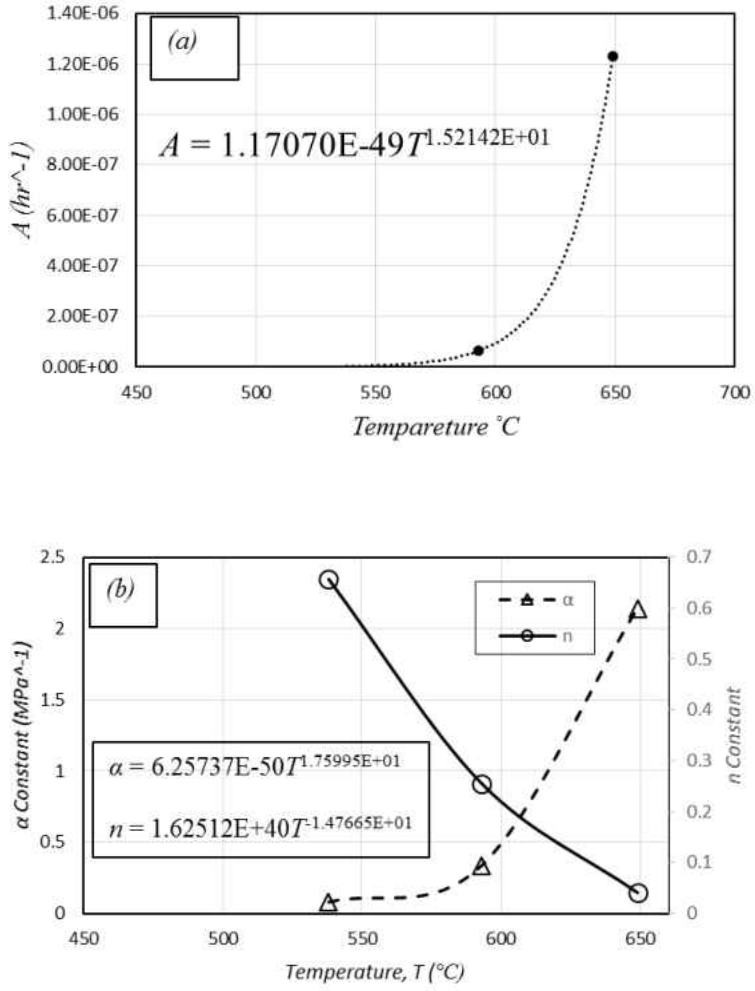

Figure 2.17: Garofalo constants for 2.25Cr-1Mo steel with various temperature: a) A and b) n and α.

2.5 Ratcheting

Ratcheting is the progressive accumulation of strain under asymmetrical cycling under stress/load control. It is caused by creep in the direction of the mean stress. Most studied ratcheting facilitated from axial stress and thermal stress. The phenomenon is detected for the loading conditions since the irremediable strain at the end of each cycle is increasing from cycle to cycle, as shown in Figure 2.18 (Liang et al., 2015), and this specimen was under different thermal aging conditions. After the strain increment during the first cycle, the increments of the residual axial strain remain almost constant (Messner et al., 2006). The ratcheting strain curve divided into three stages based on creep; primary, secondary, and tertiary. Most researchers worked to model the kinematic hardening to improve the description of ratcheting effects and to include a better modeling of multi-axial behavior (Mattos et al., 2015). The ratcheting behavior of the material studied after asymmetrical strain cycling and under biaxial compression and torsion stress cycling, but it was with different axial stress, so it shows the test control to find the ratcheting. The monotonic tensile test used to find some parameters, but it is not for the basic parameter, it also used to help the design of the biaxial compression and torsion test to know the ratcheting behavior. For the multiaxial loading has five loading paths, where axial stress the equivalent shear stress in that order (Pun et al., 2014). Inoue and co-author used the data to evaluate the performance of various conditions, but they assumed the constitutive modeling properties where already known from calibrating the models against uniaxial test data. The axial-torsional response under ratcheting must be thoroughly characterized.

The Bree diagram is used to regimes. The horizontal is the axial stress normalized by yield stress, and the vertical is the thermal stress normalized by yield stress. The stress regimes are

shown Table 2-14. Here R1 and R2 are elastic and plastic ratcheting; S1 and S2 are elastic and plastic shakedown after first half cycle, P is plastic cyclic, and E is the elastic region. As shown in the figure, the same guidance allows users to predict the threshold between regions based on elastic properties analytically. Engineers use the Bree diagram to predict how critical locations of components will balance combined pressure and thermal stress. And these stresses exceeded the yield strength limit in any region, so this diagram found the ratcheting (Bree, 1967). The Bree diagram to have yet to extended axial-torsional loading. The axial-shear analogy Bree diagram will be developed to characterize the extent of ratcheting under multi-axial behavior and to offer guidance is constitutive model development.

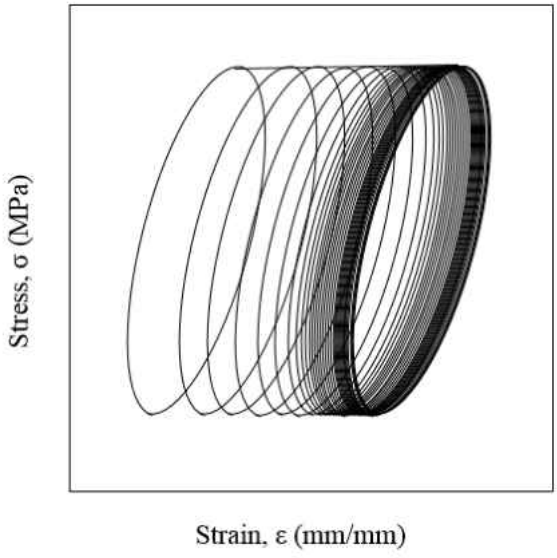

Figure 2.18: The ratcheting stress-strain curve.

Table 2-14: The Bree Diagram Stress Regimes

Stress regime	***Behavior***
R_1	Elastic Ratcheting
R_2	Plastic Ratcheting
S_1	Elastic Shakedown after first half-cycle
S_2	Plastic Shakedown after first half-cycle
P	Plastic Cycling
E	Elastic

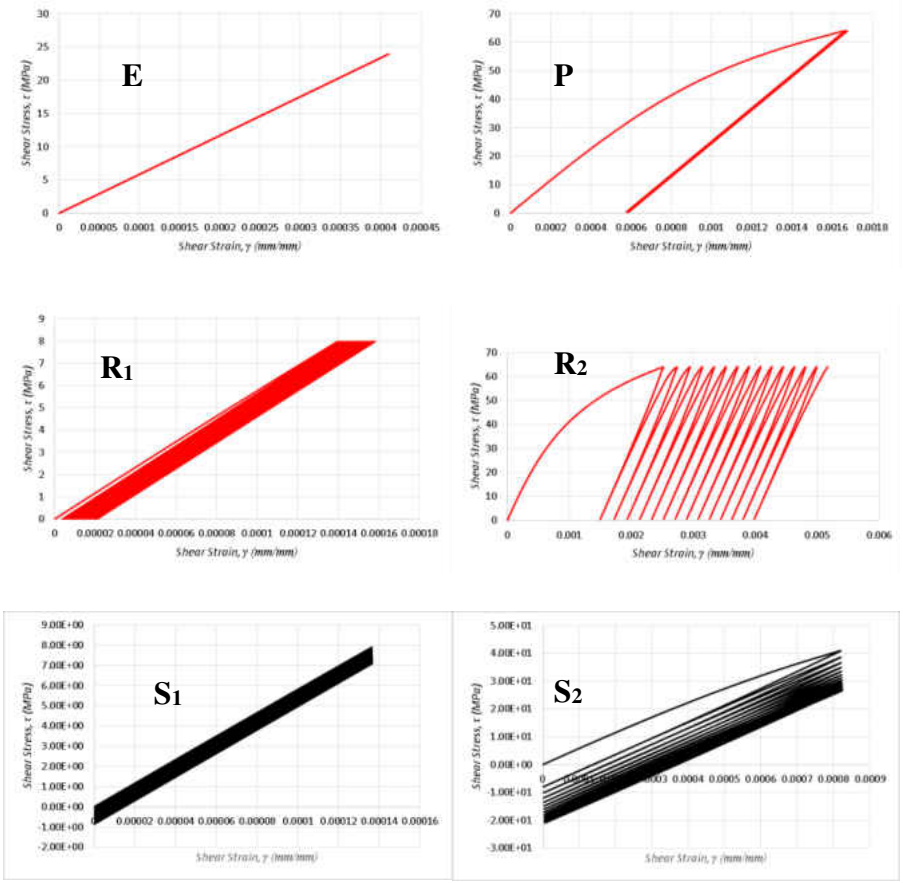

Figure 2.19: Stress-strain curve for different Bree diagram regimes.

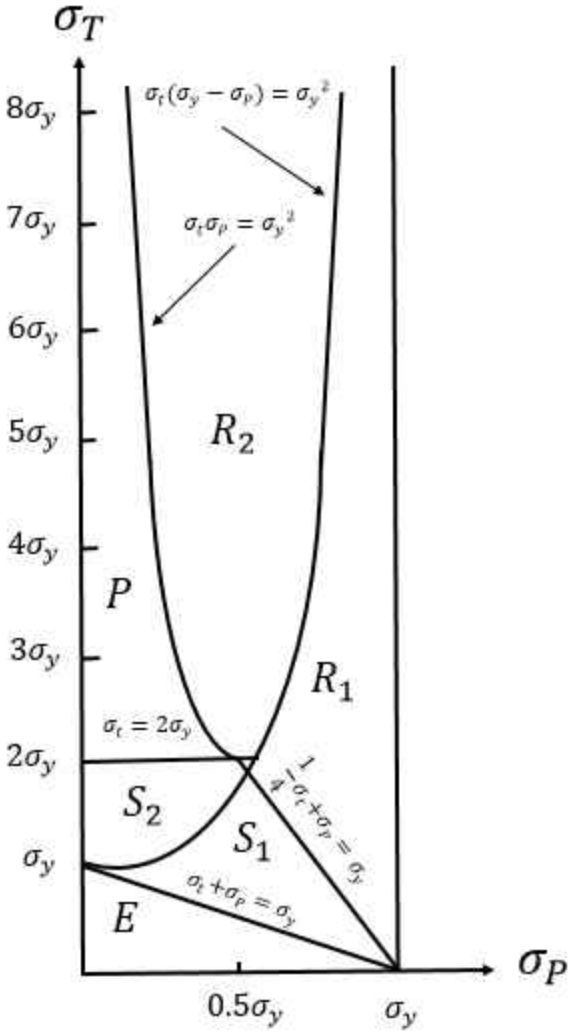

Figure 2.20: Bree diagram regimes (Bree, 1967).

2.6 Multiaxial

In the forms presented in Eq. (2.1) through Eq. (2.6), multiaxial loading is numbering not captured; however, more recent studies have attempted to modify this relation to situations where more than one component of stress is non-zero. Some methods incorporate the components of stress with a yield criterion and facilitate an effective deformation or deformation rate, while others relate tonsorial stress to tonsorial strain. Also, the location of multi-axial stress will affect failure life, stress redistribution, and damage accumulation. The candidate material was studied tested under multi-axial stresses (Barrett et al., 2014). The behavior of the material studied after symmetrical strain cycling and under biaxial compression and torsion stress cycling, but it was with different axial stress and same shear stress amplitudes.

2.6.1 Plasticity

In 1981, Garud calculated the plastic cyclic under the multi-axial load by using a power law (Garud, 1981). The theories and assumptions used the stress-strain relation to apply the general multi-axial load condition. Other assumptions were isotropy, homogeneity, etc. Fatigue process caused by the plastic strain and the shear stress. The fatigue life of a smooth specimen under uniaxial load was better than the specimen under multi-axial load (Garud, 1981). The multi-axial plasticity models are a Ramberg-Osgood model, Massing model, and Chaboche model.

$$\boldsymbol{\varepsilon} = \boldsymbol{\varepsilon_{el}} + \boldsymbol{\varepsilon_{pl}} = \boldsymbol{H}:\boldsymbol{\sigma} + \frac{\alpha}{E_R}\left(\frac{\sigma_e}{\sigma_0}\right)^{n-1}\boldsymbol{M}:\boldsymbol{\sigma}^{dev} \qquad (2.10)$$

2.6.2 Creep of Multiaxial

Creep under uniaxial stress is more widely addressed than under multi-axial stress. On the specimen with the ductile material under the multi-axial load, the strengthening observed with high axial stress across the net section redistributed and decreased below net section stress. The creep under multi-axial loading is not well-known because numerous investigations are limited in uniaxial creep (Huang et al., 2014). Currently, the most important issue in fatigue design is the fatigue behavior under multi-axial load. A complex load condition that comes from the multi-axial load will make the stress-strain analysis complex. When the multi-axial loading is applied to the material element, it exhibits different behaviors, and the probability of fatigue crack will be greater than the uniaxial loading (Li et al., 2006). Also, the Eq. (2.11) show the Norton law in the multi-axial loading condition (Penkalla et al., 1989), i.e.,

$$\dot{\varepsilon}_{ij}^{cr} = B(\sigma_v)^{n-1} S_{ij}{}^{*} \, exp^{\left(\frac{-Q}{RT}\right)} \qquad (2.11)$$

where B and n are the Norton constants, σ_v is the Mises deviatoric stress, $S_{ij}{}^{*}$ is the stress deviator, and $\dot{\varepsilon}_{ij}^{cr}$ the components of the creep strain rate tensor. The main parameters in this section are the Norton contents for multi-axial loading. In this section studied the plasticity and creep behavior for the materials under uniaxial loading, but proposed research will study the materials plasticity and creep behavior under multiaxial loading to reduce the number of experiments. This study will determine the material plasticity and creep behavior for one experiment.

The data were used to establish which constitutive model was optimal (Inoue et al., 1994). When torsion is applied, the result is shear stress. In regards to the torsion problem, the most interesting aspect is the torsion test with the experimental data for metals at a significant strain. Some research studied the two aspects individually; for example, they studied the axial load and then the torsion in separate simulations. One experiment studied the circular rod when one end is free, and the other fixed. The axial load applied to the free end, and the torsion applied to the fixed end. The axially compressive force increased with torsion (Yeganeh and Naghdabadi, 2006). The research used an axial-torsion system with closed loop feedback control. Also, the torque and axial load found from load cell by the control system. Those above the finite element method study the materials behavior under uniaxial loading. Also, the researchers never developed a finite element model capable of simulation axial-torsional fatigue to study the materials behavior under multiaxial loading.

2.7 Dynamic Recrystallization

Normally, during high temperature experiments, there are some metallurgical phenomena for example word hardening (WH), dynamic recovery (DRV), and dynamic recrystallization (DRX). Generally, the occurrence of DRX is grain modification and deformation resistance decrease in practical steel. Based on Dynamic recrystallization the stainless steels have higher deformation resistance than plain carbon steel. DRX is answerable for the high temperature deformation mechanism (Belyakov et al., 1998; Kim and Yoo, 2001).

Dynamic recrystallization (DRX) is different to static recrystallization, and the grains grown, and new grains happens through deformation in high temperature. The stress-strain curve is different when the dynamic recrystallization occurs. Sadden stress are drops as shown in Figure 2.21. This figure shows the stress is jogging during the test indicating DRX. The material used here is 304 stainless steel at 600°C, and the test type is torsion test. The continuous softening is the effect of dynamic recrystallization result, and that effective in the decrease of dynamic force of dynamic recrystallization and comparatively week softening result (Hongna et al., 2017). Also, DRX happens under both axial and torsional loading.

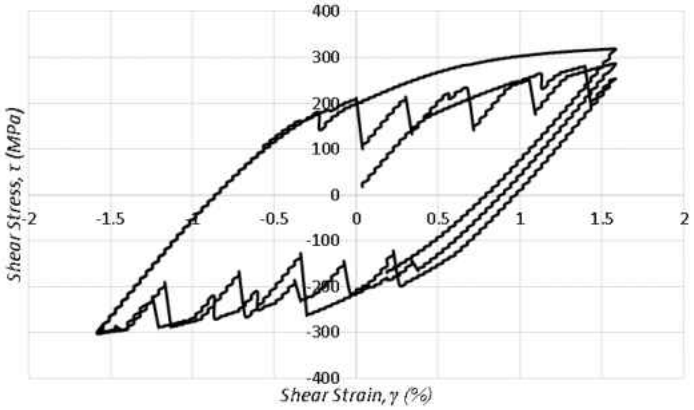

Figure 2.21: Dynamic Recrystallization behavior (present study).

The dynamic recrystallization has two relevant parameters, the first one is the critical strain, and the second parameter is the point of maximum dynamic softening. The dynamic recrystallization parameters derived from strain hardening rate-stress curves. Dynamic recrystallization is one of most important mechanism to microstructure control during the experiment at high temperature. The phenomenon is a major character in changing flow stress and the grain size. This is also a strain-rate phonomenon, and only happens when slow enough. Also, it is a great tool for the controlling mechanical properties during industrial processing. The volume fraction of dynamic recrystallization is shown in the following equation:

$$X_{DRX} = 1 - exp\left[-0.693\left(\frac{\varepsilon-\varepsilon_C}{\varepsilon^*-\varepsilon_C}\right)^2\right] \quad (2.12)$$

where X_{DRX} is the dynamic recrystallization fraction, ε is the true strain, ε^* is the strain for the maximum softening rate during the dynamic recrystallization, and ε_c is the critical strain for the onset of DRX (Shaban and Eghbali, 2010; Tsuji et al., 1997).

$$\varepsilon_C = 0.27\left(\frac{Z}{A}\right)^{0.0115} \quad (2.13)$$

$$\varepsilon^* = 0.61\left(\frac{Z}{A}\right)^{0.007} \quad (2.14)$$

Where Z is the Zener-Hollomon parameter, and A is the experimental constant.

$$Z = \dot{\varepsilon} exp\left[\frac{380}{RT}\right] = A[sinh(0.07\sigma_P)] \qquad (2.15)$$

The dynamic recrystallized is one of the most important topic, and this is occurred on the high temperature. The changing in the grain size is effective on the stress-strain curve. The stress-rate and strain rate phenomenon when the rate slow enough.

CHAPTER 3 EXPERIMENTAL APPROACH

Extensive mechanical experimentation was needed to conduct the research. Specifically, torsional and multiaxial testing used with different temperature environments, strain rate, control types, etc. These experiments will facilitate the acquisition of stress-strain behavior, and to a lesser extent, life. Experiments required the improvement of test techniques, load frame fixturing equipment, and the development of an environmental furnace. The experiments focus on 304 stainless steel; however, other materials like PLA, aluminum, and 17-4PH were tested to help with test preparation. All experiments were carried out in the Mechanical of Material Research Group (MOMRG) at the University of Central Florida (UCF).

3.1 Overview of Experimental Approach and Test Device

The experiments make use an MTS Bionix ElectroMechanical (EM) Torsion Test System. Torsion is mainly used to study the material properties of parts are rotating such as motors, turbines, and drive shafts on engines. In this research, the combination of axial and torsional loading, which are applied to real components, is studied. Based on the limitation of the test device, the axial load here is held constant for experiments. Weights are applied to generate either constant tension or compression. Torsional loading is applied via twist at one end and can be applied cyclically.

Table 3-1: Experiment test matrix of axial-torsional loading

Specimen ID	Temperature °C	Control	Torque N-m	Angle of Twist Degrees	Axial Force N
AT-20°C-01	20	Angle of Twist		±15	200
AT-20°C-02	20	Angle of Twist		15,-7	200
AT-20°C-03	20	Angle of Twist		15,-7	100
AT-20°C-04	20	Angle of Twist		15,-7	0
AT-500°C-01	500	Torque	13,-3		200
AT-500°C-01	500	Torque	14,-3		200
AT-500°C-01	500	Torque	15,-3		200
AT-500°C-01	500	Torque	16,-3		200
AT-500°C-01	500	Torque	17,-3		200
AT-500°C-01	500	Torque	18,-3		200
AT-500°C-01	500	Torque	18.5,-3		200
AT-500°C-01	500	Torque	19,-3		200
AT-500°C-01	500	Torque	19.5,-3		200
AT-600°C-01	600	Angle of Twist		±15	200
AT-600°C-02	600	Angle of Twist		15,-7	200
AT-600°C-03	600	Torque	13,0		200
AT-600°C-04	600	Torque	14,-3		200
AT-600°C-04	600	Torque	15,-3		200
AT-600°C-04	600	Torque	16,-3		200
AT-600°C-04	600	Torque	16.5,-3		200
AT-600°C-05	600	Angle of Twist		±15	200
AT-600°C-05	600	Angle of Twist		±15	200
AT-600°C-05	600	Angle of Twist		±15	200
AT-600°C-05	600	Angle of Twist		±15	200
AT-600°C-05	600	Angle of Twist		±15	200
AT-600°C-06	600	Angle of Twist		±16	0
AT-600°C-06	600	Angle of Twist		±16	0
AT-600°C-06	600	Angle of Twist		±16	0
AT-600°C-06	600	Angle of Twist		±16	200

The specimens are held from two sides by grips. The right grip applies angular rotation, the left side has a fixed position, and axial load is applied via weights, as shown in Figure 3.1. The device reads the torque by using singular load cell which in the left grip. The device specification is shown in Table 3-2. The device is highly configurable In terms of closed loop feedback control, the device can operate under either torque or twist-control. The test software (TestWorks4) allows users to develop sinusoidal, triangular, stepped, or trapezoidal waveforms. The following data are generally recorded at 20 Hz; time, axial force, axial displacement, torque, and angle of a twist.

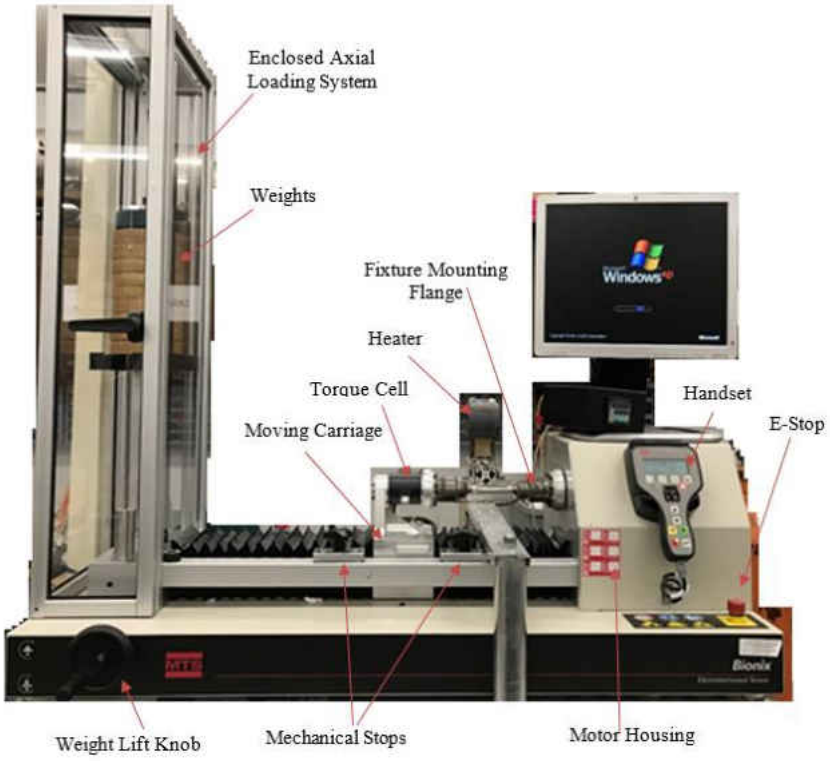

Figure 3.1: MTS Bionix ElectroMechanical (EM) Torsion Test System.

Table 3-2: Bionix EM Torsion Specifications

Specifications	Units	Value
System Torque Rating, Peak at Zero Speed	+/- N-m	45
Test Speed Maximum at 240 V(1)	RPM	175
Specimen Diameter Maximum (2)	mm	200
Test Space Maximum	mm	500
Maximum Rotation	#	26214
Rotation Resolution	arc-sec	7,9
Backlash, Maximum (3)	arc-sec	180
Torsional Stiffness, Frame Only	N-m/ deg	1691
Axial Preload/Axial Preload Maximum	+/- N	220
Frame Length	mm	1185
Frame Depth	mm	460
Frame Height	mm	420
Weight Hanger Height	mm	1130
Frame Weight	kg	68
Torque Cells available	+/- N-m	50, 20, 10, 2 and 0.2
Fixture mounting		M5 Bolt Circle

3.2 Multiaxial Specimen Design

The experiments on the test material behavior must draw out axial-torsional response. Figure 3.2 shows the specimen dimensions derived from other studies (DeMarco et al., 2013) and implemented here. The specimen has three distinct sections, and each region has importance. The first section is the gage section located in the middle of the specimen. The length is 50 mm, and the diameter is 6 mm. Next, the bulge section the grip length on two sides is identical, and the reason from that to keep the gage section in the middle. The last section is the grip section. Normally, this specimen designed for study the material under torsion loading (DeMarco et al., 2013); here it is used to investigate the material under axial-torsional loading. The American Society for Testing and Material International (ASTM) maintains test standards for multiaxial load e.g., E2207-15 (ASTM, 2015). However, the specimens recommended do not allow for compressive loading due to the tubular cross-section. Buckling is avoided due to the solid cross-section.

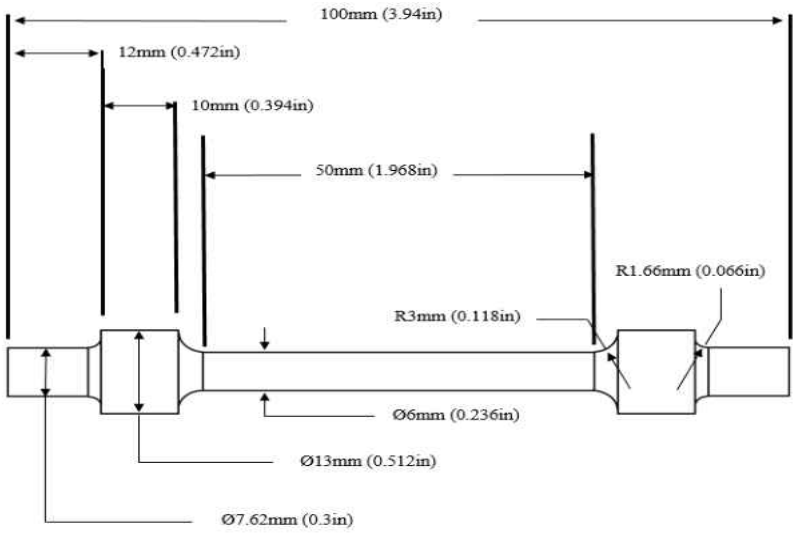

Figure 3.2: Specimen dimensions.

The primary material of the experimental portion of the study is 304 stainless steel. Test compos were machined from solid rods with 280 mm length and 13 mm diameter. Specimen fabrication was carried out by JW Machine Company (Orlando, FL). The polar moment of inertia of cylinder is *J*.

$$J = \frac{\pi d^4}{32} \qquad (3.1)$$

$$\gamma = \frac{\emptyset\, r}{L} \qquad (3.2)$$

$$\tau = \frac{Tr}{J} \qquad (3.3)$$

Where *d* is the gage section diameter, *r* the gage section radius, *L* the gage section length, and τ is the shear stress. The main section in the specimen is the gage section, and the shear stress studied on gage section. Also, the simulation will study the gage section to compare the simulation results with experiment results. Specimens were inspected to ensure the gage section were free of radial scratches which would serve as nucleation sites for fatigue cracks.

Figure 3.3: 304 stainless steel specimen.

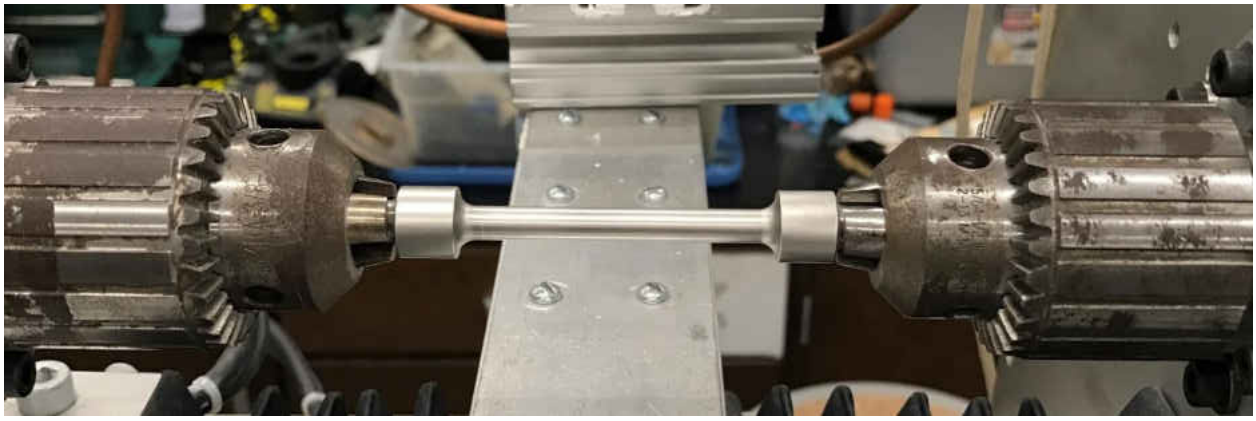

Figure 3.4: Specimen in test device.

3.3 Multiaxial Testing

This research is focused on axial-torsional fatigue loading. Sketches of the cycling are shown in Figure 3.5. The standard uses strain-controlled axial-torsional fatigue. This study used two different control models, and the control models used are stress/load and strain control. Axial load is held constant for all tests as shown in Figure 3.5 a. in one approach shear load is used the torque cyclic as shown in Figure 3.5 b. The next approach uses angular cyclic as shown on Figure 3.5 c. The main reason from using torque control in to assess the ratcheting response of the material when there are mean stresses, while the second control allows the torque of a material to evolve time. Some of material shows hardening/softening upon cycling. Some experiments have different torque and angle of twist ratio, and the temperature and axial force ratio is -1. In one approach,

$$R_T = \frac{T_{min}}{T_{max}} \qquad (3.4)$$

Where the R_T is torque ratio, T_{min} is the minimum torque, and T_{max} is the maximum torque. This is one of the most important in this study, the reason the ration will effect on the ratcheting.

$$\Delta T = T_{max} - T_{min} \quad (3.5)$$

$$R_{\phi} = \frac{\phi_{min}}{\phi_{max}} \quad (3.6)$$

$$\Delta\phi = \phi_{max} - \phi_{min} \quad (3.7)$$

Where T is the torque, R_{ϕ} is the angle of twist, $\Delta\phi$ is the angle of twist range, ϕ_{min} is the minimum angle of twist, and ϕ_{max} is the maximum angle of twist.

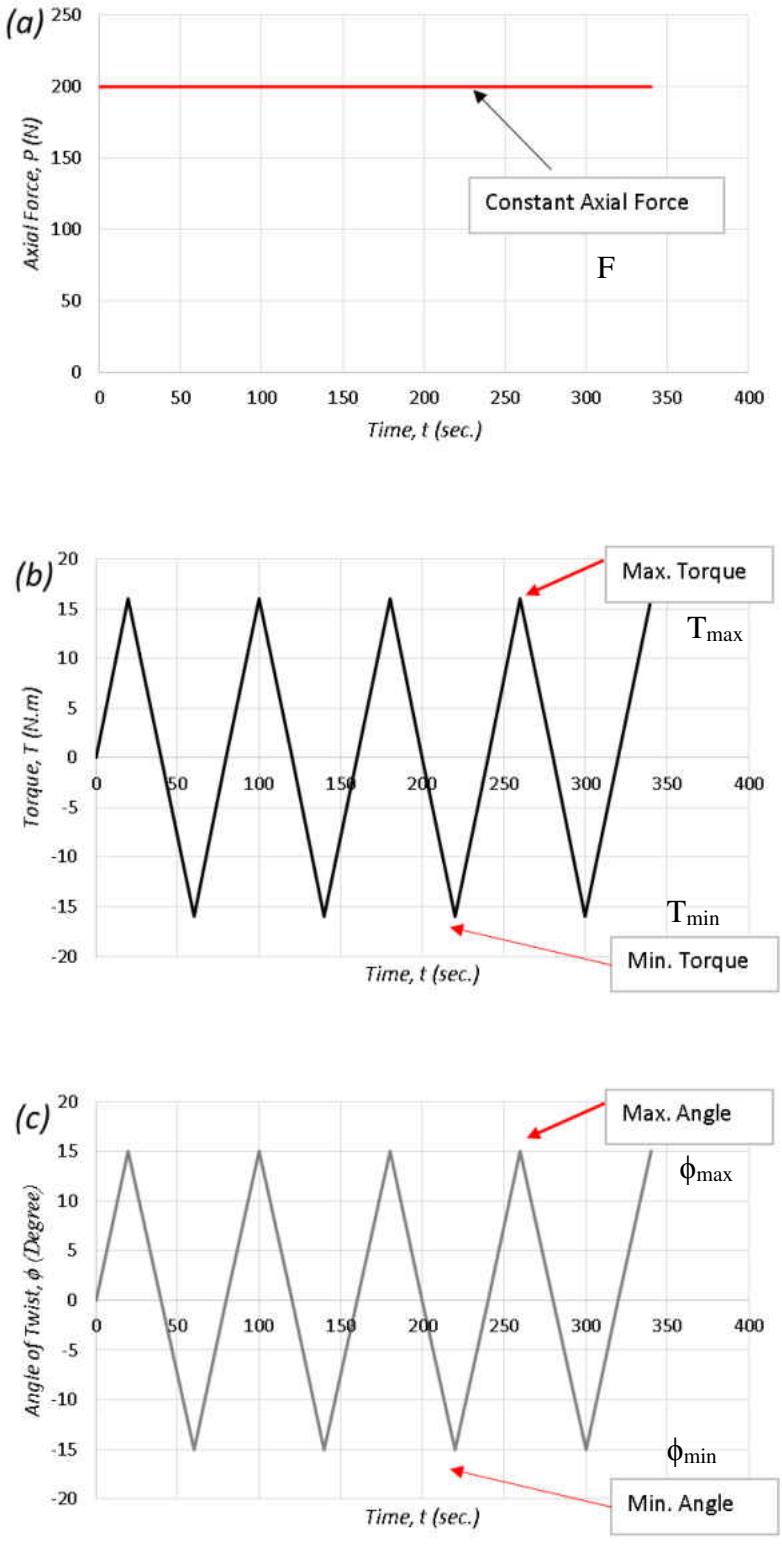

Figure 3.5: Axial-torsional control waveforms: (a) axial, (b) torque-control, and (c) angular-control.

In this research, the axial loading is constant, and shear loading is cyclic. In setting up an experiment, the specimen is fixed on the both sides by using the drill chuck as shown in Figure 3.4. The grip on the lift side rotates/translates. The maximum axial load can applied on the specimens is 200N, and the maximum torque can applied on the specimens are 50N-m. Axial load is applied via dead weights and the maximum axial load is 7 N. The shear load is applied via the angle of twist, and this load is cyclic. Load method in MTS device has applied the torque of angle of twist in the right said of the specimen. The device includes a built in extensometer to measure axial deformation. The output consists of time, axial load, extension, rotation, the angle of twist, and torque.

3.4 High-Temperature Testing

The MTS Bionix ElectroMechanical (EM) Torsion Test Systems are commonly used at room temperature; however, the material behavior at different temperatures is needed. Specifically, steel operates between Room temperature (20°C), and 600°C. A furnace was designed to supply heat to the gage section of sample. The selected furnace is manufactured by Industrial Heater Corp. This band heater is model B74772 as shown in Figure 3.6. The maximum temperature the device can reach 760°C (1400°F). The heater takes three minutes to reach 600°C.

Figure 3.6: Ceramic band heater.

To mount the heater, an aluminum frame was designed and fabricated as shown in Figure 3.7. The frame allows heater availability to be positioned horizontally or vertically to provide more space in specimen area. A cooling system was designed to keep the grips at low as needed. High temperatures could negatively effect the torque cell. Forced air was continuiusly blown on the specimen grips to keep temperature down in the test device as shown in Figure 3.8. this setup was extended from that developed by DeMarco (DeMarco et al., 2013).

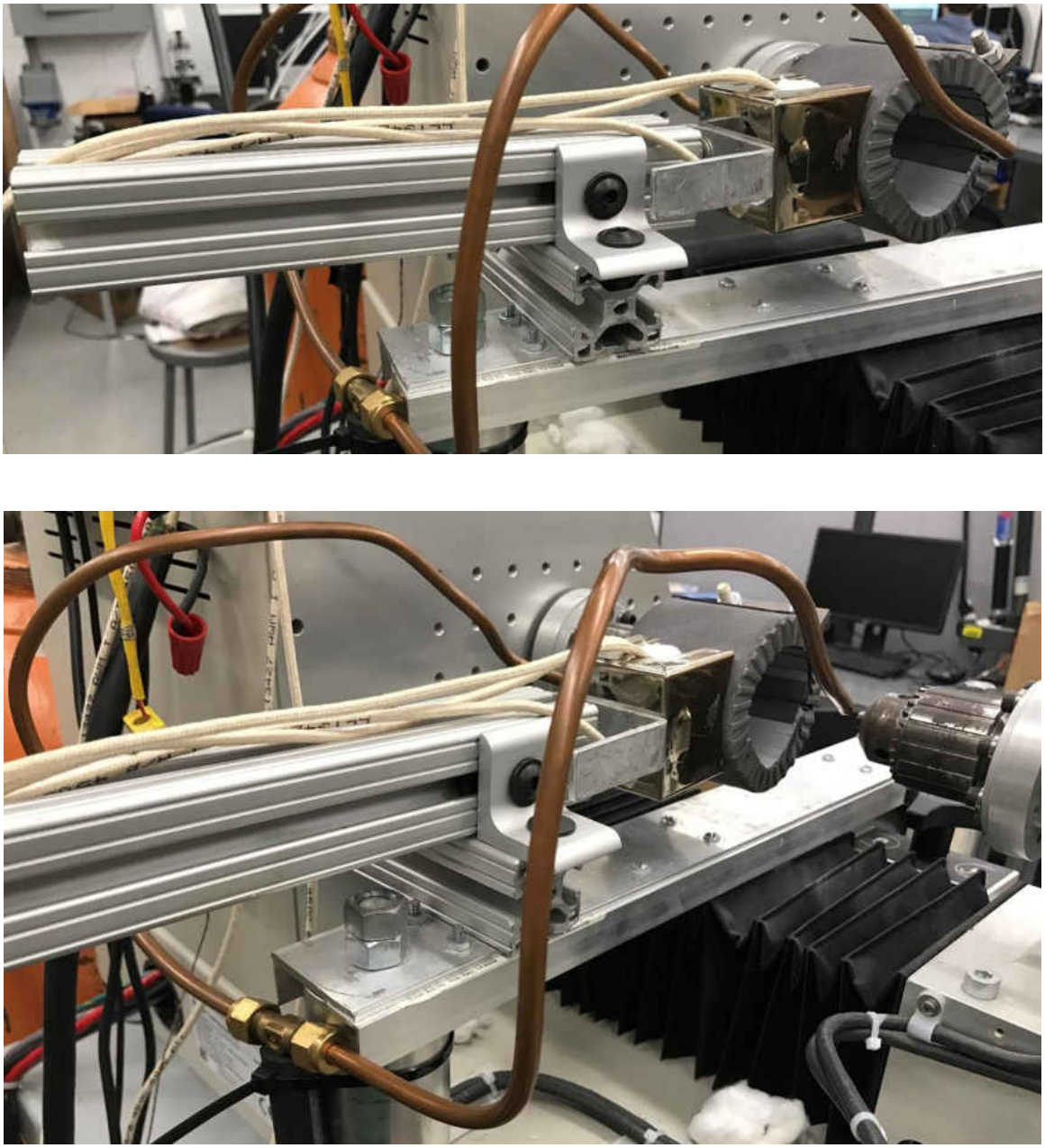

Figure 3.7: The aluminum frame and cooling system.

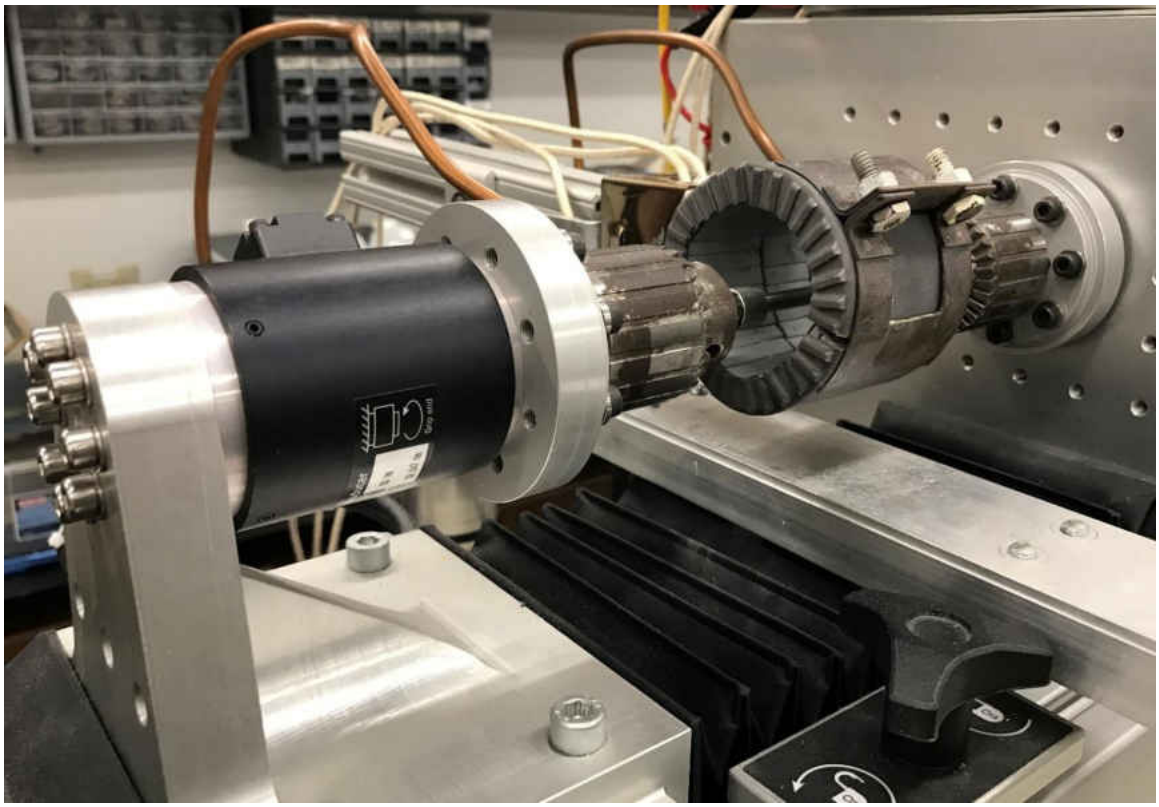

Figure 3.8: Heater in device with the cooling system.

Because the temperature of the room is not constant, and since heat is dynamically lost from the specimen, a closed-loop feedback control system is needed to keep temperature constant. Temperature was controlled by a digital temperature controller (MYPIN T-series). Each experiment was held at constant temperature. From the digital adjuster, the temperature is maintained at a set-point. The specimen is connected with a thermocouple (K-Type) to send a signal to the digital adjuster to know the specimen reach the temperature, within ± 5°C. All components were assembled to MTS the Bionix ElectroMechanical (EM) Torsion Test System, and the furnace allows the study of material behavior under axial-torsional load in high temperature. The diagram of temperature control system is shown in Figure 3.9. The power supply for the furnace was designed at UCF.

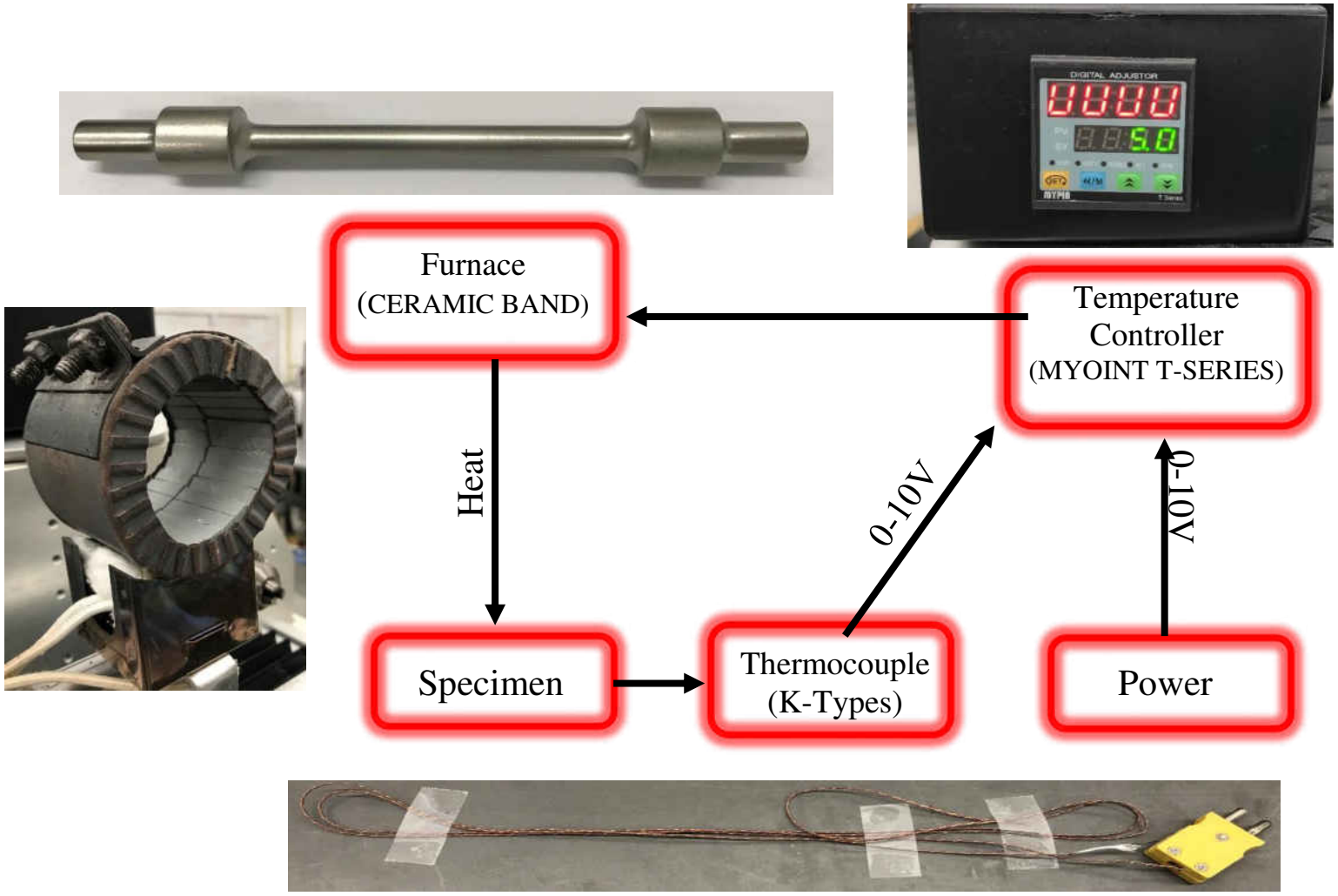

Figure 3.9: Diagram of temperature control system.

3.5 Data Processing

Data generated from the test device (i.e. T and ϕ) must be processed to achieve τ and γ. Under twist control, the device inputs are angle of twist ϕ, and axial force P. under torque control, the inputs are torque and axial load. The output data are axial displacement δ, and torque or twist. The needed data are shear stress τ, axial stress σ, axial strain ε, and shear strain γ. The gage diameter is 6mm and length 50mm. To find the axial stress the axial force is normalized by cross section area. Then, the axial strain needs the axial displacement and gage length, but for

$$\sigma = \frac{P}{A} \qquad (3.8)$$

The shear stress in all cases the torque, gage radius, and polar moment of inertia of cylinder are required.

$$\tau = \frac{Tr}{J} \qquad (3.9)$$

The axial strain needs the axial displacement and gage length.

$$\varepsilon = \frac{\delta}{L} \qquad (3.10)$$

Shear strain needs angle of twist, gage radius, and gage length. Next listed some equations need for data calculation.

$$\gamma = \frac{\phi r}{L} \qquad (3.11)$$

CHAPTER 4 EXPERIMENTAL RESULTS

In this section results from experiments described in Chapter 3 are provided. The device use here is MTS Bionix ElectroMechanical (EM) Torsion Test System. The experiments conducted in this section used two different controls the; angle of twist and torque. The outputs from the device of the experiments were the axial load, torque, axial displacement, and the rotation. Stress and strain were derived from these. Strains were calculated it. The majority of the theses experiments were used to develop the constitutive model parameter from the multiaxial loading instead of uniaxial loading. Also, from this experiments, we found the plasticity and creep parameters for material under multiaxial loading. The test were conducted under different temperatures, i.e., room temperature up to 600°C. The reason for using different temperature was that in room temperature could capture the plasticity of the material under multiaxial loading and the high temperature to captured the creep and plasticity. This section includes the experiment results, and for farther insight into test the reader should confer with in Appendix C.

4.1 Room Temperature

In this section, 304 stainless steel behavior under multiaxial loading at room temperature. The control used here is the angle of twist, and the axial force is a constant load. The axial forces used are 0, 100, 200 N, and the angle of twist rate is 2 degree per second. At room temperature the material does not creep, and at this temperature is used to know the plasticity of 304 stainless steel. The main purpose of the experiment under the room temperature is the determination of elastic modulus and the plasticity properties. Also the difference on the same experiments with different axial force are determined. In Table 4-1 shows the listing of experiments to be conducted as well as the control type.

Table 4-1: Test matrix at room temperature

Test	Temperature	Control	Axial	Shear	Loading Path
AT-20°C-01	20°C	Angle of twist	200 N	15°, -15°	Linear
AT-20°C-02	20°C	Angle of twist	200 N	15°, -7°	Linear
AT-20°C-03	20°C	Angle of twist	100 N	15°, -7°	Linear
AT-20°C-04	20°C	Angle of twist	0 N	15°, -7°	Linear

4.1.1 AT-20°C-01

The first experiment for 304 steel is conducted at room temperature. The axial load applied here is constant using dead weight, and the torsion is cyclic. Test control used the angle of twist, between (15, -15) degrees. The second load is the axial force 200 N, and this load is constant. Also, the angle of twist ratio is -1, and the angle of twist rate was 3 degree per a second. Figure 4.1 shows the torque versus the time for this angle of twist. This test used for 8.7 hours and 1540 cycles, and the maximum torque for this experiment is 17.4 N-m, and the minimum torque is -18.4 N-m. The behavior of 304 stainless steel in this experiment is the torque is increasing in the first ten cycles then it starts to decrease until the last cycle, so that means the material is hardening in the first ten cycles then it softens. After that, the torque history is almost stable. The shear strain is the same for all experiments remaining because the control was using is strain control or angle of twist control.

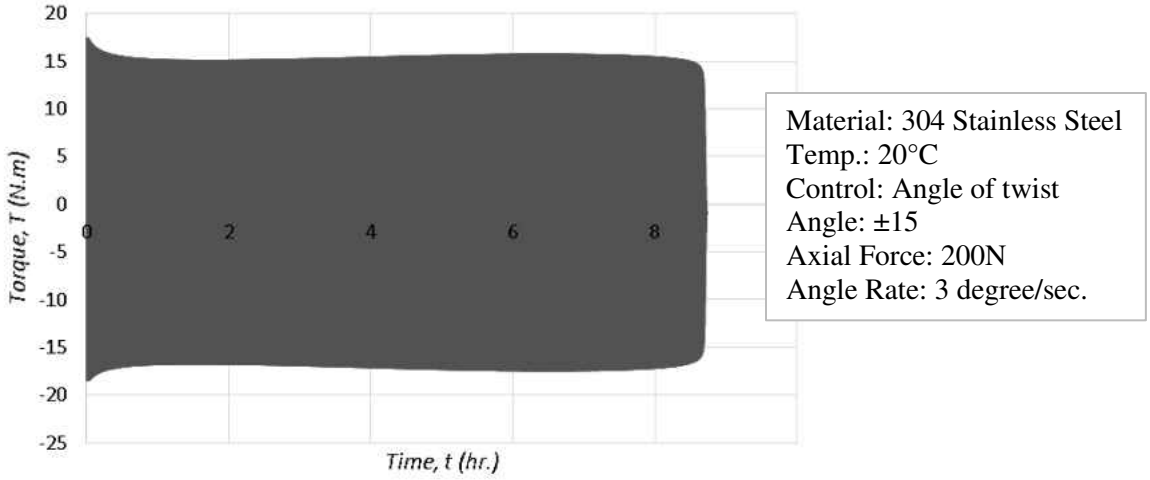

Figure 4.1: The torque history AT-20°C-01.

The torque history in one of the most important response of material. In Figure 4.2 a. shows the first few cycles of shear strain versus shear stress, and when the angle of twist is (15, -15) degrees the hysteresis loop shows the 304 stainless steel behavior when it hardening in the first ten cycles, then it goes to softening. In Figure 4.2 b shows the shear strain versus shear stress curve from the first cycles until failure, and the hysteresis loop shows the 304 stainless steel showing hardening. In the first cycle, the axial force was zero, acquire the elastic response. The output data from the experiment device are time t, axial force P, axial displacement Δ, torque T, and angle of twist ϕ. The calculated data are axial stress σ, axial strain ε, shear stress τ, and shear strain γ. In Figure 4.2 shows the data summary for this experiment, and Appendix A shows all data figures and specimen pictures.

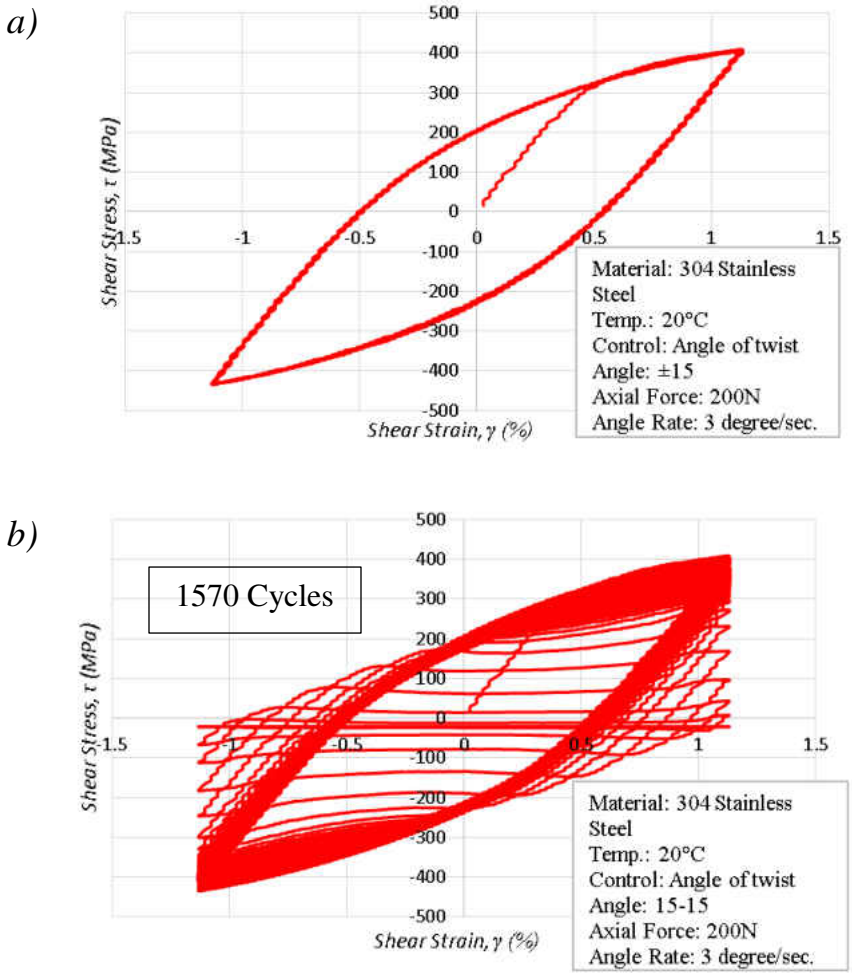

Figure 4.2: Shear strain versus shear stress for AT-20°C-01 a) first few cyclic b) from first cyclic until it broken.

4.1.2 AT-20°C-02

In the second experiment for 304 stainless steel used at room temperature, angle of twist is different. The first experiment occurred under fully reversed loading of the angle of twist; here the angle of twist ratio -0.47 is used with two degree per second. The load applied here is constant axial for by using weight for the device, and the next load is the cyclic torsion. Test control was the angle of twist, (15, -7) degrees. The second load is the axial force 200 N, and this load is

constant. Figure 4.3 shows the angle of twist versus time for this experiment, and this experiment used for 32 hours until the specimen broke. The specimen broke after 5150 cycles, and the torque increased in the first few cycles. It started to soften until stability, and broke after 3404 cycles. The maximum torque for this test is 17 N-m, and the minimum torque is -16 N-m. The behavior of 304 stainless steel in this experiment is hardening in the first few cycles then it starts to softening after that, then the material came stable until it broke. The most important part of this experiment is the elasticity and plasticity behavior for 304 stainless steel at room temperature.

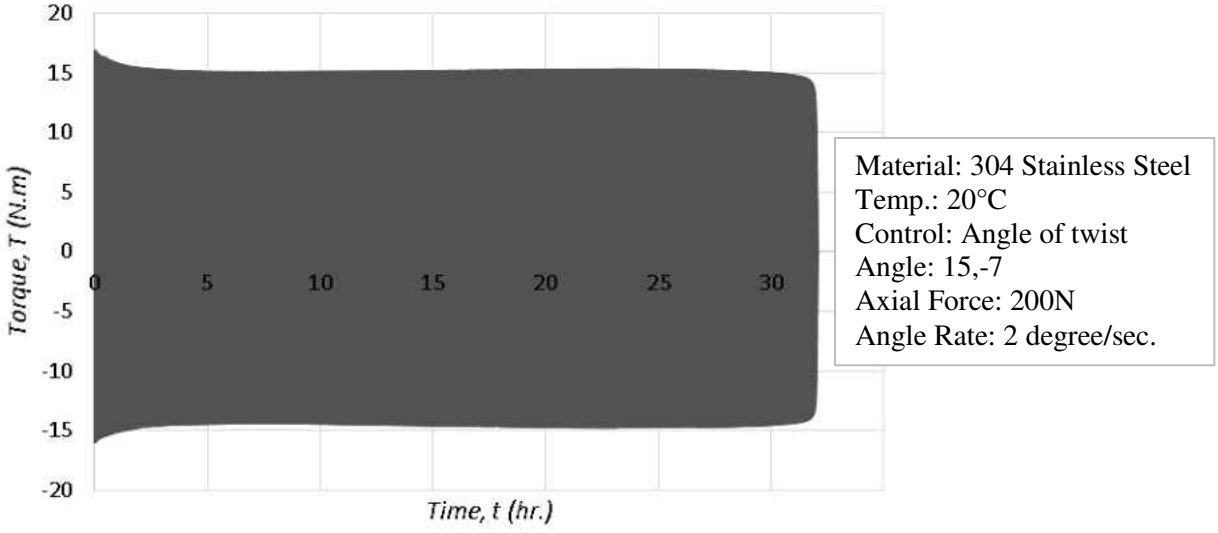

Figure 4.3: Angle of twist versus time for AT-20°C-02.

Studying the hysteresis loop of material response is important. In Figure 4.6 shows the shear strain versus shear stress, and Figure 4.4 a. hysteresis loop for the 304 stainless steel at room temperature, and this hysteresis loop for the first cycle until it came stable. The 304 stainless steel exhibits hardening behavior in the first few cycles followed by softening. Figure 4.4 b. shows the material behavior from the first cycle until fracture. The axial force does not have clear effect in this type of experiment. By focusing on the hysteresis loop, it shows the shear stress decreased very fast, and that means the crack started on the specimen. The output data from the experiment device are time t, axial force P, axial displacement Δ, torque T, and angle of twist ϕ. So, the calculation data are axial stress σ, axial strain ε, shear stress τ, and shear strain γ. In Figure 4.6 shows the shear strain is same in all cycle, and that happen because it calculated from the angle of twist. Table 4-2 shows the data summary for this experiment, and appendix A shows all data figures and specimen photograph.

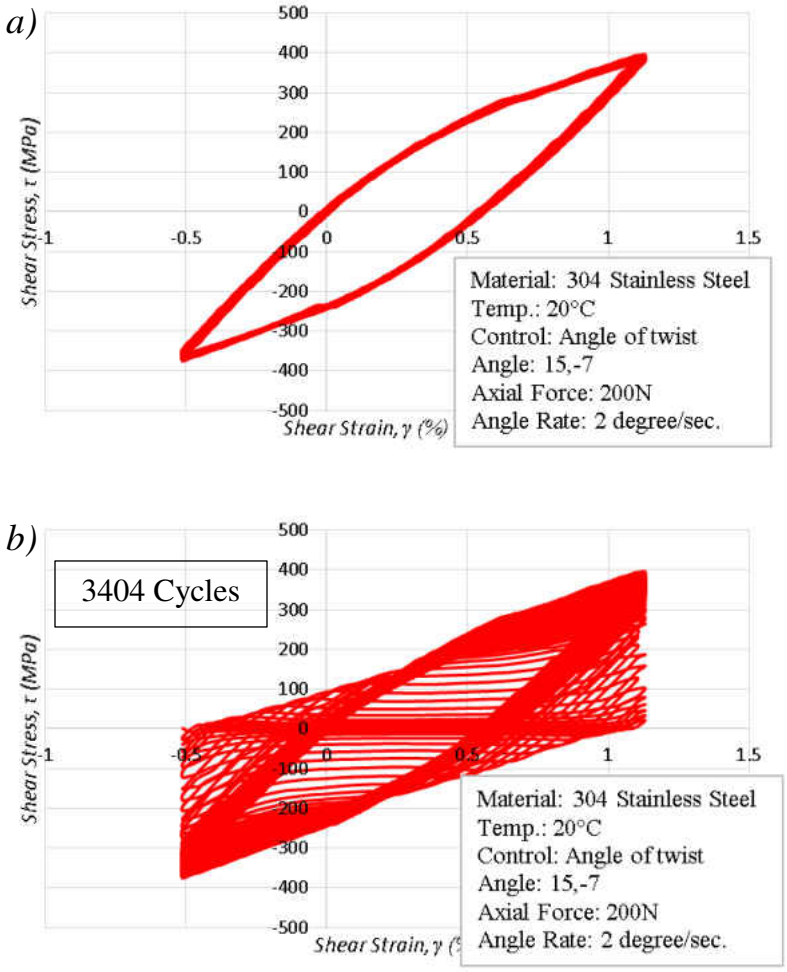

Figure 4.4: Shear strain versus shear stress for AT-20°C-02 a) first few cycles remaining loops.

4.1.3 AT-20°C-03

The next experiment is conducted in a similar mirror as AT-20°C-02. Figure 4.5 shows the torque history. The torque is increasing in the first six cycles until it reaches 17 N-m and -17.8 N-m. This specimen used 3662 cycles until it rapture. The most important part of this experiment is the elasticity and plasticity behavior for 304 stainless steel at room temperature. Of the shear strain is the same for all cyclic because the control was using is strain control or angle of twist control.

In Figure 4.5 shows that the material stability occurs after five hours, and it came stable for 16 hours then the crack is started. The first cycle was without axial force and the reason from that to find the elastic shear modulus at room temperature. In Figure 4.6 a. shows the shear strain versus shear stress, and the left hysteresis loop shows the 304 stainless steel behavior when it is hardening in the first six cycles. Figure 4.6 b. shows the material behavior from the first cycle until it is broken. Figure 4.6 shows the shear strain is same in all cycle, and that happen because it calculated from the angle of twist. Table 4-2 shows the data summary for this experiment, and Appendix A shows all data figures and specimen picture after it is broken.

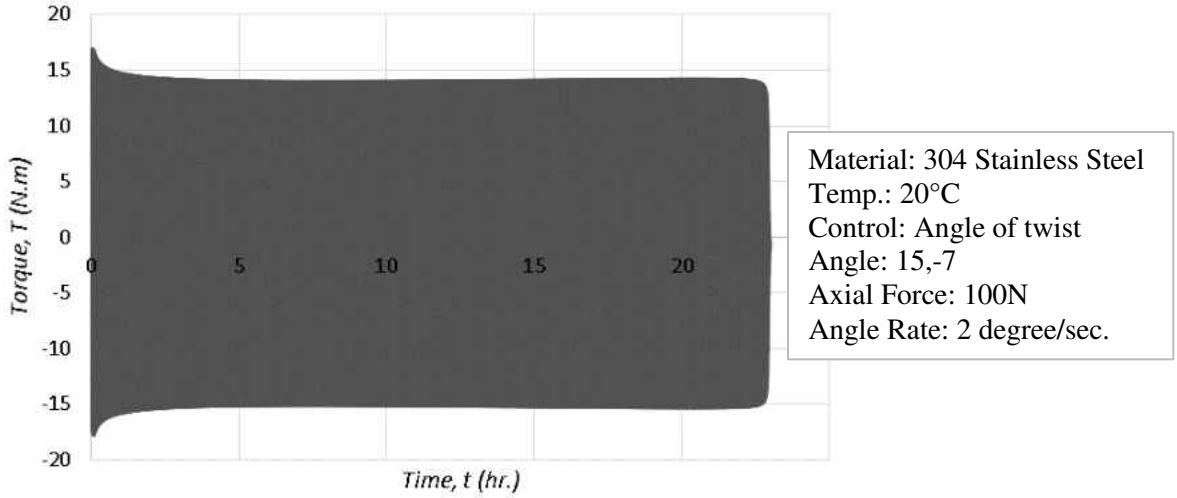

Figure 4.5: The torque versus time for AT-20°C-03.

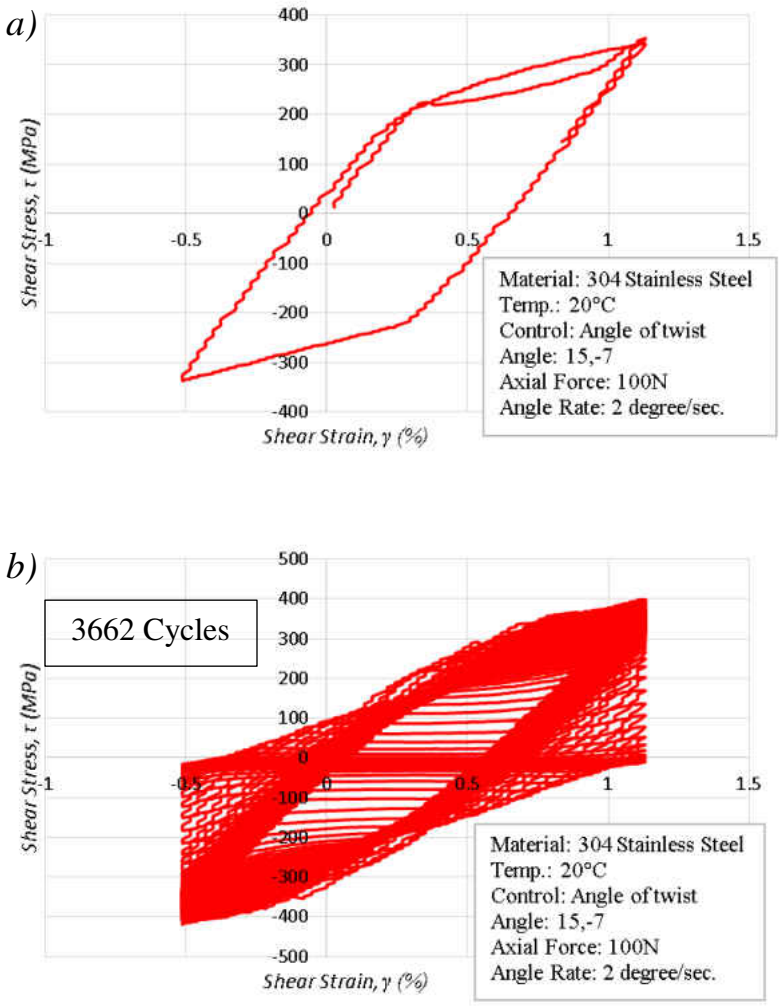

Figure 4.6: Shear strain versus shear stress for AT-20°C-03 a) first few cycles and b) first cycles until the last cycle.

4.1.4 AT-20°C-04

This experiment is the same of the AT-03, but the difference between these two is axial loading, so AT-04 has no axial loading just cyclic torque between (15,-7) degree. Also, the angle of twist ratio is -0.47, and the angle of twist rate was 3 degree per a second. Figure 4.7 shows the AT-04 torque history is nearly identical to the other. The maximum torque for this test is 17.55 N-m, and the minimum torque is 17.81 N-m. The shear strain versus shear stress shown in Figure 4.8 a., and the hysteresis loop shows the 304 stainless steel behavior when for the first seven cycles. Figure 4.8 b. Table 4-2 shows the data summary for this experiment, and Appendix A shows all data figures and specimen picture after it is broken.

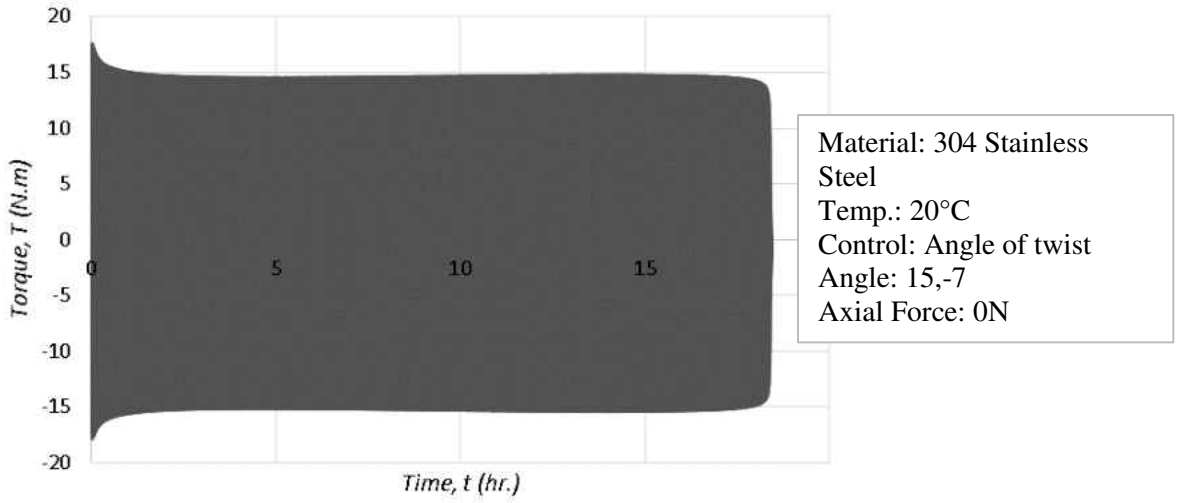

Figure 4.7: The torque versus time for AT-20°C-04.

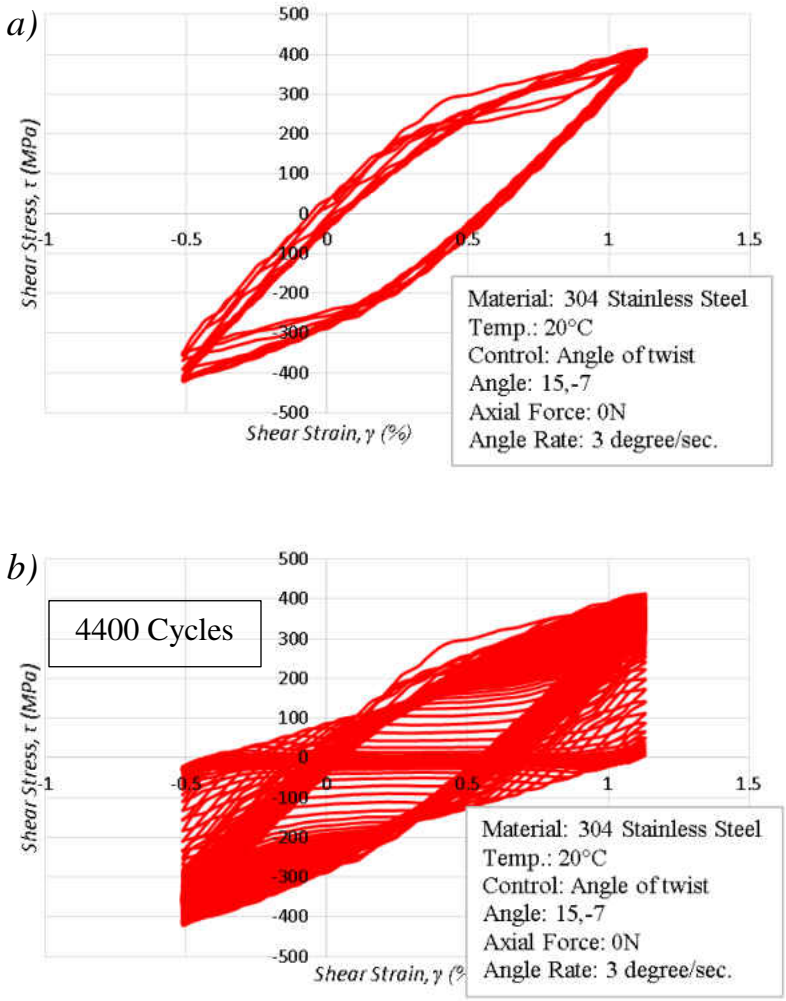

Figure 4.8: Shear strain versus shear stress for AT-20°C-04 a) first few cycle and b) the first cycle until it breaks.

4.1.5 Room Temperature Results Summary

The results are summarized in this section. Figure 4.9 shows the peak and valley torque history. All of these experiments shows the softening is almost same with different angle of twist. The first one is AT-20°C-01, the angle of twist is (15, -15) degree has the less time until it broken, and it broken after almost 8 hours. The reason from this time because the angle of twist range is 30 degree. This experiment has 1570 cycles to broken, and the maximum torque is 17.4 N-m, and the minimum torque in this experiment is -18.4 N-m. Second experiment is AT-20°C-02, and the angle of twist is (15, -7) degree with 200 N axial force. The experiment time until the specimen is broken is 32 hours, and it has 5150 cycle until it broken. The maximum torque is 16.8 N-m, and the minimum torque in this experiment is -17 N-m. AT-20°C-03 is the same of AT-20°C-02, but the different the axial force here is 100 N, so it takes 23 hours until it broken. The number of cycles here is 3630 cycles, and the maximum torque is 17 N-m, and the minimum torque in this experiment is -17.8 N-m. AT-20°C-04 is the last experiment at room temperature with 0 N axial force, so this experiment has 4400 cycles, and it takes 18.5 hours until it broken. The reason of less time because the angle of twit rate is 3 degree per second. The maximum torque here is 17.6 N-m and the minimum torque is -17.8 N-m, and the time until it broken is shown in Table 4-2. What shows in Figure 4.9 the life is increasing with decrease the axial load at room temperature with same shear strain range. Next, with same axial force and different shear strain rage the life is decrease with increasing the shear strain range as shown in this figure. By focusing in the specimen fracture for all experiments at room temperature has same model, and also the fracture occur near to torque applied side for all experiments.

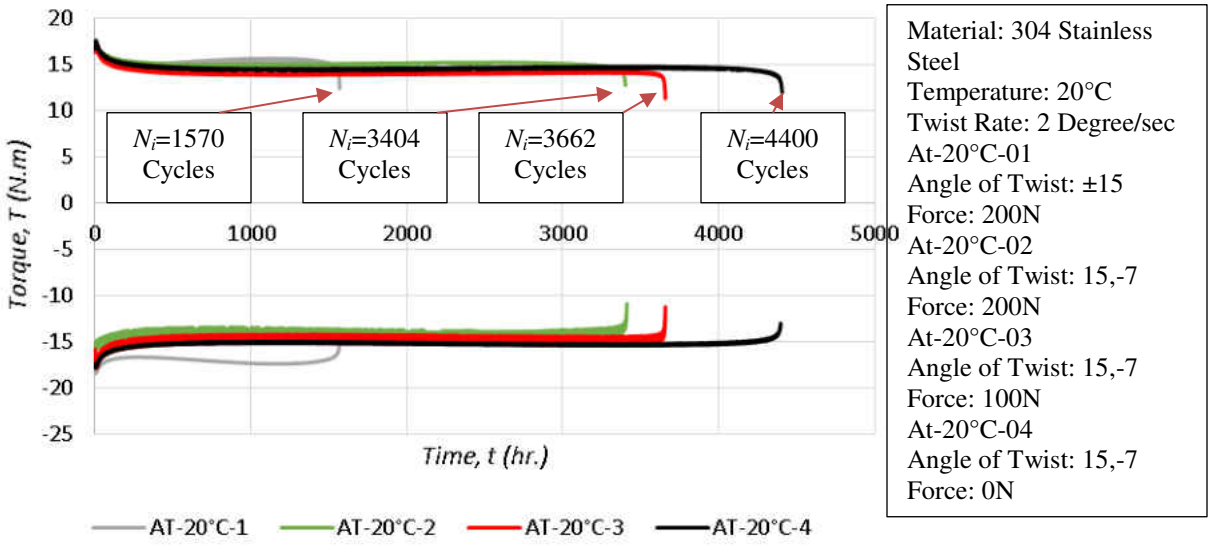

Figure 4.9: Maximum and minimum Torque for different experiments at room temperature.

Next, the second point from the summary results for different experiments under the room temperature. Figure 4.10 shows that the slope of the elastic modulus of all different experiments under room temperature are almost same. The shear strain of all different experiments are same. The different shear strain range from these experiments because the different angle of twist and axial load. The maximum torque has small different between the different experiment. From Figure 4.10 shows the elasticity and plasticity behavior for our material. The elastic properties will find from the slope of the elastic range, and from this figure the all elastic range of all experiments are almost same. Also, for plastic properties are almost same curve, so the plasticity constant will be same in all different experiments. Table 4-2 shows the result summary for all different experiments under room temperature. What shows in this table are maximum and minimum torque, time until it broken, and number of cycles, axial force, and control type.

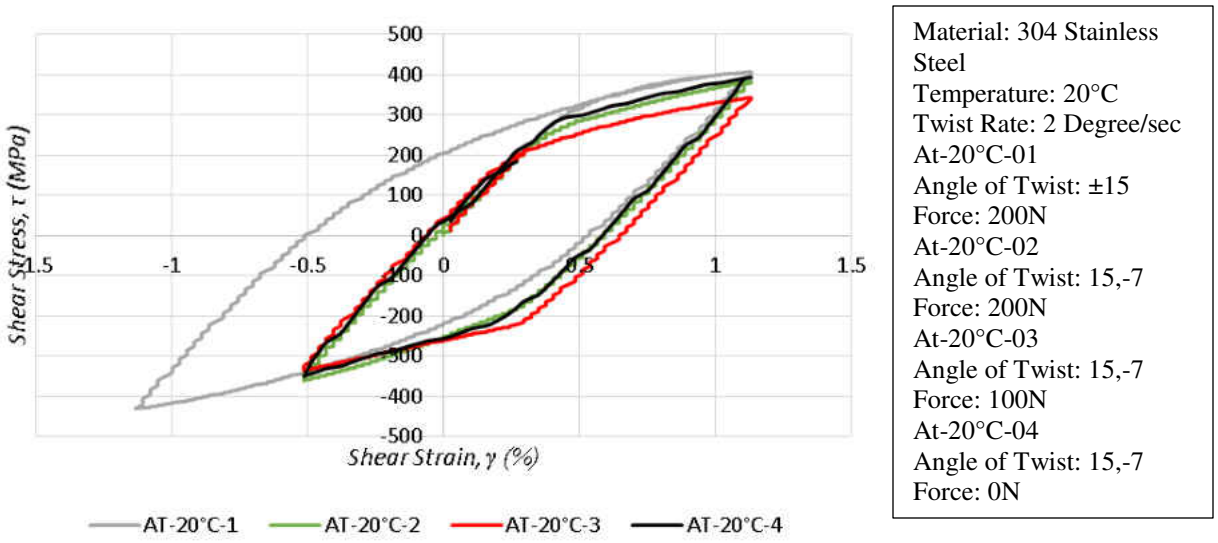

Figure 4.10: First Cyclic for different experiments under room temperature.

Table 4-2: Experiments summary results at room temperature

Specimen ID	Temperature °C	Control	Max. Torque, T_{max} N-m	Min. Torque, T_{min} N-m	Axial Force, F N	Number of Cycles Cycle	Time Hr.
AT-20°C-01	20	Angle of Twist	17.4	-18.4	200	1570	8.7
AT-20°C-02	20	Angle of Twist	17	-16.8	200	5150	32
AT-20°C-03	20	Angle of Twist	17	-17.8	100	3680	23
AT-20°C-04	20	Angle of Twist	17.6	-17.81	0	4400	18.5

4.2 500°C Temperature

In this experiment used the specimen under 500°C for 304 stainless steel. This one is important to get the material properties under 500°C. Studying the material in high temperature is important to find the creep behavior of the material. In high temperature, the materials have the creep which is one part of the study, and ratcheting is the other part occurred at high temperature. The material tested for 500°C is the 304 stainless steel under axial-torsional loading. In this particular section used different control, so the first one is the angle of twist control, and the second one is the torque control. Axial loading was constant for all different experiments, but each one has different axial force value, such as, 0, 100, 200 N. Moreover, the rates were different for each one, and the experiments have an angle of twist rate and torque rate. One of the most important in high temperature the experiment rate should be too low to capture the creep and ratcheting. In high temperature, the material has elasticity, plasticity, and creep, and this research focusing on these properties. The study did more experiment in high temperature to catch material properties.

4.2.1 AT-500°C-01

In this experiment used differently than the other experiments, so the control used here is torque control at 500°C for 304 stainless steel. The different way used here is run the experiment with various maximum torque with a same minimum torque which is zero. The maximum torques are 13 N-m, 14 N-m, 15 N-m, 16 N-m, 17 N-m, 18 N-m, 19 N-m, and 19.5 N-m. The angle of twist rate for this experiment is 0.1 degree per second. First one, the maximum torque is 13 N-m run for 8.6 hours, and it has 1238 cycles. The angle of twist versus time shows in Figure 4.11 a. Next, the maximum torque is 14 N-m run for 5.3 hours, and it has 725 cycles. The angle of twist versus time shows in Figure 4.11 b. The maximum torque is 15 N-m run for 6.7 hours, and it has

836 cycles. The angle of twist versus time shows in Figure 4.11 c. The maximum torque is 16 N-m run for 5.3 hours, and it has 737 cycles. The angle of twist versus time shows in Figure 4.11 d. Moreover, the maximum torque is 17 N-m run for 5.1 hours, and it has 547 cycles. The angle of twist versus time shows in Figure 4.11 e. The maximum torque is 18 N-m run for 16.4 hours, and it has 1603 cycles. The angle of twist versus time shows in Figure 4.11 f. The maximum torque is 18.5 N-m run for 17 hours, and it has 1598 cycles. The angle of twist versus time shows in Figure 4.11 g. The maximum torque is 19 N-m run for 11 hours, and it has 915 cycles. The angle of twist versus time shows in Figure 4.11 h, and the last test was with maximum torque is 19.5 N-m run for 12.5 hours, and it has 1000 cycles. The angle of twist versus time shows in Figure 4.11 i, and the minimum torque is the same for all of them. In this experiment is focusing on the behavior of angle of twist versus time for this material in high temperature, so in the first six torques, the angle of twist is almost constant. In the last three torques, the angle of twist came as a constant then it jumps to high value, and after then it constantly came then it jumps again, this behavior repeated. Axial force in this experiment is the highest force can apply on the device which is 200 N. The main objective for used the torque control to find if the material has ratcheting or no, and as mentioned before the main part of the specimen is the gage region. The thermocouple is connected to gage section to make sure it reaches the high temperature, but for the other sections is less than 500°C. The most important part of this experiment is the elasticity, plasticity, creep, and ratcheting behavior for 304 stainless steel at 600°C.

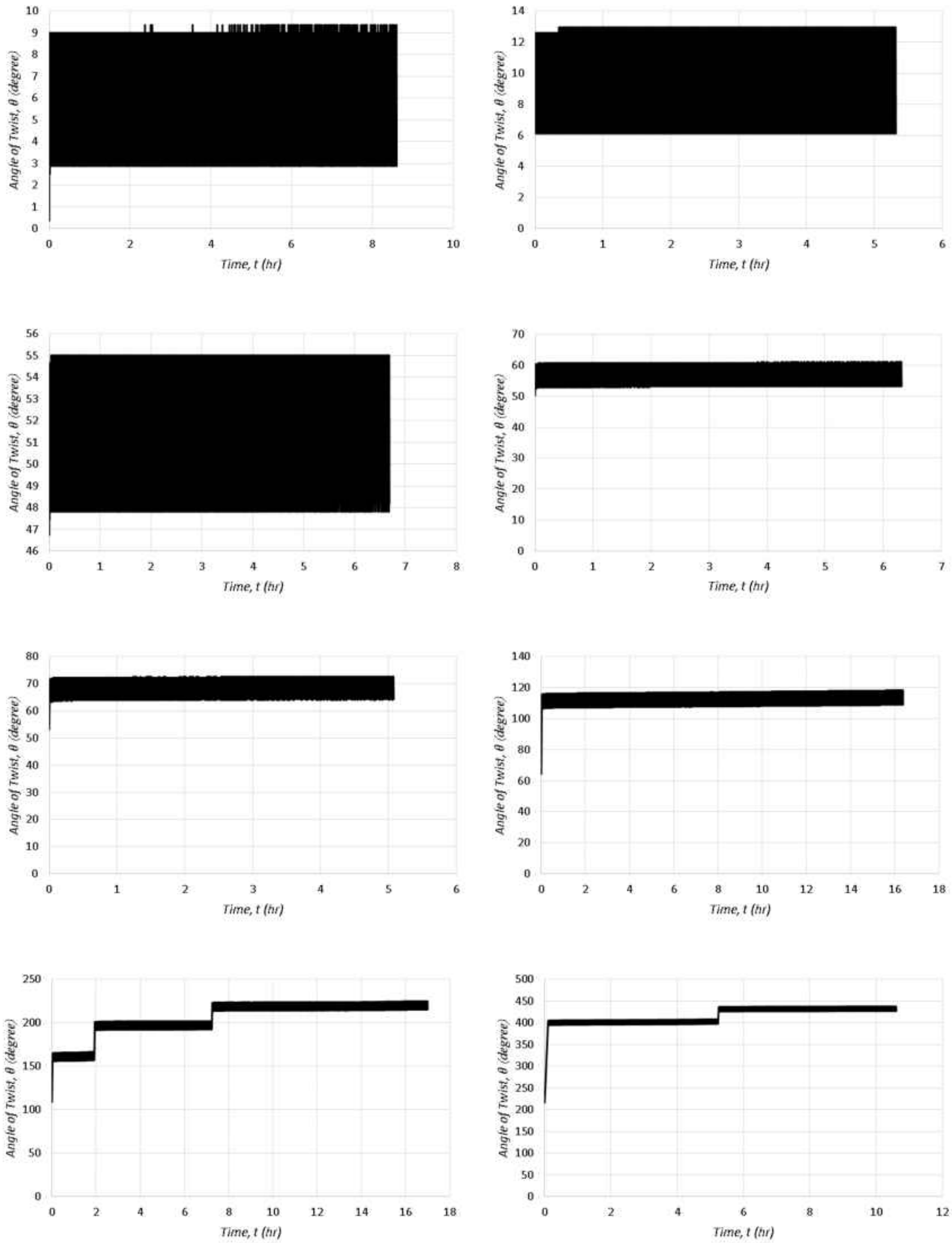
Angle of Twist, θ (degree)
Time, t (hr)

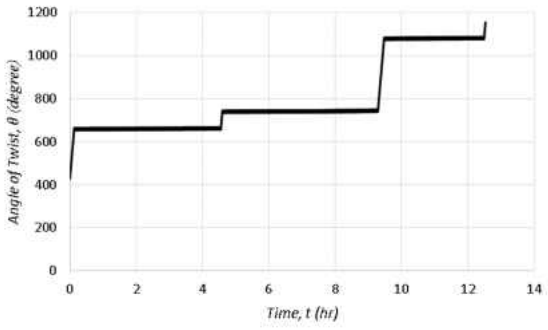

Figure 4.11: Angle of twist versus time for AT-500°C-01 a) torque (13,0), b) torque (14,0), c) torque (15,0), d) torque (16, 0), e) torque (17, 0), f) torque (18, 0), g) torque (18.5, 0), h) torque (19, 0), and i) torque (19.5, 0).

After that, the researchers studied the shear strain versus shear stress for AT-500°C-01 as shown in Figure 4.12. As mentioned before the first cycle did without axial force, and the reason from that to capture the 304 stainless steel material shear modulus at 500°C. The hysteresis loop is almost stable for all cycles, and that happens when the maximum torque is 13 N-m to 18 N-m as shown in Figure 4.12. In this experiment the shear strain increases from cycle to other cycles as shown in the figure, and there is no jump in shear strain. In the last three maximum torques which are 18.5, 19, and 19.5 N-m the first cycle the angle to twist jumps again to reach the torque value, then there are few cycles and jumped again. The jumped in the angle of twist came from the ratcheting and creep. In Table 4-3 shows the data summary for this experiment, and appendix A shows all data figures and specimen pictures.

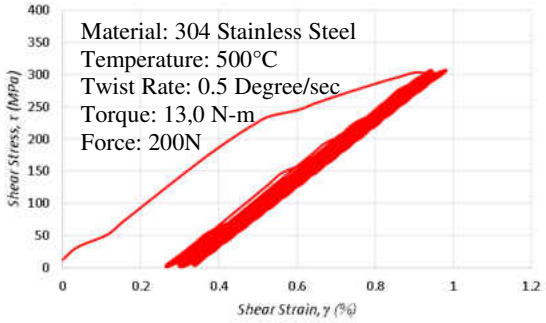

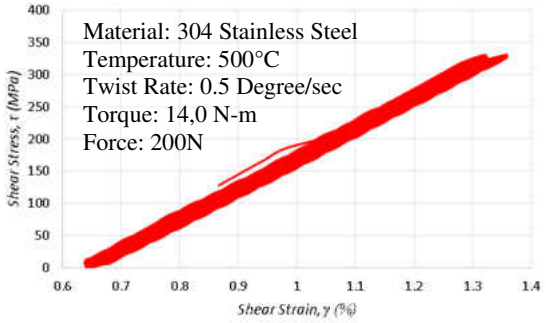

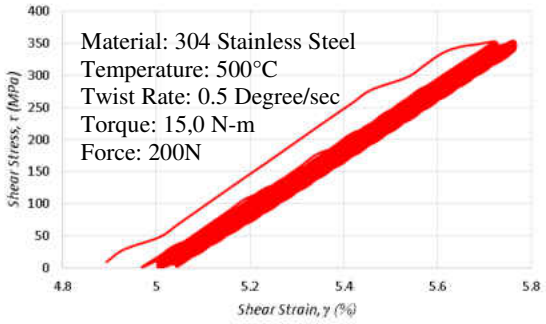

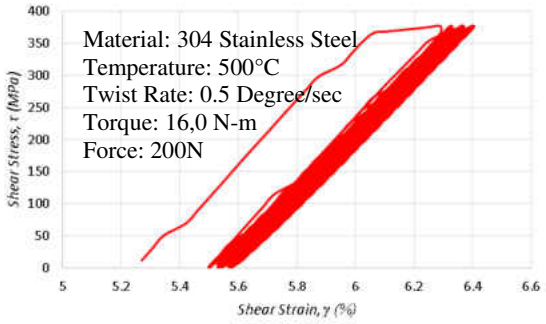

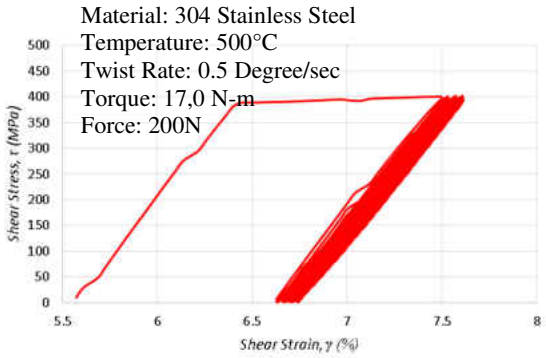

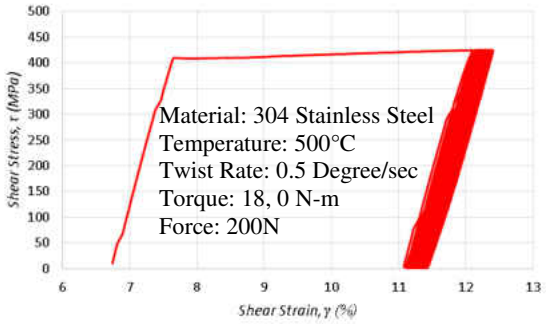

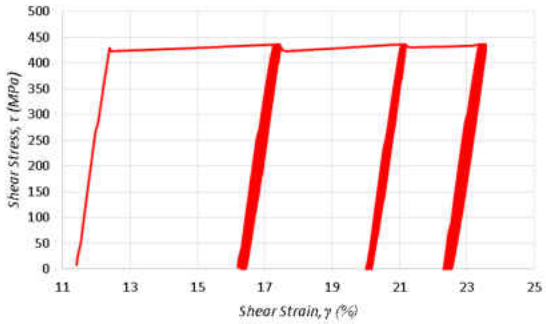

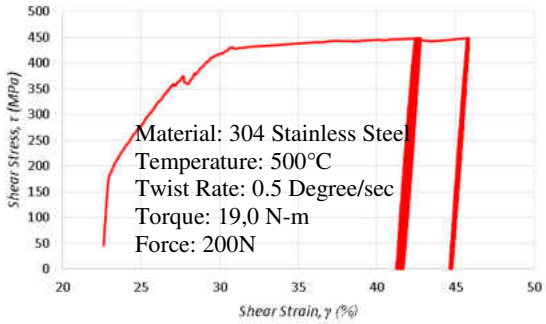

Material: 304 Stainless Steel
Temperature: 500°C
Twist Rate: 0.5 Degree/sec
Torque: 18.5,0 N-m
Force: 200N

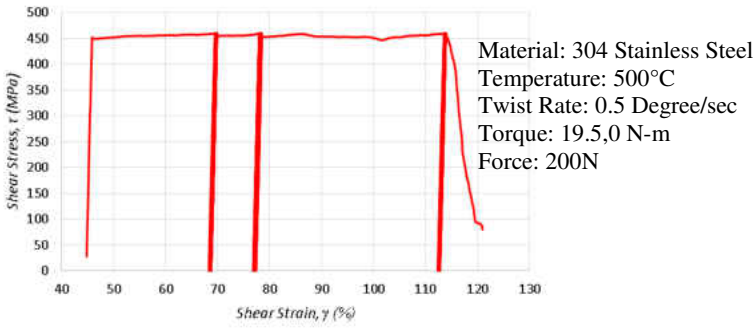

Figure 4.12: Shear stress versus shear strain for AT-500°C-01 a) torque (13,0), b) torque (14,0), c) torque (15,0), d) torque (16, 0), e) torque (16, 0), f) torque (17, 0), g) torque (18, 0), h) torque (19, 0), and i) torque (19.5, 0).

Table 4-3: AT-500°C-01 summary

Specimen ID	Temperature °C	Number of cycles cycles	Max. Torque, T_{max} N-m	Min. Torque, T_{min} N-m	Axial Force, F	Time hr.
AT-500°C-01	500	1238	13	-3	200	8.6
AT-500°C-01	500	725	14	-3	200	5.3
AT-500°C-01	500	836	15	-3	200	6.7
AT-500°C-01	500	737	16	-3	200	6.3
AT-500°C-01	500	547	17	-3	200	5.1
AT-500°C-01	500	1603	18	-3	200	16.4
AT-500°C-01	500	1598	18.5	-3	200	17
AT-500°C-01	500	915	19	-3	200	1710.6
AT-500°C-01	500	1000	19.5	-3	200	3.512.5

4.3 600°C Temperature

This part of the experiment is one of the most important parts of this study. In high temperature, materials exhibit creep which causes ratcheting. The material is tested at 600°C under axial-torsional loading. In this particular section used different control, so the first one is the angle of twist control, and the second one is the torque control. Axial loading was constant for all different experiments, but each one has different axial force value, such as, 0, 100, 200 N. Moreover, the rates were different for each one, and the experiments have an angle of twist rate and torque rate. One of the most important in high temperature the experiment rate should be too low to capture the creep, and creep causes ratcheting, so it capture creep if there is ratcheting exhibited. A variety of conditions are used to draw out elasticity, plasticity, and creep. In Table 4-4 shows the listing of experiments to be conducted, and it shows the control use for these experiments.

Table 4-4: Experiments Test types and the test control at 600°C

Test	Temperature	Control	Axial	Shear	Loading Path
AT-600°C-01	600°C	Angle of twist	200 N	15°, -15°	Linear
AT-600°C-02	600°C	Angle of twist	200 N	15°, -7°	Linear
AT-600°C-03	600°C	Torque	200 N	13, 0 N	Linear
AT-600°C-04	600°C	Torque	200 N	14,-3 N	Linear
AT-600°C-04	600°C	Torque	200 N	15, -3 N	Linear
AT-600°C-04	600°C	Torque	200 N	16, -3 N	Linear
AT-600°C-04	600°C	Torque	200 N	16.5,-3 N	Linear
AT-600°C-05	600°C	Angle of twist	200 N	16°, -16°	Linear
AT-600°C-05	600°C	Angle of twist	200 N	16°, -16°	Linear
AT-600°C-05	600°C	Angle of twist	200 N	16°, -16°	Linear
AT-600°C-05	600°C	Angle of twist	200 N	16°, -16°	Linear
AT-600°C-05	600°C	Angle of twist	200 N	16°, -16°	Linear

4.3.1 AT-600°C-01

The theories are using here is assumed the mechanical behavior is uniform throughout the gage section. The thermocouple is connected to gage section to make sure it reaches the high temperature, but for the other sections is less than 600°C, and DeMarco showed that this setup casues the temperature to be slightly lower at the ends by 10°C or less (DeMarco et al., 2013). Axial force in this experiment is the highest force can applied on the device which is 200 N. Also, the control used here is angle of twist control, so that means the shear strain is the same for all

cycles. The angle of twist goes to 15 degrees then it goes to -15 degree. The angle of twist ratio is -1, and the angle of twist rate is 0.55 degree per second. In Figure 4.13 shows the torque versus time, and from this figure, it shows that the material is hardening then it softening until it is broken. The hardening starts from the first cycle until the fourth cycle then it started softening until it is broken. The maximum torque for this test is 13.52 N-m, and the minimum torque is -13.1 N-m, but in the midlife, the material has stable torque, so when the material in stability the maximum torque is 11.05 N-m, and the minimum torque is -11.05 N-m. This specimen used for 650 cycles until it is broken. The most important part of this experiment is the elasticity, plasticity, creep, and ratcheting behavior for 304 stainless steel at 600°C. The total test time is 10 hours, and the stability was 8 hours.

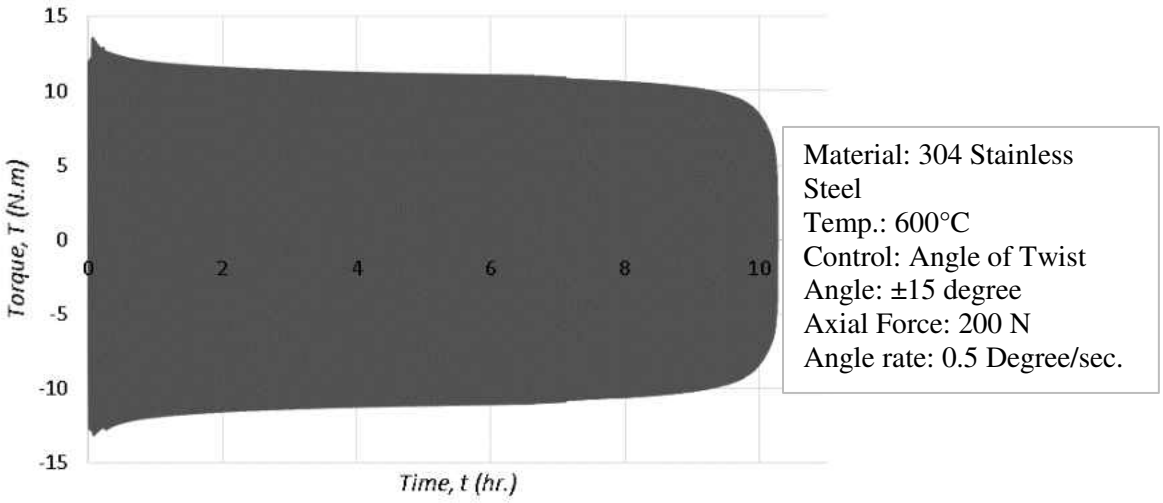

Figure 4.13: The torque versus time for AT-600°C-01.

The hysteresis response is also determined. Figure 4.14 shows the shear strain versus shear stress for AT-600°C-01. In this experiment, as anomalous behavior is drawn out in the first few cycles. The stress joys repeatedly. The behavior is called dynamic recrystallization (DRX). The

grains grown, and new grains are formed through deformation in high temperature. Mainly, in DRX, the grain modification and deformation resistance decrease in this practical steel. Based on DRX the stainless steels have higher deformation resistance than plain carbon steel. In Figure 4.14 b. shows the shear stress versus shear strain in mid life, so the maximum torque is 11.07 N-m, and the minimum torque is -11.05 N-m. Also, from this figure shows the material hardening then it softening until it is broken. Figure 4.14 c. shows the hysteresis loop from the first cycle until it is broken, and this experiment takes around 10 hours and 650 cycles. For axial load, there is small displacement in the axial direction, and if the device can apply more load the axial displacement will be clearer. The hysteresis loop shows that the shear stress decreased rapidly at rupture. From the shear stress begin to decrease until the specimen broken. The data summary for this experiment is provided in the Appendix A shows all data figures and specimen picture after it is broken.

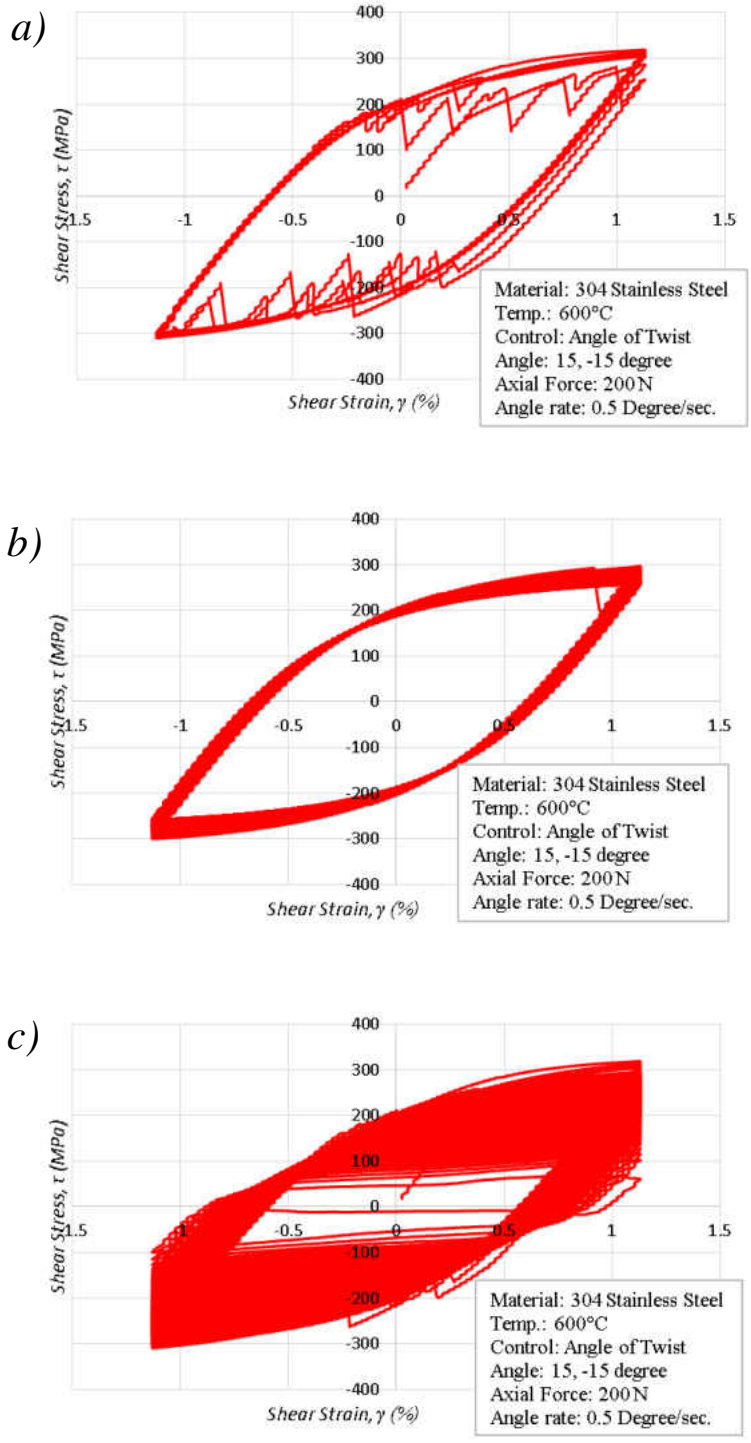

Figure 4.14: Shear strain versus shear stress for AT-600°C-01 a) first five cycles, b) midlife hysteresis loop, and c) hysteresis loop from the first cycle until broken.

4.3.2 AT-600°C-02

This experiment is the second experiment at 600°C for material. Axial force in this experiment is the highest force can applied on the device which is 200 N. Also, the control used here is angle of twist control, so that means the shear strain is the same for all cycles. The angle of twist goes to 15 degrees then it goes to -7 degree. The angle of twist ratio is -0.47, and the angle of twist rate is 0.55 degree per second. The torque versus time shown in Figure 4.15, and from this figure, it shows that the material is hardening then it softening until it is broken. From this figure, it shows that the material is softening after the first cycle until cycle number 15. After that, the material gardens from cycle number 16 until cycle number 27, and it softening again until the specimen is broken. In this experiment, have different behavior than the previous test, because in the previous experiment the material was hardening then it softens. The maximum torque for this test is 13.11 N-m, and the minimum torque is -12.17 N-m, and the midlife torque of the material have maximum torque is 11.00 N-m, and the minimum torque is -10.70 N-m. This specimen used for 1018 cycle until it is rapture

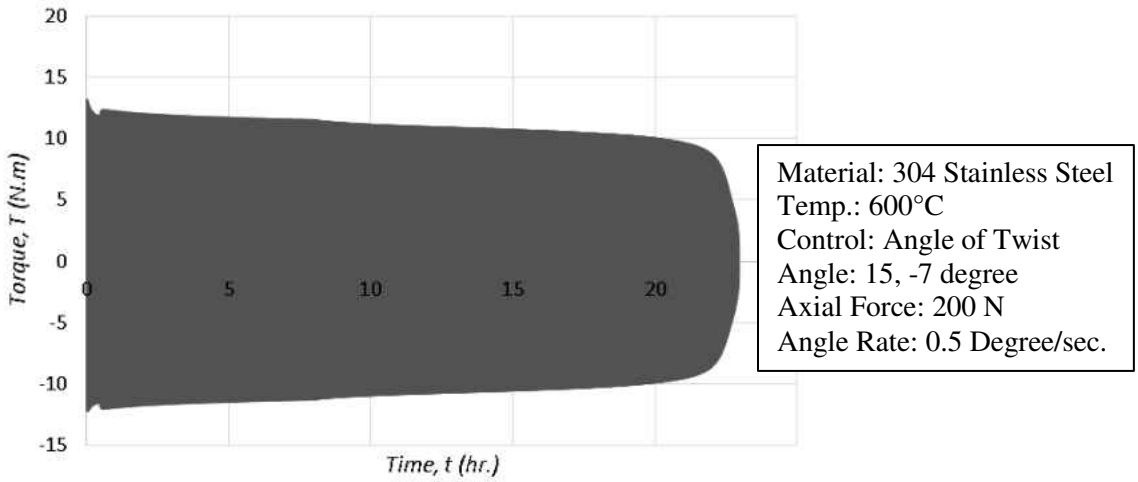

Figure 4.15: The torque versus time for AT-600°C-02.

Next, the shear strain versus shear stress for AT-600°C-02 as shown in Figure 4.16. In Figure 4.16 a. shows the first few cycles of this experiment, and the first cycle was without the axial loading. The reason from the first cycle without the axial to capture the shear elastic modulus at 600°C for 304 stainless steel. In Figure 4.16 b. shows the shear stress versus shear strain in mid life, so the maximum torque is 11 N-m, and the minimum torque is -10.7 N-m. In this hysteresis loop is almost stable, and the is small softening happen. The hysteresis loop from the first cycle until it broken shown in Figure 4.16 c, and this experiment takes around 23 hours and 1018 cycles. For axial load, there is small displacement in the axial direction, and if the device can apply more load the axial displacement will be clearer.

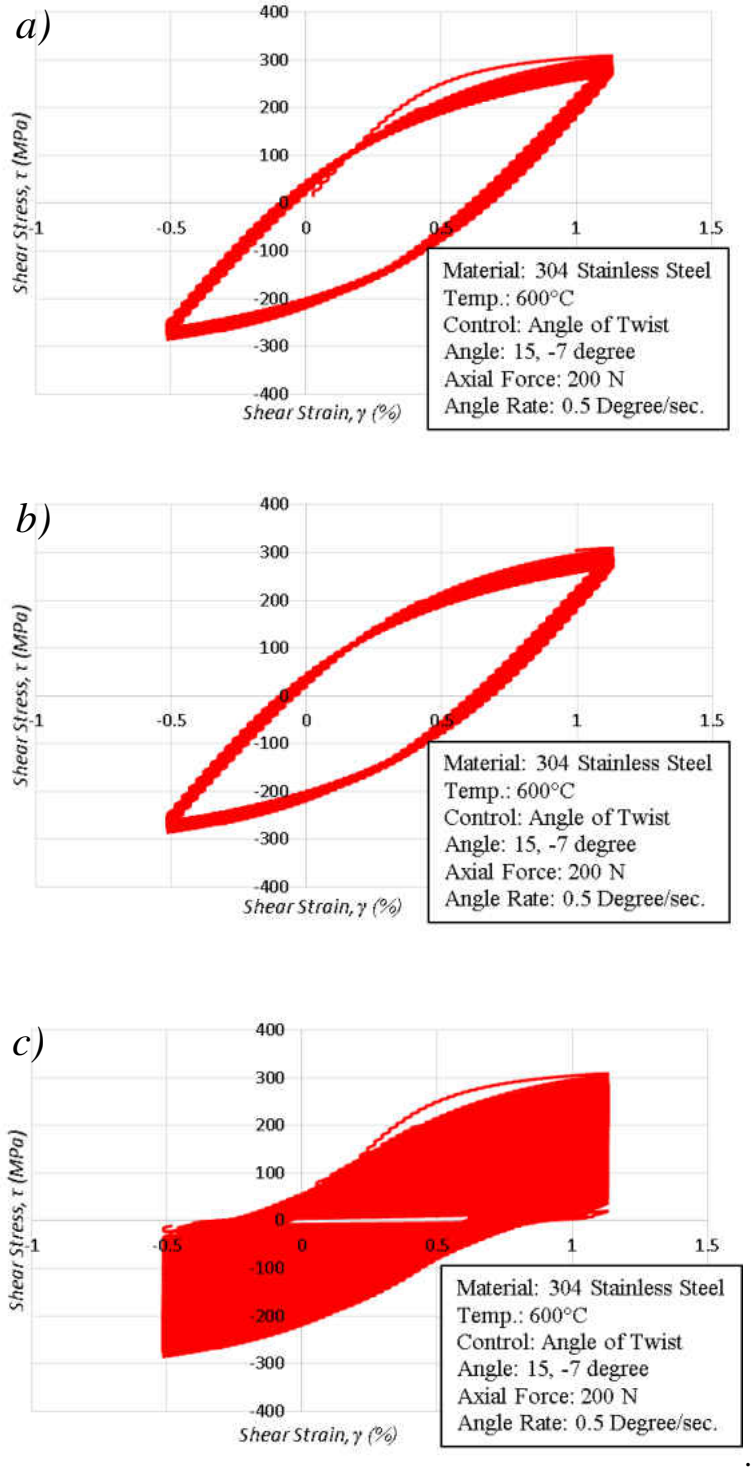

Figure 4.16: Shear strain versus shear stress for AT-600°C-02 a) first few cycles, b) midlife hysteresis loop, and c) hysteresis loop from the first cycle until broken.

4.3.3 AT-600°C-03

In this section is the first experiment by using torque control at 600°C for 304 stainless steel. The main objective for used the torque control to find if the material has ratcheting or no, and as mentioned before the main part of the specimen is the gage region. The thermocouple is connected to gage section to make sure it reaches the high temperature, but for the other sections is less than 600°C.. Figure 4.17 shows the angle of twist versus the time, so the angle of twist is increasing from the cycle to other cycles, and the reason from that is using the torque control. The Figure 4.17 shows the increasing on the angle of twist, then after 40 hours the angle of twist has small increasing, and the increasing happen in the angle of twist came from creep response. In this experiment used for almost 88 hours with 12313 cycles. The most important part of this experiment is the elasticity, plasticity, creep, and ratcheting behavior for 304 stainless steel at 600°C and the total test time is 23 hours. The shear strain versus shear stress for AT-600°C-03 as shown in Figure 4.18.

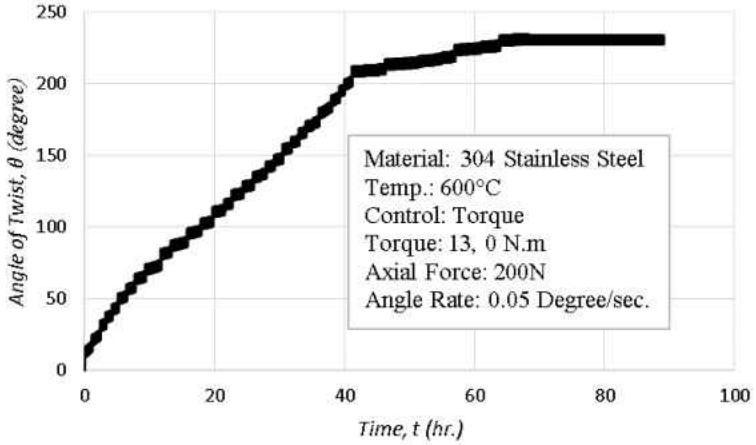

Figure 4.17: Angle of twist versus time for AT-600°C-03.

a)

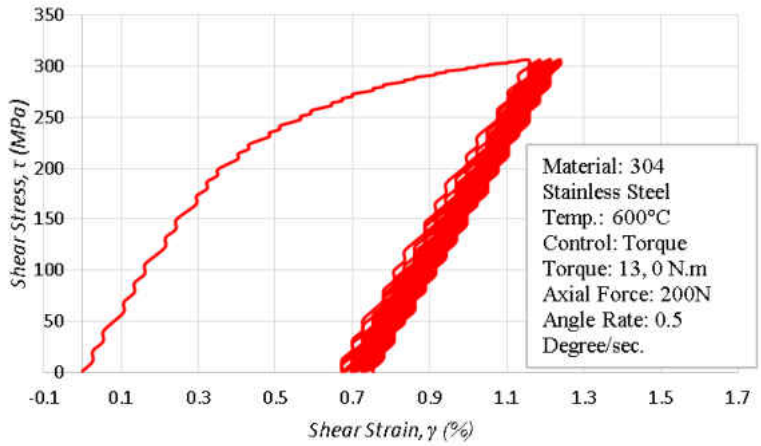

b)

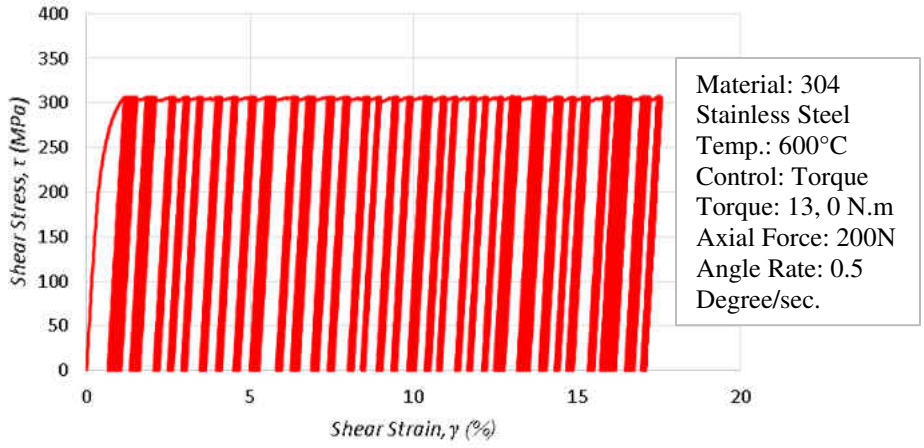

Figure 4.18: Shear strain versus shear stress for AT-600°C-03 a) first few cycles and b) from the first cycle until least.

4.3.4 AT-600°C-04

In this experiment used differently than the other experiments, so the control used here is torque control at 600°C for 304 stainless steel. The different way used here is run the experiment with maximum torque 14 N-m and minimum torque -3 N-m for 13 hours, then the maximum torque is increasing to 15 N-m for five hours. The different here than the other experiment focused on the angle of twist, the mean torque for this particular experiment is 5.5 N-m, 6 N-m, 6.5 N-m, and 6.75 N-m, and the angle of twist rate is 0.5 degree per second. Figure 4.19 a. shows the angle of twist versus the time for the first torque which is maximum torque is 14 N-m. The angle of twist has small increasing, but there is three significant increase as shown in Figure 4.19 a., and as mentioned before that could happen from creep or ratcheting. This experiment used for 13 hours with 1333 cycles. Figure 4.19 b. shows the angle of twist versus time for 304 stainless steel with maximum torque 15 N-m, and with this torque value, the angle of twist has more increasing. In this experiment has seven big increasing the angle of twist. In Figure 4.19 c. is the angle of twist versus time with maximum torque 16 N-m. In the first cycle, the angle of twist is very high to reach the highest torque as shown in the figure. Moreover, the same behavior happens in Figure 4.19 d.

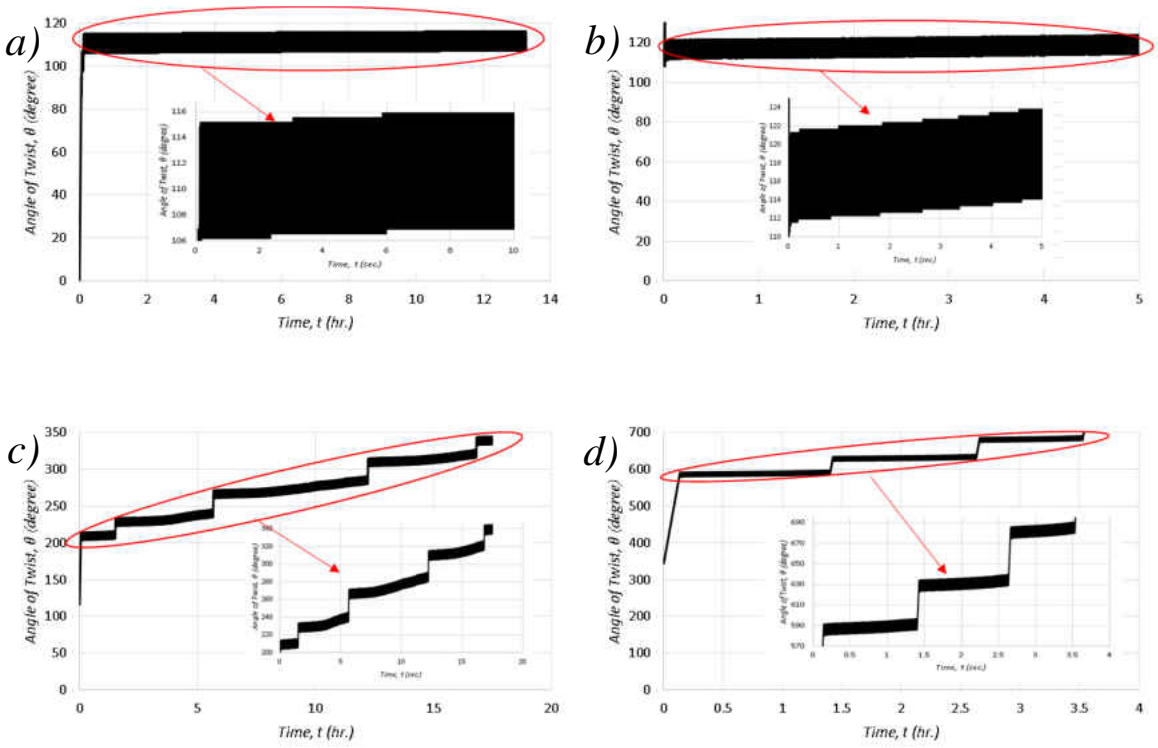

Figure 4.19: Angle of twist versus time for AT-600°C-04 a) torque (14,-3), b) torque (15,-3), c) torque (16,-3), and d) torque (16.5, -3).

Next step will go to the shear strain versus shear stress for AT-600°C-04 as shown in Figure 4.20. The first maximum torque 14 N-m shows in Figure 4.20 a., so the first cycle has the biggest angle of twist to reach that torque. Also, in the first cycle shows the Dynamic recrystallization (DRX). Mainly, the happening of DRX the grain modification and deformation resistance decrease in practical steel. Based on DRX the stainless steels have higher deformation resistance than plain carbon steel. The first few cycles of this experiment and the first cycle were without the axial loading. The reason from the first cycle without the axial to capture the shear elastic modulus at 600°C for 304 stainless steel. After the first cycle the angle to twist jumps again to reach the torque value, then there are few cycles and jumped again. The jumped in the angle of

twist came from the ratcheting and creep. This experiment used for 13 hours, and during that experiment have 1333 cycles. Next, the maximum torque is 15 N-m shows in below Figure 4.20 b. in this experiment the shear strain versus shear strain behavior is different, so the shear strain has small increasing from cycle to other cycles as shown in the figure, and there are no jumped in shear strain. The increasing on the shear strain is the same value from cycle to other cycles. The third experiment which is 16 N-m torque as shown in Figure 4.20 c. In this part of the experiment the shear strain in jumped after first few cycles then it has a small increase. After that, the shear strain jumped again, and this jumped occurred four times. The part of experiment used for almost 17 hours and 1711 cycles. Last part of this experiment is torque 16.5 N-m as shown in Figure 4.20 d. this part used for 3.5 hours and 273 cycles. There are increasing in the hysteresis loop from cycle to another cycle. The increasing happen after the first cycle then it jumped to different shear strain, and that behavior repeated for three times. The output data from the experiment device are time t, axial force P, axial displacement Δ, torque T, and angle of twist ϕ. So, the calculation data are axial stress σ, axial strain ε, shear stress τ, and shear strain γ. In Table 4-5 shows the data summary for this experiment, and appendix A shows all data figures and specimen pictures.

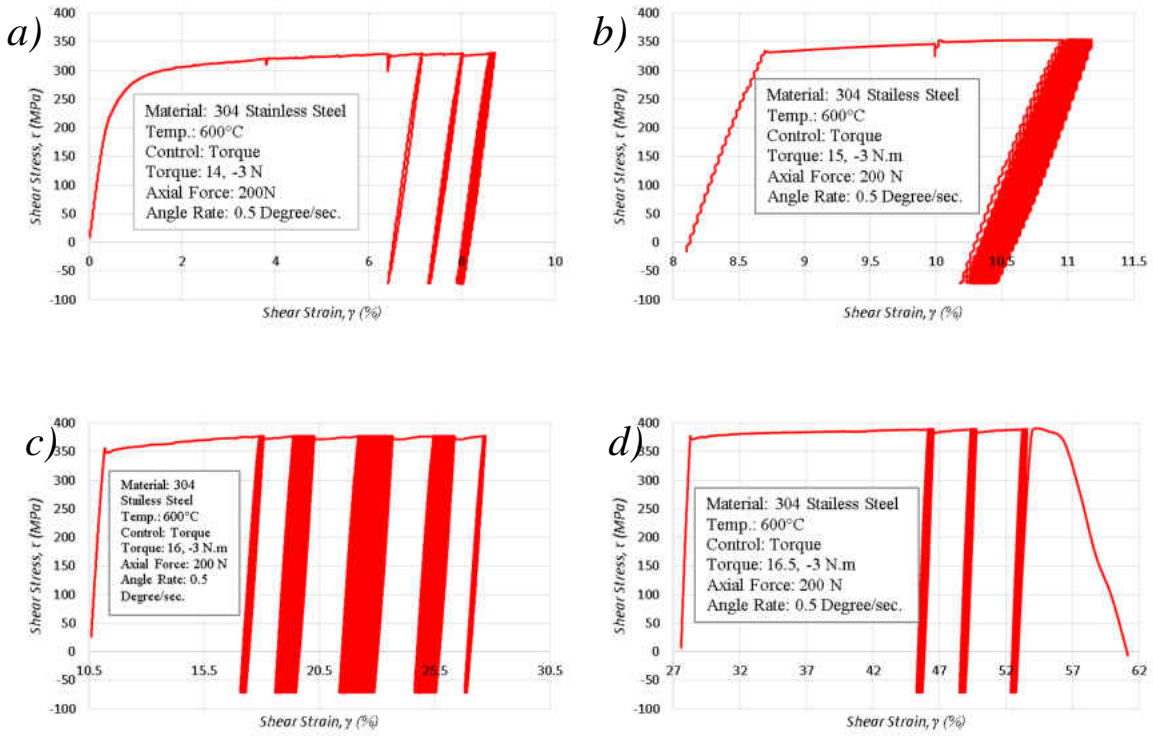

Figure 4.20: Shear strain versus shear stress for AT-600°C-04 a) torque (14,-3), b) torque (15,-3), c) torque (16,-3), and d) torque (16.5, -3).

4.3.5 AT-600°C-05

In this type of experiment is different from the other experiments for 304 stainless steel at 600°C, and the controller used here is the angle of twist control, but the angle of twist is started with 0.00025 degrees per second and raised to 2.5 degrees per second. Also, the angle of twist applied here is 16, -16 degree. The main idea of used different angle of twist rate is to find the creep constant for 304 stainless steel at 600°C. Axial force in this experiment is the highest force can apply on the device which is 200 N. The thermocouple is connected to gage section to make sure it reaches the high temperature, but for the other sections is less than 600°C. Figure 4.21 a. shows the torque versus time for the first angle of twist which is 0.0005 degrees per second. The

maximum torque for this test is 11.7 N-m, and the minimum torque for this experiment is -8.34 N-m. This experiment used for 72 hours and one cycle. After that, the angle of twist is increased to 0.0025 degrees per second as shown in Figure 4.21 b. The second angle of twist which is 0.0025 degree per second, and this part of experiment used for 22 hours and six cycles. The maximum torque here is 11.15 N-m, and the minimum torque is -9.8 N-m. Next, the angle of twist is 0.025 degree per second, and the maximum torque is 10.76 N-m, and the minimum torque is -10.74 N-m as shown in Figure 4.21 c. This part of experiment used for 1.8 hour and 3 cycles. After that, the angle of twist is 0.25 degree per second, and the maximum torque is 10.79 N-m, and the minimum torque is -11.44 N-m as shown in Figure 4.21 d. This part of experiment used for 0.54 hour and 3 cycles. Finally, the last angle of twist rate applied here is 2.5 degree per second as shown in Figure 4.21 e. The maximum torque here is 110.81 N-m, and the minimum torque in this part of the experiment is -11.44 N-m. This part of experiment used for 0.036 hours with 6 cycles.

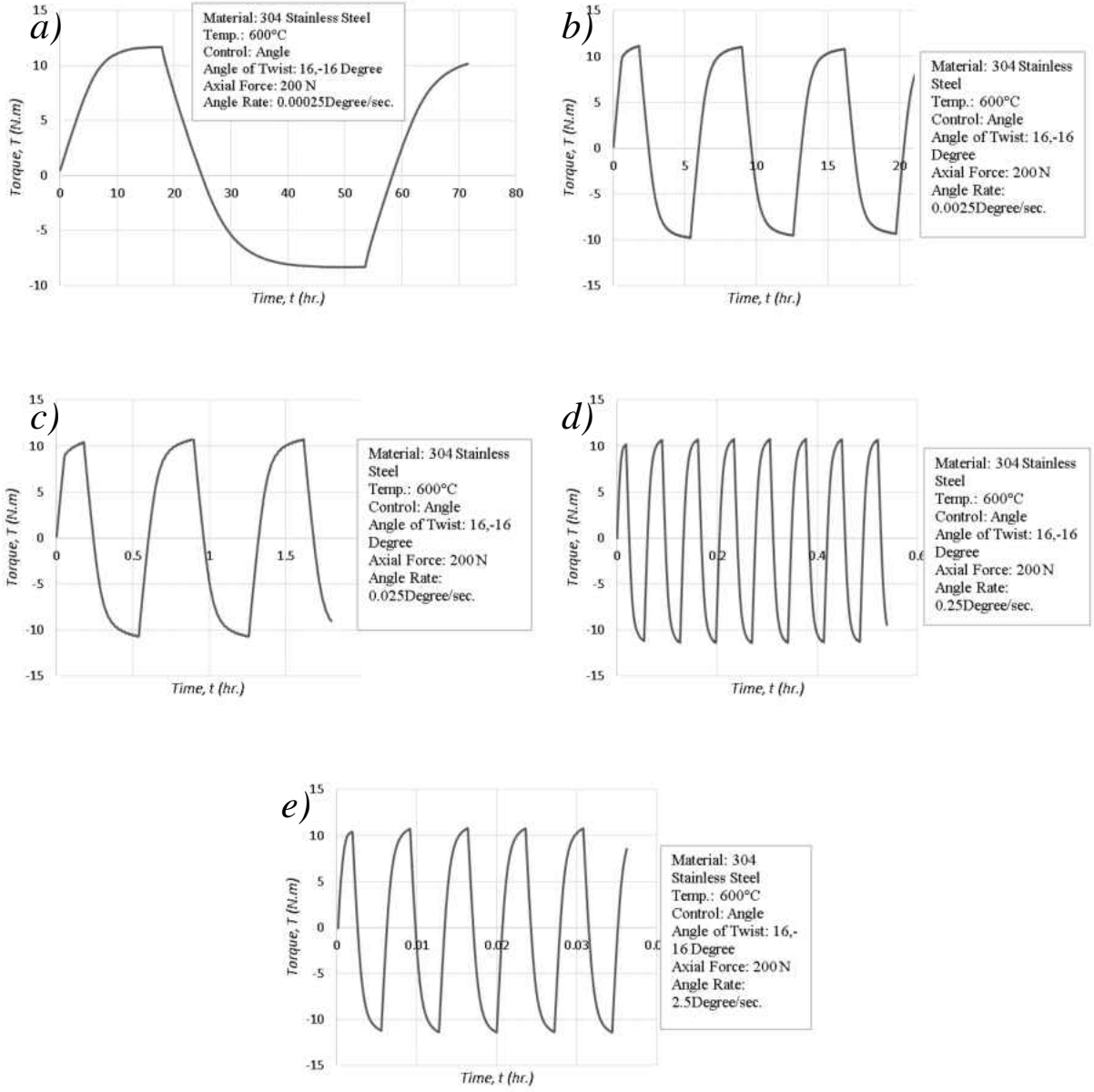

Figure 4.21: Torque versus time for AT-600°C-05 a) angle of twist rate is 0.00025 degree per second, b) 0.0025 degree per second, c) 0.025 degree per second, d) 0.25 degree per second, and e) 2.5 degree per second.

Next step will go to the shear strain versus shear stress for AT-600°C-05 as shown in Figure 4.22. The first angle of twist rate is 0.0005 degree per second as shown in Figure 4.22 a, and the hysteresis loop shown for this angle of twist rate. Then, the angle of twist rate is 0.005 degree per second as shown in Figure 4.22 b, and the hysteresis loop indicated for this angle of twist rate. The third angle of twist rate is 0.05 degree per second as shown in Figure 4.22 c. The hysteresis loop for this experiment is stable. Finally, the angle of twist is 0.5 degree per second as shown in Figure 4.22 d. The output data from the experiment device are time t, axial force P, axial displacement Δ, torque T, and angle of twist ϕ. So, the calculation data are axial stress σ, axial strain ε, shear stress τ, and shear strain γ. In Table 4-5 shows the data summary for this experiment, and appendix A shows all data figures and specimen pictures.

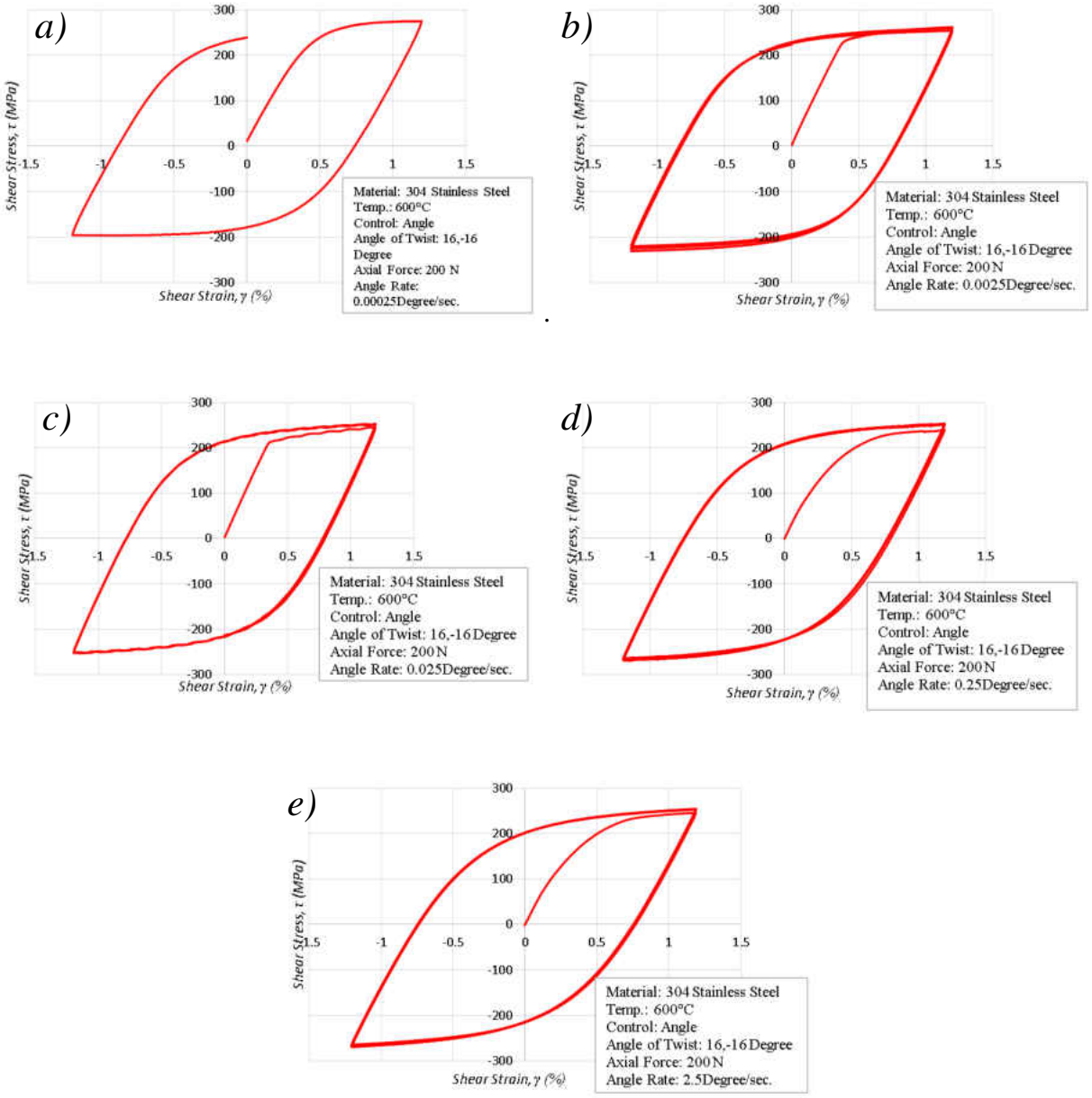

Figure 4.22: Shear stress versus shear strain for AT-600°C-05 a) angle of twist rate is 0.00025 degrees per second, b) 0.0025 degree per second, c) 0.025 degree per second, d) 0.25 degree per second, and e) 2.5 degree per second.

4.3.6 AT-600°C-06

This experiment is different from previous experimints for 304 stainless steel at 600°C. This part of experiments to find the relaxation of our material to find the creep constants, the controller used here is the angle of twist control than applied axial force. The hold time here is 2 min, 20 min, and 200 min. the angle of twist applied here is 16, -16 degree, and the angle of twist rate is 2 degree per second. The main idea of the used different angle of twist rate is to find the creep constant at 600°C by using relaxation. Axial force in this experiment is the highest force can apply on the device which is 200 N. Figure 4.23 shows the torque versus time without axial force, and this experiment has three different dwell time which is 2, 20, and 200 min. Figure 4.23 a. did not show the relaxation, and that why the dwell time increased. For 200 min dwell time to show good relaxation curve, and for 20 min holding time is shows the relaxation, but it not clear as 200 min when the torque came as constant during the time. Figure 4.23 d. shows the torque versus the time, but the difference here is the axial load. The axial load applied in this experiment to see the difference between the relaxation with and without axial load. From comparing between the relaxation with a without axial load found is almost the same relaxation, and the reason from that is the axial load is very small comparing to shear stress.

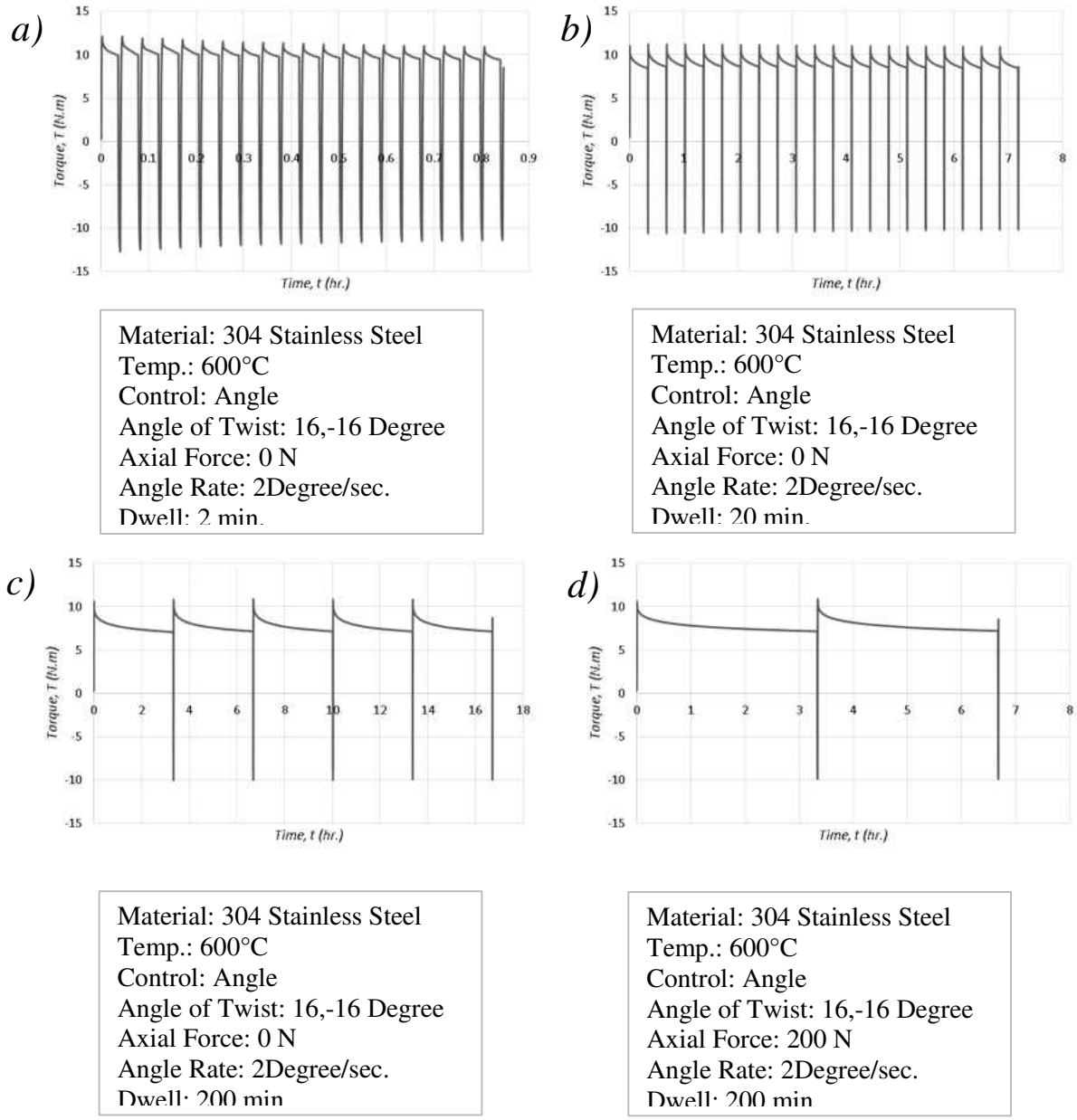

Figure 4.23: Torque versus time for AT-600°C-06 a) dwell 2 min, b) dwell 20 min, c) dwell 200 min, and d) dwell 200 min with axial load.

The second part of this section is to see the shear stress-strain curve for this material under 600°C as shown in Figure 4.24. The main reason for this experiment to find the creep constants from the relaxation curve. The differences between a, b, and c. are the dwell time, d. is with the axial load to see if there were any different in relaxation curve when the axial load applied, but there are no different because the axial load is minimal comparing to shear load. The output data from the experiment device are time t, axial force P, axial displacement Δ, torque T, and angle of twist ϕ. So, the calculation data are axial stress σ, axial strain ε, shear stress τ, and shear strain γ. In Table 4-5 shows the data summary for this experiment, and appendix A shows all data figures and specimen pictures.

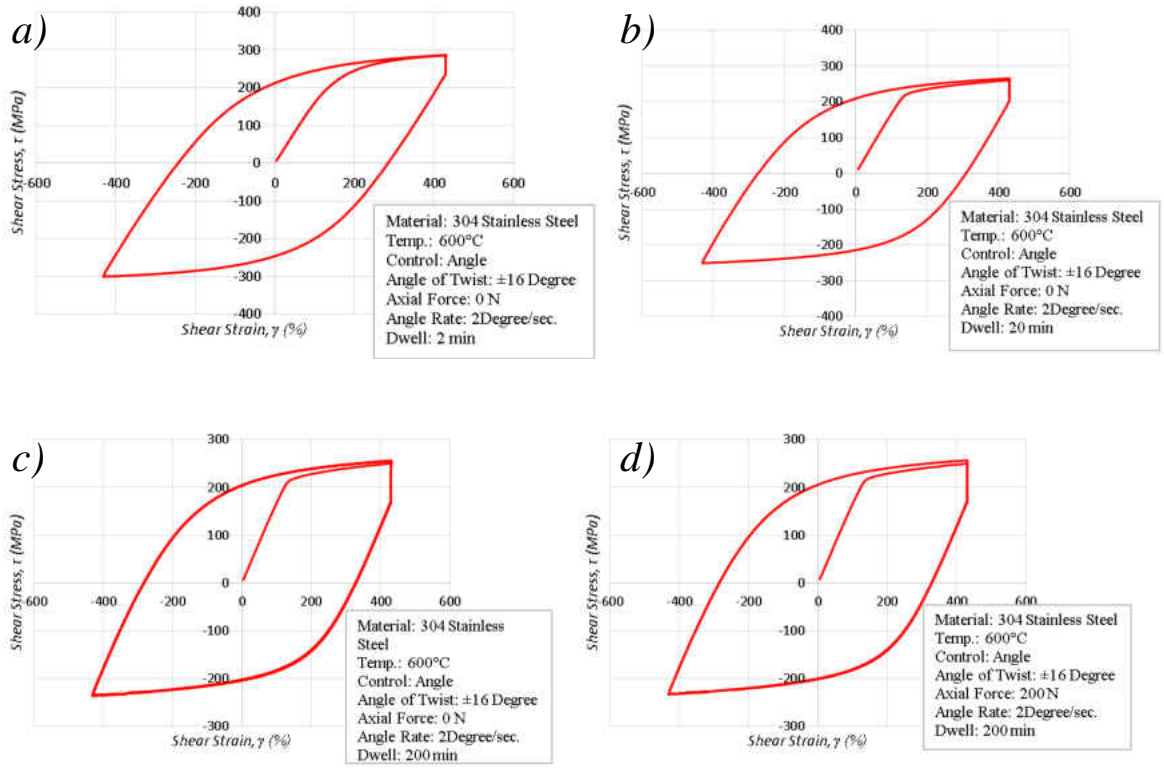

Figure 4.24: Shear stress- strain curve for AT-600°C-06 a) dwell 2 min, b) dwell 20 min, c) dwell 200 min, and d) dwell 200 min with axial load.

4.3.7 600°C Results Summary

The results of testing at 600°C are summarized here. The first parts in this section is the peak and valley torque versus the time, the second parts is the first cycle of different experiments under room temperature. Figure 4.25 shows the peak and valley torque versus the time. All of these experiments shows the softening is almost same with different angle of twist. The first one is AT-600°C-01, the angle of twist is (15, -15) degree has the less time until it broken, and it broken after almost 10.3 hours. The reason from this time because the angle of twist range is 30 degree. This experiment has 650 cycles to broken, and the maximum torque is 13.5 N-m, and the minimum torque in this experiment is -13.1 N-m. Second experiment is AT-600°C-02, and the angle of twist is (15, -7) degree with 200 N axial force. The experiment time until the specimen is broken is 23 hours, and it has 2700 cycle until it broken. The maximum torque is 13.1 N-m, and the minimum torque in this experiment is -12.2 N-m. Figure 4.25 shows the second experiment take more time to broken, and the reason from that the first experiment has large angle of twist range which is 30 degree. The second experiment has smaller angle of twist range which is 22 degree. Also, the number of cycles of the second experiment is larger than the first experiment, and the reason is the angle of twist range, and the time until it broken is shown in Table 4-5.

.

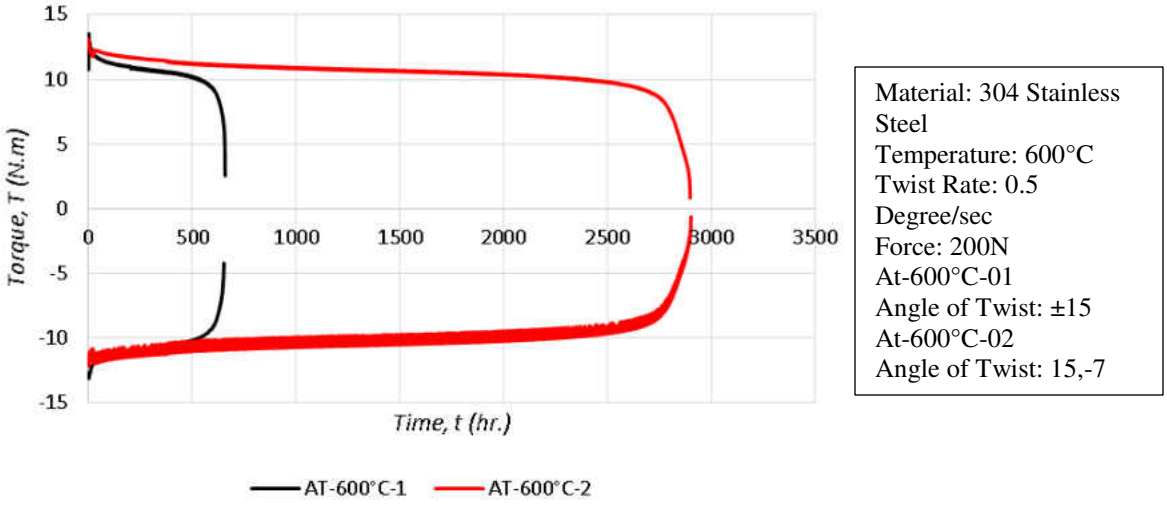

Figure 4.25: Maximum and minimum Torque for different experiments at 600°C.

Next, the second point from the summary results for different experiments at 600°C. Figure 4.26 shows that the slope of the elastic modulus of all different experiments under room temperature are almost same. The shear strain of all different experiments are same. Next, but looking to the plasticity curve has almost same curve. The different shear strain range from these experiments because the different angle of twist. The maximum torque has small different between the different experiment, and the different cloud come from the specimen defect, or it cloud come from the heater. From Figure 4.26 a. can find the elasticity, plasticity, and creep behavior for our material. The elastic properties will find from the slope of the elastic range, and from this figure the all elastic range of all experiments are almost same. Also, for plastic properties are almost same curve, so the plasticity constant will be same in all different experiments. Figure 4.26 b. shows the hysteresis loop the same experiment but with different angle of twist rate. The reason from the AT-600°C-05 to extract the creep constant at 600°C. Table 4-5 shows the result summary for all different experiments under room temperature. What shows in this table are maximum and minimum torque, time until it broken, and number of cycles, axial force, and control type.

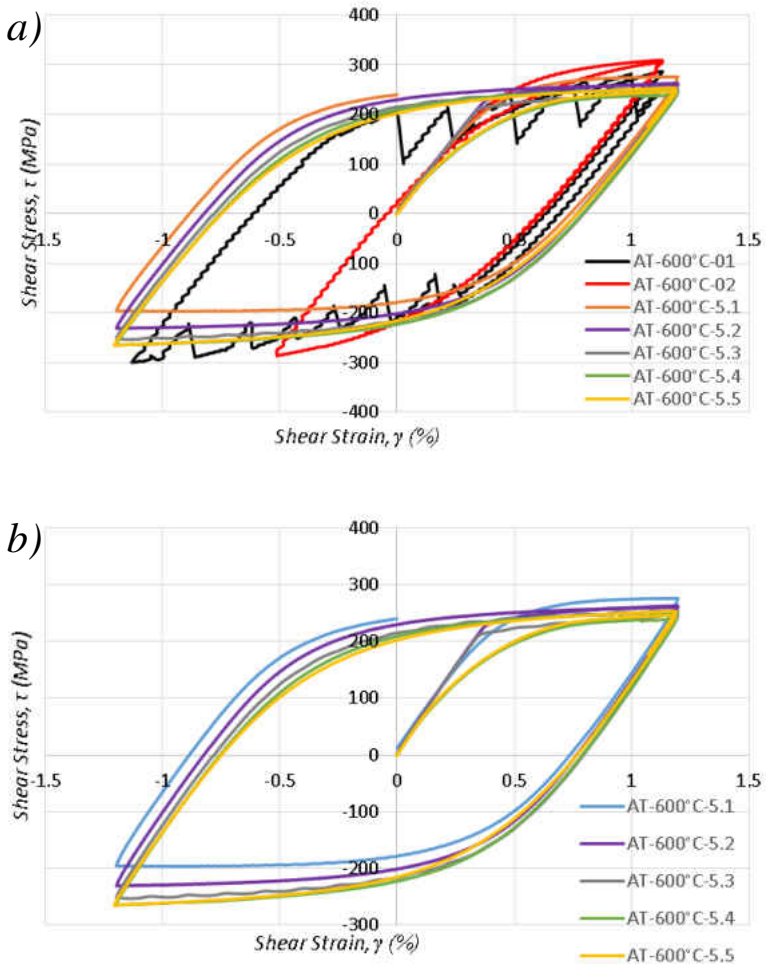

Figure 4.26: First Cyclic for different experiments at 600°C a) all experiments, and b) AT-600°C-5.

The last experiment type in this study is shear stress relaxation under high temperature. The differences are the dwell time but the same specimen. The dwell is incrementally increases, the relaxation needs more time to be more evident, so the dwell time increased to 200 min, and this one was the more evident relaxation as shown Figure 4.27. This figure proves that there are no different in relaxation curve wit and without axial load, and the reason from that is the axial

load is small, but if the axial load can increase the relaxation curve will be different from the relaxation without axial load.

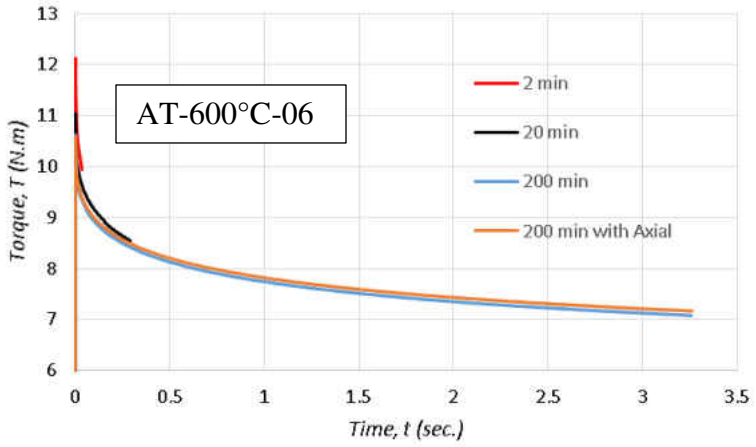

Figure 4.27: Relaxation of 304 stainless steel under high temperature with different dwell time.

Figure 4.28 shows the shear stress-strain for 304 stainless steel at 600°C, but the difference between the curves is the dwell time. First, when the dwell is 2 min, the relaxation is very small, so it is not clear to find the creep constant from this relaxation. Second, the dwell time is 20 min, and this one has good relaxation curve, but it needs more time to have good relaxation curve. Last dwell time is 200 min, but there are two different experiments with and without axial load. Figure 4.28 shows that there are no different when there is axial load and without axial load, and the reason from that the axial load is small to make the different curve. Also, this figure shows the minimum shear stress is decreasing with increase the dwell time, and the reason from that the experiment did for one specimen, and as mentioned before the material is softening with time at high temperature.

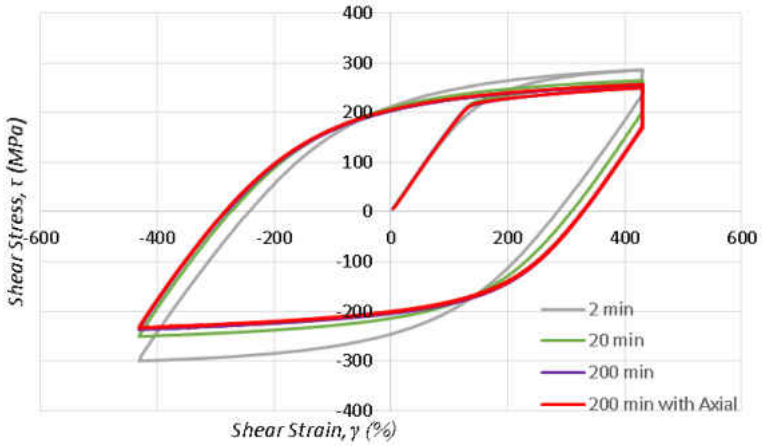

Figure 4.28: Shear stress-strain curve for 304 stainless steel with different dwell time.

Table 4-5: Experiments summary results at 600°C

Specimen ID	Temperature °C	Number of cycles cycles	Angle of twist rate Degree/sec.	Max. Torque, T_{max} N-m	Min. Torque, T_{min} N-m	Axial Force, P N	Time hr.
AT-600°C-01	600	650	0.5	13.5	-13.1	200	10.5
AT-600°C-02	600	2900	0.5	13.1	-12.2	200	23
AT-600°C-03	600	4632	0.5	13	0	200	90
AT-600°C-04	600	1326	0.5	14	-3	200	13.5
AT-600°C-04	600	464	0.5	15	-3	200	5
AT-600°C-04	600	1711	0.5	16	-3	200	20
AT-600°C-04	600	221	0.5	16.5	-3	200	3.5
AT-600°C-05	600	1	0.00025	11.7	-8.34	200	71.6
AT-600°C-05	600	3	0.0025	11.15	-9.8	200	21.6
AT-600°C-05	600	3	0.025	10.76	-10.74	200	1.8
AT-600°C-05	600	3	0.25	10.79	-11.44	200	0.54
AT-600°C-05	600	2	2.5	10.81	-11.44	200	0.036
AT-600°C-06	600	20	2	12.13	-11.2	0	2 min dwell
AT-600°C-06	600	6	2	11.2	-10.6	0	20 min dwell
AT-600°C-06	600	6	2	10.9	-10	0	200 min dwell
AT-600°C-06	600	2	2	10.9	-10	200	200 min dwell

CHAPTER 5 NUMERICAL SIMULATIONS

The most important part of this research is the numerical simulation. From the simulation can the researcher know how the material behavior will look like, then the researcher can imagine which experiments need to do? Without numerical simulation the researcher will do many experiments, and that experiments it will not need it, so that is wasting time and material. The Finite Element Method (FEM) is a numerical approach that can be leveraged to study the stress-strain response of a material under a wide range of conditions which might be too unwieldy to investigate with experiments fully. In constitutive model development, either uniaxial or multiaxial approach can take, but the former has received the most emphasis. The FEM method is used to study the material behavior because it will lower the cost and time the experimentation is resource intensive. For example, to observe the creep behavior of some material, the FEM is used because of the lower cost, shorter period, and repeatability.

5.1 Multiaxial FE Model Description

In this research is the focus in finite element analysis under axial-torsional loading. Most of the prior study is studying different conditions. In some paper has material behavior under uniaxial loading. A few paper did finite element analysis for multiaxial loading, but the multiaxial used is not axial-torsional loading. The past paper was a focus to study the finite element of the pressure vessel, so the multiaxial was axial and pressure. From the literature review, not one has reviewed and considered the finite element analysis for axial-torsional type, but there is some experiment for this types of multiaxial without FEA. The reason from this study is comparing the

finite element analysis results and experiment result which came from the past paper. In this research will use ANSYS to do the finite element analysis. Axial-torsional loading in one of the most important study because most components subjected to this loading. Figure 5.1 shows the finite element analysis model with stress/load control, strain control, and the cross section.

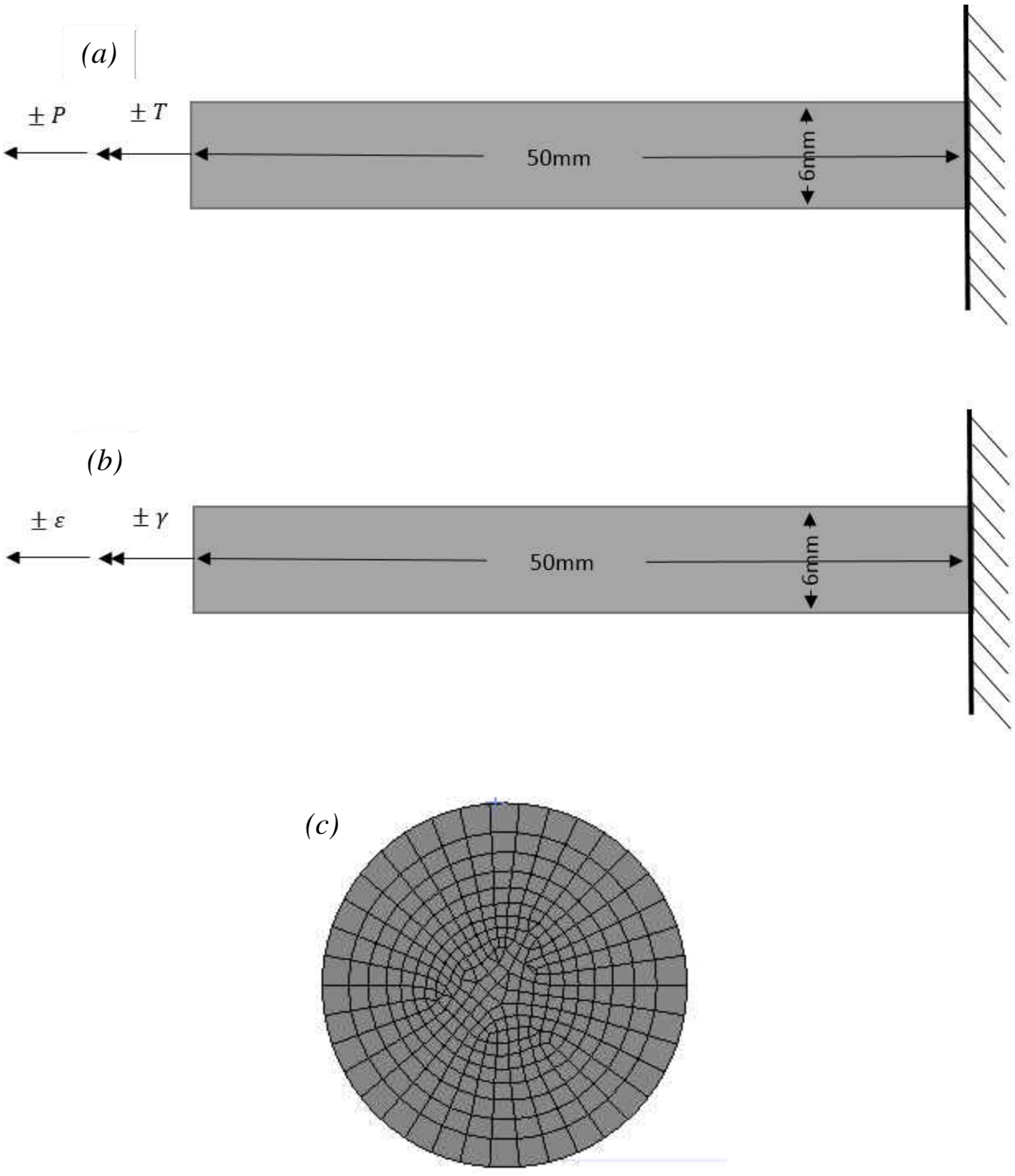

Figure 5.1: Finite Element Model a) Stress/Load-control b) Strain Control c) Cross Section.

Some research studied the two aspects individually; for example, they studied the axial load/strain and then the torsion/angle of twist in separate simulations. One experiment studied the circular rod when one end is free, and the other fixed. The axial load/strain applied to the free end, and the torsion/angle of twist applied to the fixed end. The axially compressive force increased with torsion (Yeganeh and Naghdabadi, 2006). The research used an axial-torsion system with closed loop feedback control. Also, the torque and axial load found from load cell by the control system. Also, researchers never developed a finite element model capable of simulation axial-torsional fatigue to study the materials behavior under multiaxial loading. The study will focus on the gage section. The main idea is to study the material behaviors under axial-torsion loading. Figure 5.1 shows the FEM model shows the boundary conditions by using ANSYS. The axial force and shear forces applied to the left end, and the right end fixed. The FEM is 50 mm length. In this simulation used Hexahedral Meshing, and it has 3106 nodes and 661 elements. The main reason from this simulation is to compare the simulation results and results presented by others.

5.2 Multiaxial FE Modeling For 2.25Cr-1Mo Steel Results

This section is used to compare the experiments results and the numerical simulation results. The study included four different models with four various types of axial-torsional loading. All axial-torsional loading types came from literature, and Table 5-1 will shows the four different load paths for each case. Figure 5.2 shows the load steps applied on 2.25Cr-1Mo steel. Each test loads to a different response.

Table 5-1: Simulation Test types and the test control

Test	Paper	Test Control	Axial	Shear	Rate	Loading Path
M1	Inoue et al., 1994	Stress/Load Control	60MPa	-160 to200 MPa	$\dot{\sigma} = 10\text{MPa/s}$ $\sqrt{3}\,\dot{\tau} = 0.1\text{MPa/s}$	Linear
M2	Inoue et al., 1994	Strain Control	$\pm 0.2\%$	$\pm \frac{0.4}{\sqrt{3}}$ %	$\dot{\varepsilon} = 0.01\%/\text{s}$ $\sqrt{3}\,\dot{\gamma} = 0.01\%/\text{s}$	Diamond CCW
M3	Inoue et al., 1989	Strain Control	$\pm 0.6\%$	$\pm \frac{0.6}{\sqrt{3}}$ %	$\dot{\varepsilon} = 0.1\%/\text{s}$ $\sqrt{3}\,\dot{\gamma} = 0.1\%/\text{s}$	Cruciform CCW
M4	Inoue et al., 1989	Strain Control	$\pm 0.6\%$	$\pm \frac{0.6}{\sqrt{3}}$ %	$\dot{\varepsilon} = 0.1\%/\text{s}$ $\sqrt{3}\,\dot{\gamma} = 0.1\%/\text{s}$	Elliptical CCW

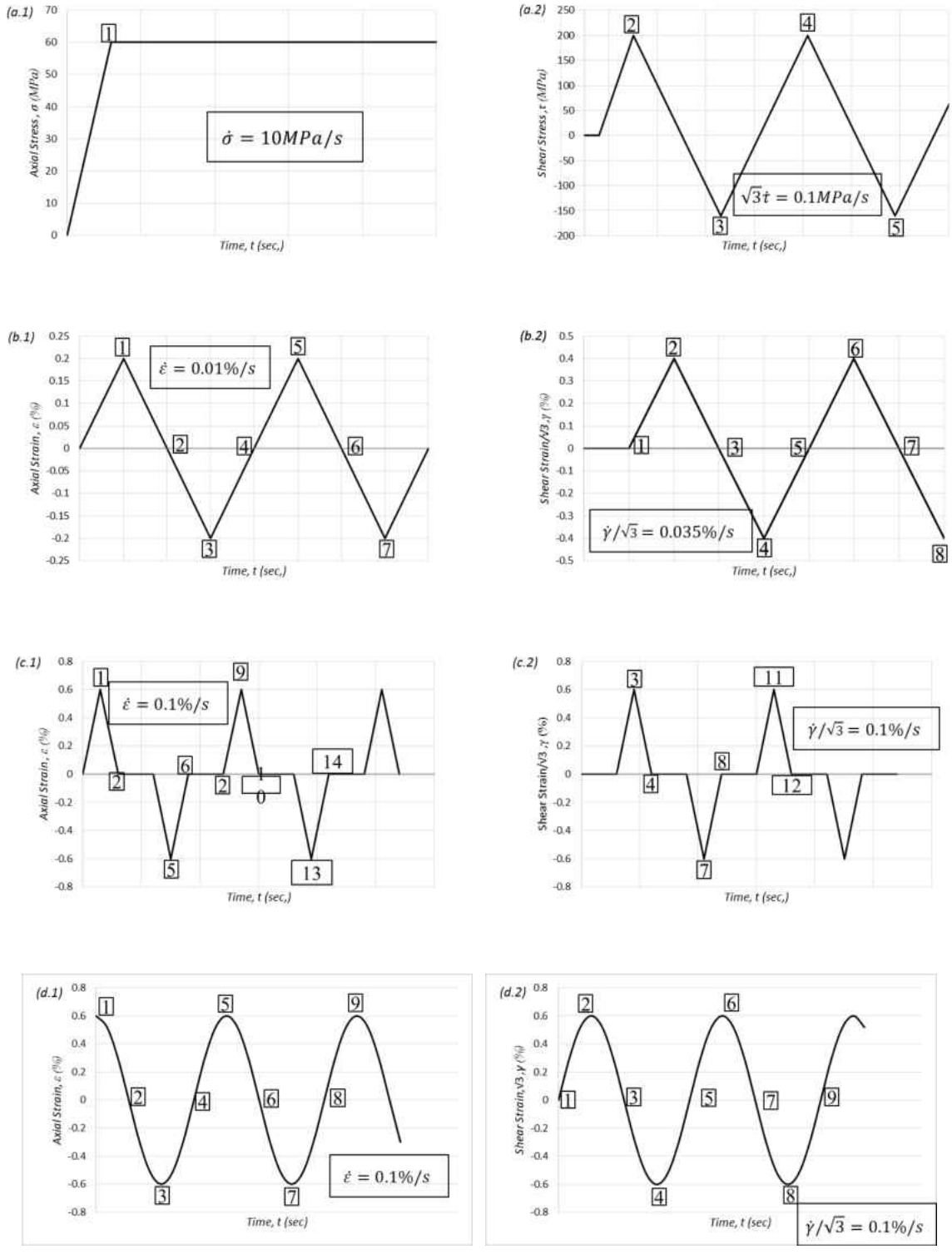

Figure 5.2: Load steps applied in2.25Cr-1Mo at T=600°C a) Linear, b) Diamond CCW, c) Cruciform CCW, and d) Elliptical CCW.

Initially, the simulation results are compared with the experimental results presented by Inoue et al., 1989 and 1994. In Table 5-1 shows the different experiments date from these sources are provided. The stress or strain controls and stress/strain rate for 2.25Cr-1Mo. Inoue et al., 1989 and 1994 show various multiaxial loading test. The main objective of this study is to prove that constitutive models develop under uniaxial conditions can translate over to multiaxial ones. The temperature for these four different experiments happens under 600°C.

The first test was using stress control, and the loading path have used in Test 1 is linear; whereas Test 2 used strain control, and the loading path is Diamond CCW. In Test 3, the loading path is Cruciform CCW, the control is strain control, and the last test is strain control with Elliptical CCW loading path. The finite element analysis will use four different models, and these models are Chaboche-Garofalo, Chaboche-Norton, Romberg-Osgood-Garofalo, and Ramberg-Osgood-Norton. The goal of using different models is to determin which model will capture experiment data optimally. The output data from FEA have axial stress, shear stress, equivalent stress, equivalent strain, plastic axial and shear strain, creep axial and shear strain, and total axial and shear strain.

The modeling and data are reviewed Figure 5.3 show the simulation results for four models, and compare it with experimental data. Chaboche-Garofalo and Ramberg-Osgood-Garofalo have more accurate results than Chaboche-Norton and Ramberg-Osgood-Norton model. In Figure 5.9 a. shows that the total strain is mostly creep strain, and the plastic strain is near to zero, so that why shows different between Garofalo and Norton. There are no differences between the plasticity model which are Ramberg-Osgood and Chaboche. As mentioned before the total strain is almost creep, so the plasticity model will have a small effect on the results. The simulation data show that

the good fitting between the data and the simulation. The slope of the simulation was approximately identical. Also, the trend from one cycle to another is close, which means the simulation and boundary condition is have designed well. The space in each cycle looks the same, but in the Inoue data, the space between the cycles reduced. There were many reasons for this difference. The first reason was that the data used to calibrate the computational model derived from a material with a slightly different heat treatment compared to that of the experimental data. Other discrepancies could be due to experimental scatter. The reasons of Garofalo model capture multiaxial responses more accurately than Norton model are Garofalo has three constants, but Norton has two constants. By viewing at Figure 2.15, it shows that the Garofalo model is caverd over a range of strain rates, while Norton model is linear on a log graph line. However, by focusing on 539°C and 649°C data which came from the experiment, and compare it the Garofalo and Norton models. Norton model cannot capture the all data because it is a straight line and the stress is too low on low creep strain rate. Garofalo has almost captured the most data because it came as curve, so it starts with low stress, then it will go through the high stress. Now, from knowing the difference between the creep models we are aware why Garofalo model capture the data more accurate than Norton model.

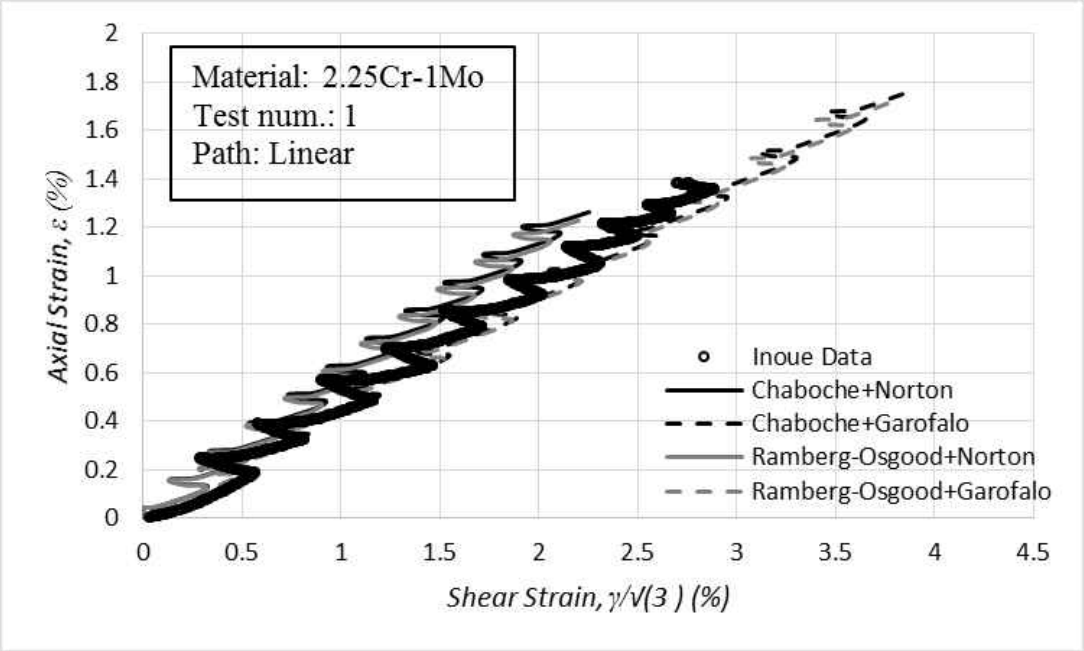

Figure 5.3: Comparison between the simulation and Inoue results for 2.25Cr-1Mo Steel Test 1 (Inoue et al., 1994).

Test 2 has different loading path, and the path used for this test is Diamond CCW, and the control used here is strain control. The simulation used for this test was displacement control, so this could be one the cause differences between the simulation and experiment results. In Figure 5.4 shows the comparison between the simulation and experiment total strain for four models. In Figure 5.5 a. and b. shows the axial stress versus axial strain, and shear stress versus shear strain. This figure reveals that there are no differences between Chaboche-Garofalo and Chaboche-Norton, and the same with Ramberg-Osgood-Norton and Ramberg-Osgood-Garofalo, so the difference in this test is between plasticity models. In Figure 5.5 b. shows the total, creep, and plastic strain for this test, so the total strain is an almost plastic strain, so the difference between the plasticity models came because the total strain is a nearly plastic strain. Test 2 used isotropic

hardening and Non-Linear Kinematic Hardening (NLKH) models, and NLKH model captures the axial-torsional response more accurately than isotropic hardening. The creep strain in this test is almost zero, so creep models did not effect in this type of test. Finally, from this test, we know the NLKH is more accurate that isotropic hardening.

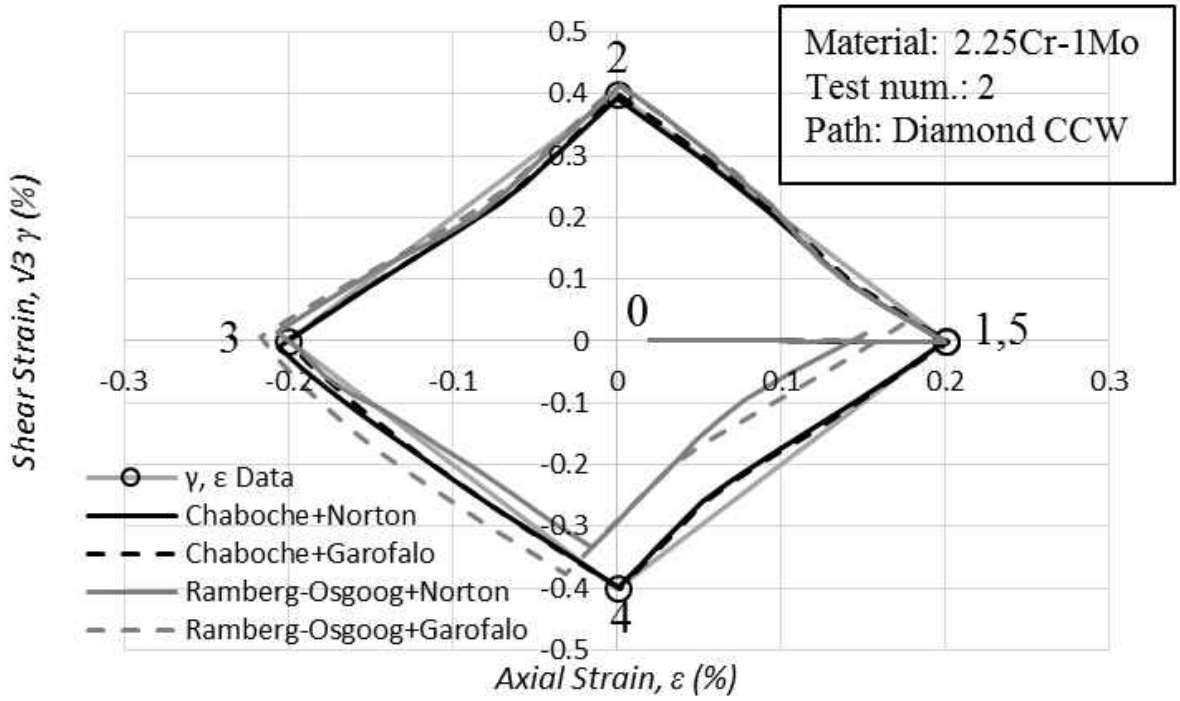

Figure 5.4: Comparison of strain control between the simulation and Inoue et al., 1994 results of 2.25Cr-1Mo Steel. Test 2 (Inoue et al., 1994).

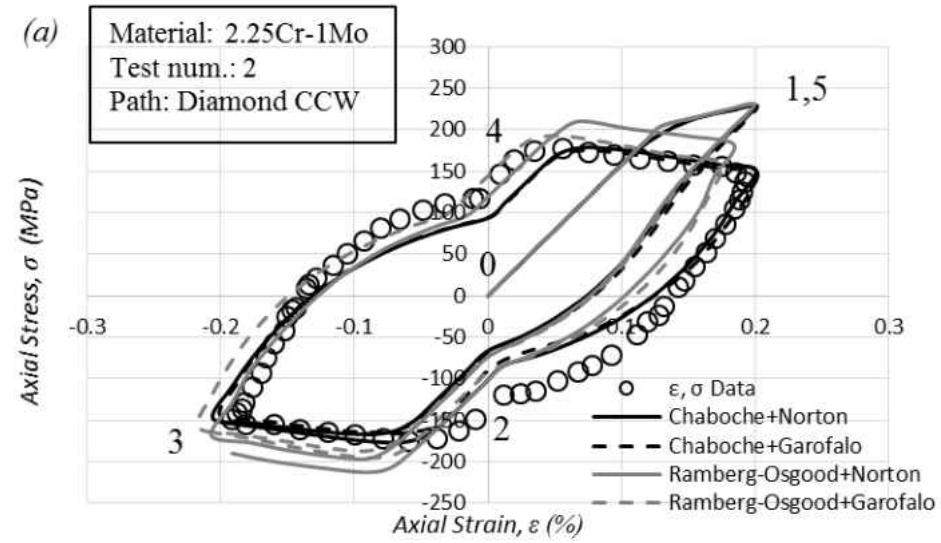

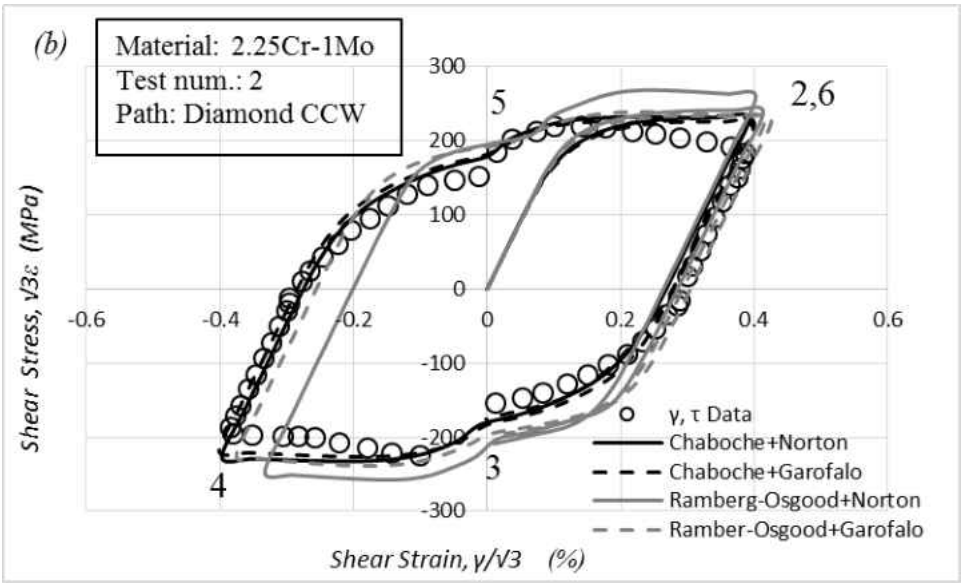

Figure 5.5: Comparison of stress-strain between the simulation and Inoue et al., 1994 results of 2.25Cr-1Mo Steel a) axial stress-strain, b) Shear stress-strain. Test 2(Inoue et al., 1994).

The third test, this test has Cruciform CCW loading path, and it used strain control. As mention in test 2 the simulation use displacement control which causes differences between the simulation and experiment results. In Figure 5.6 a. shows the axial versus shear strain for four models. Figure 5.6 b. shows the axial versus shear stress, and this simulation did under 600°C, and it did not show there significant differences between the models. In Figure 5.7, there are significant differences between the plasticity models, and these various because in Figure 5.9 c. shows the total strain is an almost plastic strain. In this test, the creep strain is nearby to zero, so the creep models in not affected. The model is affected plasticity model, and the plasticity models use Romberg-Osgood and Chaboche model. Figure 5.7 shows that the NLKH is closer to the experimental data more than isotropic hardening, so from the comparing between the experimental results and simulation results we know that the nonlinear kinematic hardening is more accurate than isotropic hardening. Test 2 and test 3 are shows the nonlinear kinematic hardening has a better fitting with experiment data, and it is more accurate than isotropic hardening.

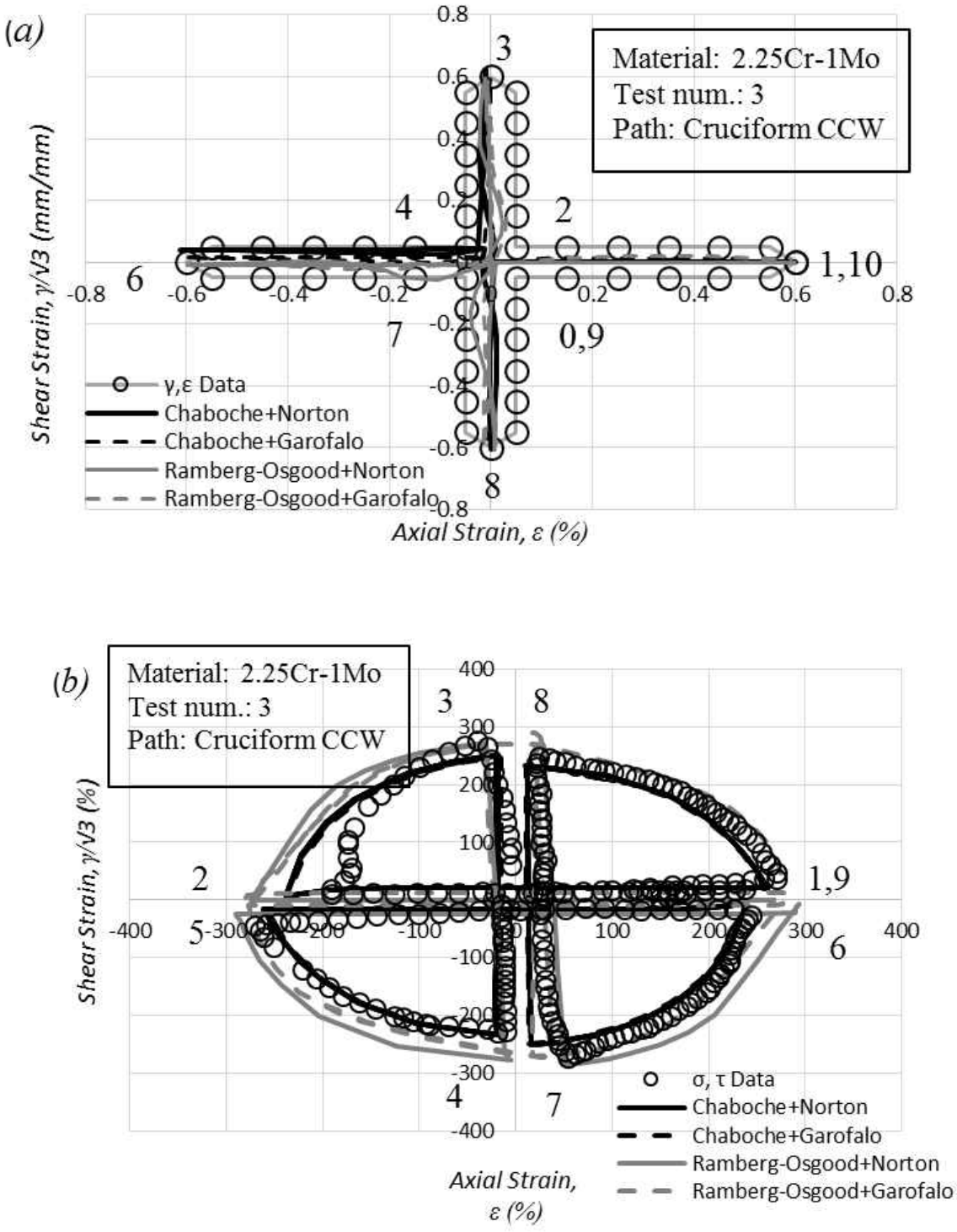

Figure 5.6: Comparing between the simulation and Inoue et al., 1989 a) The strain control of test 3, and b) Axial stress versus Shear Stress of test 3 (Inoue et al., 1989).

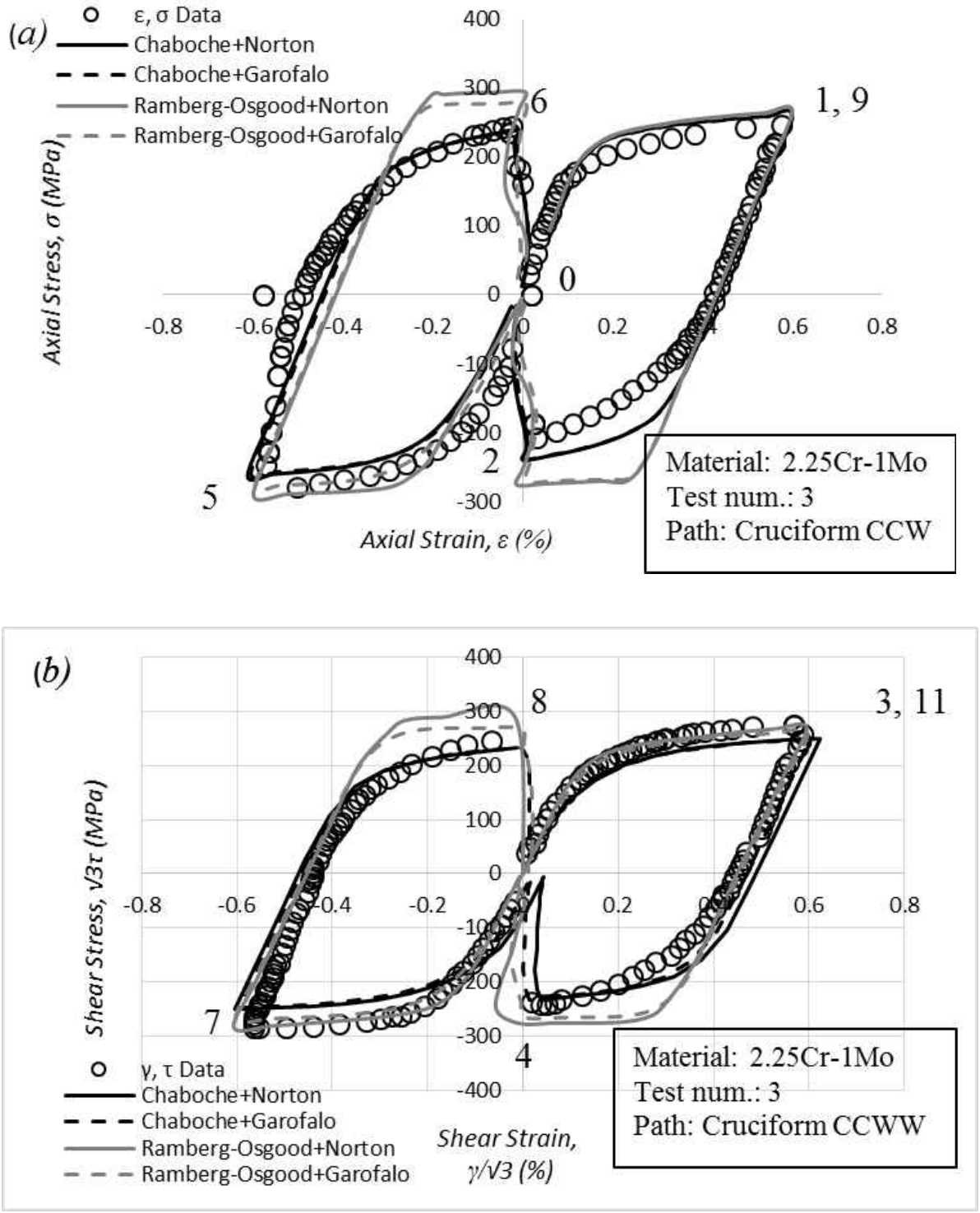

Figure 5.7: Comparison of stress-strain between the simulation and Inoue et al., 1989 results of 2.25Cr-1Mo Steel a) axial stress-strain, b) Shear stress-strain. Test 3 (Inoue et al., 1989).

The last test type is this study is Test 4, and this test has elliptical CCW loading path, and the controlled use of Test 4 is strain control, so the different minor cloud came from the simulation because the simulation used displacement control. In Figure 5.8 a. shows the axial versus shear strain, and b. shows the axial versus shear stress. The difference here is that there no difference between the plasticity and creep models. From Figure 5.9 d. shows that the plastic strain is bigger than the creep strain, but creep strain is not zero. Because test 4 has creep strain and plastic strain, so the plasticity and creep models will effect in this type of test. The elliptical CCW loading is one of the most complex conditions, and it difficult to control it.

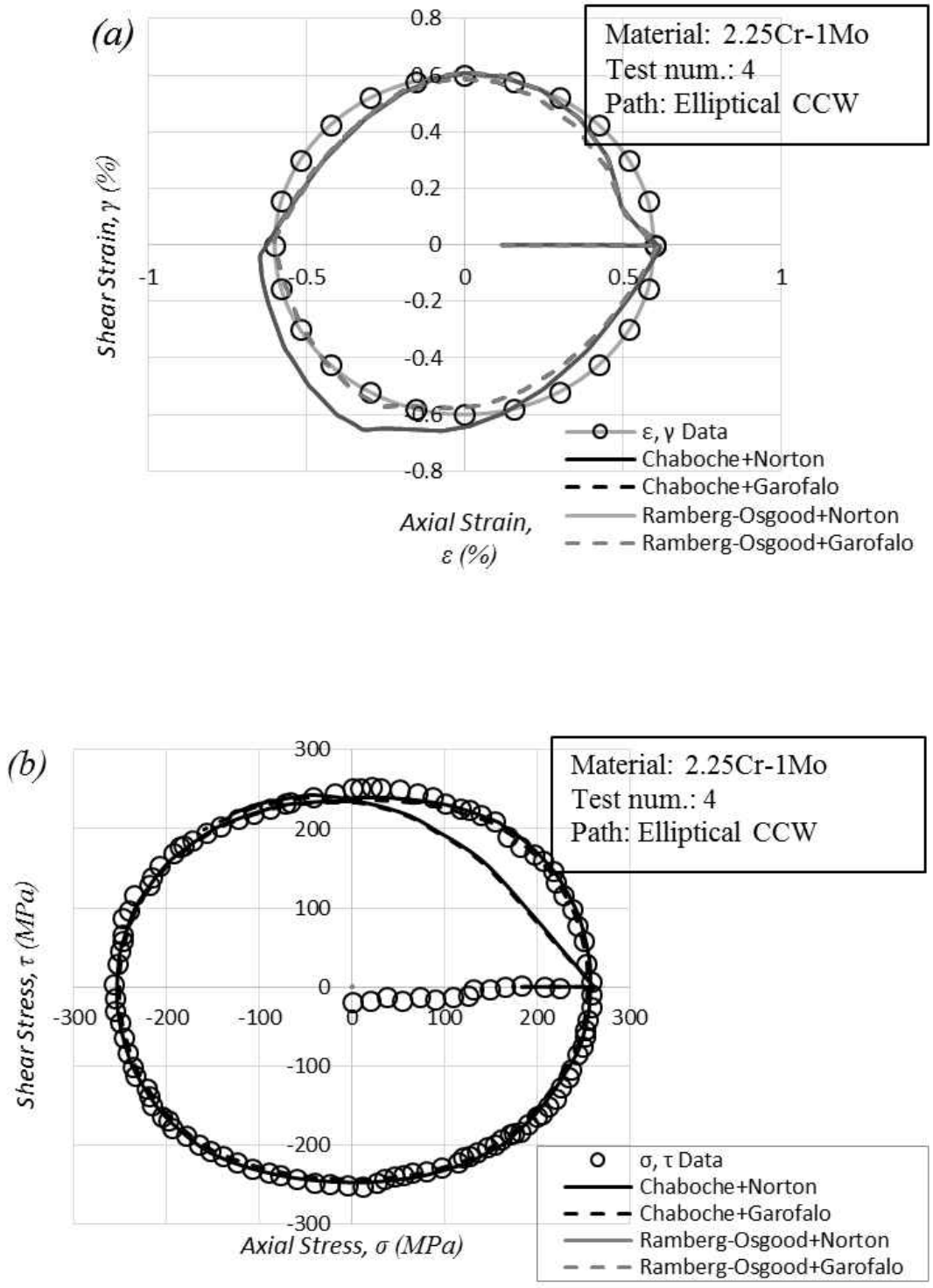

Figure 5.8: Comparison of between the simulation and Inoue et al., 1989 results of 2.25Cr-1Mo Steel a) Strain control, b) Axial stress versus shear stress. Test 4 (Inoue et al., 1989).

The simulation needs to modify the material properties to get results, which will be closer to the previous study's data. Also, the difference may come from the different kinds of heat treatments, and it could be the models used. In test 1 the total strain was close to creep strain, so the creep models made the difference between the simulation and experiment results. Garofalo model captures the multiaxial more accurately than the Norton model is this test. Test 2 used strain control and the total strain was an almost plastic strain, so the plasticity models affected in this type of test. Comparing between isotropic hardening and non-linear kinematic hardening will have that the non-linear kinematic hardening is more accurate because it captures the experiment data. Test 3 has the same impression from test 2, which is the plastic strain is closer to total strain, and creep strain is nearly zero. Non-linear kinematic hardening is more accurate in diamond CCW loading path and cruciform CCW loading path. Test 4 did not displays different between plasticity and creep models, and because the plastic strain is near to creep strain, so the models did not effect on simulation results. The study found that the more accurate plasticity model is non-linear kinematic hardening, and that found from the simulation results from test1 to test 4. On the other side, the Garofalo model captures the experiment result more than the Norton model. Chaboche-Garofalo model is the most accurate model have been using in the simulation. Garofalo is capture experiment data because it is curved, but Norton came as a straight line. In high temperature the stress in low creep strain rate is low, and to get better fitting need to use Garofalo model. Non-linear kinematic hardening model is better because this model has more constant than isotropic hardening, and it will capture more experimental data. The best comparison, which will be more accurate, will be between the simulation and actual experimental data. Now, the simulation is working which more important in this section because the proposal needs axial-torsion load data that will use in the next section.

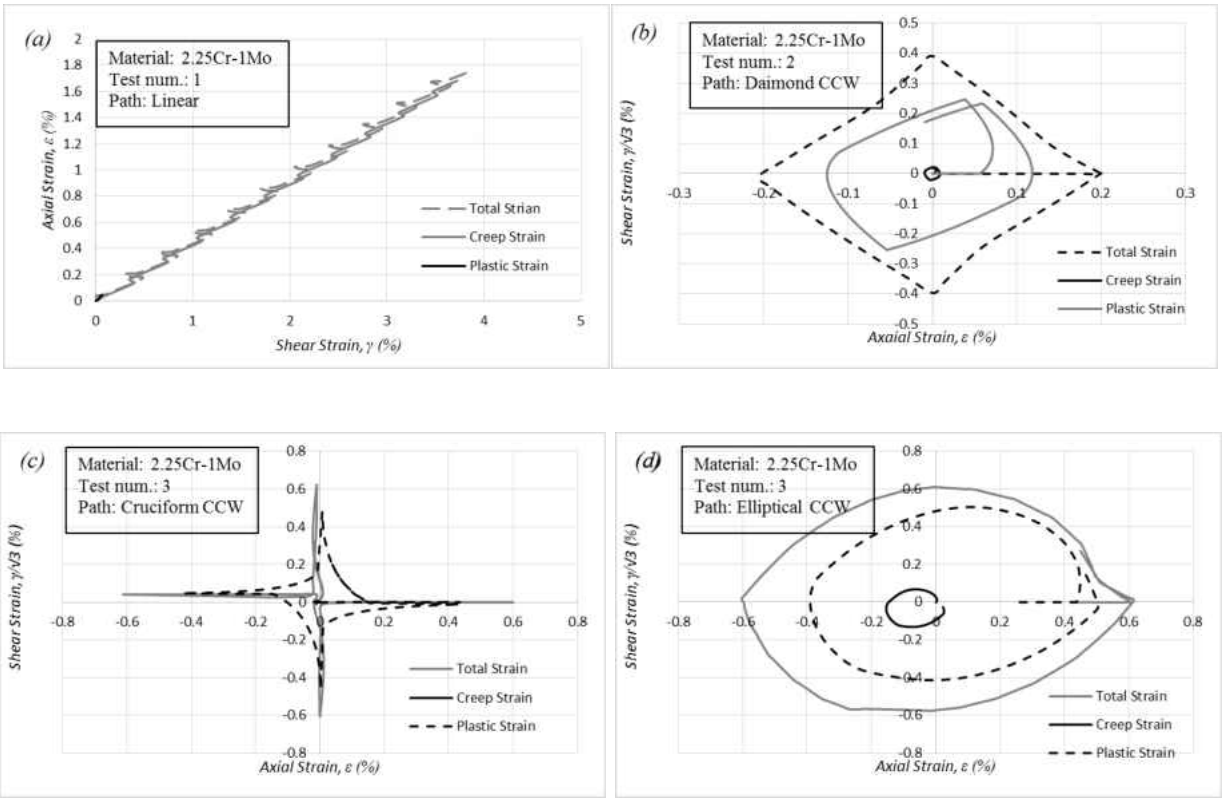

Figure 5.9: The strain for different tests a) Linear, b) Diamond CCW, c) Cruciform CCW, and d) Elliptical CCW.

5.3 Multiaxial FE Modeling for 304 Stainless Steel

This section is one of the most critical sections as it is used to compare the experiment results and the numerical simulation results. Through this, we can know if our simulation is working and if we can show that the material properties found in the experiment are correct. The study used the Chaboche model for plasticity properties and the Norton model for creep properties, with four various types of axial-torsional loading. All axial-torsional loading types came from the MOMRG lab. The material used in this research was 304 stainless steel.

5.3.1 Room Temperature

The first part contains the comparison between the simulation and experiments. The simulation described here was completed at room temperature, but with different conditions. Chapter 4 outlined various experiments conducted at room temperature, as shown in Table 4-1. Figure 5.10 shows the comparison between the simulation and the experiments, and also shows that it has a proper fitting. The plastic model used here is the Chaboche model, used because it has better results. The previous section used both the Ramberg-Osgood model and the Chaboche model, and shows that the Chaboche model captured the results better than Ramberg-Osgood model. The path used here is a linear path, so the axial loading is constant the shear is cycling. The control for these experiments was the angle of twist control. In general, the elastic range is situated perfectly between the simulation and experiments, and the plastic range is almost same between the simulation and experiments. The difference between the simulation and experiment could come from the model used in the simulation but still capture the experiment data. Creep properties were not utilized in this section because they occur at room temperature, which means there is no creep. Figure 5.10 a. shows there were small differences between the simulation and experiment, and for that reason could have some affect on the experiment, but in the elastic range returned perfect results. Figure 5.10 b. to d. show that the simulation was almost the same as the experiment results. From this simulation result, it can be concluded that the material properties extracted from the experiment were acceptable properties. The next section will include the creep properties because they occur at a high temperature. The next chapter will also show the procedure used to find the 304 stainless steel properties.

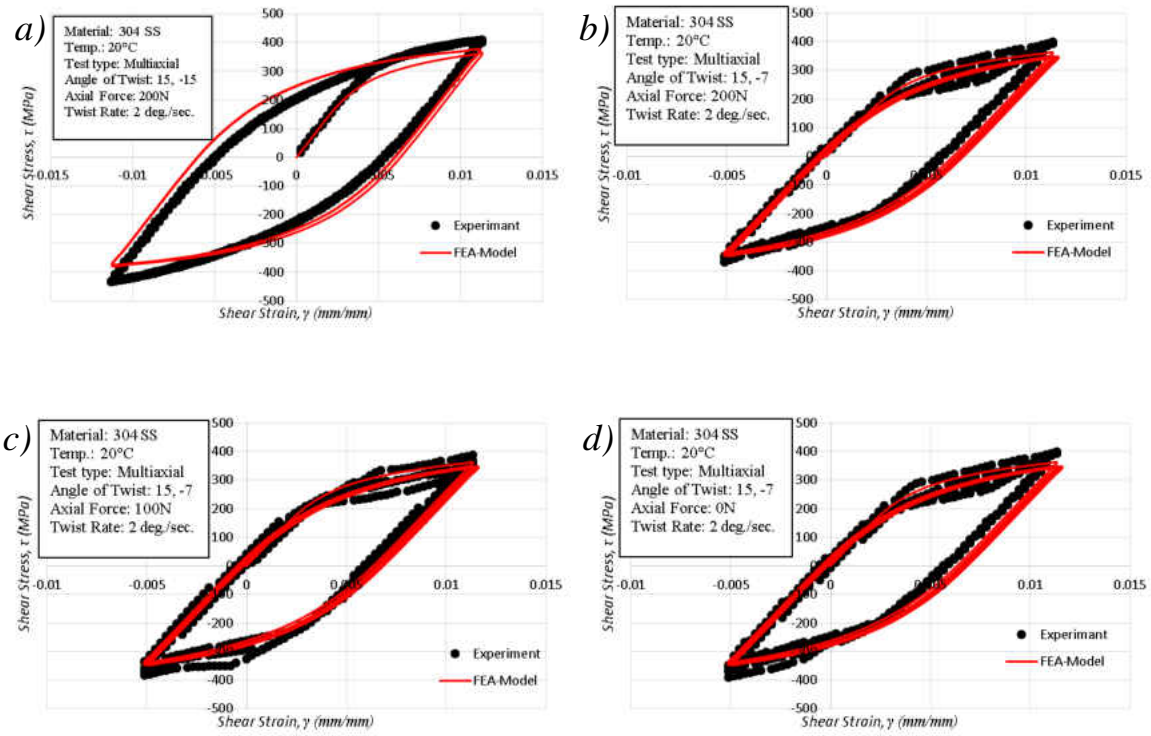

Figure 5.10: Shear stress versus shear strain for different simulation at room temperature a) AT-20°C-01, b) AT-20°C-02, c) AT-20°C-03, and d) AT-20°C-04.

5.3.2 High Temperature

In high temperatures, the main reason for comparison between the simulation and experiments, prove that the material properties found from experiment results was correct. Also, the challenge in high temperature was finding the elasticity, plasticity, and creep constants for 304 stainless steel. The key part in high temperature was finding the creep constants from the multiaxial loading, then converting the multiaxial creep parameters to uniaxial creep parameters. The simulation used in high temperature had a different condition, and the following chapter shows the procedure used to find the constant in high temperatures.

In the first simulation, the control used was the angle of twist. The angle was 15, -15 degrees with the angle of twist rate 0.5 degrees per second, and the axial force is 200 N. The plastic model used here was the Chaboche model; the reason for using that model because it has better results, the previous section used the Ramberg-Osgood model and Chaboche model and shows that the Chaboche model captures the results better than Ramberg-Osgood model, and finally because the creep model used in simulation is the Norton model. The path used here is a linear path, so the axial loading was constant the shear was cycling. The control for these experiments was the angle of twist control. hows the shear stress-strain curve for simulation and experiment. The figure shows that the curve, in general, is almost same as in the elastic range and that the simulation fit the experiment well. Next, the plasticity and creep were compared for the simulation and the experiment, and in this part, the simulation is fit the experiment result perfectly. The experiment results show the shear stress dropping then going back again repeatedly; this happened in the first cycles and is called *Dynamic recrystallization*. Dynamic recrystallization (DRX) is different from static recrystallization as when the grains grow, new grains happen through a

deformation in high temperatures. Finally, the simulation captured the experiment result, so the material properties extracted from the experiment were acceptable properties.

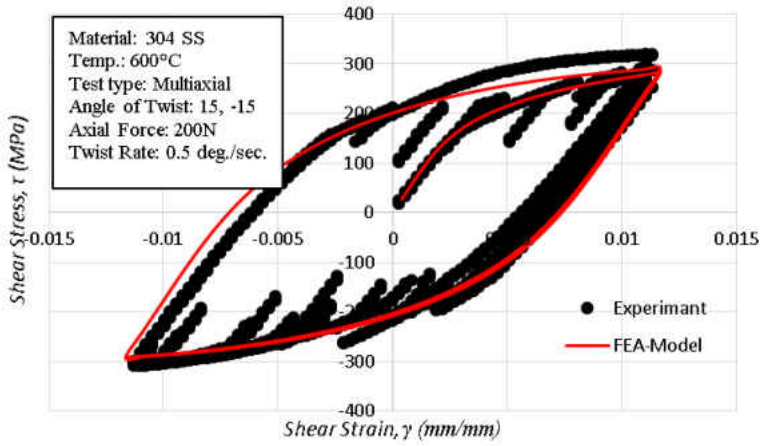

Figure 5.11: Simulation and experiment for AT-600°C-01.

Next, the simulation was compared with experiments in different conditions, so in this simulation the control used was the angle of twist for shear load and for the axial load was force. The angle of twist used here was 15, -7 degree and the angle of twist rate was 0.5 degrees per second. The axial load applied in this simulation was 200 N. The plasticity model used in the simulation was the Chaboche model, and the reason from that was the Chaboche model captured the experiment results better than other models. The creep model used was the Norton model. In this simulation, the axial load was constant during the test, and the shear loading was cycling. Figure 5.12 shows the shear stress-strain curve for simulation versus the experiment results, and from this comparison the simulation elastic results were the same as the experiment result. Moreover, the simulation curve fit the experiment curve, but there was a difference when the shear was going from the positive to the negative direction. The reason could be the plasticity model used in simulation, because the plasticity model used here had the average plasticity and creep

parameters for all experiments at 600°C. As a final point, the simulation captured the experiment result, so the material properties extracted from the experiment were acceptable properties.

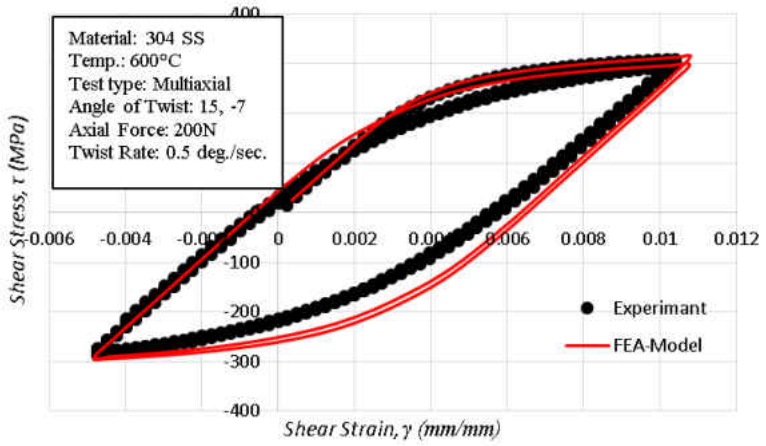

Figure 5.12: Simulation and experiment for AT-600°C-02.

The comparison of simulation results and experiment results for AT-600°C-05, and the control used was the angle of twist for shear load, and for the axial load was a force. This experiment used the specimen for a different angle of twist rate, starting with 0.00025 degrees per second increasing to 0.25 degrees per second. The angle of twist used here was 16, -16 degrees and the angle of twist rate was 0.5 degrees per second. The axial load applied in this simulation was 200 N. The plasticity model used in the simulation was the Chaboche model, and the reason was that the Chaboche model captures the experiment results better than other models, and the creep model used was the Norton model. In this simulation, the axial load was constant during the test, and the shear loading was cycling. Figure 5.13 shows the shear stress-strain curve for simulation versus the experiment results with a different angle of twist rate. Figure 5.13 a shows the shear stress-strain curve for 0.25 degrees per second, and the elastic range was same between the simulation and experiment, but the yield point was different. The specimen used in this

experiment utilized a different angle of twist rate, so the yield was different because the material softened after some cycles. In this condition, the simulation shear stress was higher than the experiment shear stress, and as mentioned before the specimen was used for an extended period time, so it could have been softening. In general, the simulation results fit the experiment results perfectly, so the material properties found from the experiment result were correct, and it proved that the new method used was accurate.

Figure 5.13 b shows the shear stress-strain curve for 0.025 degrees per second, and the elastic range was same between the simulation and experiment. Furthermore, the yield point was almost the same as the experiment yield point. The specimen used in this experiment used for a different angle of twist rate so there was some difference between the yield point of simulation and the experiment, but in this condition, the simulation yield point was same yet the experiment yield point was different because the material was softening after a number of cycles. In this condition, the simulation shear stress was higher than experiment shear stress, and as mentioned previously the specimen was used for a length of time, so it could have been softening. The simulation curve fit the experiment curve, but there was a difference in the shear stress. The reason could be the plasticity model used in simulation, because the plasticity model used here was of the average plasticity and creep parameters for all experiments at 600°C.In general, the simulation results fit the experiment results perfectly, so the material properties found from the experiment results were correct and it proved that the new method used was accurate.

Figure 5.13 c shows the shear stress-strain curve for simulation and experiment at 0.0025 degrees per second. The first part is the elasticity section; the elastic simulation is equal to elastic of the experiment. In general, the simulation results fit the experiment results perfectly, but there

are some differences between the simulation and the experiment. Also, as mentioned before, this specimen was used many times, so the material could be softening. The simulation shear stress was higher than the experiment shear stress, and this came from the plasticity and creep parameters. In the second cycle, the shear stress was less than the first cycle, and the changing of the shear stress came from the creep properties. The creep properties used in this simulation were accurate, so the material properties found from the experiment result were correct, proving that the new method used was accurate. As a final point, the simulation captured the experiment result, so the material properties extracted from the experiment were acceptable properties. Figure 5.13 d. shows the shear stress-strain curve for simulation with a different angle of twist rate, and also shows the maximum shear stress for all was the same in the first cycle, and that the minimum shear stress was different with a different angle of twist rate. Thus, the creep had an effect on the simulation results. During the second cycle, the maximum shear stress was different with a different angle of twist rate, so the maximum shear stress decreased with decreasing the angle of twist rate. The summary for the simulation in this condition is that the simulation was working and the material properties found from the multiaxial experiment converted to uniaxial were perfect.

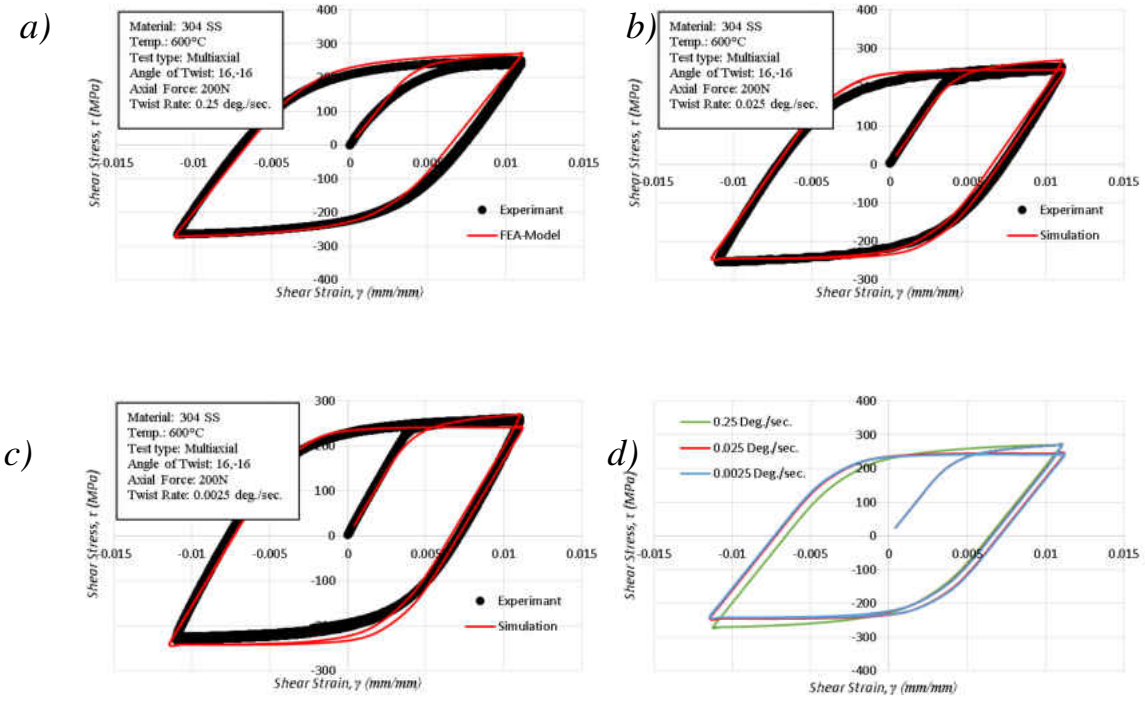

Figure 5.13: Shear stress-strain curve for simulation and experiment for AT-600C-05 with different angle of twist rate a) 0.25 degree/sec, b) 0.025 degree/sec, c) 0.0025 degree/sec, and d) simulation for all different rates.

The last type of comparison between the simulation and experiment are concerned with dwell time. The main difference is this simulation used dwell time, and the reason for using it in this type of experiment was to see the relaxation curve and also to determine if the creep constants could be found from the relationship between the relaxation and creep. The control used this simulation was the angle of twist for shear load, and for the axial load was force. The angle of twist used here was 16, -16 degrees and the angle of twist rate was 2 degrees per second. Also, dwell time was added in this simulation, and the relaxation showed that the creep parameters found from the multiaxial experiment were accurate. The axial load applied in this simulation aws 200 N. The plasticity model used in the simulation was the Chaboche model, and the reason for that is the Chaboche model captures the experiment results better than other models. The creep model

used was the Norton model. In this simulation, the axial load was constant during the test, and the shear loading was cycling. The elasticity of simulation and experiment was almost the same, and for the relaxation of the simulation was the same as experiment exactly. This means that the creep constant applied on the simulation was accurate, and the new method used to extract the creep parameters from the multiaxial loading was also accurate. By looking at the curve in the negative section, the simulation is different from the experiment. The reason for the difference in the negative section is that the specimen was used for many cycles. The experiment used this specimen with a 2-minute, 20-minute, and then a 200-minute dwell time, and the relaxation was perfect at 200 minutes. This is the reason for the difference between the simulation and the experiment in the negative section on shear stress. In general, the simulation curve fit the experiment curve, and this proves that the constants used in the simulation were accurate. This chapter proves that the new method used to find the plasticity and creep parameters from the multiaxial load converted to uniaxial parameters is accurate. This parameter found that even when using simulation with different conditions, all of these experiments fit the results with changed conditions.

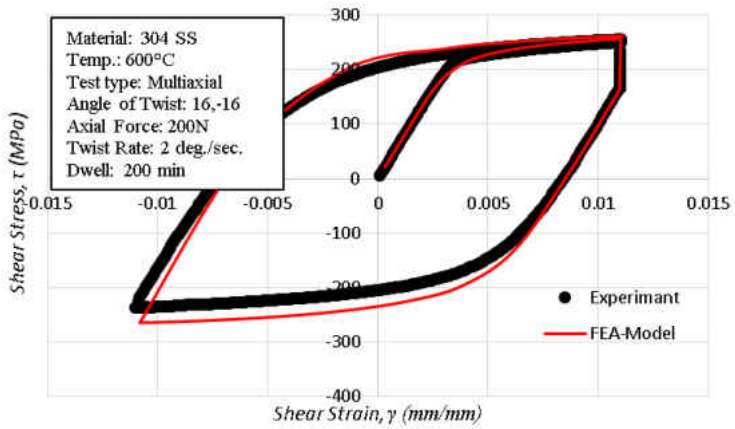

Figure 5.14: Shear stress-strain curve for AT-600°C-06 with dwell time.

CHAPTER 6 ELASTICITY, PLSTICITY, AND CREEP PARAMETER FROM MULTIAXIAL

The present study used experiments to extract constitutive model properties of 304 stainless steel. The properties found here correspond to three temperatures (20°C, 500°C, and 600°C). Room temperature was used to determine the elasticity properties and plasticity properties. High temperatures were used to determine the elasticity, plasticity, and creep properties for 304 stainless steel. The first deformation model the experiments was determined from elasticity by determining the slope of the elastic range for each temperature. The next step was plasticity modeling via Ramberg-Osgood. Finally, the creep properties were found at high temperatures, such as 600°C.

6.1 Material Properties at Room Temperature

At room temperature there are four different experiments. The slope found from the elastic range is the shear modulus, as shown in Figure 6.1. Elasticity properties for the material are acquired easily. Then the uniaxial elastic modulus, *E*, is established assuming isotropy.

$$E = 2(1+\nu)G \qquad (6.1)$$

The Poisson's Ratio is assumed as 0.3 at room temperature consistent with most steel in literature.

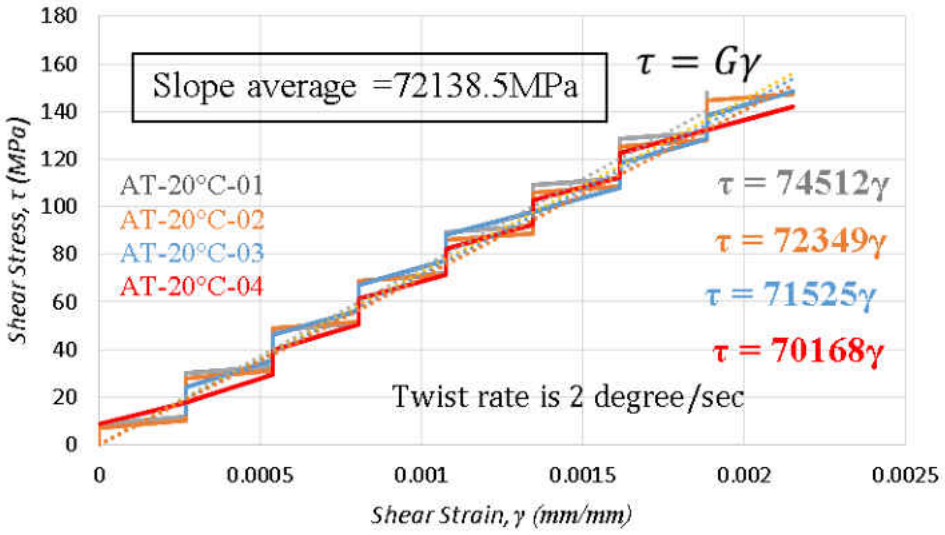

Figure 6.1: Elastic modulus for 304 stainless steel at room temperature.

The next part of this study focused on the plasticity properties for 304 stainless steel at room temperature. The Ramberg-Osgood constants found here are K_s' and n_s'. As mentioned previously, the shear loading is the main load for this study, so the Ramberg-Osgood constants are shear Ramberg-Osgood parameters. This study assumes von Mises-type yielding and isotropy. The shear correction is 0.577. No change is needed in the strain hardening exponent, i.e.

$$K = K_s/\sqrt{3} \qquad (6.2)$$

$$n = n_s \qquad (6.3)$$

A uniaxial Ramberg-Osgood parameter found from shear constant is illustrated in Figure 6.2. The second model is the Chaboche model, and a Chaboche constant was obtained from the Ramberg-Osgood parameter by using Thomas techniques (Bouchenot et al., 2016a).

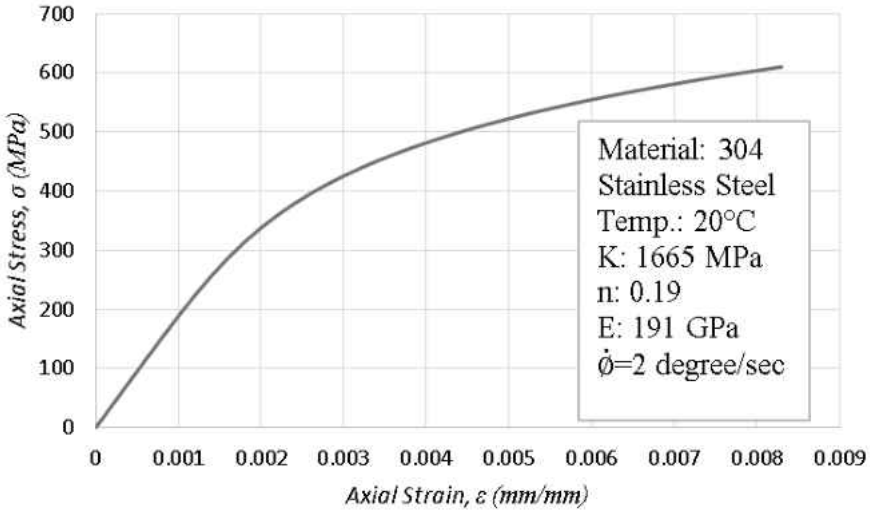

Figure 6.2: Tensile response of 304 steel via Romberg-Osgood model.

6.2 Material Properties at 500°C

This section follows the same approach as the one employed at room temperature, but the difference is that this experiment was conducted at 500°C. Here used the same equations which are used in the room temperature. The material properties found from the experiment is shear properties then it converted to axial properties. The Poisson's Ratio is assumed as 0.29 at room temperature consistent with most steel in literature.

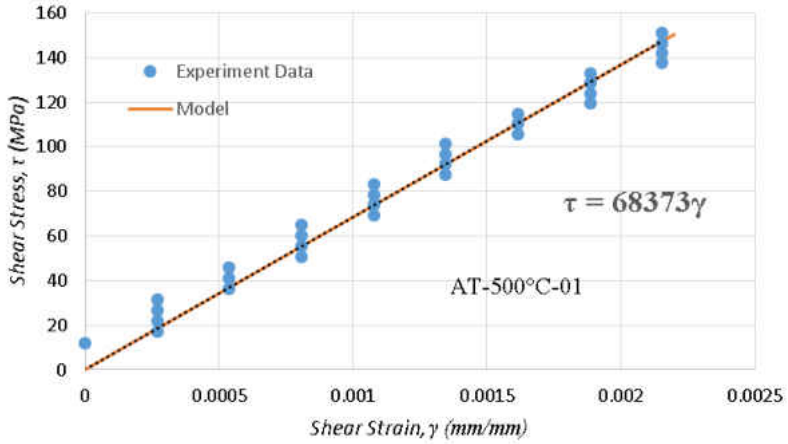

Figure 6.3: Elastic modulus for 304 stainless steel at 500°C

Plasticity properties were determined at 500°C for 304 Steel. The second important material properties were the plasticity properties for 304 stainless steel at 500°C. The first model used here was shear Romberg-Osgood, then from the shear properties determined the uniaxial Romberg-Osgood constants. The reason for that it is easy to find the curve fitting with Ramberg-Osgood. As mentioned previously, a 0.577 correction was applied. The uniaxial Ramberg-Osgood parameter found from shear constant is shown in Figure 6.4.

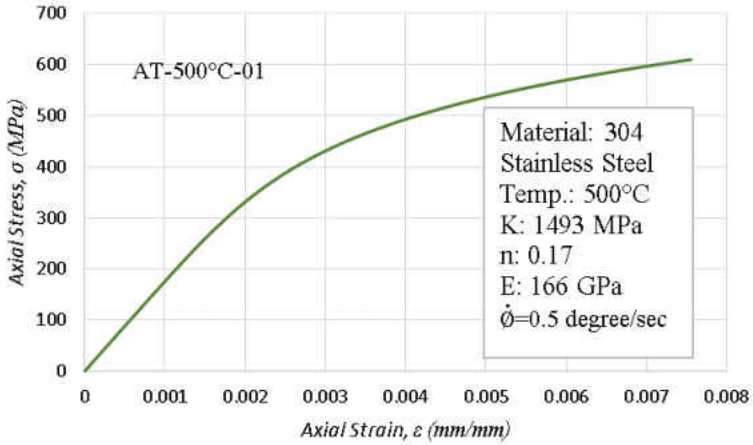

Figure 6.4: Stress versus strain at 500°C for Romberg-Osgood model

6.3 Material Properties at 600°C

At 600°C, the experiment was conducted for 304 stainless steel. This section follows the same approach as the one employed at room temperature. In this used different temperature which is 600°C. Here used the same equations which are used in the room temperature. The material properties found from the experiment is shear properties then it converted to axial properties. The Poisson's Ratio is assumed as 0.28 at room temperature consistent with most steel in literature.

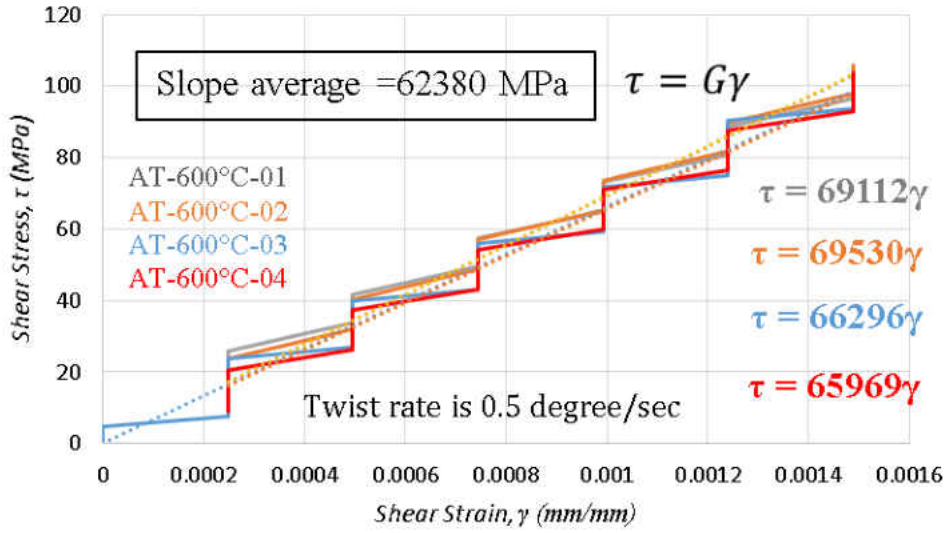

Figure 6.5: Elastic modulus for 304 stainless steel at 600°C

The next part of this study was the plasticity properties were determined for 304 stainless steel at 600°C. The first model used here was shear Romberg-Osgood; then from the shear properties the uniaxial Romberg-Osgood constants were found. The reason for that was that by using the Ramberg-Osgood model, it is easy to find the curve fitting. The main idea of finding the Chaboche model parameter was to use the Chaboche model in the simulation. The Chaboche model is more accurate than the Ramberg-Osgood because the Chaboche model captures the curve

fitting better than the others models. A uniaxial Ramberg-Osgood parameter was found from a shear constant, as shown in Figure 6.6. In Table 6-1 shows the 304 stainless steel elasticity, and Table 6-2 is showing the Ramberg-Osgood constants, and Table 6-3 is showing the Chaboche constants for 304 steel with various temperatures.

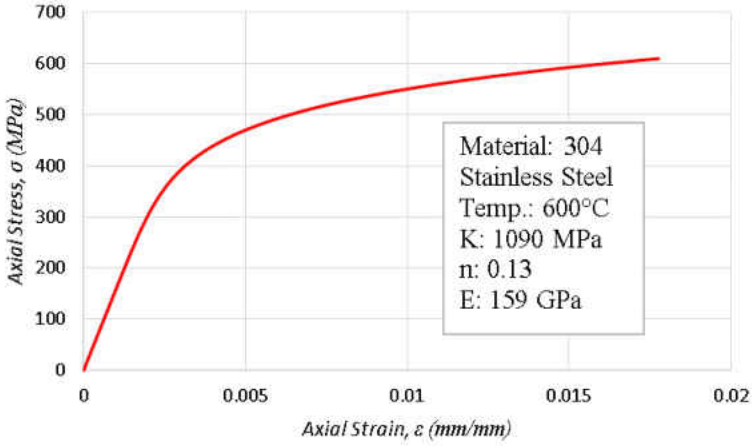

Figure 6.6: Stress versus strain at 600°C for Romberg-Osgood model.

Table 6-1: Elasticity properties of 304 stainless steel with various temperatures

Elasticity properties		
T °C	Shear Elastic Modulus, G GPa	Uniaxial Elastic Modulus, E GPa
20	73	191
500	68	158
600	62	159

Table 6-2: Ramberg-Osgood constants of 304 stainless steel with various temperatures

Plasticity properties Romberg-Osgood Model				
T	**Shear Monotonic Plasticity Coefficient,** K_s	**Shear Monotonic Plasticity Exponent,** n_s	**Uniaxial Monotonic Plasticity Coefficient,** K	**Uniaxial Monotonic Plasticity Coefficient,** n
°C	MPa		MPa	
20	960	0.19	1664	0.19
500	882	0.17	1583	0.17
600	629	0.13	1089	0.13

Table 6-3: Chaboche constants of 304 stainless steel with various temperatures

Plasticity properties Chaboche Model						
T	$C1$	$\gamma 1$	$C2$	$\gamma 2$	$C3$	$\gamma 3$
°C	MPa		MPa		MPa	
20	1312169	12630	175546	1992	73124	289
500	1350727	12252	173741.4	2398	82162	334
600	1087429	12424	126780	1755	43770	270

Finding the creep constant from the multiaxial loading was the most challenging part of this research. There were two separate approaches attempted to identify the Norton steady state creep constants. The first approach involved cycling the material at various rates and observing the stress. The next approach focused on shear stress relaxation during dwell periods.

For the first approach, the angle of twist control was used with a different angle of twist rate; so the first rate was 0.00025 degree per second then 0.0025, 0.025, and 0.25 degree per second. Figure 6.7 shows the maximum shear stress was almost identical across the different twist rates as shown in the solid circle, but in minimum shear stresses were different with a different angle of a twist as shown in the dotted circle. In this study, the difference between the minimum stresses can

be used to find the creep constants. Figure 6.8 shows the shear stress versus shear strain rate, the shear strain used here was the minimum shear stresses. The model used here to find the creep constants was the Norton model, and the constants found here were A_s and n_s. Afterwards, the Norton constants were found under uniaxial load.

$$A = A_s/\sqrt{3} \qquad (6.4)$$

The relation used here is the same relation between the axial and shear stress/strain. Most researcher used this relation, but for n constant obtain from the simulation. In the first try, there were problem with dwell section between the simulation and experiment result, and when the n change the dwell section was working very well.

$$n = n_s/0.9 \qquad (6.5)$$

To show the procedure utilized here was accurate, the research was simulated and compared to the experimental results with simulation results. This is first way creep parameters were found, as shown in Table 6-4.

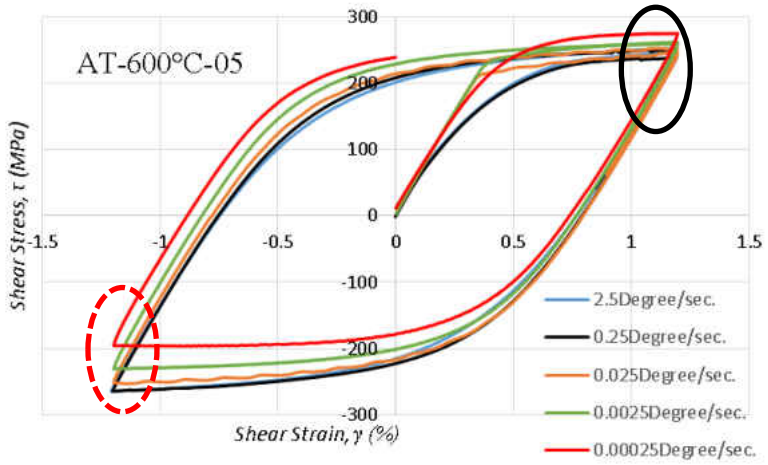

Figure 6.7: Shear stress-strain curve with different angle of twist rate

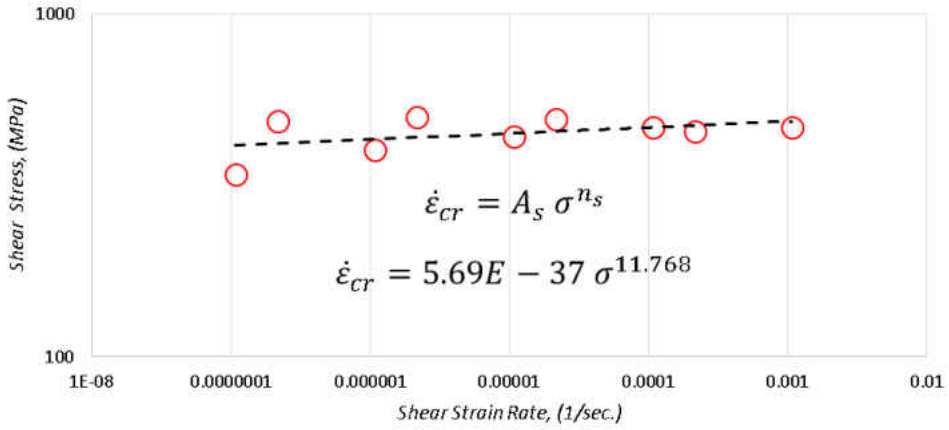

Figure 6.8: Shear stress versus shear strain rate

Shear stress relaxation was used to find the creep constants. The dwell times used here were 2 minutes, 20 minutes, and 200 minutes, to allow the matrix to relaxation. Figure 6.9 shows that the relaxation was nearly identical across dwell times; the dotted circle shows the relaxation curve with different dwell times. The solid circle shows minimal variation in dwell response even with a small axial load. The procedure used to find the shear creep constant by the relation between the relaxations and creep is shown.

$$\dot{\gamma}_{total} = \dot{\gamma}_{el} + \dot{\gamma}_{cr} = 0 \qquad (6.6)$$

$$\dot{\gamma}_{el} = -\dot{\gamma}_{cr} = -A_s \tau^{n_s} \qquad (6.7)$$

$$\dot{\gamma}_{el} = \frac{\dot{\tau}}{G} \qquad (6.8)$$

$$Error = \sum_{i=1}^{m} \left(\frac{\dot{\tau}}{G} - A_s \tau^{n_s} \right) \qquad (6.9)$$

The procedure used here to find the creep constants to fit the curve by using the scroll bar in Excel. Figure 6.10 shows the relaxation curve from the experiment and the model used, and this model fit the best. The model in Figure 6.10 has the best fit and also the minimum error value, and this did by used regression analysis. This is the second way to find the creep constants ant the constants compared the first way, which is to find the creep constant by experimenting with the different shear rates. From the simulation, the study found that the creep constants determined from the relaxation were more accurate than by using different shear strain rates. Norton constants were found here from shear, then an attempt was made to find the uniaxial creep parameters. The ns constant was equal 0.9 *n* constant, and A_s constant was equal to 1.732 times *A* constant. One of the most important aspects of this study is that a relationship was found between the A_s and ns, so when the ns was increasing the A_s was decreasing. Table 6-4 shows the Norton parameters found

from the relaxation. The comparison between the experiment results with simulation result proves that the constants found from relaxation was best model used. In this study was using the creep constants came from relaxation because more accurate that creep constants came from different shear strain rate. Also, this study prove that the creep constants can found from the relaxation.

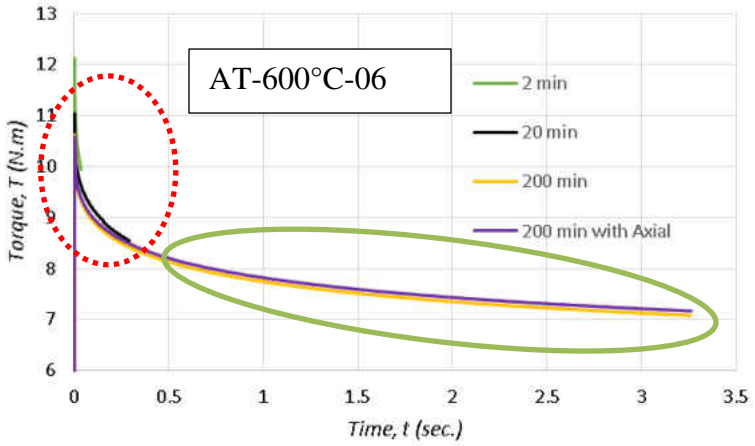

Figure 6.9: Relaxation for 304 stainless steel at high temperature

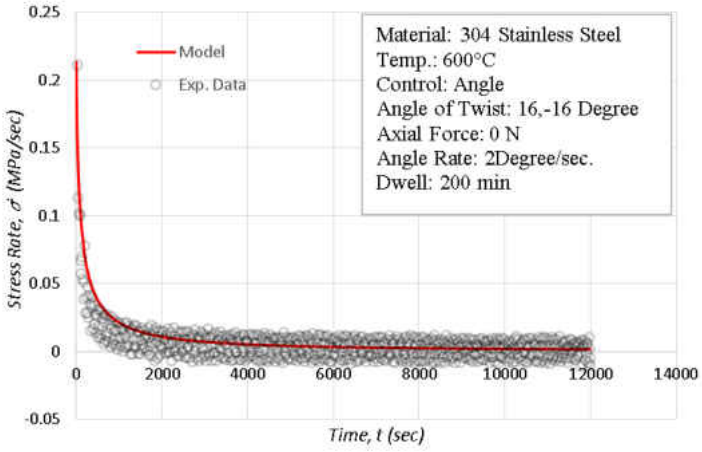

Figure 6.10: Shear stress relaxation modeling.

Table 6-4: Norton parameters found from different shear strain rate and relaxation

Different Shear Strain Rate				
Temperature °C	A_s $(\mathrm{MPa}^{-n} - hr^{-1})$	n_s Unitless	A $(\mathrm{MPa}^{-n} - hr^{-1})$	n Unitless
600	5.69E-37	11.77	9.86E-37	10.47
Relaxation				
Temperature °C	A_s $(\mathrm{MPa}^{-n} - hr^{-1})$	n_s Unitless	A $(\mathrm{MPa}^{-n} - hr^{-1})$	n Unitless
600	4.625E-44	16.024	8.016E-44	14.261

6.4 Bree Diagram

In this section is building the Bree diagram for axial-torsion loading and 304 stainless steel material, the main reason from the Bree diagram is dividing the test to different regimes. Bree diagram will show the researcher in which regimes they will be before they do the test. For example, the researcher would study the material behavior on ratcheting regimes, and they do not want to study the material in elastic regime, so Bree diagram give researcher which load they need. Mainly, ratcheting is evaluated by using Bree diagram which developed by constant axial load and cyclic shear loading.

6.4.1 Torque Control

The modified Bree diagram is used to capture the different regimes, as shown in Figure 6.11. In this figure the *x*-axis is the axial stress over axial yield stress, and the *y*-axis is the shear stress over shear yield stress, so the maximum axial stress over axial yield stress used in *x*-axis is 1.25, and the maximum shear stress over shear yield stress used in *y*-axis is 2. The control used to build this modified Bree diagram is torque control. The stress regimes are shown in Table 6-5, so Rp is plastic ratcheting, Rcr is plastic creep ratcheting, P plastic, and E is elastic. As

shown in the figure, the same guidance allows users to predict the threshold between regions based on elastic properties analytically.

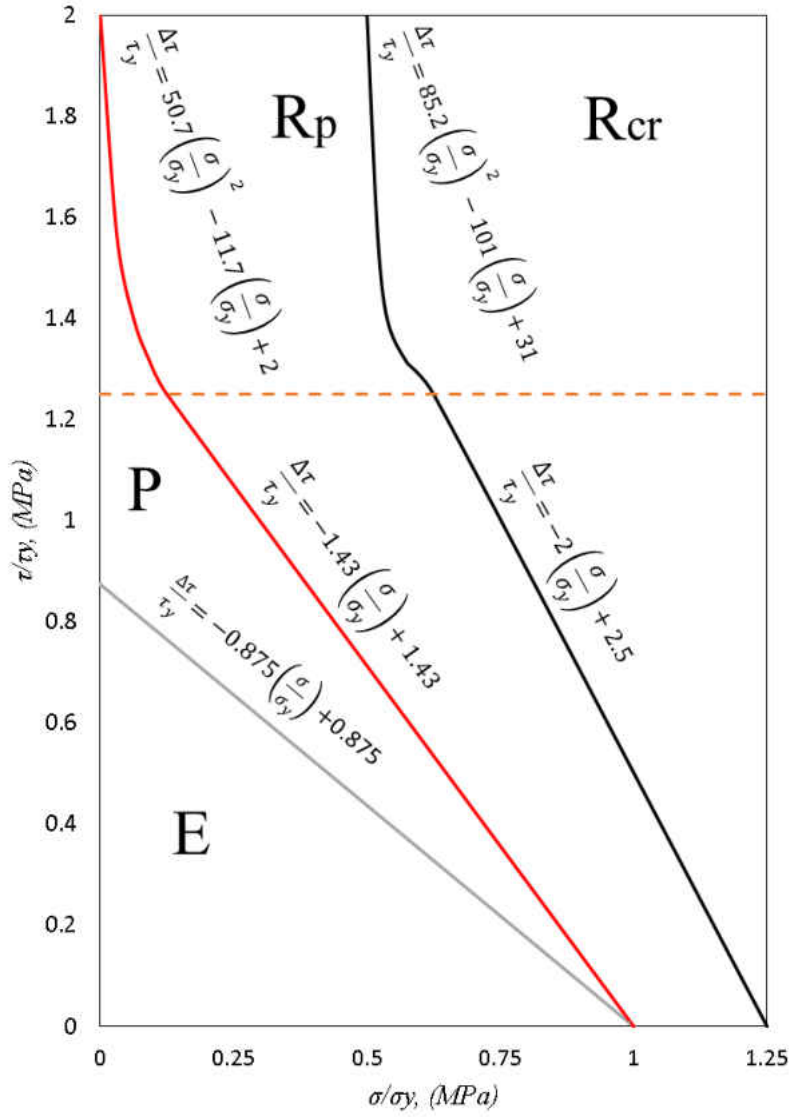

Figure 6.11: Modified Bree diagram for multiaxial loading (Torque control).

Table 6-5: Bree diagram regimes for axial-torsional loading

Stress regime	***Behavior***
E	Elastic
P	Plastic
R_P	Plastic Ratcheting
R_{cr}	Plastic Creep Ratcheting

Figure 6.12 is showing the elastic, plastic, plastic ratcheting, and plastic and creep ratcheting regimes obtained from the modified Bree diagram. Figure 6.12 a in the elastic regimes, so there is no deformation on that regime. By have a series number of simulation to build the modified Bree diagram, so when the equivalent strain is less the 0.0005 mm/mm that mean it is elastic. The plastic regime for modified Bree diagram when the equivalent strain is higher than 0.0005 mm/mm and less the 0.0007 mm/mm as shown in figure b. Next, the plastic ratcheting when the equivalent strain is higher than 0.0007 mm/mm, and it less than 0.001 mm/mm. Figure 6.12 c shows the ratcheting, but the total strain is almost plastic strain, and there are no creep strain. The last regimes is creep ratcheting, and this regime has creep and plastic strain. Also, in this regime the distance between the cycles to the other cycle is higher than the distance in plastic ratcheting, and this regime when the equivalent strain more than 0.001 mm/mm. Figure 6.15 shows the axial strain versus shear strain for different regimes of modified Bree diagram. In plastic regimes, the shear strain has plastic strain then it came constant. Plastic ratcheting shows the shear strain is same for each cycle, but the axial strain is increasing with each cycle as shown in

Figure 6.15 c. the last regimes is creep ratcheting, so the axial strain and shear strain is increasing from cycle to other cycle as shown in Figure 6.15, the reason from that the creep strain.

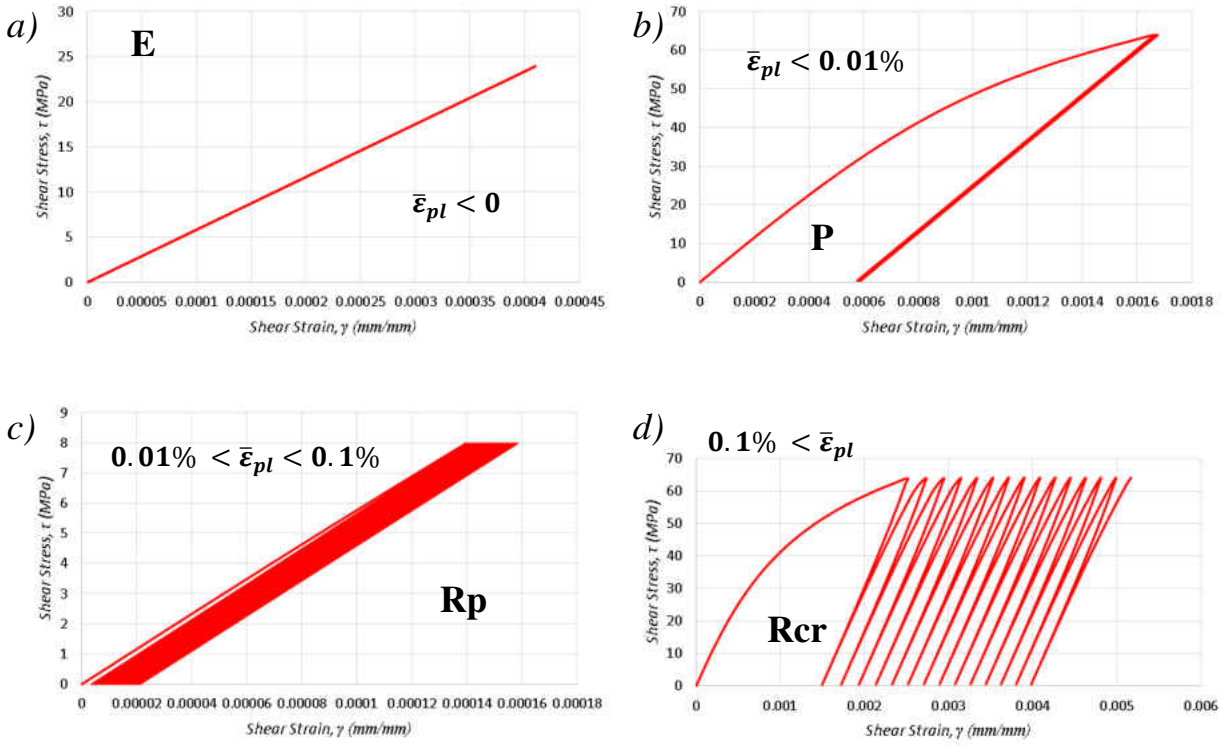

Figure 6.12: The regimes for modified Bree diagram (Torque control) a) elastic, b) plastic, c) plastic ratcheting, and d) plastic and creep ratcheting.

6.4.2 Twist Control

Second part of modified Bree diagram build with angle of twist control, and the reason from that to found the different between the torque and twist control. In the torque control have elasticity, plasticity, and ratcheting regimes, but when the angle of twist control used the Bree diagram will have elasticity, plasticity, and shakedown. So, the main differences between the two different controls are ratcheting and shakedown. The modified Bree diagram with twist control is used to capture the different regimes, as shown in Figure 6.15. In this figure the *x*-axis is the axial stress over axial yield stress, and the *y*-axis is the shear stress over shear yield stress, so the

maximum axial stress over axial yield stress used in *x*-axis is 1, and the maximum shear stress over shear yield stress used in *y*-axis is 2. The control used to build this modified Bree diagram is angle of twist control. The stress regimes are shown in Table 6-6, so Sp is plastic ratcheting, Scr is plastic creep ratcheting, P plastic, and E is elastic. As shown in the figure, the same guidance allows users to predict the threshold between regions based on elastic properties analytically. Figure 6.15 shows two different lines, and the differences between these two is the strain rate. In the solid lines the strain rate use are 1e-3 sec^{-1}, and the dash lines used strain rate 1e-6 sec^{-1}. The main reason from that is found the Bree diagram response with changing the strain rate.

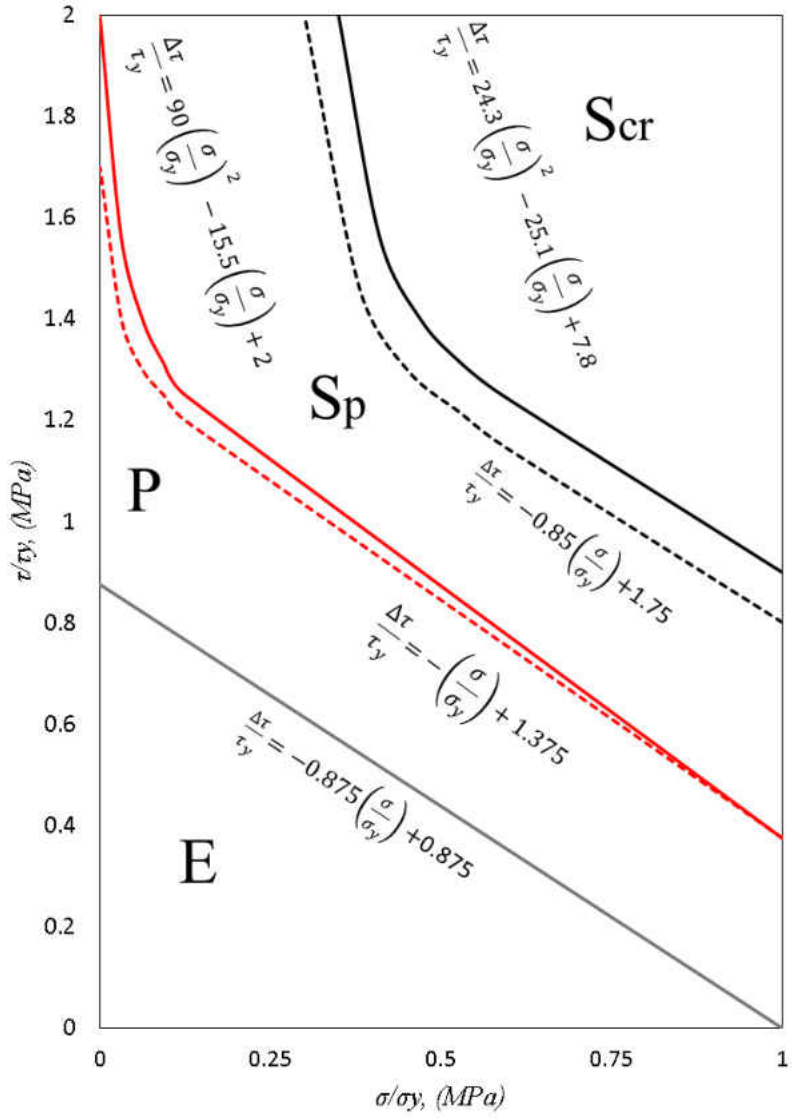

Figure 6.13: Modified Bree diagram for multiaxial loading (Twist control).

Table 6-6: Modified Bree diagram regimes for axial-torsional loading (Twist control)

Stress regime	***Behavior***
E	Elastic
P	Plastic
S_P	Plastic Shakedown
S_{cr}	Plastic Creep Shakedown

Figure 6.14 is showing the elastic, plastic, plastic shakedown, and plastic and creep shakedown regimes obtained from the modified Bree diagram with twist control. Figure 6.14 a shows the elastic regimes for modified Bree diagram with twist control, so there is no deformation on that regime. By have a series number of simulation to build the modified Bree diagram with twist control, so when the equivalent plastic strain is zero that mean it is elastic. The plastic regime for modified Bree diagram with twist control when the equivalent plastic strain is less than 0.01% as shown in Figure 6.14 b. Next, the plastic shakedown when the equivalent plastic strain is higher than 0.01%, and the equivalent plastic strain less than 0.1%. Figure 6.12 c shows the Shakedown, but the total equivalent strain is almost equivalent plastic strain, and there are no creep strain. The last regimes is creep shakedown, and this regime has creep and plastic strain. Also, in this regime the distance between the cycles to the other cycle is higher than the distance in plastic shakedown, and this regime when the equivalent plastic strain more than 0.1%.

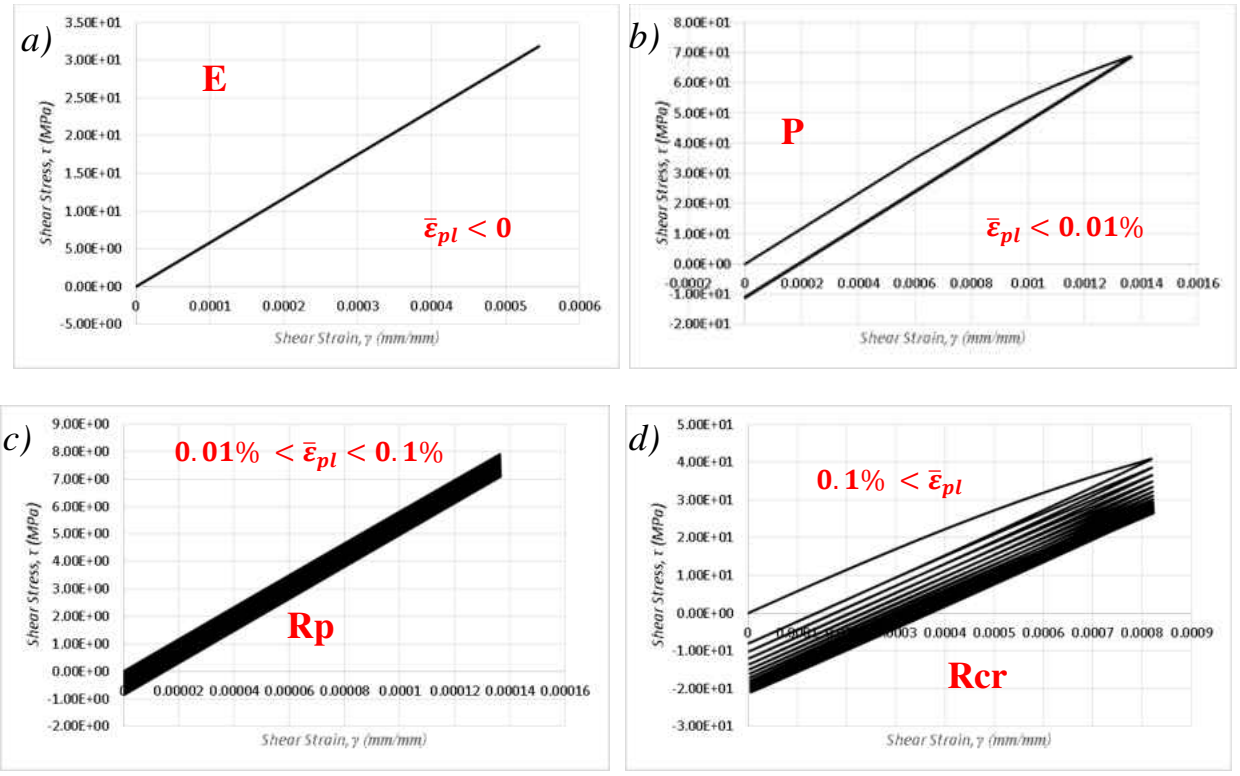

Figure 6.14: The regimes for modified Bree diagram (Twist control) a) elastic, b) plastic, c) plastic ratcheting, and d) plastic and creep ratcheting

Figure 6.15 shows the axial strain versus shear strain for different regimes of modified Bree diagram with twist control. In plastic regimes, the shear strain has plastic strain then it came constant. Plastic shakedown shows the shear strain is same for each cycle, but the axial strain is increasing with each cycle as shown in Figure 6.15 c. The last regimes is plastic and creep shakedown, so the axial strain and shear strain is increasing from cycle to other cycle as shown in Figure 6.15 d, the reason from that the creep strain.

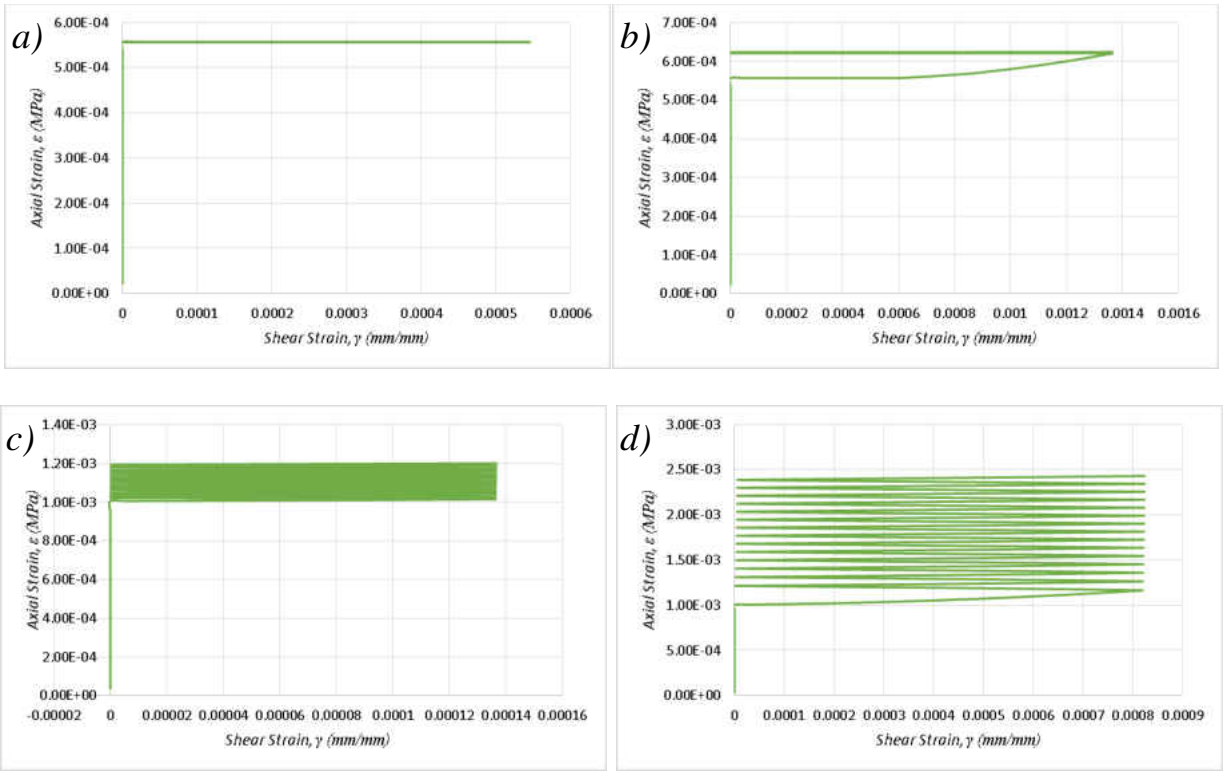

Figure 6.15: Axial strain versus shear strain a) elastic, b) plastic, c) plastic ratcheting, and d) creep ratcheting

In this part of study obtained modified Bree diagram with two different controls, and the main purpose is to predict how critical locations of components will balance combined axial and shear stress. And these stresses exceeded the yield strength limit in any region, so this diagram found the ratcheting and shakedown. Modified Bree diagram extended axial-torsional loading for 304 stainless steel with different controls. The axial-shear analogy modified Bree diagram developed to characterize the extent of ratcheting and shakedown under multi-axial behavior and to offer guidance is constitutive development. The results from the modified Bree diagram are when study used torque control the material will have ratcheting, by the control used is twist control we do not have ratcheting, and will have shakedown. Modified Bree diagram has four different regimes for each control, but the elastic regimes for both control happen when the

equivalent plastic strain is zero. Plastic regimes for both control happen when the equivalent plastic strain is less than 0.01%, plastic ratcheting and shakedown regimes for both control occur when the equivalent plastic strain is higher than 0.01% and less than 0.1%. The last regimes is plastic and creep ratcheting and shakedown for both control occur when the equivalent plastic strain is higher than 0.1%.

6.5 Life Prediction

Life prediction is one of the most important part for fatigue test, and it has different approaches have been established to predict fatigue life of material and structure are subjected to complex loading. The main reason of studying the life prediction to predict the life of any components allowing fatigue damage or surprising structure failure might happen.

The damage occur on specimen when the effects of fatigue is omnipresent in low cycle fatigue, creep-fatigue, thermomechanical fatigue, and corrosion. For example, when the loading is pure fatigue, so the fatigue damage can deliver start from zero to which the properties of oxidation- and creep- ambitious mechanisms can be added (Halford et al., 1993). In this research used the different experimental conditions, and the method selected in this study is the Manson- Coffin relation as the central component. Also, in this study the load is multiaxial, but the axial load is very low, so it will study the shear load. The control used here is strain-controlled, and with a shear strain ratio value of $R\varepsilon = -1$. The strain-life approach is the Basquin-augmented Manson-Coffin approach. The following equation is the Manson-Coffin for axial and shear loading total strain range $\Delta\varepsilon$ to life N_f as

$$\frac{\Delta\varepsilon}{2} = \frac{\sigma_{f'}}{E}(2N_i)^b + \varepsilon_{f'}(2N_i)^c \qquad (6.10)$$

$$\frac{\Delta\gamma}{2} = \frac{\tau_{f'}}{E}(2N_i)^b + \gamma_{f'}(2N_i)^c \qquad (6.11)$$

where $\sigma_{f'}$ is fatigue strength coefficient, $\varepsilon_{f'}$ fatigue ductility coefficient, b is fatigue strength exponent, and c is fatigue ductility exponents. For shear loading is used the same equation, and the constants are the same way, but with using the shear stress and shear strain. For 304 stainless steel properties found from the experiments results, and fatigue strength coefficient is found from the previous study (Karl, 2013). The fatigue ductility coefficient, fatigue strength exponent, and fatigue ductility exponents are found from the Ramberg-Osgood model, and in the following equation shows the relation between the Ramberg-Osgood model and Manson-Coffin. Table11111 shows the Manson-Coffin constants.

$$K = \frac{\sigma'_f}{\left(\varepsilon'_f\right)^n}$$

$$n = \frac{b}{c}$$

In this study has multiaxial loading test, and the torsion load is cycling. Fatigue is one part of this research, and the material failure after number of cyclic. In this part will have the strain range versus the number of cyclic, and also see the different between the numbers of cyclic with different conditions. In Figure shows some multiaxial experiments with different temperatures, and also different strain range. The fires and second curve are used when the axial load is 200 N, and there is one experiment when the axial load is zero and 100 N. When they have high strain range the specimen under 600°C is failure before the specimen at room temperature, and the same with low strain range. Moreover, the specimen under high temperature is failure faster than the specimen at room temperature, so when the temperature is increasing the number of cyclic is decreasing. The specimen in room temperature has three different conditions. The difference of the conditions are the axial load are different, so when the axial load is zero the specimen has the highest number of cycles. Also, by increase the axial load the number of cycles is decreasing as shown in Figure 6.16.

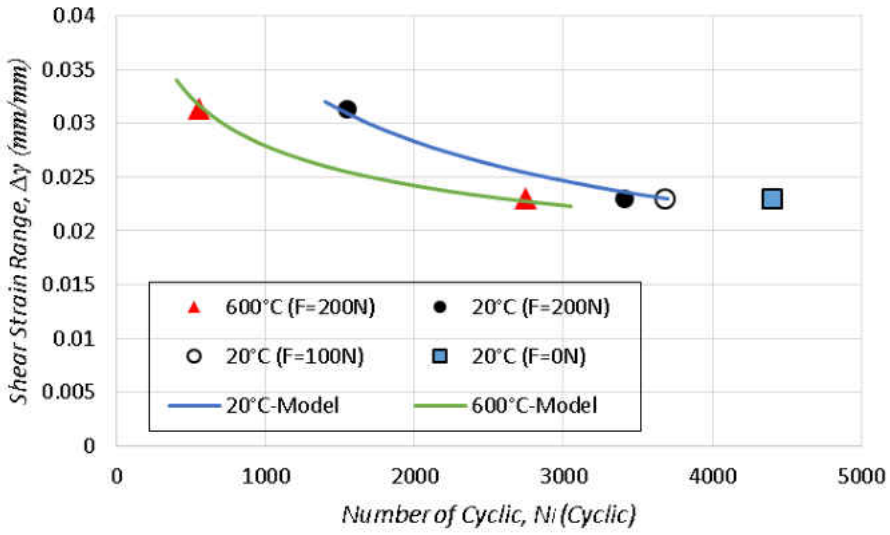

Figure 6.16: Shear strain range versus number of cycles and Mason-Coffin model.

Table 6-7: Mason-Coffin constants

Temperature, T °C	Shear Fatigue Strength Coefficient, τ'_f MPa	Shear Fatigue Ductility Coefficient, γ'_f	Shear Fatigue Strength Exponent, b	Shear Fatigue Ductility Exponents, c
20	569	0.0634	-0.0497	-0.26158
600	420	0.0730	-0.0375	-0.30072

CHAPTER 7 CONCLUSIONS

Most machine components are subjected to complex cyclic loading and subsequent deformation. The present work demonstrates two frameworks. First, a complex axial-torsional loading path can be used to verify the constitutive modeling approach for 2.25Cr-1Mo steel. Secondly, axial-torsional experiments can be used to generate constitutive models. Increasingly, there is a desire to develop approaches to reduce the number of experiments required characterize a material. The non-interaction model shown here uses only a small collection of plasticity-dominant experiments and creep deformation data. A range of temperatures were considered based on available uniaxial and axial-torsional responses. This study demonstrates a method of constitutive modeling that can carry over to axial-torsion conditions with high accuracy. These proposed methodology can be used to design creep and plasticity constitutive models that correlate strongly with axial-torsional fatigue data. The models are applied under service-like conditions to gain an understanding of how this and other key alloys behave under complex conditions. Included in this work are four different multiaxial test types having differences in control path. Moreover, from finite element analysis, some conditions exhibited dominantly-plastic condition, while others display creep-dominant deformation. A test with mean stress shows dominantly creep deformation, but the other three types were dominantly-plastic. Several constitutive modeling combinations were explored. Comparing between Multi-linear Isotropic Hardening (MISO) and Non Linear Kinematic Hardening (NLKH) models, the NLKH model captures the multiaxial responses more accurately than MISO. Differences between the Garofalo and Norton models were also drawn out when creep deformation was dominant. Garofalo shows slightly better results compared to Norton because the model simulates creep rate more accurately across a range of stresses. At wide

range of applied stress especially those facilitating very low strain rates, Garofalo captures the non-linear creep stress-strain rate trend more accurately. In this research used ANSYS software, and the results were obtain from finite element analysis have good fit model creep, and plasticity with experiments data were found from the literature review. Then did some experiment with multiaxial loading to found the material properties under multiaxial loading. The axial loading was in elastic range, so the axial did not effect in the shear stresses. The research found the plasticity from the shear experiments data, and convert the shear plasticity to uniaxial plasticity parameters. The simulation used with the plasticity parameters found from the multiaxial loading, and the simulation results compared to experiment results and it has good fitting.

One of the most important contributions here was based on shear relaxation, and relating it with a creep model to find the creep parameters. The creep parameters were found from relaxation to here very good accuracy after it simulated, and fit the simulation carve with experiment curve.

The last part was studying in this research was to build the Bree Diagram for this type of test. The Bree Diagram was modified for axial-torsional loading. This diagram allows designers to predict the hysteresis character under axial-torsional loading. The collection of these methods help support the evaluation and implementation of materials under complex loading at elevated temperature.

CHAPTER 8 FUTURE WORK

While significant determination has been exhausted in the completion of this dissertation. To improve the research need to increase the axial load, and use the multiaxial plasticity equation, so in the multiaxial equation will use the equivalent stress and strain. Also, for stress relaxation curve the equation used for shear because the axial stress did not make a change in relaxation curve, but when axial load increase the stress relaxation will use the equivalent stress and strain. Below are listed some subjects of future work apply to the improvement of models.

Increase the axial loading to reach the plastic range. For axial loading can apply in the MTS Bionix ElectroMechanical (EM) Torsion Test Systems is 200 N, and this axial force in elastic range, so the axial load did not shows any plasticity and creep in the axial direction. The axial loading need to be increased to 300 MPa because the axial yield strength for 304 stainless steel is almost 300 MPa, and the axial stress will be in plastic range. The reason from increase the axial stress and reach the plasticity is to show the effect axial stress in shear stress. The maximum axial load used in this research was 7 MPa which is in elastic range, so the shear stress did not effect. In chapter 6 shows the plasticity properties found from the shear data, but when the axial loading increase the equation will use for the equivalent stress and strain. The plasticity constants will be more accurate for multiaxial loading.

Using the new plasticity and creep model with varying material types. In this research the material used to define the plasticity and creep constants were 304 stainless steel. One of the important future work is using the new plasticity and creep model with different materials, and compare the experimental results and simulation results. When the simulation results are fitting

the experimental data so that means the new model found for plasticity and creep can be used for any material.

Optimize the constants determination process. In the current research, a large number of experiments are needed to define the material properties of the unified mechanical model for multiaxial types of test. The determination procedure includes a series of numerical optimization for collections of constants connected with each experiment. It can simplify with using the multiaxial test, and the mechanical experiment can do with different boundary conditions for the same specimen. This procedure will reduce the number of experiments, the time, and the cost.

Increase the experiment number. One of the main section in this research is developing Bree diagram for axial-torsion loading. Determine the stress regimes and capture the modes of deformation and relate it to the mechanical tests. The first step will run some experiments for multiaxial loading to build the Bree diagram. Afterwards, analysis and observation will be used to identify the transitions between adjacent regions. It is expecting that constitutive modeling constants will be useful. To increase the Bree diagram accuracy need to run more experiments to make Bree diagram more accurate.

APPENDIX A:
EXPERIMENT DATA

Different test types and controls

Specimen ID	Temperature °C	Control	Torque N-m	Angle of Twist Degree	Axial Force N
AT-20°C-01	20	Angle of Twist		±15	200
AT-20°C-02	20	Angle of Twist		15,-7	200
AT-20°C-03	20	Angle of Twist		15,-7	100
AT-20°C-04	20	Angle of Twist		15,-7	0
AT-500°C-01	500	Torque	13,-3		200
AT-500°C-01	500	Torque	14,-3		200
AT-500°C-01	500	Torque	15,-3		200
AT-500°C-01	500	Torque	16,-3		200
AT-500°C-01	500	Torque	17,-3		200
AT-500°C-01	500	Torque	18,-3		200
AT-500°C-01	500	Torque	18.5,-3		200
AT-500°C-01	500	Torque	19,-3		200
AT-500°C-01	500	Torque	19.5,-3		200
AT-600°C-01	600	Angle of Twist		±15	200
AT-600°C-02	600	Angle of Twist		15,-7	200
AT-600°C-03	600	Torque	13,0		200
AT-600°C-04	600	Torque	14,-3		200
AT-600°C-04	600	Torque	15,-3		200

AT-600°C-04	600	Torque	16,-3		200
AT-600°C-04	600	Torque	16.5,-3		200
AT-600°C-05	600	Angle of Twist		±15	200
AT-600°C-05	600	Angle of Twist		±15	200
AT-600°C-05	600	Angle of Twist		±15	200
AT-600°C-05	600	Angle of Twist		±15	200
AT-600°C-05	600	Angle of Twist		±15	200
AT-600°C-06	600	Angle of Twist		±16	0
AT-600°C-06	600	Angle of Twist		±16	0
AT-600°C-06	600	Angle of Twist		±16	0
AT-600°C-06	600	Angle of Twist		±16	200

Room Temperature (20°C)

AT-20°C-01

Test ID	Temp.	Control	Axial Force, F_a	Angle of Twist, ∅	Twist Rate, $\dot{\emptyset}$
AT-20°C-01	°C		N	Degree	Degree/sec.
	20	Angle	200	15,-15	3

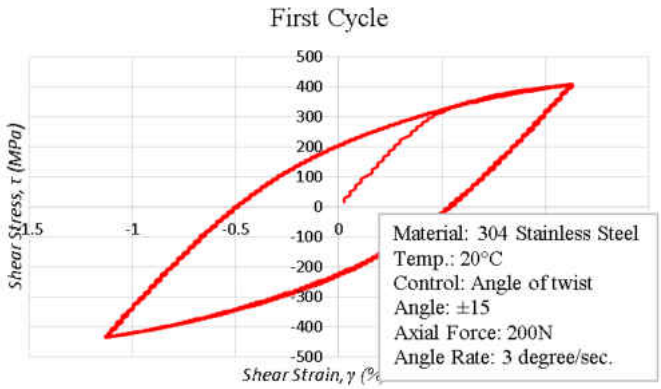

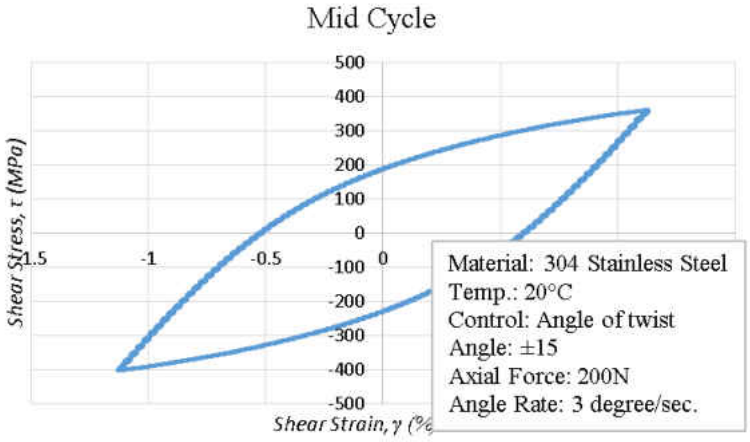

Test ID	Modulus of Elasticity, E	Yield Strength, $\sigma_{0.2\%}$	Number of Cycle, N_i	Max. Torque, T_{max}	Min. Torque, T_{min}	Torque Range, ΔT	Mean Torque, T_m	Time, t
AT-20°C-01	GPa	MPa	Cycles	N-m	N-m	N-m	N-m	hr
	194	294.5	1570	17.4	-18.40	35.8	-0.4	8.7

AT-20°C-02

Test ID	Temp.	Control	Axial Force, F_a	Angle of Twist, $\emptyset$	Twist Rate, $\dot{\emptyset}$
AT-20°C-02	°C		N	Degree	Degree/sec.
	20	Angle	200	15,-7	2

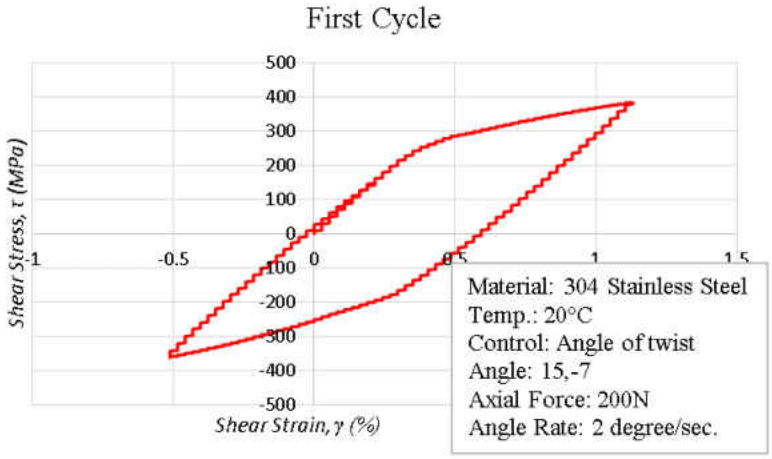

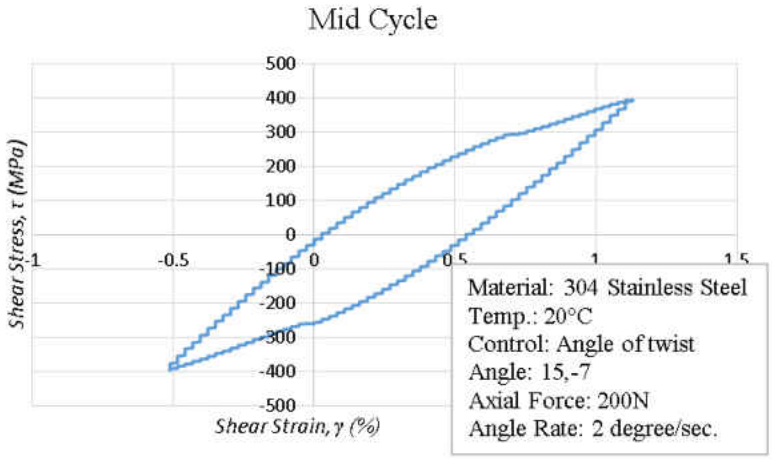

Test ID	Modulus of Elasticity, E	Yield Strength, $\sigma_{0.2\%}$	Number of Cycle, N_i	Max. Torque, T_{max}	Min. Torque, T_{min}	Torque Range, ΔT	Mean Torque, T_m	Time, t
AT-20°C-02	GPa	MPa	Cycles	N-m	N-m	N-m	N-m	hr
	188	303	3404	17	-16	33	0.5	32

AT-20°C-03

Test ID	Temp.	Control	Axial Force, F_a	Angle of Twist, $\emptyset$	Twist Rate, $\dot{\emptyset}$
AT-20°C-03	°C		N	Degree	Degree/sec.
	20	Angle	100	15,-7	2

First Cycle

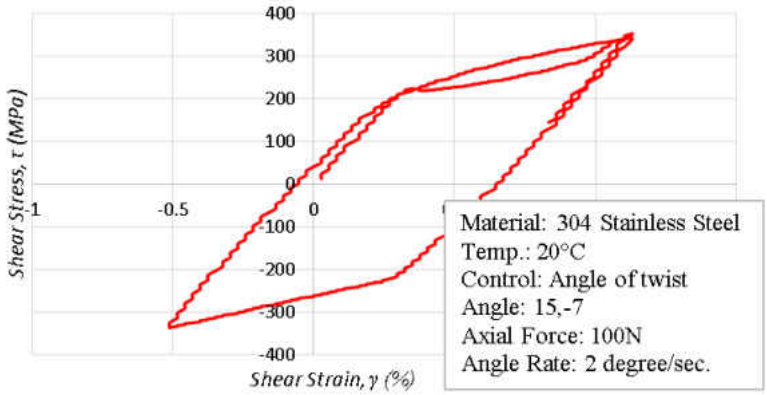

Mid Cycle

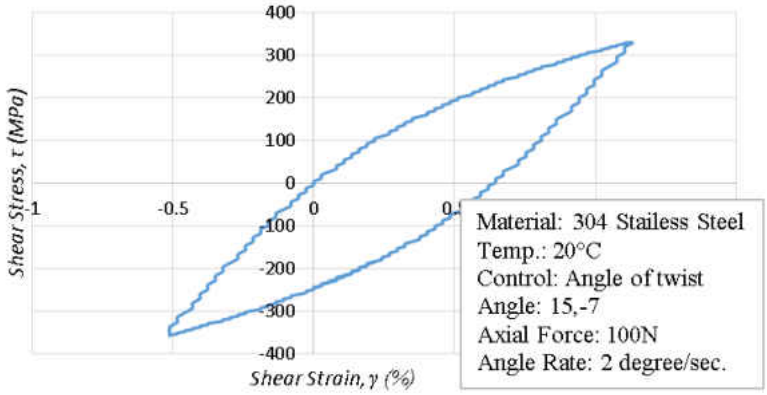

Test ID	Modulus of Elasticity, E	Yield Strength, $\sigma_{0.2\%}$	Number of Cycle, N_i	Max. Torque, T_{max}	Min. Torque, T_{min}	Torque Range, ΔT	Mean Torque, T_m	Time, t
AT-20°C-03	GPa	MPa	Cycles	N-m	N-m	N-m	N-m	hr
	186	260	3662	17	-17.8	34.8	-0.4	23

AT-20°C-04

Test ID	Temp.	Control	Axial Force, F_a	Angle of Twist, $\emptyset$	Twist Rate, $\dot{\emptyset}$
AT-20°C-04	°C		N	Degree	Degree/sec.
	20	Angle	0	15,-7	3

First Cycle

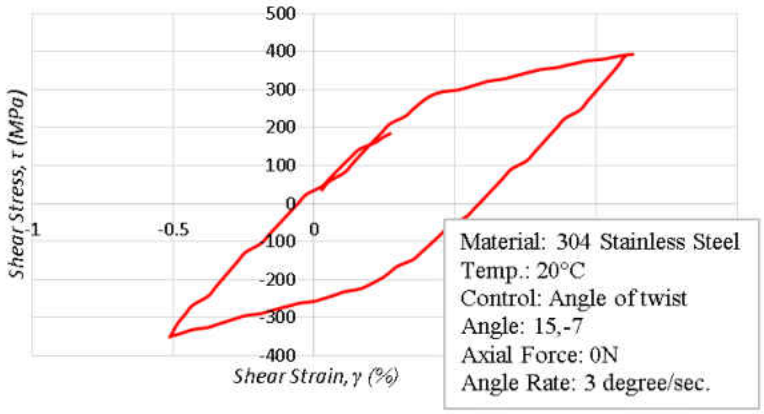

Mid Cycle

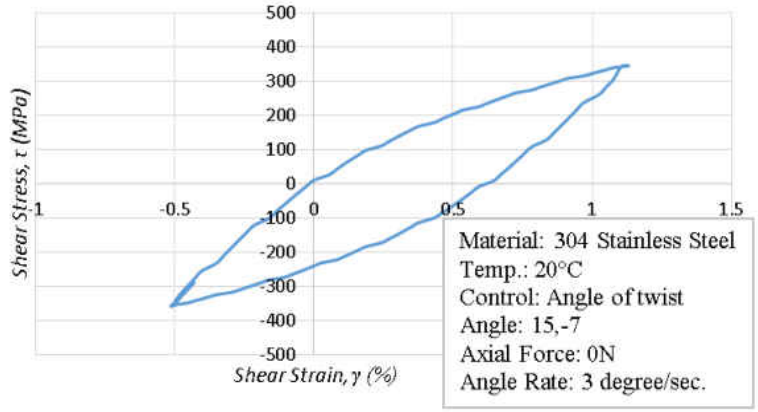

Test ID	Modulus of Elasticity, E	Yield Strength, $\sigma_{0.2\%}$	Number of Cycle, N_i	Max. Torque, T_{max}	Min. Torque, T_{min}	Torque Range, ΔT	Mean Torque, T_m	Time, t
AT-20°C-04	GPa	MPa	Cycles	N-m	N-m	N-m	N-m	hr
	203	330	4400	17	-17.8	34.8	-0.4	18.4

High Temperature (500°C)

AT-500°C-01

Test ID	Temp.	Control	Axial Force, F_a	Torque, T	Rate
AT-500°C-01	°C		N	N-m	Degree/sec.
	500	Torque	200	13,0	0.2

First Cycle

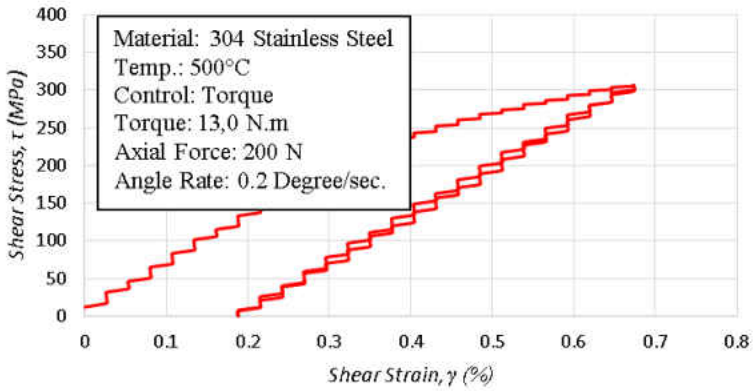

Mid Cycle

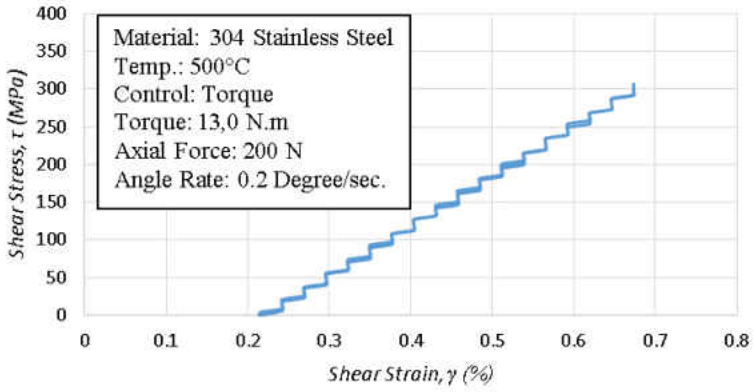

Test ID	Modulus of Elasticity, E	Yield Strength, $\sigma_{0.2\%}$	Number of Cycle, N_i	Max. Torque, T_{max}	Min. Torque, T_{min}	Torque Range, ΔT	Mean Torque, T_m	Time, t
AT-500°C-01	GPa	MPa	Cycles	N-m	N-m	N-m	N-m	hr
	176	267	1240	13	0	13	6.5	8.6

Test ID	Temp.	Control	Axial Force, F_a	Torque, T	Rate
AT-500°C-01	°C		N	N-m	Degree/sec.
	500	Torque	200	14,0	0.2

First Cycle

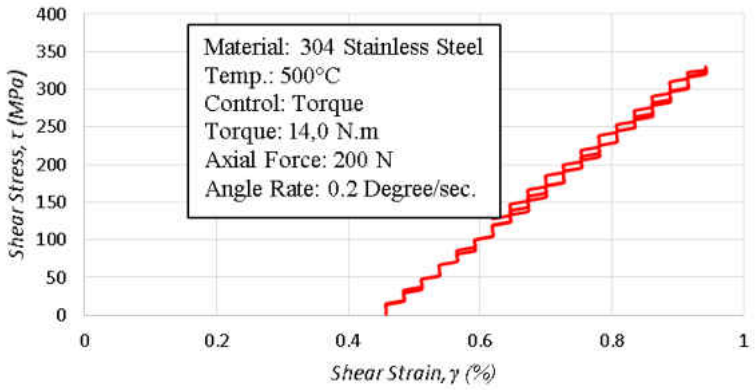

Mid Cycle

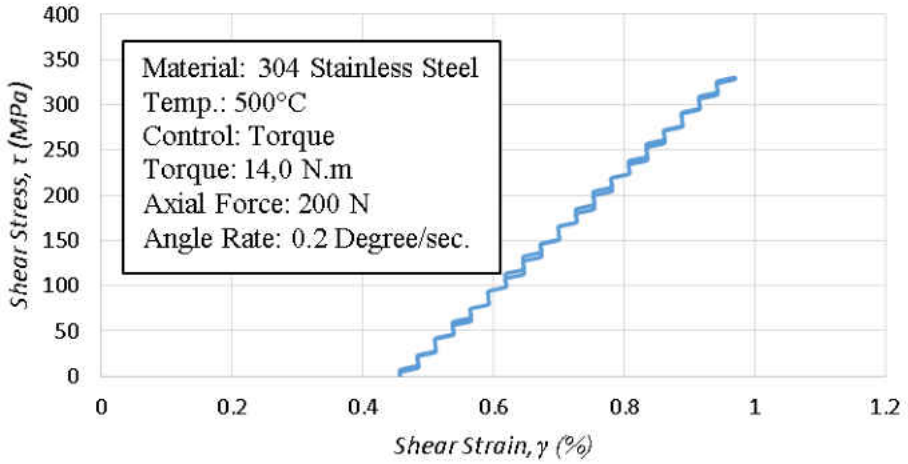

Test ID	Modulus of Elasticity, E	Yield Strength, $\sigma_{0.2\%}$	Number of Cycle, N_i	Max. Torque, T_{max}	Min. Torque, T_{min}	Torque Range, ΔT	Mean Torque, T_m	Time, t
AT-500°C-01	GPa	MPa	Cycles	N-m	N-m	N-m	N-m	hr
	176	267	725	14	0	14	7	5.3

Test ID	Temp.	Control	Axial Force, F_a	Torque, T	Rate
AT-500°C-01	°C		N	N-m	Degree/sec.
	500	Torque	200	15,0	0.2

First Cycle

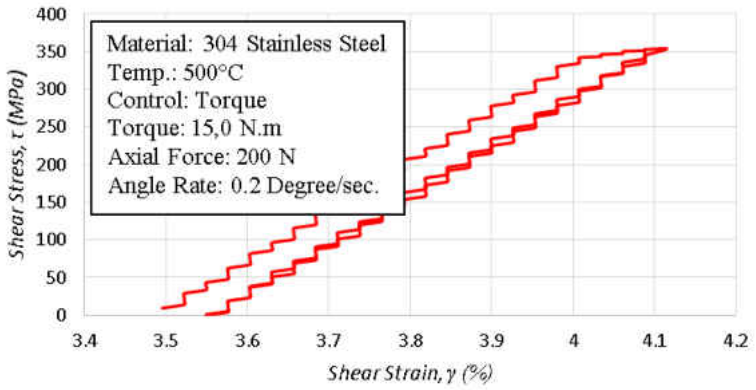

Mid Cycle

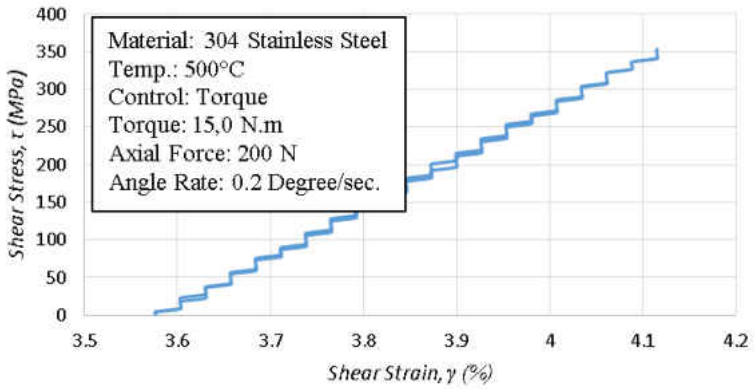

Test ID	Modulus of Elasticity, E	Yield Strength, $\sigma_{0.2\%}$	Number of Cycle, N_i	Max. Torque, T_{max}	Min. Torque, T_{min}	Torque Range, ΔT	Mean Torque, T_m	Time, t
AT-500°C-01	GPa	MPa	Cycles	N-m	N-m	N-m	N-m	hr
	176	267	6.7	15	0	15	7.5	6.7

Test ID	Temp.	Control	Axial Force, F_a	Torque, T	Rate
AT-500°C-01	°C		N	N-m	Degree/sec.
	500	Torque	200	16,0	0.2

First Cycle

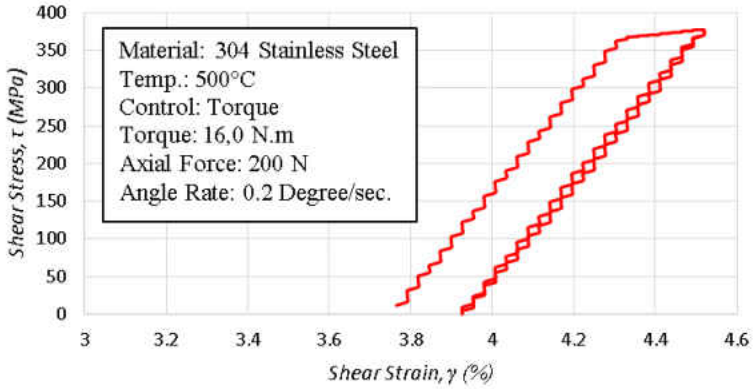

Mid Cycle

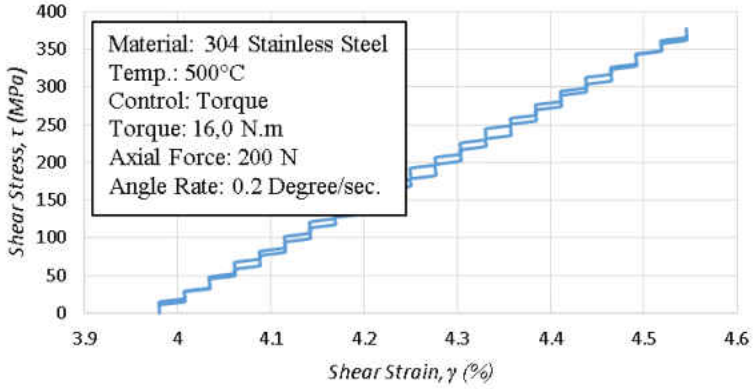

Test ID	Modulus of Elasticity, E	Yield Strength, $\sigma_{0.2\%}$	Number of Cycle, N_i	Max. Torque, T_{max}	Min. Torque, T_{min}	Torque Range, ΔT	Mean Torque, T_m	Time, t
AT-500°C-01	GPa	MPa	Cycles	N-m	N-m	N-m	N-m	hr
	176	267	730	16	0	16	8	6.3

Test ID	Temp.	Control	Axial Force, F_a	Torque, T	Rate
AT-500°C-01	°C		N	N-m	Degree/sec.
	500	Torque	200	17,0	0.2

First Cycle

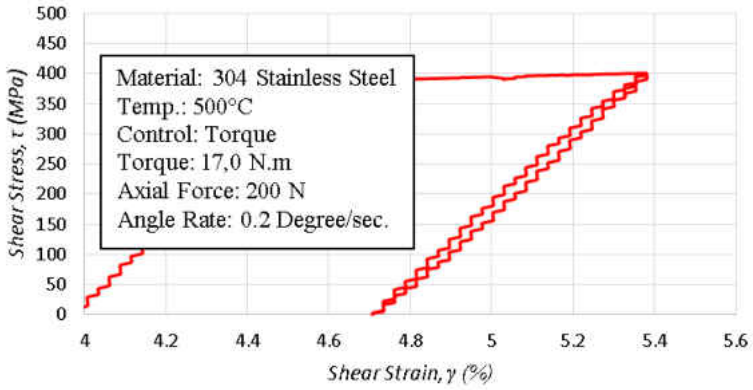

Mid Cycle

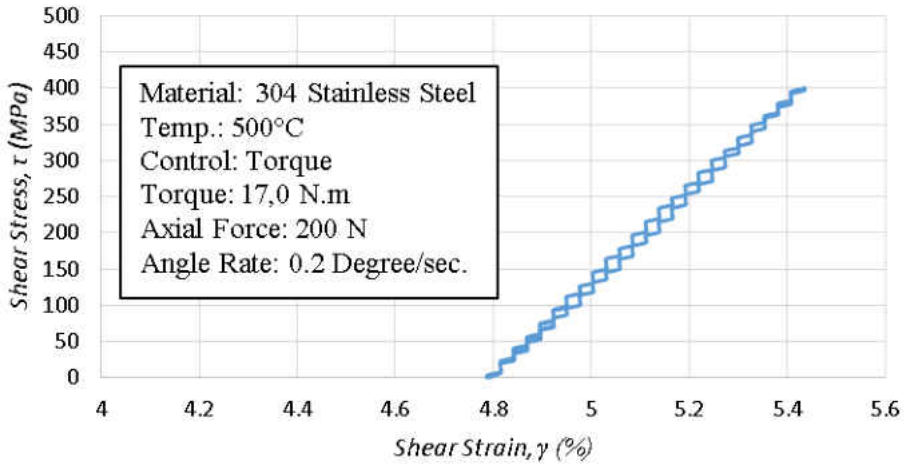

Test ID	Modulus of Elasticity, E	Yield Strength, $\sigma_{0.2\%}$	Number of Cycle, N_i	Max. Torque, T_{max}	Min. Torque, T_{min}	Torque Range, ΔT	Mean Torque, T_m	Time, t
AT-500°C-01	GPa	MPa	Cycles	N-m	N-m	N-m	N-m	hr
	176	267	547	17	0	17	8.5	5

Test ID	Temp.	Control	Axial Force, F_a	Torque, T	Rate
AT-500°C-01	°C		N	N-m	Degree/sec.
	500	Torque	200	18,0	0.2

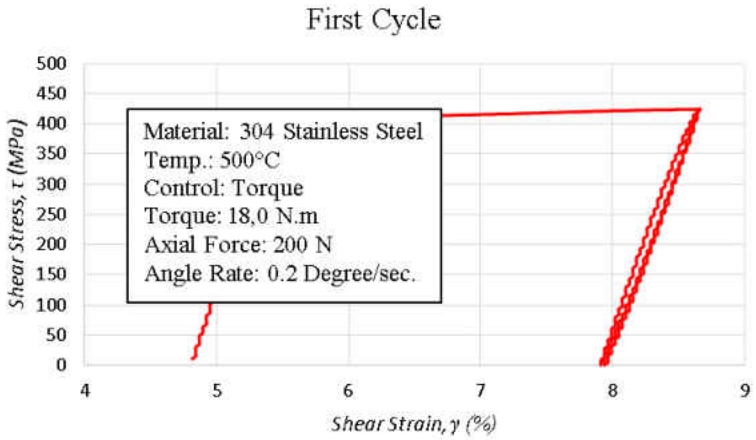

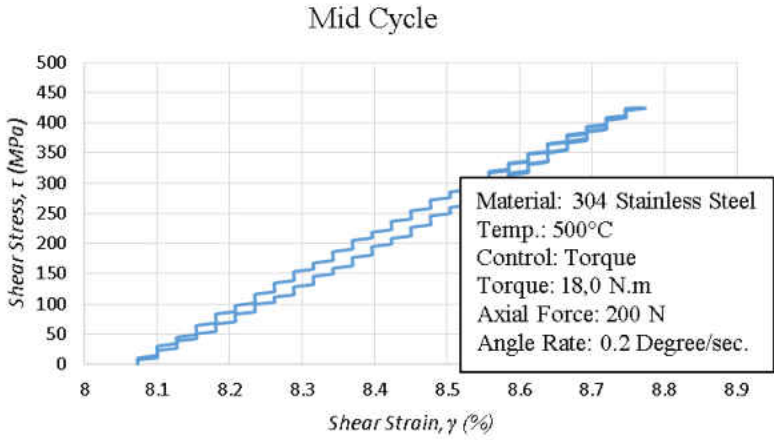

Test ID	Modulus of Elasticity, E	Yield Strength, $\sigma_{0.2\%}$	Number of Cycle, N_i	Max. Torque, T_{max}	Min. Torque, T_{min}	Torque Range, ΔT	Mean Torque, T_m	Time, t
AT-500°C-01	GPa	MPa	Cycles	N-m	N-m	N-m	N-m	hr
	176	267	1603	18	0	18	9	16.4

Test ID	Temp.	Control	Axial Force, F_a	Torque, T	Rate
AT-500°C-01	°C		N	N-m	Degree/sec.
	500	Torque	200	18.5,0	0.2

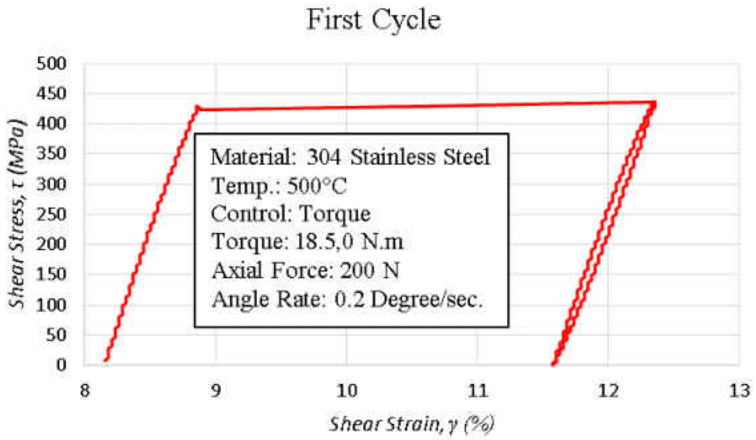

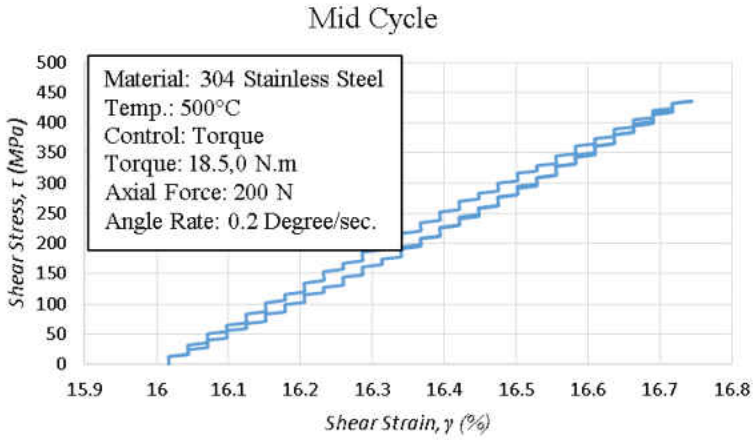

Test ID	Modulus of Elasticity, E	Yield Strength, $\sigma_{0.2\%}$	Number of Cycle, N_i	Max. Torque, T_{max}	Min. Torque, T_{min}	Torque Range, ΔT	Mean Torque, T_m	Time, t
AT-500°C-01	GPa	MPa	Cycles	N-m	N-m	N-m	N-m	hr
	176	267	1615	18.5	0	18.5	9.25	17

Test ID	Temp.	Control	Axial Force, F_a	Torque, T	Rate
AT-500°C-01	°C		N	N-m	Degree/sec.
	500	Torque	200	19,0	0.2

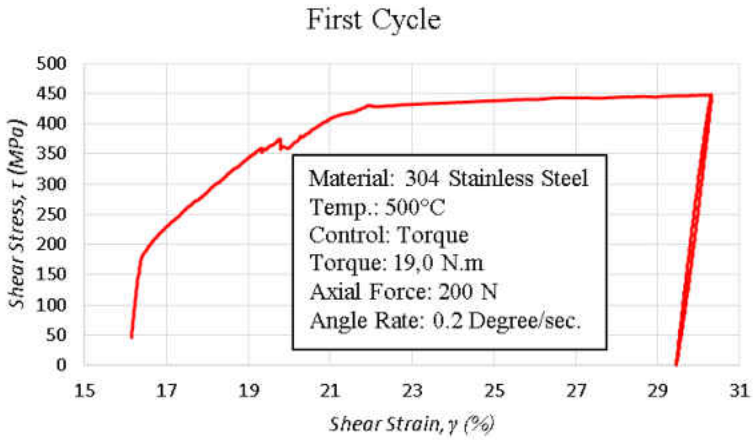

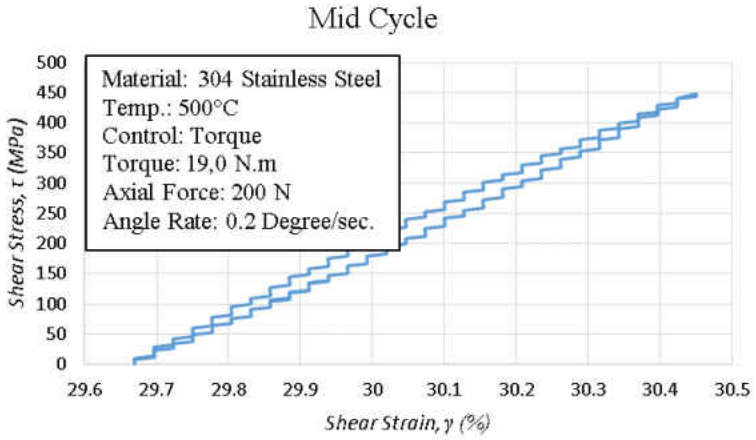

Test ID	Modulus of Elasticity, E	Yield Strength, $\sigma_{0.2\%}$	Number of Cycle, N_i	Max. Torque, T_{max}	Min. Torque, T_{min}	Torque Range, ΔT	Mean Torque, T_m	Time, t
AT-500°C-01	GPa	MPa	Cycles	N-m	N-m	N-m	N-m	hr
	176	267	915	19	0	19	9.5	10.5

Test ID	Temp.	Control	Axial Force, F_a	Torque, T	Rate
AT-500°C-01	°C		N	N-m	Degree/sec.
	500	Torque	200	19.5,0	0.2

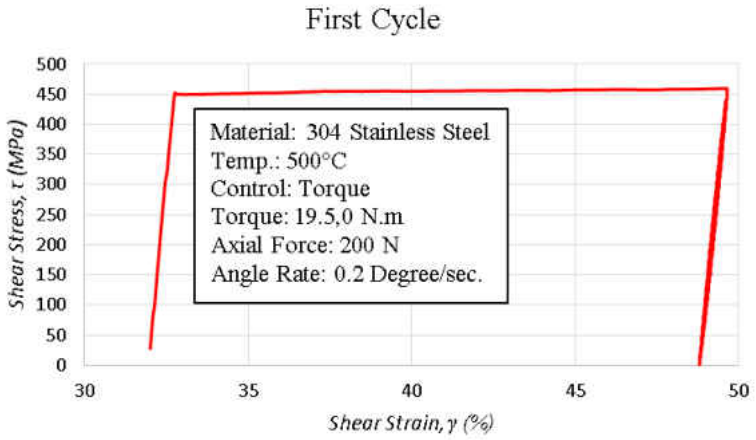

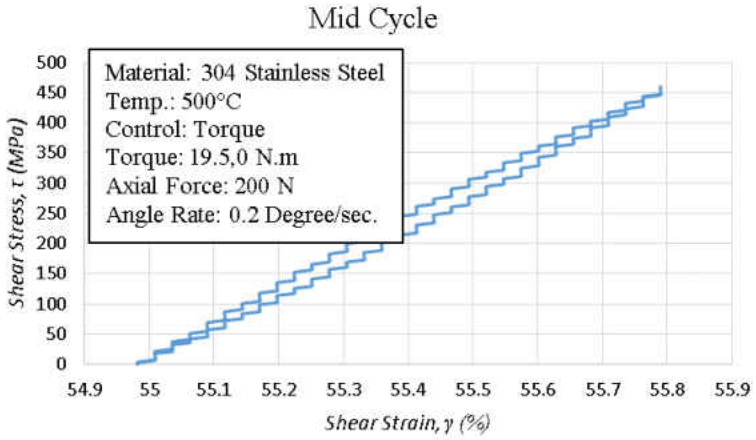

Test ID	Modulus of Elasticity, E	Yield Strength, $\sigma_{0.2\%}$	Number of Cycle, N_i	Max. Torque, T_{max}	Min. Torque, T_{min}	Torque Range, ΔT	Mean Torque, T_m	Time, t
AT-500°C-01	GPa	MPa	Cycles	N-m	N-m	N-m	N-m	hr
	176	267	100	19.5	0	19.5	9.75	12.5

High Temperature (600°C)

AT-600°C-01

Test ID	Temp.	Control	Axial Force, F_a	Angle of Twist, $\emptyset$	Twist Rate, $\dot{\emptyset}$
AT-600°C-01	°C		N	Degree	Degree/sec.
	600	Angle	200	15, -15	0.5

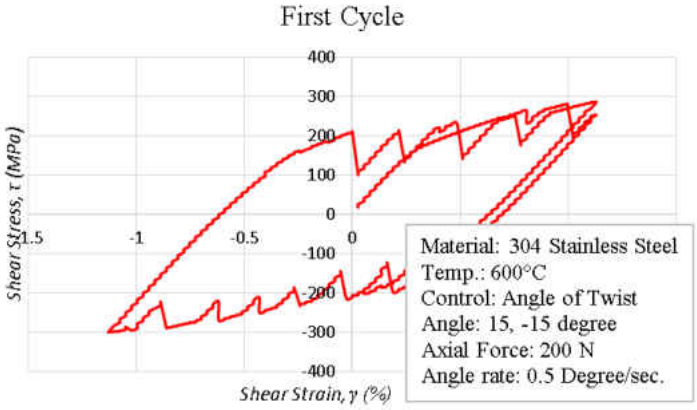

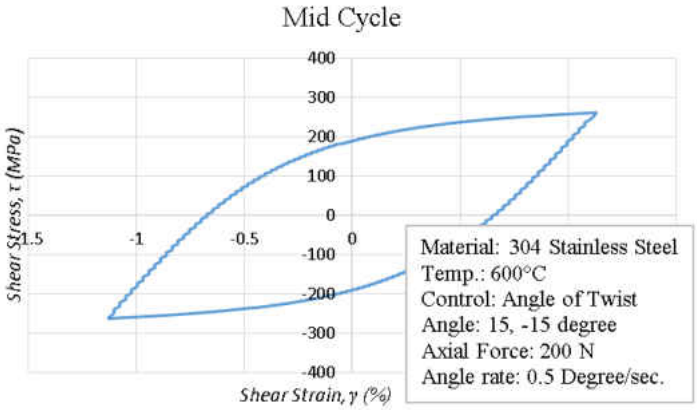

Test ID	Modulus of Elasticity, E	Yield Strength, $\sigma_{0.2\%}$	Number of Cycle, N_i	Max. Torque, T_{max}	Min. Torque, T_{min}	Torque Range, ΔT	Mean Torque, T_m	Time, t
AT-600°C-01	GPa	MPa	Cycles	N-m	N-m	N-m	N-m	hr
	162	147	335	13.52	-13.1	26.62	0.21	10.3

AT-600°C-02

Test ID	Temp.	Control	Axial Force, F_a	Angle of Twist, $\emptyset$	Twist Rate, $\dot{\emptyset}$
AT-600°C-02	°C		N	Degree	Degree/sec.
	600	Angle	200	15,-7	0.5

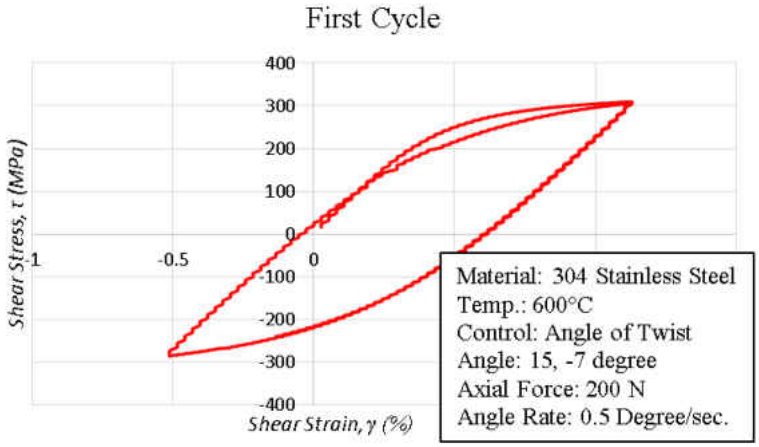

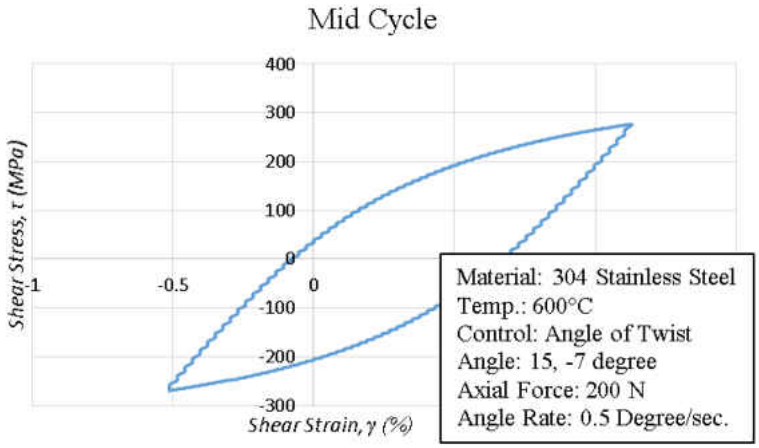

Test ID	Modulus of Elasticity, E	Yield Strength, $\sigma_{0.2\%}$	Number of Cycle, N_i	Max. Torque, T_{max}	Min. Torque, T_{min}	Torque Range, ΔT	Mean Torque, T_m	Time, t
AT-600°C-02	GPa	MPa	Cycles	N-m	N-m	N-m	N-m	hr
	163	207	265	13.1	-12.2	25.3	0.45	8

Test ID	Temp.	Control	Axial Force, F_a	Angle of Twist, $\emptyset$	Twist Rate, $\dot{\emptyset}$
AT-600°C-02	°C		N	Degree	Degree/sec.
	600	Angle	200	15,-7	2

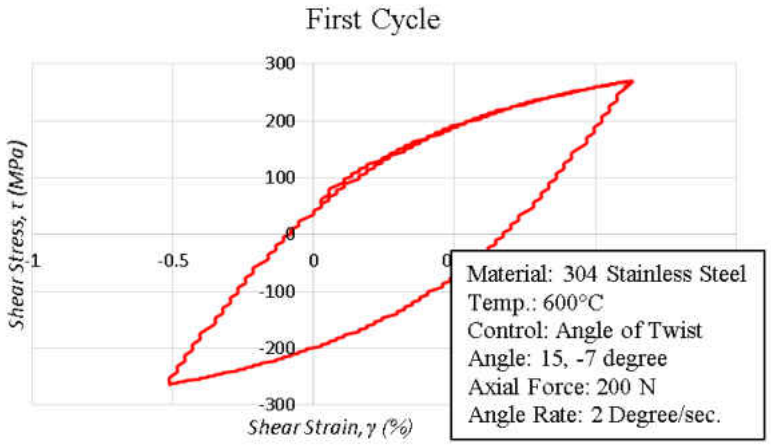

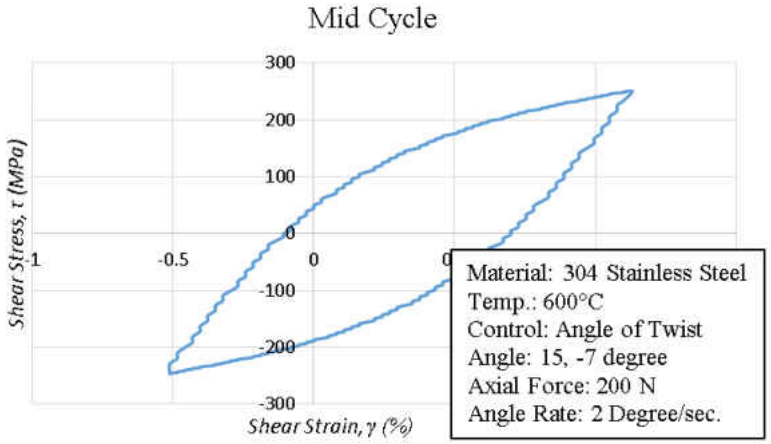

Test ID	Modulus of Elasticity, E	Yield Strength, $\sigma_{0.2\%}$	Number of Cycle, N_i	Max. Torque, T_{max}	Min. Torque, T_{min}	Torque Range, ΔT	Mean Torque, T_m	Time, t
AT-600°C-02	GPa	MPa	Cycles	N-m	N-m	N-m	N-m	hr
	163	207	2380	11.45	-11.2	22.65	0.125	14

AT-600°C-03

Test ID	Temp.	Control	Axial Force, F_a	Torque, T	Rate
AT-600°C-03	°C		N	N-m	Degree/sec.
	600	Torque	200	13,0	0.5

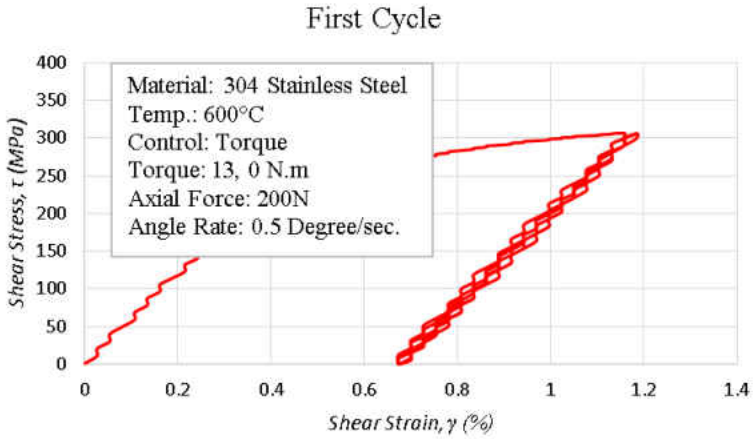

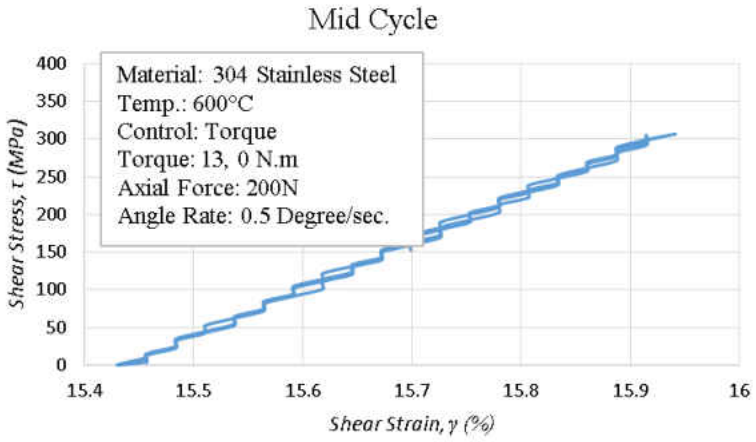

Test ID	Modulus of Elasticity, E	Yield Strength, $\sigma_{0.2\%}$	Number of Cycle, N_i	Max. Torque, T_{max}	Min. Torque, T_{min}	Torque Range, ΔT	Mean Torque, T_m	Time, t
AT-600°C-03	GPa	MPa	Cycles	N-m	N-m	N-m	N-m	hr
	156	208	4632	13	0	13	6.5	90

AT-600°C-04

Test ID	Temp.	Control	Axial Force, F_a	Torque, T	Rate
AT-600°C-04	°C		N	N-m	Degree/sec.
	600	Torque	200	14,-3	0.5

First Cycle

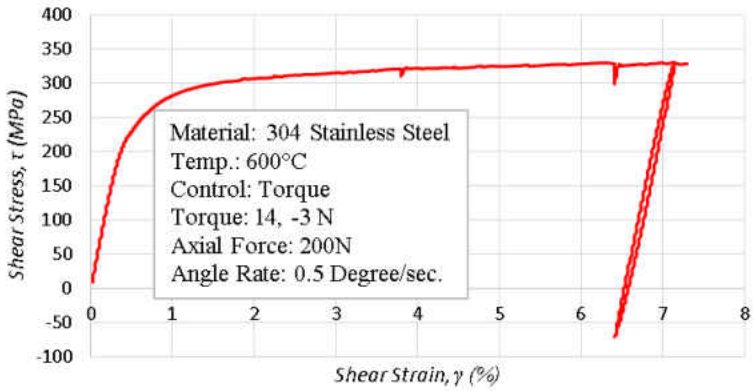

Mid Cycle

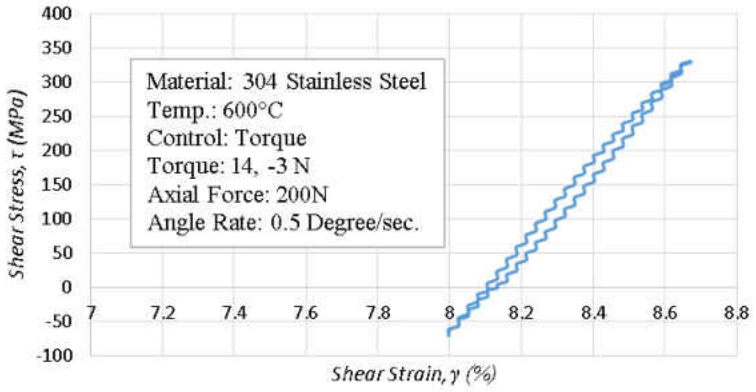

Test ID	Modulus of Elasticity, E	Yield Strength, $\sigma_{0.2\%}$	Number of Cycle, N_i	Max. Torque, T_{max}	Min. Torque, T_{min}	Torque Range, ΔT	Mean Torque, T_m	Time, t
AT-600°C-04	GPa	MPa	Cycles	N-m	N-m	N-m	N-m	hr
	154	242	1333	14	-3	17	5.5	13

Test ID	Temp.	Control	Axial Force, F_a	Torque, T	Rate
AT-600°C-04	°C		N	N-m	Degree/sec.
	600	Torque	200	15,-3	0.5

First Cycle

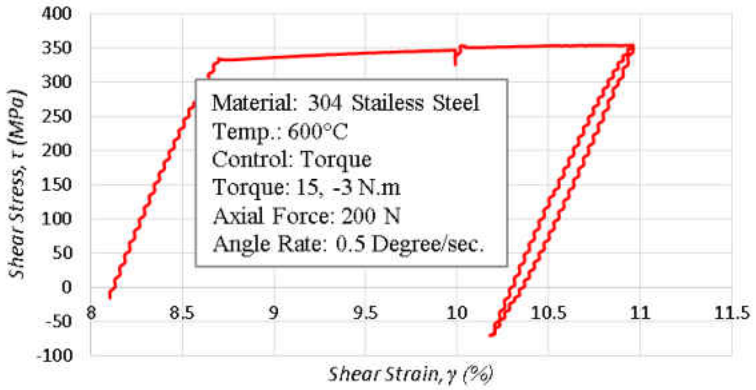

Mid Cycle

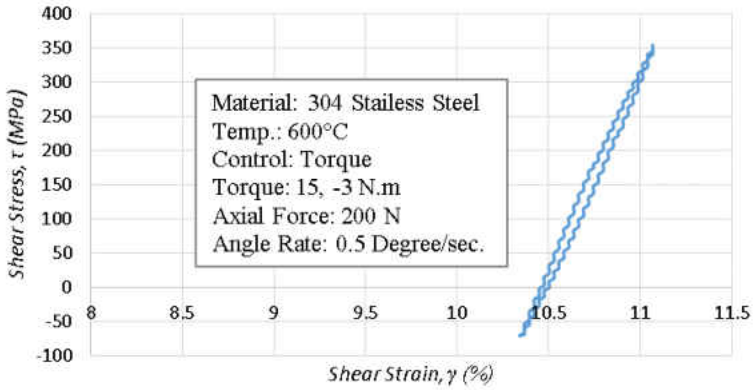

Test ID	Modulus of Elasticity, E	Yield Strength, $\sigma_{0.2\%}$	Number of Cycle, N_i	Max. Torque, T_{max}	Min. Torque, T_{min}	Torque Range, ΔT	Mean Torque, T_m	Time, t
AT-600°C-04	GPa	MPa	Cycles	N-m	N-m	N-m	N-m	hr
	154	242	464	15	-3	18	6	5

Test ID	Temp.	Control	Axial Force, F_a	Torque, T	Rate
AT-600°C-04	°C		N	N-m	Degree/sec.
	600	Torque	200	16,-3	0.5

First Cycle

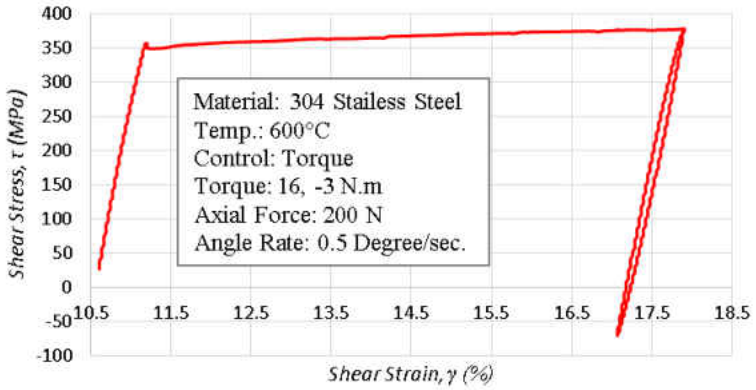

Mid Cycle

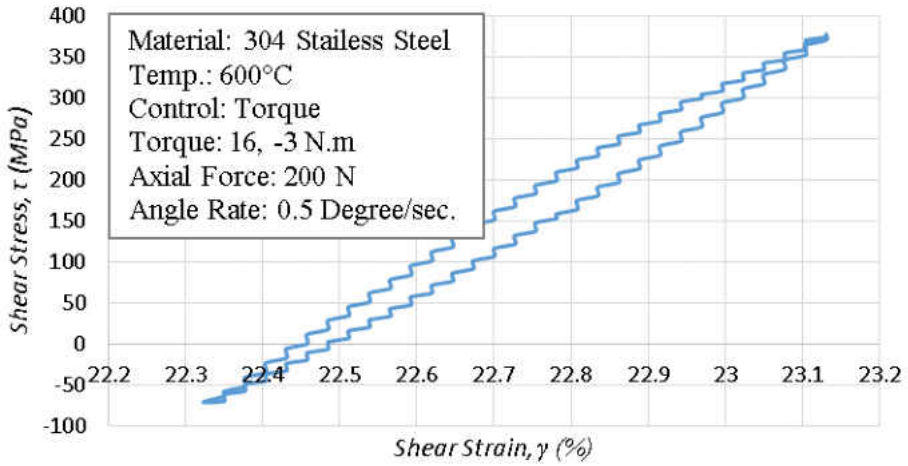

Test ID	Modulus of Elasticity, E	Yield Strength, $\sigma_{0.2\%}$	Number of Cycle, N_i	Max. Torque, T_{max}	Min. Torque, T_{min}	Torque Range, ΔT	Mean Torque, T_m	Time, t
AT-600°C-04	GPa	MPa	Cycles	N-m	N-m	N-m	N-m	hr
	154	242	1711	16	-3	19	6.5	

Test ID	Temp.	Control	Axial Force, F_a	Torque, T	Rate
AT-600°C-04	°C		N	N-m	Degree/sec.
	600	Torque	200	16.5,-3	0.5

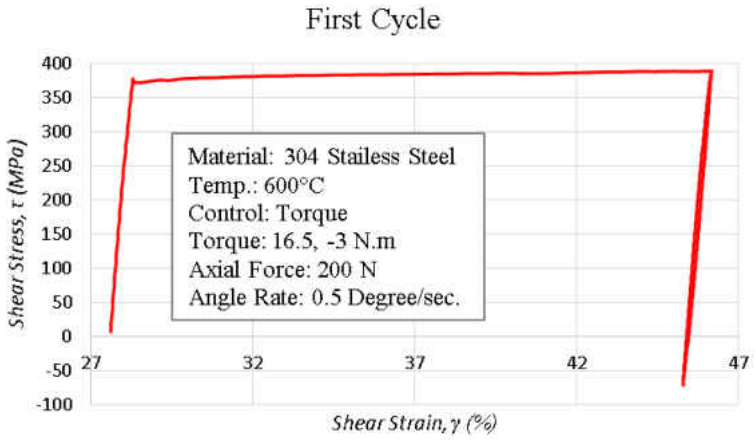

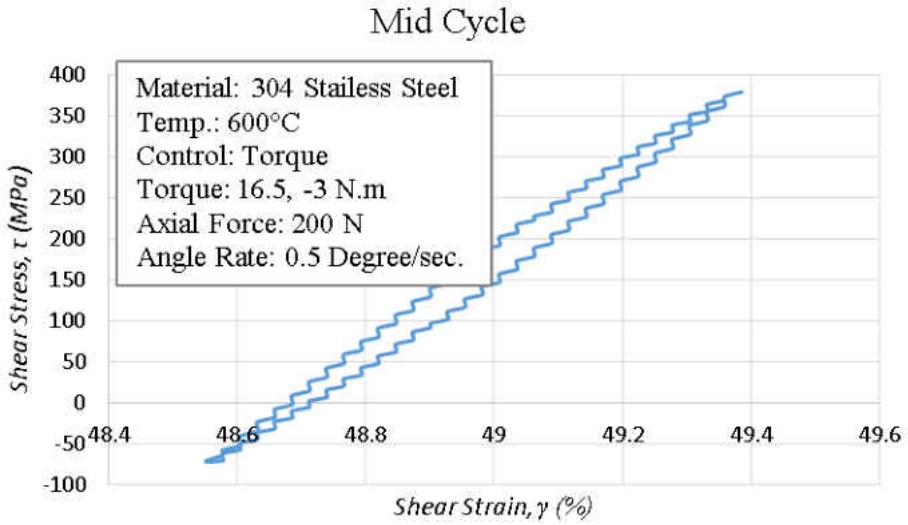

Test ID	Modulus of Elasticity, E	Yield Strength, $\sigma_{0.2\%}$	Number of Cycle, N_i	Max. Torque, T_{max}	Min. Torque, T_{min}	Torque Range, ΔT	Mean Torque, T_m	Time, t
AT-600°C-04	GPa	MPa	Cycles	N-m	N-m	N-m	N-m	hr
	154	242	273	16.5	-3	19.5	6.75	3.6

AT-600°C-06

Test ID	Temp.	Control	Axial Force, F_a	Angle of Twist, ∅	Twist Rate, $\dot{\emptyset}$	Dwell Time
AT-600°C-06	°C		N	Degree	Degree/sec.	Min.
	600	Angle of Twist	0	±16	2	2

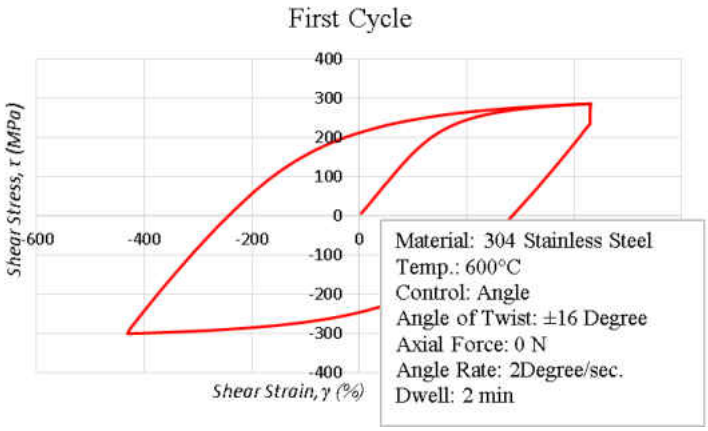

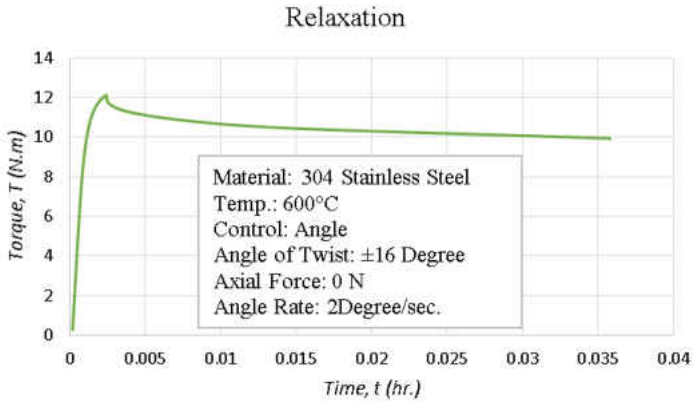

Test ID	Modulus of Elasticity, E	Yield Strength, $\sigma_{0.2\%}$	Number of Cycle, N_i	Max. Torque, T_{max}	Min. Torque, T_{min}	Torque Range, ΔT	Mean Torque, T_m	Time, t
AT-600°C-04	GPa	MPa	Cycles	N-m	N-m	N-m	N-m	hr
	153	235	20	12	-12.5	24.5	-0.25	0.8

Test ID	Temp.	Control	Axial Force, F_a	Angle of Twist, ∅	Twist Rate, $\dot{\emptyset}$	Dwell Time
AT-600°C-06	°C		N	Degree	Degree/sec.	Min.
	600	Angle of Twist	0	±16	2	20

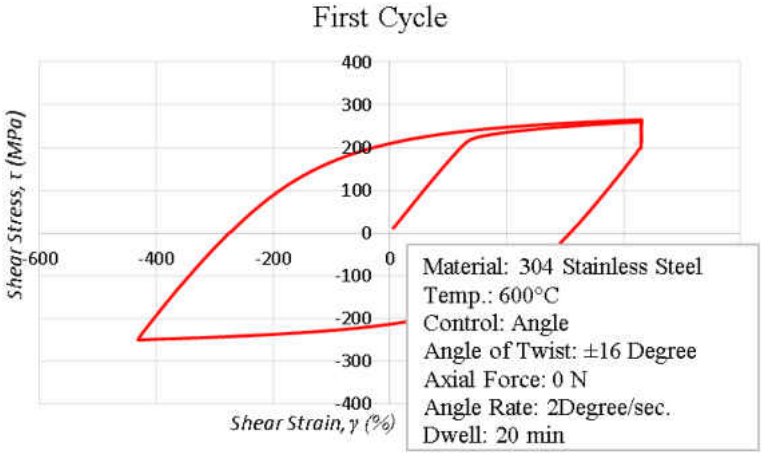

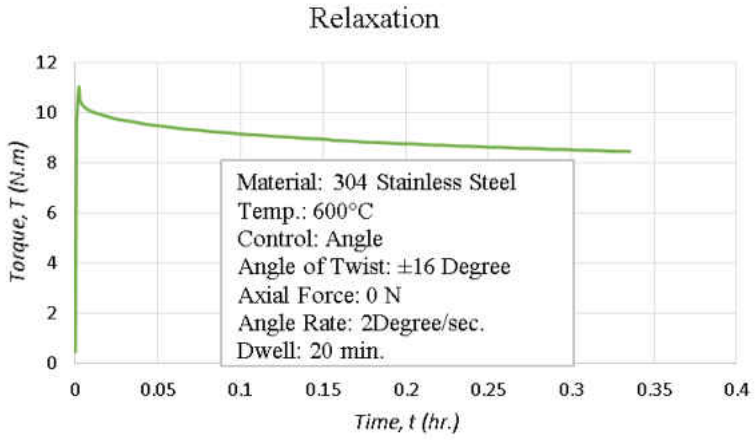

Test ID	Modulus of Elasticity, E	Yield Strength, $\sigma_{0.2\%}$	Number of Cycle, N_i	Max. Torque, T_{max}	Min. Torque, T_{min}	Torque Range, ΔT	Mean Torque, T_m	Time, t
AT-600°C-04	GPa	MPa	Cycles	N-m	N-m	N-m	N-m	hr
	153	230	20	11	-10.6	21.6	0.2	7

Test ID	Temp.	Control	Axial Force, F_a	Angle of Twist, ∅	Twist Rate, $\dot{\emptyset}$	Dwell Time
AT-600°C-06	°C		N	Degree	Degree/sec.	Min.
	600	Angle of Twist	0	±16	2	200

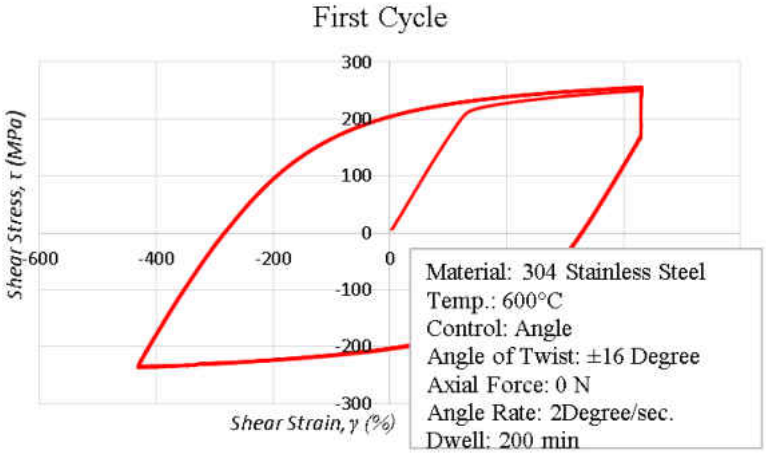

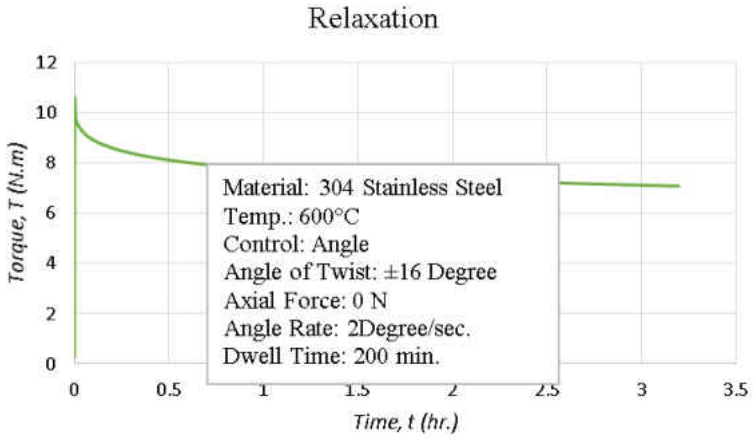

Test ID	Modulus of Elasticity, E	Yield Strength, $\sigma_{0.2\%}$	Number of Cycle, N_i	Max. Torque, T_{max}	Min. Torque, T_{min}	Torque Range, ΔT	Mean Torque, T_m	Time, t
AT-600°C-04	GPa	MPa	Cycles	N-m	N-m	N-m	N-m	hr
	153	235	20	11	-10	21	0.5	17

Test ID	Temp.	Control	Axial Force, F_a	Angle of Twist, ∅	Twist Rate, $\dot{\emptyset}$	Dwell Time
AT-600°C-06	°C		N	Degree	Degree/sec.	Min.
	600	Angle of Twist	200	±16	2	200

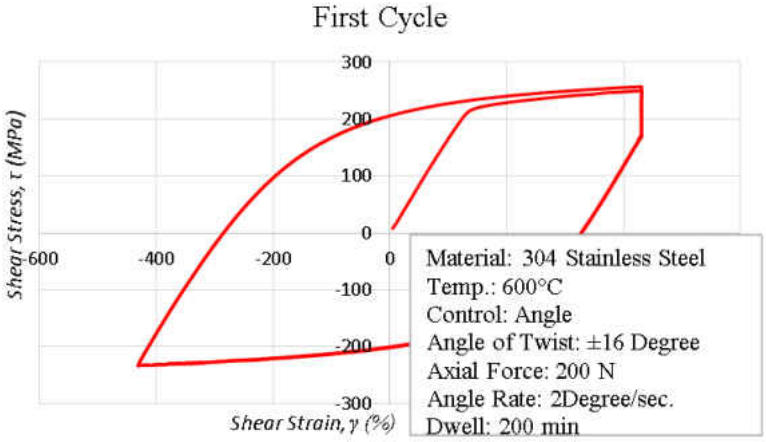

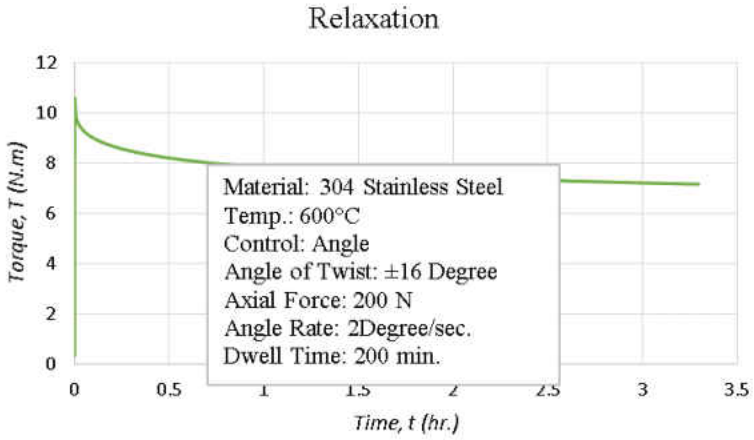

Test ID	Modulus of Elasticity, E	Yield Strength, $\sigma_{0.2\%}$	Number of Cycle, N_i	Max. Torque, T_{max}	Min. Torque, T_{min}	Torque Range, ΔT	Mean Torque, T_m	Time, t
AT-600°C-04	GPa	MPa	Cycles	N-m	N-m	N-m	N-m	hr
	153	235	2	11	-10	21	0.5	6

APPENDIX B:
CODS

- List the codes that are included in this research to do the simulations and compared the simulation results with the experiment results. The reason form that to approve that the material properties found from the experiments are working well.
- The first code used in ANSYS is APDL file for single element model, and the material used here is 2.25Cr-1Mo Steel, CODE1.
- The second code used in ANSYS is Workbench, and that one used for axial-torsional loading, and the material used is 304 Stainless Steel, CODE2.

CODE1:

```
! ANSYS Finite Element Modeling (FEM) Simulation of Fatigue
! Author: Various (Bassem Felemban)
! ver. 10
! Date: 11/01/17
!!!!!!!!!!!!!!!!!!!!!!!!!!!!!!!!!!!!!!!!!!!!!!!!!!!!!!!!!!!!!!!!!!!!!!!!!!!!!!!
Finish
/Clear
/Prep7
!!!!!!!!!!!!!!!!!!!!!!!!!!!!!!!!!!!!!!!!!!!!!!!!!!!!!!!!!!!!!!!!!!!!!!!!!!!!!!!
! Description: A Solid185 Element is subjected to strain-controlled
! fatigue in units of (m, N, MPa). Results are collected in a text file
! for later post-processing.
!!!!!!!!!!!!!!!!!!!!!!!!!!!!!!!!!!!!!!!!!!!!!!!!!!!!!!!!!!!!!!!!!!!!!!!!!!!!!!!
/inquire, numtes,lines,testconditions,csv
!!!!!!!!!!!!!!!!!!!!!!!!!!!!!!!!!!!!!!!!!!!!!!!!!!!!!!!!!!!!!!!!!!!!!!!!!!!!!!!
RADIUS=3                !MM
AREA=(3.14159265*RADIUS*RADIUS)
POLAR=((3.14159265*RADIUS*RADIUS*RADIUS*RADIUS)/2)
SHEAR_STRESS_MAX=(200/(3**0.5))
SHEAR_STRESS_MIN=(-200/(3**0.5))
MOMENT_MAX=((SHEAR_STRESS_MAX*POLAR)/RADIUS)
MOMENT_MIN=((SHEAR_STRESS_MIN*POLAR)/RADIUS)
!!!!!!!!!!!!!!!!!!!!!!!!!!!!!!!!!!!!!!!!!!!!!!!!!!!!!!!!!!!!!!!!!!!!!!!!!!!!!!!
! Parametric File Setup
! Thermal Cycling
isotherm=1.0            ! 0=Yes, 1=No
SINGLEHOLD=1                ! 0=two holds (normal), 1= single hold at the max temperature
firstholdon=0           ! Different first hold than rest of cycles
holdnumber_ini=1    ! For use when singlehold=1
holdnumber_inc=2    ! 1=0hr, 2=2/60hr, 3=20hr
holdnumber_fin=1
!!!!!!!!!!!!!!!!!!!!!!!!!!!!!!!!!!!!!!!!!!!!!!!!!!!!!!!!!!!!!!!!!!!!!!!!!!!!!!!
! Material Orientation
ang_ini=0.0         ! 90 is L-oriented 0 is T-oriented
ang_inc=-45.0
ang_fin=0.0 !90.0
!!!!!!!!!!!!!!!!!!!!!!!!!!!!!!!!!!!!!!!!!!!!!!!!!!!!!!!!!!!!!!!!!!!!!!!!!!!!!!!
! Parametric Simulation Initiation
!
I=1
J=1
K=1
```

```
L=1
M=1
*DO,holdnumber,holdnumber_ini,holdnumber_fin,holdnumber_inc          !hold time for single
hold
!*DO,strainstuff,1,4,1
*DO,csvlist,1,numtes,1
PARSAV,,FEA_Parameters1,txt
*IF,I,GT,1,THEN
!!!!!!!!!!!!!!!!!!!!!!!!!!!!!!!!!!!!!!!!!!!!!!!!!!!!!!!!!!!!!!!!!!!!!!!!!!!!


! File Naming Convention
Finish
/clear
/PREP7
PARRES,,FEA_Parameters1,txt
*ENDIF
Finish
/FILNAME, C1-S1-Ph1a
/title, C1-S1-Ph1a Isothermal Fatigue Simulation
/prep7
/OUTPUT, FEA_Junk1,txt,,
!!!!!!!!!!!!!!!!!!!!!!!!!!!!!!!!!!!!!!!!!!!!!!!!!!!!!!!!!!!!!!!!!!!!!!!!!!!!
! Simulations set conditions
/inquire, numtes,lines,testconditions,csv
*DIM,tespar,array,numtes,8
*VREAD,tespar(1,1),testconditions,csv,,JIK,8,numtes
(F10.0,F10.0,F10.0,F10.0,F10.0,F10.0,F10.0,F10.0)
AXIAL_STRESS=tespar(csvlist,1)
sr=tespar(csvlist,2)              ! Strain Range
tmc=tespar(csvlist,3)             ! Temperature in compression
tmt=tespar(csvlist,4)             ! Temperature in tension
mrat=tespar(csvlist,5)            ! Strain Ratio -1=ZtC, 0=CR, 1=ZtT
strain_rate=tespar(csvlist,6)     ! Strain rate mm/mm/sec
holdtime=tespar(csvlist,7)        ! Dwell in seconds
dwelltype=tespar(csvlist,8)       !1=dwell in tension, 0=dwell in compression
!!!!!!!!!!!!!!!!!!!!!!!!!!!!!!!!!!!!!!!!!!!!!!!!!!!!!!!!!!!!!!!!!!!!!!!!!!!!
FORCE=(AXIAL_STRESS*AREA)
!!!!!!!!!!!!!!!!!!!!!!!!!!!!!!!!!!!!!!!!!!!!!!!!!!!!!!!!!!!!!!!!!!!!!!!!!!!!
holdtime=holdtime/3600
*IF, holdtime, eq, 0, then
holdtime=1.02e-2/3600
*ENDIF
!!!!!!!!!!!!!!!!!!!!!!!!!!!!!!!!!!!!!!!!!!!!!!!!!!!!!!!!!!!!!!!!!!!!!!!!!!!!
FINISH
```

```
/FILNAME,FEA_N_%tmc%_%tmt%_%AXIAL_STRESS%_%sr%_%mrat%_%strain_rate%_
%holdtime%_%dwelltype%
/Prep7
!!!!!!!!!!!!!!!!!!!!!!!!!!!!!!!!!!!!!!!!!!!!!!!!!!!!!!!!!!!!!!!!!!!!!!!!!!!
! Define the specimen dimensions
side_length=1.00   ! in units of mm
!!!!!!!!!!!!!!!!!!!!!!!!!!!!!!!!!!!!!!!!!!!!!!!!!!!!!!!!!!!!!!!!!!!!!!!!!!!
! Input parameters:
! Geometric:
*SET,DIA_GAGE,6.0          ! Diameter of gage section [mm]
*SET,LEN_SHLD_GRIP,1.66 ! Radius of grip-side shoulder [mm]
*SET,LEN_SHLD_GAGE,3.0  ! Radius of gage-side shoulder [mm]
*SET,DIA_BULG,12.9         ! Diameter of bulge section     [mm]
*SET,DIA_GRIP,7.62         ! Diameter of specimen grip [mm]
*SET,LEN_GRIP,10.34        ! Length of specimen grip [mm]
*SET,LEN_GAGE,50.0         ! Length of gage section [mm]
*SET,LEN_SPEC,100          ! Length of entire specimen     [mm]
*SET,LEN_BULG,10.0         ! Length of bulge section       [mm]
!*****************************************************************************
**
! Parameters derived from geometric relationships
*AFUN, DEG
*SET,l1,LEN_SPEC
*SET,l2,LEN_GRIP
*SET,l3,LEN_BULG
*SET,d1,DIA_GRIP/2  ! grip  radius
*SET,d2,DIA_GAGE/2  ! gage  radius
*SET,d3,DIA_BULG/2  ! bulge radius
*SET,d4,DIA_GAGE/3  ! mesh  radius
*SET,l4,d1-d4
*SET,l5,d2-d4
*SET,l6,LEN_SHLD_GRIP
*SET,l7,LEN_SHLD_GAGE
*SET,r1,(LEN_SHLD_GRIP*LEN_SHLD_GRIP + (d3-d1)*(d3-d1))/(2.0*(d3-d1))
*SET,r2,(LEN_SHLD_GAGE*LEN_SHLD_GAGE + (d3-d2)*(d3-d2))/(2.0*(d3-d2))
!y1=sqrt((r1*r1)-(d3-d1)*(d3-d1))
!y2=sqrt((r2*r2)-(d3-d2)*(d3-d2))
*SET,m1,r1/SQRT(2.0)
*SET,m2,r2/SQRT(2.0)
!*****************************************************************************
**
! 2D Geometry:
!!!!!!!!!!!!!!!!!!!!!!!!!KEY POINTS!!!!!!!!!!!!!!!!!!!!!!!!!!!!
!*****************************************************************************
**
```

```
! 2D Geometry:
! Geometry Keypoints
k,  1,   0.0,    0.0
k,  2,   0.0,    l1
k,  3,   d1,     l1
k,  4,   d1,     l1-l2
k,  5,   d3,     l1-l2-l6
k,  6,   d3,     l1-l2-l6-l3
k,  7,   d2,     l1-l2-l6-l3-l7
k,  8,   d2,     l2+l6+l3+l7
k,  9,   d3,     l2+l6+l3
k, 10,   d3,     l2+l6
k, 11,   d1,     l2
k, 12,   d1,     0.0
k, 13,   d1+r1,  l1-l2
k, 14,   d2+r2,  l1-l2-l6-l3-l7
k, 15,   d2+r2,  l2+l6+l3+l7
k, 16,   d1+r1,  l2
! Mapped meshing keypoints
k, 17,   d1+r1-m1, l1-l2-m1
k, 18,   d2+r2-m2, l1-l2-l6-l3-l7+m2
k, 19,   d2+r2-m2, l2+l6+l3+l7-m2
k, 20,   d1+r1-m1, l2+m1
k, 21,   d3      , l1-l2-l6-l4
k, 22,   d3      , l1-l2-l6-l3+l5
k, 23,   d3      , l2+l6+l3-l5
k, 24,   d3      , l2+l6+l4
k, 25,   d4      , l1
k, 26,   d4      , l1-l2
k, 27,   d4      , l1-l2-l6-l4
k, 28,   d4      , l1-l2-l6-l3+l5
k, 29,   d4      , l1-l2-l6-l3-l7
k, 30,   d4      , l2+l6+l3+l7
k, 31,   d4      , l2+l6+l3-l5
k, 32,   d4      , l2+l6+l4
k, 33,   d4      , l2
k, 34,   d4      , 0.0
k, 35,   0.0     , l1-l2
k, 36,   0.0     , l1-l2-l6-l4
k, 37,   0.0     , l1-l2-l6-l3+l5
k, 38,   0.0     , l1-l2-l6-l3-l7
k, 39,   0.0     , l2+l6+l3+l7
k, 40,   0.0     , l2+l6+l3-l5
k, 41,   0.0     , l2+l6+l4
k, 42,   0.0     , l2
```

```
k, 43,   d2      , l1/2
k, 44,   d4      , l1/2
k, 45,   0.0     , l1/2
!!!!!!!!!!!!!!!!!!!!!!!!!!!!!!!! Geometry Lines!!!!!!!!!!!!!!!!!!!!!!!!!!!!!!!!!!!!
L,     1,  42  ! Line 1
L,    42,  41  ! Line 2
L,    41,  40  ! Line 3
L,    40,  39  ! Line 4
L,    39,  38  ! Line 5 * replaced
L,    38,  37  ! Line 6
L,    37,  36  ! Line 7
L,    36,  35  ! Line 8
L,    35,   2  ! Line 9
L,     2,  25          ! Line 10
L,    25,   3          ! Line 11
L,     3,   4     ! Line 12
Larc,  4,  17, 13, r1 ! Line 13
Larc, 17,   5, 13, r1 ! Line 14
L,     5,  21  ! Line 15
L,    21,  22  ! Line 16
L,    22,   6   ! Line 17
Larc,  6,  18, 14, r2   ! Line 18
Larc, 18,   7, 14, r2   ! Line 19
L,     7,  8           ! Line 20 * replaced
Larc,  8, 19, 15, r2    ! Line 21
Larc, 19,  9, 15, r2    ! Line 22
L,     9, 23           ! Line 23
L,    23, 24           ! Line 24
L,    24, 10           ! Line 25
Larc, 10, 20, 16, r1    ! Line 26
Larc, 20, 11, 16, r1    ! Line 27
L,    11, 12           ! Line 28
L,    12, 34           ! Line 29
L,    34,  1           ! Line 30
! Mapped meshing lines
L,    25, 26           ! Line 31
L,    26, 27           ! Line 32
L,    27, 28           ! Line 33
L,    28, 29           ! Line 34
!L,   29, 30           ! Line 35 * replaced
L,    30, 31           ! Line 36
L,    31, 32           ! Line 37
L,    32, 33           ! Line 38
L,    33, 34           ! Line 39
L,    35, 26           ! Line 40
```

```
L,    36, 27          ! Line 41
L,    37, 28          ! Line 42
L,    38, 29          ! Line 43
L,    39, 30          ! Line 44
L,    40, 31          ! Line 45
L,    41, 32          ! Line 46
L,    42, 33          ! Line 47
L,    26,  4          ! Line 48
L,    27, 17          ! Line 49
L,    27, 21          ! Line 50
L,    28, 22          ! Line 51
L,    28, 18          ! Line 52
L,    29,  7          ! Line 53
L,    30,  8          ! Line 54
L,    31, 19          ! Line 55
L,    31, 23          ! Line 56
L,    32, 24          ! Line 57
L,    32, 20          ! Line 58
L,    33, 11          ! Line 59
L,     7, 43  ! Line 60
L,    43,  8  ! Line 61
L,    29, 44  ! Line 62
L,    44, 30  ! Line 63
L,    38, 45  ! Line 64
L,    45, 39  ! Line 65
L,    43, 44  ! Line 66
L,    44, 45  ! Line 67
! Areas
AL,31,11,12,47
AL,10,9,31,39
AL,8,39,40,32
AL,32,47,13,48
AL,14,48,49,15
AL,8,39,32,40
AL,49,16,33,50
AL,7,40,33,41
AL,41,6,34,42
AL,19,34,52,51
AL,50,17,18,51
AL,42,63,61,66
AL,52,61,59,65
AL,66,64,62,43
AL,65,62,60,53
AL,4,35,44,43
AL,53,35,21,54
```

```
AL,22,23,55,54
AL,44,3,36,45
AL,55,36,56,24
AL,45,2,46,37
AL,37,58,27,57
AL,26,25,56,57
AL,46,1,38,30
AL,58,38,28,29

ksel,all
!*****************************************************************************
**
! 3D Geometry
VROTAT,ALL,,,,,,1,2,360,8
VGLUE, ALL
!!!!!!!!!!!!!!!!!!!!!!!!!!!!!!!!!!!!!!!!!!!!!!!!!!!!!!!!!!!!!!!!!!!!!!!!!!!
! Define the material: Generic materials
!!!!!!!!!!!!!!!!!!!!!!!!!!!!!!!!!!!!!!!!!!!!!!!!!!!!!!!!!!!!!!!!!!!!!!!!!!!
! Elastic Properties (Hooke's Law):
MPTEMP,1,20,300,400,500,600, 650
MPDATA,EX,1,1,193000,175500,168000,159370,148000,145500    !  Long
MPDATA,EY,1,1,193000,175500,168000,159370,148000,145500    !  Trans
MPDATA,EZ,1,1,193000,175500,168000,159370,148000,145500    !  Trans
MPDATA,PRYZ,1,1,0.29,0.29,0.29,0.29,0.29    !  TT
MPDATA,PRXZ,1,1,0.29,0.29,0.29,0.29,0.29    !  TL
MPDATA,PRXY,1,1,0.29,0.29,0.29,0.29,0.29    !  TL
!MPDATA,GXY,1,1,82128.90625,75781.25,75000,68652.34375,58637.10938    !  TL
!MPDATA,GYZ,1,1,82128.90625,75781.25,75000,68652.34375,58637.10938    !  TT
!MPDATA,GXZ,1,1,82128.90625,75781.25,75000,68652.34375,58637.10938    !  TL

TB,PLAS,1,6,38
TBTEMP,20.0
TBPT,DEFI,0,288.4226476
TBPT,DEFI,0.00001,288.4226476
TBPT,DEFI,0.00002,302.3426386
TBPT,DEFI,0.00003,310.7947003
TBPT,DEFI,0.00004,316.9344428
TBPT,DEFI,0.00005,321.7802017
TBPT,DEFI,0.00006,325.7944219
TBPT,DEFI,0.00007,329.2274407
TBPT,DEFI,0.00008,332.2304836
TBPT,DEFI,0.00009,334.9020839
TBPT,DEFI,0.0001,337.3101108
TBPT,DEFI,0.0002,353.5895317
TBPT,DEFI,0.0003,363.4742127
```

TBPT,DEFI,0.0004,370.6546379
TBPT,DEFI,0.0005,376.3217499
TBPT,DEFI,0.0006,381.016378
TBPT,DEFI,0.0007,385.0312914
TBPT,DEFI,0.0008,388.5433482
TBPT,DEFI,0.0009,391.6677832
TBPT,DEFI,0.001,394.4839691
TBPT,DEFI,0.002,413.522742
TBPT,DEFI,0.003,425.0828704
TBPT,DEFI,0.004,433.4803733
TBPT,DEFI,0.005,440.1080573
TBPT,DEFI,0.006,445.5984221
TBPT,DEFI,0.007,450.2938608
TBPT,DEFI,0.008,454.4012092
TBPT,DEFI,0.009,458.0552339
TBPT,DEFI,0.01,461.3487617
TBPT,DEFI,0.02,483.614595
TBPT,DEFI,0.03,497.1341581
TBPT,DEFI,0.04,506.9550325
TBPT,DEFI,0.05,514.706105
TBPT,DEFI,0.06,521.1270833
TBPT,DEFI,0.07,526.618396
TBPT,DEFI,0.08,531.4219374
TBPT,DEFI,0.09,535.6953171
TBPT,DEFI,0.1,539.5470958

TBTEMP,300.0
TBPT,DEFI,0,159.6604192
TBPT,DEFI,0.00001,159.6604192
TBPT,DEFI,0.00002,171.8329494
TBPT,DEFI,0.00003,179.3792146
TBPT,DEFI,0.00004,184.933515
TBPT,DEFI,0.00005,189.3599305
TBPT,DEFI,0.00006,193.0551083
TBPT,DEFI,0.00007,196.2355367
TBPT,DEFI,0.00008,199.0328692
TBPT,DEFI,0.00009,201.5333718
TBPT,DEFI,0.0001,203.7967553
TBPT,DEFI,0.0002,219.3342453
TBPT,DEFI,0.0003,228.966591
TBPT,DEFI,0.0004,236.0563155
TBPT,DEFI,0.0005,241.7063641
TBPT,DEFI,0.0006,246.4230325
TBPT,DEFI,0.0007,250.4826547
TBPT,DEFI,0.0008,254.0532785

TBPT,DEFI,0.0009,257.2450171
TBPT,DEFI,0.001,260.1340875
TBPT,DEFI,0.002,279.9667428
TBPT,DEFI,0.003,292.2618427
TBPT,DEFI,0.004,301.3114422
TBPT,DEFI,0.005,308.5233835
TBPT,DEFI,0.006,314.543922
TBPT,DEFI,0.007,319.7257813
TBPT,DEFI,0.008,324.2834642
TBPT,DEFI,0.009,328.3575232
TBPT,DEFI,0.01,332.0452448
TBPT,DEFI,0.02,357.3604157
TBPT,DEFI,0.03,373.0543583
TBPT,DEFI,0.04,384.6056184
TBPT,DEFI,0.05,393.8112202
TBPT,DEFI,0.06,401.4960691
TBPT,DEFI,0.07,408.1103955
TBPT,DEFI,0.08,413.9279987
TBPT,DEFI,0.09,419.1282858
TBPT,DEFI,0.1,423.8354367

TBTEMP,400.0
TBPT,DEFI,0,139.402307
TBPT,DEFI,0.00001,139.402307
TBPT,DEFI,0.00002,150.760077
TBPT,DEFI,0.00003,157.8282215
TBPT,DEFI,0.00004,163.0432186
TBPT,DEFI,0.00005,167.2066599
TBPT,DEFI,0.00006,170.6872386
TBPT,DEFI,0.00007,173.6864903
TBPT,DEFI,0.00008,176.3271262
TBPT,DEFI,0.00009,178.6896362
TBPT,DEFI,0.0001,180.8297829
TBPT,DEFI,0.0002,195.5628467
TBPT,DEFI,0.0003,204.7314974
TBPT,DEFI,0.0004,211.4962834
TBPT,DEFI,0.0005,216.8970132
TBPT,DEFI,0.0006,221.4119477
TBPT,DEFI,0.0007,225.3025149
TBPT,DEFI,0.0008,228.7278931
TBPT,DEFI,0.0009,231.792492
TBPT,DEFI,0.001,234.568646
TBPT,DEFI,0.002,253.680071
TBPT,DEFI,0.003,265.5734545
TBPT,DEFI,0.004,274.3485947

TBPT,DEFI,0.005,281.3543094
TBPT,DEFI,0.006,287.2109889
TBPT,DEFI,0.007,292.257752
TBPT,DEFI,0.008,296.7010816
TBPT,DEFI,0.009,300.6764157
TBPT,DEFI,0.01,304.2775852
TBPT,DEFI,0.02,329.0685295
TBPT,DEFI,0.03,344.4963801
TBPT,DEFI,0.04,355.8793101
TBPT,DEFI,0.05,364.966978
TBPT,DEFI,0.06,372.5641412
TBPT,DEFI,0.07,379.1106977
TBPT,DEFI,0.08,384.8744927
TBPT,DEFI,0.09,390.0312138
TBPT,DEFI,0.1,394.7025762

TBTEMP,500.0
TBPT,DEFI,0,126.5404407
TBPT,DEFI,0.00001,126.5404407
TBPT,DEFI,0.00002,137.4206227
TBPT,DEFI,0.00003,144.2137839
TBPT,DEFI,0.00004,149.236303
TBPT,DEFI,0.00005,153.2522196
TBPT,DEFI,0.00006,156.6135527
TBPT,DEFI,0.00007,159.512973
TBPT,DEFI,0.00008,162.0679173
TBPT,DEFI,0.00009,164.3554847
TBPT,DEFI,0.0001,166.4291299
TBPT,DEFI,0.0002,180.7390155
TBPT,DEFI,0.0003,189.6735497
TBPT,DEFI,0.0004,196.2792915
TBPT,DEFI,0.0005,201.5611248
TBPT,DEFI,0.0006,205.9820336
TBPT,DEFI,0.0007,209.7954232
TBPT,DEFI,0.0008,213.1557494
TBPT,DEFI,0.0009,216.1644147
TBPT,DEFI,0.001,218.8917245
TBPT,DEFI,0.002,237.7124413
TBPT,DEFI,0.003,249.4633626
TBPT,DEFI,0.004,258.1513983
TBPT,DEFI,0.005,265.0981966
TBPT,DEFI,0.006,270.9126856
TBPT,DEFI,0.007,275.9281502
TBPT,DEFI,0.008,280.3477347
TBPT,DEFI,0.009,284.3048061

TBPT,DEFI,0.01,287.8918316
TBPT,DEFI,0.02,312.6453057
TBPT,DEFI,0.03,328.1004092
TBPT,DEFI,0.04,339.5271295
TBPT,DEFI,0.05,348.6637311
TBPT,DEFI,0.06,356.3110915
TBPT,DEFI,0.07,362.9075551
TBPT,DEFI,0.08,368.7203023
TBPT,DEFI,0.09,373.9247409
TBPT,DEFI,0.1,378.6424859

TBTEMP,600.0
TBPT,DEFI,0,109.7700209
TBPT,DEFI,0.00001,109.7700209
TBPT,DEFI,0.00002,119.208251
TBPT,DEFI,0.00003,125.1011137
TBPT,DEFI,0.00004,129.4579978
TBPT,DEFI,0.00005,132.9416845
TBPT,DEFI,0.00006,135.8575397
TBPT,DEFI,0.00007,138.3726995
TBPT,DEFI,0.00008,140.5890367
TBPT,DEFI,0.00009,142.5734325
TBPT,DEFI,0.0001,144.3722573
TBPT,DEFI,0.0002,156.785652
TBPT,DEFI,0.0003,164.5360913
TBPT,DEFI,0.0004,170.2663734
TBPT,DEFI,0.0005,174.8482047
TBPT,DEFI,0.0006,178.6832099
TBPT,DEFI,0.0007,181.9912105
TBPT,DEFI,0.0008,184.9061922
TBPT,DEFI,0.0009,187.5161188
TBPT,DEFI,0.001,189.8819779
TBPT,DEFI,0.002,206.2083828
TBPT,DEFI,0.003,216.4019531
TBPT,DEFI,0.004,223.9385624
TBPT,DEFI,0.005,229.9647006
TBPT,DEFI,0.006,235.0085948
TBPT,DEFI,0.007,239.3593592
TBPT,DEFI,0.008,243.1932156
TBPT,DEFI,0.009,246.6258559
TBPT,DEFI,0.01,249.7374925
TBPT,DEFI,0.02,271.2103857
TBPT,DEFI,0.03,284.6172225
TBPT,DEFI,0.04,294.5295581
TBPT,DEFI,0.05,302.4552848

TBPT,DEFI,0.06,309.0891396
TBPT,DEFI,0.07,314.8113731
TBPT,DEFI,0.08,319.8537562
TBPT,DEFI,0.09,324.3684499
TBPT,DEFI,0.1,328.4609516

TBTEMP,650.0
TBPT,DEFI,0,98.28951722
TBPT,DEFI,0.00001,98.28951722
TBPT,DEFI,0.00002,106.2976324
TBPT,DEFI,0.00003,111.2812265
TBPT,DEFI,0.00004,114.9582068
TBPT,DEFI,0.00005,117.8937582
TBPT,DEFI,0.00006,120.3478381
TBPT,DEFI,0.00007,122.4625449
TBPT,DEFI,0.00008,124.3243996
TBPT,DEFI,0.00009,125.9901536
TBPT,DEFI,0.0001,127.4991243
TBPT,DEFI,0.0002,137.8870853
TBPT,DEFI,0.0003,144.3517003
TBPT,DEFI,0.0004,149.121403
TBPT,DEFI,0.0005,152.9293394
TBPT,DEFI,0.0006,156.1127209
TBPT,DEFI,0.0007,158.8558748
TBPT,DEFI,0.0008,161.271034
TBPT,DEFI,0.0009,163.4318156
TBPT,DEFI,0.001,165.3892211
TBPT,DEFI,0.002,178.8642688
TBPT,DEFI,0.003,187.2500333
TBPT,DEFI,0.004,193.4371928
TBPT,DEFI,0.005,198.3767689
TBPT,DEFI,0.006,202.5061855
TBPT,DEFI,0.007,206.0645478
TBPT,DEFI,0.008,209.1974423
TBPT,DEFI,0.009,212.0003634
TBPT,DEFI,0.01,214.5394693
TBPT,DEFI,0.02,232.0190218
TBPT,DEFI,0.03,242.8968617
TBPT,DEFI,0.04,250.9227167
TBPT,DEFI,0.05,257.3302325
TBPT,DEFI,0.06,262.6868261
TBPT,DEFI,0.07,267.3026599
TBPT,DEFI,0.08,271.3665857
TBPT,DEFI,0.09,275.0024769
TBPT,DEFI,0.1,278.2961523

TB,Creep,1,27,,10
TBTEMP,20
TBDATA,1,9.39E-40,1,0
TBTEMP,400
TBDATA,1,9.39E-40,1,0
TBTEMP,410
TBDATA,1,9.39E-40,1,0
TBTEMP,420
TBDATA,1,9.39E-40,1,0
TBTEMP,430
TBDATA,1,9.39E-40,1,0
TBTEMP,440
TBDATA,1,9.39E-40,1,0
TBTEMP,450
TBDATA,1,1.22343E-18,6.545051233,0
TBTEMP,460
TBDATA,1,4.14792E-18,6.348537577,0
TBTEMP,470
TBDATA,1,1.36987E-17,6.161962885,0
TBTEMP,480
TBDATA,1,4.41166E-17,5.984628698,0
TBTEMP,490
TBDATA,1,1.38692E-16,5.815898842,0
TBTEMP,500
TBDATA,1,4.26042E-16,5.655192739,0
TBTEMP,510
TBDATA,1,1.27997E-15,5.501979562,0
TBTEMP,520
TBDATA,1,3.76419E-15,5.355773098,0
TBTEMP,530
TBDATA,1,1.08447E-14,5.216127229,0
TBTEMP,540
TBDATA,1,3.0632E-14,5.082631951,0
TBTEMP,550
TBDATA,1,8.48902E-14,4.954909844,0
TBTEMP,560
TBDATA,1,2.30974E-13,4.832612953,0
TBTEMP,570
TBDATA,1,6.17411E-13,4.715420012,0
TBTEMP,580
TBDATA,1,1.6224E-12,4.60303397,0
TBTEMP,590
TBDATA,1,4.19344E-12,4.495179794,0
TBTEMP,600

```
TBDATA,1,1.06672E-11,4.391602491,0
TBTEMP,610
TBDATA,1,2.67195E-11,4.292065351,0
TBTEMP,620
TBDATA,1,6.59357E-11,4.196348358,0
TBTEMP,630
TBDATA,1,1.60375E-10,4.104246769,0
TBTEMP,640
TBDATA,1,3.84657E-10,4.015569835,0
TBTEMP,650
TBDATA,1,9.10164E-10,3.93013964,0



!!!!!!!!!!!!!!!!!!!!!!!!!!!!!!!!!!!!!!!!!!!!!!!!!!!!!!!!!!!!!!!!!!!!!!!!!!!!!!!!
! Create Boundary Conditions
!************************************************************************************
**
! Meshing
! Element type
ET, 1, 186, 0
ESIZE,3,0,
MSHAPE,0,3D
MSHKEY,1
FLST,5,192,6,ORDE,2
FITEM,5,1
FITEM,5,-192
CM,_Y,VOLU
VSEL, , , ,P51X
CM,_Y1,VOLU
CHKMSH,'VOLU'
CMSEL,S,_Y
VMESH,_Y1
CMDELE,_Y
CMDELE,_Y1
CMDELE,_Y2
FINISH
/PREP7
N,30000,0,101,0,,,,
!!!!!!!!!!!!!!!!!!!!!!!!!!!!!!!!!Select Node!!!!!!!!!!!!!!!!!!!!!!!!!!!!!!!!!!!!!!
FLST,5,16,5,ORDE,16
FITEM,5,28
FITEM,5,30
FITEM,5,106
```

```
FITEM,5,108
FITEM,5,184
FITEM,5,186
FITEM,5,262
FITEM,5,264
FITEM,5,340
FITEM,5,342
FITEM,5,418
FITEM,5,420
FITEM,5,496
FITEM,5,498
FITEM,5,574
FITEM,5,-575
ASEL,S, , ,P51X
NSEL,ALL
NSLL,S,1
nsel,a,,,30000
!!!!!!!!!!!!!!!!!!!
et,2,184
keyop,2,1,1    !set option for beam behavior, MPC184
type,2
E,30000,1
E,30000,2
E,30000,3
E,30000,4
E,30000,5
E,30000,54
E,30000,62
E,30000,63
E,30000,64
E,30000,65
E,30000,86
E,30000,87
E,30000,88
E,30000,89
E,30000,90
E,30000,91
E,30000,92
E,30000,93
E,30000,94
E,30000,95
E,30000,96
E,30000,142
E,30000,143
E,30000,144
```

E,30000,145
E,30000,146
E,30000,147
E,30000,148
E,30000,149
E,30000,150
E,30000,151
E,30000,152
E,30000,1779
E,30000,1780
E,30000,1781
E,30000,1782
E,30000,1819
E,30000,1827
E,30000,1828
E,30000,1829
E,30000,1843
E,30000,1844
E,30000,1845
E,30000,1846
E,30000,1847
E,30000,1848
E,30000,1849
E,30000,1850
E,30000,1883
E,30000,1884
E,30000,1885
E,30000,1886
E,30000,1887
E,30000,1888
E,30000,1889
E,30000,3004
E,30000,3005
E,30000,3006
E,30000,3007
E,30000,3044
E,30000,3052
E,30000,3053
E,30000,3054
E,30000,3068
E,30000,3069
E,30000,3070
E,30000,3071
E,30000,3072
E,30000,3073

E,30000,3074
E,30000,3075
E,30000,3108
E,30000,3109
E,30000,3110
E,30000,3111
E,30000,3112
E,30000,3113
E,30000,3114
E,30000,4229
E,30000,4230
E,30000,4231
E,30000,4232
E,30000,4269
E,30000,4277
E,30000,4278
E,30000,4279
E,30000,4293
E,30000,4294
E,30000,4295
E,30000,4296
E,30000,4297
E,30000,4298
E,30000,4299
E,30000,4300
E,30000,4333
E,30000,4334
E,30000,4335
E,30000,4336
E,30000,4337
E,30000,4338
E,30000,4339
E,30000,5454
E,30000,5455
E,30000,5456
E,30000,5457
E,30000,5494
E,30000,5502
E,30000,5503
E,30000,5504
E,30000,5518
E,30000,5519
E,30000,5520
E,30000,5521
E,30000,5522

E,30000,5523
E,30000,5524
E,30000,5525
E,30000,5558
E,30000,5559
E,30000,5560
E,30000,5561
E,30000,5562
E,30000,5563
E,30000,5564
E,30000,6679
E,30000,6680
E,30000,6681
E,30000,6682
E,30000,6719
E,30000,6727
E,30000,6728
E,30000,6729
E,30000,6743
E,30000,6744
E,30000,6745
E,30000,6746
E,30000,6747
E,30000,6748
E,30000,6749
E,30000,6750
E,30000,6783
E,30000,6784
E,30000,6785
E,30000,6786
E,30000,6787
E,30000,6788
E,30000,6789
E,30000,7904
E,30000,7905
E,30000,7906
E,30000,7907
E,30000,7944
E,30000,7952
E,30000,7953
E,30000,7954
E,30000,7968
E,30000,7969
E,30000,7970
E,30000,7971

```
E,30000,7972
E,30000,7973
E,30000,7974
E,30000,7975
E,30000,8008
E,30000,8009
E,30000,8010
E,30000,8011
E,30000,8012
E,30000,8013
E,30000,8014
E,30000,9129
E,30000,9130
E,30000,9131
E,30000,9156
E,30000,9157
E,30000,9158
E,30000,9172
E,30000,9173
E,30000,9174
E,30000,9175
E,30000,9176
E,30000,9196
E,30000,9197
E,30000,9198
E,30000,9199
E,30000,9164
E,30000,9165
E,30000,9166
E,30000,9167
E,30000,9168
E,30000,9169
E,30000,9170
E,30000,9171
ALLS
 FINISH
/SOL
FINISH
/PREP7
!*
FINISH
/SOL
!!!!!!!!!!!!!!!!!!!!!!!!!!!!!!!!!!!!!!!!!!!!!!!!!!!!!!!!
FINISH
/PREP7
```

```
N,20000,0,105,0,,,,
!!!!!!!!!!!!!!!!!!!!!!!!
FLST,5,8,5,ORDE,8
FITEM,5,27
FITEM,5,105
FITEM,5,183
FITEM,5,261
FITEM,5,339
FITEM,5,417
FITEM,5,495
FITEM,5,573
ASEL,S, , ,P51X
NSLA,S,1
nsel,a,,,20000
!!!!!!!!!!!!!!!!!!!!!!!!!!!!!!!!!!!!!!!!!!!!!!!!!!!!!!!!!!!!
et,2,184
keyop,2,1,1    !set option for beam behavior, MPC184
type,2
!!!!!!!!!!!!!!!!!!!!!!!!!!!!!!!!!!!!!!!!!!!!!!!!!!!!!!!!!!!!
E,20000,38
E,20000,42
E,20000,43
E,20000,44
E,20000,45
E,20000,54
E,20000,55
E,20000,56
E,20000,57
E,20000,58
E,20000,59
E,20000,60
E,20000,61
E,20000,66
E,20000,67
E,20000,68
E,20000,69
E,20000,70
E,20000,71
E,20000,72
E,20000,73
E,20000,74
E,20000,75
E,20000,76
E,20000,77
E,20000,78
```

E,20000,79
E,20000,80
E,20000,81
E,20000,82
E,20000,83
E,20000,84
E,20000,85
E,20000,1807
E,20000,1811
E,20000,1812
E,20000,1813
E,20000,1820
E,20000,1821
E,20000,1822
E,20000,1823
E,20000,1824
E,20000,1825
E,20000,1826
E,20000,1830
E,20000,1831
E,20000,1832
E,20000,1833
E,20000,1834
E,20000,1835
E,20000,1836
E,20000,1837
E,20000,1838
E,20000,1839
E,20000,1840
E,20000,1841
E,20000,1842
E,20000,3032
E,20000,3036
E,20000,3037
E,20000,3038
E,20000,3045
E,20000,3046
E,20000,3047
E,20000,3048
E,20000,3049
E,20000,3050
E,20000,3051
E,20000,3055
E,20000,3056
E,20000,3057

E,20000,3058
E,20000,3059
E,20000,3060
E,20000,3061
E,20000,3062
E,20000,3063
E,20000,3064
E,20000,3065
E,20000,3066
E,20000,3067
E,20000,4257
E,20000,4261
E,20000,4262
E,20000,4263
E,20000,4270
E,20000,4271
E,20000,4272
E,20000,4273
E,20000,4274
E,20000,4275
E,20000,4276
E,20000,4280
E,20000,4281
E,20000,4282
E,20000,4283
E,20000,4284
E,20000,4285
E,20000,4286
E,20000,4287
E,20000,4288
E,20000,4289
E,20000,4290
E,20000,4291
E,20000,4292
E,20000,5482
E,20000,5486
E,20000,5487
E,20000,5488
E,20000,5495
E,20000,5496
E,20000,5497
E,20000,5498
E,20000,5499
E,20000,5500
E,20000,5501

E,20000,5505
E,20000,5506
E,20000,5507
E,20000,5508
E,20000,5509
E,20000,5510
E,20000,5511
E,20000,5512
E,20000,5513
E,20000,5514
E,20000,5515
E,20000,5516
E,20000,5517
E,20000,6707
E,20000,6711
E,20000,6712
E,20000,6713
E,20000,6720
E,20000,6721
E,20000,6722
E,20000,6723
E,20000,6724
E,20000,6725
E,20000,6726
E,20000,6730
E,20000,6731
E,20000,6732
E,20000,6733
E,20000,6734
E,20000,6735
E,20000,6736
E,20000,6737
E,20000,6738
E,20000,6739
E,20000,6740
E,20000,6741
E,20000,6742
E,20000,7932
E,20000,7936
E,20000,7937
E,20000,7938
E,20000,7945
E,20000,7946
E,20000,7947
E,20000,7948

```
E,20000,7949
E,20000,7950
E,20000,7951
E,20000,7955
E,20000,7956
E,20000,7957
E,20000,7958
E,20000,7959
E,20000,7960
E,20000,7961
E,20000,7962
E,20000,7963
E,20000,7964
E,20000,7965
E,20000,7966
E,20000,7967
E,20000,9148
E,20000,9149
E,20000,9150
E,20000,9159
E,20000,9160
E,20000,9161
E,20000,9162
E,20000,9163
E,20000,9164
E,20000,9165
E,20000,9166
E,20000,9167
E,20000,9168
E,20000,9169
E,20000,9170
E,20000,9171

ALLS
FINISH
/SOL
!!!!!!!!!!!!!!!!!!!!!!!!!!!!!!!!!!!!!!!!!!!!!!!!!!!!!!!!!!!!
FLST,2,16,5,ORDE,16
FITEM,2,98
FITEM,2,101
FITEM,2,176
FITEM,2,179
FITEM,2,254
FITEM,2,257
FITEM,2,332
```

```
FITEM,2,335
FITEM,2,410
FITEM,2,413
FITEM,2,488
FITEM,2,491
FITEM,2,566
FITEM,2,569
FITEM,2,622
FITEM,2,624
!*
/GO
DA,P51X,ALL,0
!!!!!!!!!!!!!!!!!!!!!!!!!!!!!!!!!!!!!!!!!!!!!!!!!!!!!!!!!!!!!!!!!!!!!!!!!!!!!!
! Define Fatigue Cycling Parameters:
! Mechanical Loading
strain_range = sr                                    ! Difference in Max and Min strains
[mm/mm]
tol=0.0001
re=(mrat-1+tol)/(mrat+1+tol)                         ! Strain ratio (0 = Z-to-T, -1 = CR, -900 = Z-
to-C)
strain_ratio=re
*IF, mrat, EQ, 2, THEN
strain_ratio=0.5
*ENDIF
*IF, mrat, EQ, 3, THEN
strain_ratio=0.267
*ENDIF
*IF, mrat, EQ, 4, THEN
strain_ratio=0.333
*ENDIF
*IF, mrat, EQ, 5, THEN
strain_ratio=0.5
*ENDIF
*IF, mrat, EQ, 6, THEN
strain_ratio=0.667
*ENDIF
tens_hold = 18          !1.01e-2/3600                      ! Tension hold [hr]
comp_hold = 1.02e-2/3600                    !1.00e-2/3600          !18.0
        ! Compression hold [hr]
first_hold = 20         !5000.0                            !5000.00 !
        ! First hold [hr] ex:5000 hr hold
displ_range = strain_range*side_length                     ! Displacement [mm]
displ_max = displ_range/(1.0-strain_ratio)                 ! Displacement [mm]
displ_min = displ_max-displ_range                    ! Displacement [mm]
displ_mean = 0.5*(displ_max+displ_min)                     ! Displacement [mm]
```

```
strain_rate_hr = strain_rate*3600.0                    ! Strain rate [mm/mm/hr]
half_cycle = strain_range/strain_rate_hr/2.0           ! Half cycle [hr] ! needs to be modified for
z-t and z-c
full_cycle = 2.0*half_cycle                            ! Full cycle [hr]
!displ_rate = displ_range/half_cycle
! Cycle Stepping and Ramping Time
num_cycles = 1
tot_load_steps=num_cycles*4+2
load_init_time = 1.0E-2/3600.0                               ! Initial Load Time [hr]
load_mini_time = 1.0E-4/3600.0                               ! Minimum Deltim step time [hr]
load_mini_dwell_time = 1.0E-4/3600.0                                 ! Minimum Deltim step time
[hr]
load_maxi_time = 1.0E-1/3600.0                               ! Maximum Deltim step time [hr]
load_maxi_dwell_time = 300          !10000.0/3600.0                          ! Maximum Deltim
step time [hr]
load_ramp_time = 1.0E-10/3600.0                              ! Ramp time used in Deltim [hr]
data_freq = 1.0                                              ! Frequency of data capture
tmca=tmc*isotherm+(1-isotherm)*tmt
max_temp=0.5*(tmt+tmca+abs(tmt-tmca))
min_temp=0.5*(tmt+tmca-abs(tmt-tmca))
temp_range=abs(tmt-tmca)
!temp_rate=temp_range/full_cycle
!
*IF, tmt, NE, tmca, THEN                               !temp controlled strain rate for TMF
temp_rate = 3          !3 degress per second for TMF
temp_rate_hr = temp_rate*3600.0
half_cycle = temp_range/temp_rate_hr/2.0               ! Half cycle [hr] ! needs to be modified for
z-t and z-c
full_cycle = 2.0*half_cycle                            ! Full cycle [hr]
*ENDIF

load_init_time = half_cycle/100.0                      ! Initial Load Time [hr]
load_mini_time = half_cycle/200.0                      ! Minimum Deltim step time [hr]
load_maxi_time = half_cycle/50.0                             ! Maximum Deltim step time [hr]

!!!!!!!!!!!!!!!!!!!!!!!!!!!!!!!!!!!!!!!!!!!!!!!!!!!!!!!!!!!!!!!!!!!!!!!!!!
! Assign the Peak-Valley-Period Values (based on strain ratio and phasing)
! Cycling rules:
valley_displ=displ_min
mean_temp=0.5*(tmt+tmca)
temp_init=mean_temp
peak_temp=tmt
valley_temp=tmca
*IF,dwelltype,EQ,1,THEN
peak_hold=holdtime
```

```
valley_hold=1.01e-2/3600
*ENDIF
*IF,dwelltype,EQ,0,THEN
peak_hold=1.01e-2/3600
valley_hold=holdtime
*ENDIF
*IF, SINGLEHOLD, EQ, 0, THEN
*IF,mrat,eq,0,and,comp_hold,gt,tens_hold,THEN ! See Rule #2
peak_displ=displ_min
valley_displ=displ_max
*ENDIF
*ENDIF
*IF,mrat,eq,-1,THEN ! See Rule #3 (only in Z-to-C case)
peak_displ=displ_min
valley_displ=displ_max
half_cycle=half_cycle*2
peak_temp=tmca
valley_temp=tmt
temp_init=tmt
*IF,dwelltype,EQ,0,THEN
peak_hold=holdtime
valley_hold=1.01e-2/3600
*ENDIF
*IF,dwelltype,EQ,1,THEN
peak_hold=1.01e-2/3600
valley_hold=holdtime
*ENDIF
*ENDIF
*IF,mrat,eq,1,THEN  ! See Rule #4 (only in Z-to-T case)
peak_displ=displ_max
valley_displ=displ_min
half_cycle=half_cycle*2
peak_temp=tmt
valley_temp=tmca
temp_init=tmca
*IF,dwelltype,EQ,1,THEN
peak_hold=holdtime
valley_hold=1.01e-2/3600
*ENDIF
*IF,dwelltype,EQ,0,THEN
peak_hold=1.01e-2/3600
valley_hold=holdtime
*ENDIF
*ENDIF
*IF, SINGLEHOLD, EQ, 1, THEN
```

```
*IF,mrat,eq,0,and,tmca,gt,tmt,THEN ! See Rule #2
peak_displ=displ_min
valley_displ=displ_max
peak_temp=tmca
valley_temp=tmt
*ENDIF
*IF, peak_temp, GT, valley_temp, THEN
peak_hold=holdtime
valley_hold=1.01e-2/3600
*ENDIF
*IF, peak_temp, LT, valley_temp, THEN
peak_hold=1.01e-2/3600
valley_hold=holdtime
*ENDIF
! Fixing the substep times
load_init_dwell_time_peak = 1.0E-2/3600.0
load_init_dwell_time_valley = 1.0E-2/3600.0
load_init_dwell_time_first = 1.0E-2/3600.0
*IF, first_hold, GT, 2.0E-2/3600, THEN
load_init_dwell_time_first = first_hold/20
*ENDIF
*IF, peak_hold, GT, 2.0E-2/3600, THEN
load_init_dwell_time_peak = peak_hold/20
*ENDIF
*IF, valley_hold, GT, 2.0E-2/3600, THEN
load_init_dwell_time_valley = valley_hold/20
*ENDIF
*IF, firstholdon, EQ, 0, THEN
first_hold=peak_hold
*ENDIF
!tref,temp_init             !ignore CTE for single element case
FINISH                      ! Finish pre-processing
!switch back to the global system to define boundry conditions
!local,12,0,0,0,0,0,-ang,0,,          ! trying to get reference frame back to global
!rsys,0
! Begin Initial Solution Stage
/CONFIG,NRES,500000
/NERR,5000000,5000000,,0
/SOLU
ALLSEL
!!!!!!!!!!!!!!!!!!!!!!!!!!!!!!!!!!!!!!!!!!!!!!!!!!!!!!!!!!!!!!!!!!!!!!!!!!!!!!!!!!!!!!!!!!!!!!!!!!!!!!!!!!!!!!!!!!!!!!!!!!!!!!!!
!!!!!!!!!!!!!!!!!!!!!!!!!!!!!!!!!!!!!!!!!!!!!!!!!!!!
! Step 1                                        ! renamed step
total_time = abs(load_ramp_time)                ! Total time [s]
```

```
Antype, trans                                    ! ANTYPE, Antype, Status, LDSTEP,
SUBSTEP, Action
nropt,auto                                       ! Uses Newton-Raphson
lnsrch,auto                                      ! Auto line searching for NR
NLGEOM,auto                             ! Non-linear geometry
Solcontrol, 1                                    ! Optimizes nonlinear solutions
Cnvtol,F,3
Time, total_time                                 ! Time at end of step
NSUBST,5,1000,5                                  ! Specifies substeps
!Deltim, load_init_time, load_mini_time, load_maxi_time   ! DELTIM, DTIME, DTMIN,
DTMAX, Carry
Autots, 1                                        ! Auto Time Stepping
!D, TOP , UZ , displ_init                                             ! modified
displacement
!NSEL,ALL
BF,ALL,TEMP,temp_init                                 ! Nodal body force load
Outres, All, data_freq                           ! Outputs data to be read by ESOL
Crplim, 20, 1                                    ! CRPLIM, CRCR, Option, !Creep Ratio
Limit
Rate, 0                                          ! Activates Creep for step
Kbc, 0                                           ! Specifies stepped or ramped load,
1=stepped
Solve
!!!!!!!!!!!!!!!!!!!!!!!!!!!!!!!!!!!!!!!!!!!!!!!!!!!!!!!!!!!!!!!!!!!!!!!!!!!!!!!!!!!!!!!!!!!!!!!!!!!!!!!!!!!!!!!!!
!!!!!!!!!!!!!!!!!!!!!!!!!!!!!!!!!!!!!!!!!!!!!!!!
! Step 2:
*SET,total_time , (6/3600)+total_time
Antype, trans
nropt,auto
lnsrch,auto
NLGEOM,auto
Solcontrol, 1
Cnvtol,F,3
Time, total_time
NSUBST,50,200,50 !NSUBST,20,400,20
!Deltim, load_init_time, load_mini_time, load_maxi_time
Autots, 1
FLST,2,1,1,ORDE,1
FITEM,2,20000
!*
/GO
F,P51X,FY,FORCE
NSEL,ALL
BF,ALL,TEMP,peak_temp
Outres, All, data_freq
```

```
Crplim, 20, 1
Rate, 1
Kbc, 0
Solve
!!!!!!!!!!!!!!!!!!!!!!!!!!!!!!!!!!!!!!!!!!!!!!!!!!!!!!!!!!!!!!!!!!!!!!!!!!!!!!!!!!!!!!!!!!!!!!!!!!!!!!!!!!!!!!!!!!!!!!!!
!!!!!!!!!!!!!!!!!!!!!!!!!!!!!!!!!!!!!!!!!!!!!!!!
! Step 3:
total_time = abs(half_cycle)+total_time
Antype, trans
nropt,auto
lnsrch,auto
NLGEOM,auto
Solcontrol, 1
Cnvtol,F,3
Time, total_time
NSUBST,50,150,50    !NSUBST,70,100,70
Autots, 1
FLST,2,1,1,ORDE,1
FITEM,2,20000
/GO
F,P51X,FY,FORCE
FLST,2,1,1,ORDE,1
FITEM,2,30000
/GO
F,P51X,MY,peak_displ                                    ! modified
displacement
NSEL,ALL
BF,ALL,TEMP,peak_temp
Outres, All, data_freq
Crplim, 20, 1
Rate, 1
Kbc, 0
Solve
!!!!!!!!!!!!!!!!!!!!!!!!!!!!!!!!!!!!!!!!!!!!!!!!!!!!!!!!!!!!!!!!!!!!!!!!!!!!!!!!!!!!!!!!!!!!!!!!!!!!!!!!!!!!!!!!!!!!!!!!
!!!!!!!!!!!!!!!!!!!!!!!!!!!!!!!!!!!!!!!!!!!!!!!!
! Continue Solution Stage with Subsequent Cycling
total_cycles=num_cycles                          ! Number of cycles
*do,cycle,1,total_cycles,1                  ! Do cycles from 1 to total_cycles with
increment 1
!!!!!!!!!!!!!!!!!!!!!!!!!!!!!!!!!!!!!!!!!!!!!!!!!!!!!!!!!!!!!!!!!!!!!!!!!!!!!!!!!!!!!!!!!!!!!!!!!!!!!!!!!!!!!!!!!!!!!!!!
!!!!!!!!!!!!!!!!!!!!!!!!!!!!!!!!!!!!!!!!!!!!!!!!
! Step 4:
!*GET, LOADNUM,ACTIVE,0,SOLU, NCMLS
!*IF, LOADNUM, EQ, 2, THEN                  ! Equal to 2 because the 3rd load step
hasn't started yet
```

```
!total_time = abs(first_hold) + total_time
total_time = abs(peak_hold) + total_time
Antype, trans
nropt,auto
lnsrch,auto
NLGEOM,auto                ! Non-linear geometry
Solcontrol, 1
Cnvtol,F,3
Time, total_time
NSUBST,30,100,30
Autots, 1
FLST,2,1,1,ORDE,1
FITEM,2,20000
/GO
F,P51X,FY,FORCE
FLST,2,1,1,ORDE,1
FITEM,2,30000
/GO
F,P51X,MY,peak_displ                                          ! modified
displacement
NSEL,ALL
BF,ALL,TEMP,peak_temp
Outres, All, data_freq
Crplim, 20, 1
Rate, 1
Kbc, 0
Solve
!!!!!!!!!!!!!!!!!!!!!!!!!!!!!!!!!!!!!!!!!!!!!!!!!!!!!!!!!!!!!!!!!!!!!!!!!!!!!!!!!!!!!!!!!!!!!!!!!!!!!!!!!!!!!!!!!!!!!!!!!!!!!!!!!
!!!!!!!!!!!!!!!!!!!!!!!!!!!!!!!!!!!!!!!!!!!!!!!!!!!
! Step 5:
total_time = abs(full_cycle) + total_time
Antype, trans
nropt,auto
lnsrch,auto
NLGEOM,auto                ! Non-linear geometry
Solcontrol, 1
Cnvtol,F,3
Time, total_time
NSUBST,50,300,50
Autots, 1
FLST,2,1,1,ORDE,1
FITEM,2,20000
/GO
F,P51X,FY,FORCE
FLST,2,1,1,ORDE,1
```

```
FITEM,2,30000
/GO
F,P51X,MY,valley_displ                                          ! modified
displacement
NSEL,ALL
BF,ALL,TEMP,valley_temp
Outres, All, data_freq
Crplim, 20, 1
Rate, 1
Kbc, 0
Solve
!!!!!!!!!!!!!!!!!!!!!!!!!!!!!!!!!!!!!!!!!!!!!!!!!!!!!!!!!!!!!!!!!!!!!!!!!!!!!!!!!!!!!!!!!!!!!!!!!!!!!!!!!!!!!!!!!!!!
!!!!!!!!!!!!!!!!!!!!!!!!!!!!!!!!!!!!!!!!!!!!!!!!
! Step 6:
total_time = abs(valley_hold) + total_time
Antype, trans
nropt,auto
lnsrch,auto
NLGEOM,auto             ! Non-linear geometry
Solcontrol, 1
Cnvtol,F,3
Time, total_time
NSUBST,50,100,50
!Deltim, load_init_dwell_time_valley, load_mini_dwell_time, load_maxi_dwell_time
Autots, 1
FLST,2,1,1,ORDE,1
FITEM,2,20000
/GO
F,P51X,FY,FORCE
FLST,2,1,1,ORDE,1
FITEM,2,30000
/GO
F,P51X,MY,valley_displ                                          ! modified
displacement
NSEL,ALL
BF,ALL,TEMP,valley_temp
Outres, all, data_freq
Crplim, 20, 1
Rate, 1
Kbc, 0
Solve
!!!!!!!!!!!!!!!!!!!!!!!!!!!!!!!!!!!!!!!!!!!!!!!!!!!!!!!!!!!!!!!!!!!!!!!!!!!!!!!!!!!!!!!!!!!!!!!!!!!!!!!!!!!!!!!!!!!!
!!!!!!!!!!!!!!!!!!!!!!!!!!!!!!!!!!!!!!!!!!!!!!!!
! Step 7:
total_time = abs(full_cycle) + total_time
```

```
Antype, trans
nropt,auto
lnsrch,auto
NLGEOM,auto                    ! Non-linear geometry
Solcontrol, 1
Cnvtol,F,3
Time, total_time
NSUBST,50,300,50
Autots, 1
FLST,2,1,1,ORDE,1
FITEM,2,20000
/GO
F,P51X,FY,FORCE
FLST,2,1,1,ORDE,1
FITEM,2,30000
/GO
F,P51X,MY,peak_displ                                        ! modified displacement
NSEL,ALL
BF,ALL,TEMP,peak_temp
Outres, all, data_freq
Crplim, 20, 1
Rate, 1
Kbc, 0
Solve
*enddo
FINISH
!!!!!!!!!!!!!!!!!!!!!!!!!!!!!!!!!!!!!!!!!!!!!!!!!!!!!!!!!!!!!!!!!!!!!!!!!!!!!!!!!!!!!!!!!!!!!!!!!!!!!!!!!!!!!!!!!!!!!!!!!!!!!!!!!!!
!!!!!!!!!!!!!!!!!!!!!!!!!!!!!!!!!!!!!!!!!!!!!!!
/Post1
allsel
SAVE
/OUTPUT, FEA_Junk3,txt
ALLSEL
RSYS,0                 ! global
*GET,LSTSET, ACTIVE, 0, SET, NSET
TOTARRAYSTEPS=LSTSET
*dim,atime,array,TOTARRAYSTEPS
*dim,acurlo,array,TOTARRAYSTEPS
*dim,acursb,array,TOTARRAYSTEPS
*dim,TEMPERATUREVALUE,array,TOTARRAYSTEPS
*dim,EFFECTIVESTRESS,array,TOTARRAYSTEPS
*dim,YYSTRESS,array,TOTARRAYSTEPS
*dim,XYSTRESS,array,TOTARRAYSTEPS
*dim,EFFECTIVESTRAIN,array,TOTARRAYSTEPS
*dim,YYSTRAIN,array,TOTARRAYSTEPS
```

```
*dim,XYSTRAIN,array,TOTARRAYSTEPS
*dim,EYYSTRAIN,array,TOTARRAYSTEPS
*dim,EXYSTRAIN,array,TOTARRAYSTEPS
*dim,PYYSTRAIN,array,TOTARRAYSTEPS
*dim,PXYSTRAIN,array,TOTARRAYSTEPS
*dim,CYYSTRAIN,array,TOTARRAYSTEPS
*dim,CXYSTRAIN,array,TOTARRAYSTEPS
!t=1
!*DO,tttt,RFTSET,LSTSET,1
*DO,t,1,LSTSET,1
!SET,,,,,,tttt
SET,,,,,,t

*GET,acurlo(t), ACTIVE, 0, SET, LSTP
*GET,acursb(t), ACTIVE, 0, SET, SBST                    !get the current sub step
*GET,atime(t), ACTIVE,0, SET, TIME
!!!!!!!!!!!!!!!!!!!!!!!!!!!!!!!!!!!!!!!!!!!!!!!!!!!!!!!!!!!!!!!!!!!!!!!!!!!!!!!!!!!!!!!!!!!!!!!!!!!!!!!!!!!!!!!!!!!!!!!!!!!!!!!
!!!!!!!!!!!!!!!!!!!!!!!!!!!!!!!!!!!!!!!!!!!!!!!!!!
ETABLE, CSTRVALN, EPCR, Z                               ! Make an element table for
other stresses and strains
ETABLE, TEMPVAL, BFE, TEMP
ETABLE, ESTRESS, S, EQV
ETABLE, STRESSX, S, X
ETABLE, STRESSY, S, Y
ETABLE, STRESSZ, S, Z
ETABLE, STRESSXY, S, XY
ETABLE, STRESSYZ, S, YZ
ETABLE, STRESSXZ, S, XZ
ETABLE, ESTRAIN, EPTO, EQV
ETABLE, STRAINX, EPTO, X
ETABLE, ESTRINY, EPEL, Y
ETABLE, PSTRINY, EPPL, Y
ETABLE, CSTRINY, EPCR, Y
ETABLE, STRAINY, EPTO, Y
ETABLE, STRAINZ, EPTO, Z
ETABLE, ESTRINXY, EPEL, XY
ETABLE, PSTRINXY, EPPL, XY
ETABLE, CSTRINXY, EPCR, XY
ETABLE, STRAINXY, EPTO, XY
ETABLE, STRAINYZ, EPTO, YZ
ETABLE, STRAINXZ, EPTO, XZ
!!!!!!!!!!!!!!!!!!!!!!!!!!!!!!!!!!!!!!!!!!!!!!!!!!!!!!!!!!!!!!!!!!!!!!!!!!!!!!!!!!!!!!!!!!!!!!!!!!!!!!!!!!!!!!!!!!!!!!!!!!!!!!!
!!!!!!!!!!!!!!!!!!!!!!!!!!!!!!!!!!!!!!!!!!!!!!!!!!
*GET,TEMPERATUREVALUE(t),ELEM,1430,ETAB,TEMPVAL
*GET,EFFECTIVESTRESS(t),ELEM,1430,ETAB,ESTRESS
```

```
*GET,YYSTRESS(t),ELEM,1430,ETAB,STRESSY
*GET,XYSTRESS(t),ELEM,1430,ETAB,STRESSXY
*GET,EFFECTIVESTRAIN(t),ELEM,1430,ETAB, ESTRAIN
*GET,YYSTRAIN(t),ELEM,1430,ETAB, STRAINY
*GET,XYSTRAIN(t),ELEM,1430,ETAB, STRAINXY
*GET,EYYSTRAIN(t),ELEM,1430,ETAB, ESTRINY
*GET,EXYSTRAIN(t),ELEM,1430,ETAB, ESTRINXY
*GET,PYYSTRAIN(t),ELEM,1430,ETAB, PSTRINY
*GET,PXYSTRAIN(t),ELEM,1430,ETAB, PSTRINXY
*GET,CYYSTRAIN(t),ELEM,1430,ETAB, CSTRINY
*GET,CXYSTRAIN(t),ELEM,1430,ETAB, CSTRINXY
!!!!!!!!!!!!!!!!!!!!!!!!!!!!!!!!!!!!!!!!!!!!!!!!!!!!!!!!!!!!!!!!!!!!!!!!!!!!!!!!!!!!!!!!!!!!!!!!!!!!!!!!!!!!!!!!!!!!!!!!!!!!!!!!!!!!!!!!!!!!!!!!!!!!!!!!!!!!!!!!!!!!!!!!!!!!!!!!
!t=t+1
*ENDDO
!CYYSTRAIN(1),CXYSTRAIN(1),
!,6X E11.5,6X E11.5
! Hysteresis File
!!!!!!!!!!!!!!!!!!!!!!!!!!!!!!!!!!!!!!!!!!!!!!!!!!!!!!!!!!!!!!!!!!!!!!!!!!!!!!!!!!!!!!!!!!!!!!!!!!!!!!!!!!!!!!!!!!!!!!!!!!!!!!!!!!!!!!!!!!!!!!!!!!!!!!!!!!!!!!!!!!!!!!!!!!!!!!!!
*CFOPEN,
FEA_N_%tmc%_%tmt%_%AXIAL_STRESS%_%sr%_%mrat%_%strain_rate%_%holdtime%
_%dwelltype%,data,,
*VWRITE, atime(1),acurlo(1), acursb(1),
TEMPERATUREVALUE(1),EFFECTIVESTRESS(1),YYSTRESS(1),XYSTRESS(1),EFFECT
IVESTRAIN(1),EYYSTRAIN(1),EXYSTRAIN(1),PYYSTRAIN(1),PXYSTRAIN(1),CYYSTR
AIN(1),CXYSTRAIN(1),YYSTRAIN(1),XYSTRAIN(1)
(E11.5,6X F10.2,6X F10.2,6X F10.2,6X F10.3,6X F10.3,6X F10.3,6X E11.5,6X E11.5,6X
E11.5,6X E11.5,6X E11.5,6X E11.5,6X E11.5,6X E11.5,6X E11.5)
*CFCLOS
! Index File
*CFOPEN, FEA_Index_N,txt,,append
JOB_NAME1='FEA_N_%tmc%_%tmt%_%AXIAL_STRESS%_%sr%_'
JOB_NAME2='%mrat%_%strain_rate%_%holdtime%_%dwelltype%'
*VWRITE, JOB_NAME1,JOB_NAME2
%C%C
/OUTPUT, FEA_Junk22,txt
!!!!!!!!!!!!!!!!!!!!!!!!!!!!!!!!!!!!!!!!!!!!!!!!!!!!!!!!!!!!!!!!!!!!!!!!!!!!!!!!!!!!!!!!!!!!!!!!!!!!!!!!!!!!!!!!!!!!!!!!!!!!!!!!!!!!!!!!!!!!!!!!!!!!!!!!!!!!!!!!!!!!!!!!!!!!!!!!
! Parametric Simulation Termination
!
I=I+1
J=J+1
K=K+1
L=L+1
```

```
M=M+1
FINISH
*ENDDO
*ENDDO
!*ENDDO
*ENDDO
```

CODE2:

```
/batch
*get,_wallstrt,active,,time,wall
! ANSYS input file written by Workbench version 17.2 RELEASE
! File used for geometry attach: C:\Users\Bassem Felemban\Desktop\Exp. Vs Simu. 304
SS_files\dp0\SYS\DM\SYS.scdoc
/title,Exp. Vs Simu. 304 SS--Static Structural (A5)
*DIM,_wb_ProjectScratch_dir,string,248
_wb_ProjectScratch_dir(1) = 'C:\Users\Bassem Felemban\Desktop\Exp. Vs Simu. 304
SS_files\dp0\SYS\MECH\'
*DIM,_wb_SolverFiles_dir,string,248
_wb_SolverFiles_dir(1) = 'C:\Users\Bassem Felemban\Desktop\Exp. Vs Simu. 304
SS_files\dp0\SYS\MECH\'
*DIM,_wb_userfiles_dir,string,248
_wb_userfiles_dir(1) = 'C:\Users\Bassem Felemban\Desktop\Exp. Vs Simu. 304
SS_files\user_files\'
/com,--- Data in consistent NMM units. See Solving Units in the help system for more
information.
/units,MPA
/nopr
/wb,file,start              !  signify a WB generated input file
/prep7
SHPP,OFF,,NOWARN
/nolist
etcon,set            ! allow ANSYS to choose best KEYOP's for 180x elements
/com,************ Nodes for the whole assembly ************
nblock,3
(1i9,3e20.9e3)
 /wb,elem,start            !  set before creation of elements
/com,************ Elements for Body 1 "SYS\Solid" ************
et,1,187
eblock,19,solid,,22
(19i9)
/wb,elem,end               !  done creating elements
/com,************ Send User Defined Coordinate System(s) ************
csys,0
toffst,273.15,  ! Temperature offset from absolute zero
/com,************ Set Reference Temperature ************
tref,20.
/wb,mat,start              !  starting to send materials
/com,************ Send Materials ************
TB,CHABOCHE,1,8,3
TBTEMP,20
TBDATA,1,290,1381244.424,12353.82459,185916.3245,2325.56608,87448.43818
TBDATA,7,321.8990903
```

```
TBTEMP,100
TBDATA,1,225.4,633226.4354,12276.06252,71441.44849,1767.548183,24251.89822
TBDATA,7,272.6672033
TBTEMP,200
TBDATA,1,160,593369.0024,12387.62089,62435.89276,1804.619158,20515.73648
TBDATA,7,283.2572208
TBTEMP,300
TBDATA,1,147.04,594729.233,12324.96128,63123.37745,1760.562368,20661.19939
TBDATA,7,275.2539867
TBTEMP,400
TBDATA,1,134,571139.2842,12323.30114,62521.65416,1782.84014,20721.39792
TBDATA,7,278.5002919
TBTEMP,500
TBDATA,1,123.05,529528.251,12326.81138,61357.02868,1795.221686,20955.47694
TBDATA,7,275.2643483
TBTEMP,600
TBDATA,1,110,458336.0828,12592.11826,49239.45914,1752.015753,16474.91431
TBDATA,7,273.3822468
TBTEMP,650
TBDATA,1,102.79,395527.4677,12314.05026,42631.67594,1756.936412,14312.25083
TBDATA,7,274.1085117
MPTEMP,,,,,,,,
MPTEMP,1,20
MPTEMP,2,100
MPTEMP,3,200
MPTEMP,4,300
MPTEMP,5,400
MPTEMP,6,500
MPTEMP,7,600
MPTEMP,8,650
MPDATA,EX,1, ,137540,191340,183000,174660,166320,157980,
MPDATA,EX,1, ,149640,145470,     ! tonne s^-2 mm^-1
MPTEMP,,,,,,,,
MPTEMP,,,,,,,,
MPTEMP,1,20
MPTEMP,2,100
MPTEMP,3,200
MPTEMP,4,300
MPTEMP,5,400
MPTEMP,6,500
MPTEMP,7,600
MPTEMP,8,650
MPDATA,NUXY,1, ,0.3,0.3,0.29,0.29,0.29,0.28,
MPDATA,NUXY,1, ,0.28,0.28,
MPTEMP,,,,,,,,
```

```
TB,CREEP,1,8,4,8
TBTEMP,20
TBDATA,1,3.46329e-10,0.001956949,2.986175078,0
TBTEMP,100
TBDATA,1,7.80331e-10,0.002492447,3.011286543,0
TBTEMP,200
TBDATA,1,2.1541e-09,0.003372361,3.042973037,0
TBTEMP,300
TBDATA,1,5.94638e-09,0.004562912,3.074992955,0
TBTEMP,400
TBDATA,1,1.6415e-08,0.006173766,3.107349805,0
TBTEMP,500
TBDATA,1,4.53134e-08,0.008353303,3.140047133,0
TBTEMP,600
TBDATA,1,1.25087e-07,0.011302287,3.173088521,0
TBTEMP,650
TBDATA,1,2.0783e-07,0.013146809,3.189739367,0

/wb,mat,end               !  done sending materials
!************************ Model Summary ********************
!SYS\Solid,     304SS Ch+Ga,           matid,  1
!************************ End Model Summary ********************
! get the diagonal of the bounding box. Needed later for other things
*get,_xmin,node,,mnloc,x
*get,_ymin,node,,mnloc,y
*get,_zmin,node,,mnloc,z
*get,_xmax,node,,mxloc,x
*get,_ymax,node,,mxloc,y
*get,_zmax,node,,mxloc,z
_ASMDIAG=(_xmax-_xmin)*(_xmax-_xmin)+(_ymax-_ymin)*(_ymax-_ymin)+(_zmax-
_zmin)*(_zmax-_zmin)
_ASMDIAG=SQRT(_ASMDIAG)
/wb,contact,start          !  starting to send contact
/wb,contact,end            !  done creating contacts
CMBLOCK,SELECTION,ELEM,        1
(8i10)
       767
/golist
/wb,load,start             !  starting to send loads
/com,*********** Fixed Supports ***********
CMBLOCK,_FIXEDSU,NODE,       82
(8i10)
cmsel,s,_FIXEDSU
d,all,all
```

```
nsel,all
nsel,all
/com,********** Define Force Using Surface Effect Elements **********
local,12,0,0.,0.,0.,-0.,0.,0.
csys,0
et,3,154
eblock,10,,,24
(15i9)
 esel,s,type,,3
keyop,3,2,1              ! Apply load in local coordinate system
keyop,3,7,1              ! Use original area so load is constant in large deformation
keyop,3,11,2              ! Use real and not project area
esel,all
*DIM,_loadvari47x,TABLE,2,1,1,TIME,
! Time values
_loadvari47x(1,0,1) = 0.
_loadvari47x(2,0,1) = 6.
! Load values
_loadvari47x(1,1,1) = 0.
_loadvari47x(2,1,1) = 0.
*DIM,_loadvari47y,TABLE,2,1,1,TIME,
! Time values
_loadvari47y(1,0,1) = 0.
_loadvari47y(2,0,1) = 6.
! Load values
_loadvari47y(1,1,1) = 0.
_loadvari47y(2,1,1) = 7.07435170460317
*DIM,_loadvari47z,TABLE,2,1,1,TIME,
! Time values
_loadvari47z(1,0,1) = 0.
_loadvari47z(2,0,1) = 6.
! Load values
_loadvari47z(1,1,1) = 0.
_loadvari47z(2,1,1) = 0.
/com,********** Create Remote Point "Internal Remote Point 2" **********
! -------- Remote Point Used by "Shear" --------
*set,tid,5
*set,cid,4
et,cid,174
et,tid,170
keyo,tid,2,1             ! Don't fix the pilot node
keyo,tid,4,111111
keyo,cid,12,5             ! Bonded Contact
keyo,cid,4,1             ! Deformable RBE3 style load
keyo,cid,2,2             ! MPC style contact
```

```
eblock,10,,,24
(15i9)
*set,_npilot,4094
_npilot39=_npilot
type,tid
mat ,cid
real,cid
tshape,pilo
en,937,_npilot
tshape
/com,********** Construct Remote Displacement **********
*DIM,_loadvari38roty,TABLE,21,1,1,TIME,
! Time values
_loadvari38roty(1,0,1) = 0.
_loadvari38roty(2,0,1) = 6.
_loadvari38roty(3,0,1) = 13.5
_loadvari38roty(4,0,1) = 24.5
_loadvari38roty(5,0,1) = 35.5
_loadvari38roty(6,0,1) = 46.5
_loadvari38roty(7,0,1) = 57.5
_loadvari38roty(8,0,1) = 68.5
_loadvari38roty(9,0,1) = 79.5
_loadvari38roty(10,0,1) = 90.5
_loadvari38roty(11,0,1) = 101.5
_loadvari38roty(12,0,1) = 112.5
_loadvari38roty(13,0,1) = 123.5
_loadvari38roty(14,0,1) = 134.5
_loadvari38roty(15,0,1) = 145.5
_loadvari38roty(16,0,1) = 156.5
_loadvari38roty(17,0,1) = 167.5
_loadvari38roty(18,0,1) = 178.5
_loadvari38roty(19,0,1) = 189.5
_loadvari38roty(20,0,1) = 200.5
_loadvari38roty(21,0,1) = 211.5
! Load values
_loadvari38roty(1,1,1) = 0.
_loadvari38roty(2,1,1) = 0.
_loadvari38roty(3,1,1) = 0.305432619099008
_loadvari38roty(4,1,1) = -0.183259571459405
_loadvari38roty(5,1,1) = 0.296705972839036
_loadvari38roty(6,1,1) = -0.183259571459405
_loadvari38roty(7,1,1) = 0.296705972839036
_loadvari38roty(8,1,1) = -0.183259571459405
_loadvari38roty(9,1,1) = 0.296705972839036
_loadvari38roty(10,1,1) = -0.183259571459405
```

```
_loadvari38roty(11,1,1) = 0.296705972839036
_loadvari38roty(12,1,1) = -0.183259571459405
_loadvari38roty(13,1,1) = 0.296705972839036
_loadvari38roty(14,1,1) = -0.183259571459405
_loadvari38roty(15,1,1) = 0.296705972839036
_loadvari38roty(16,1,1) = -0.183259571459405
_loadvari38roty(17,1,1) = 0.296705972839036
_loadvari38roty(18,1,1) = -0.183259571459405
_loadvari38roty(19,1,1) = 0.296705972839036
_loadvari38roty(20,1,1) = -0.183259571459405
_loadvari38roty(21,1,1) = 0.296705972839036
/COM,*** Create a component for all remote displacements ***
CMBLOCK,REMOTEDISPALL,NODE,        1
(8i10)
      4094
tblist
/gst,on,on
fini
*get,_numnode,node,0,count
*get,_numelem,elem,0,count
*get, _MAXELEMNUM, elem, 0, NUM, MAX
*get, _MAXNODENUM, node, 0, NUM, MAX
*get, _MAXELEMTYPE, etyp, 0, NUM, MAX
*get, _MAXREALCONST, real, 0, NUM, MAX
/go
/wb,load,end               !  done creating loads
/com,--- Number of total nodes = %_numnode%
/com,--- Number of contact elements = 48
/com,--- Number of spring elements = 0
/com,--- Number of bearing elements = 0
/com,--- Number of solid elements = 886
/com,--- Number of total elements = %_numelem%
*get,_wallbsol,active,,time,wall
/com,*********************************************************************
***
/com,************************    SOLUTION      *******************************
/com,*********************************************************************
***
/solu
antype,0                ! static analysis
eqsl,pcg,1e-8,,,,,1
cntr,print,1            ! print out contact info and also make no initial contact an error
dmpopt,emat,no            ! Don't combine emat file for DANSYS
dmpopt,esav,no           ! Don't combine esav file for DANSYS
nldiag,cont,iter         ! print out contact info each equilibrium iteration
```

```
resc,define,last,last,,dele            ! Program Controlled
/com,*************************************************
/com,****************** SOLVE FOR LS 1 ***************
esel,s,type,,3
nsle
sfe,all,1,pres,1,%_loadvari47x%
sfe,all,2,pres,1,%_loadvari47y%
sfe,all,3,pres,1,%_loadvari47z%
nsel,all
esel,all
d,4094,roty,%_loadvari38roty%
/nopr
/gopr
autots,on                  ! User turned on automatic time stepping
nsub,30,300,30,OFF
time,6.
outres,erase
outres,all,none
outres,nsol,all
outres,rsol,all
outres,strs,all
outres,epel,all
outres,eppl,all
outres,epcr,all
stabilize,off                  ! Stabilization turned OFF by user
RATE,OFF                                        ! Creep is turned Off by the user
! *********** WB SOLVE COMMAND ***********
! check interactive state
*get,ANSINTER_,active,,int
*if,ANSINTER_,ne,0,then
/eof
*endif
solve
/com *************** Write FE CONNECTORS *********
CEWRITE,file,ce,,INTE
/com,*************************************************
/com,*************** FINISHED SOLVE FOR LS 1 *************
/com,*************************************************
/com,****************** SOLVE FOR LS 2 ***************
/nopr
/gopr
autots,on                  ! User turned on automatic time stepping
nsub,30,300,30,OFF
time,13.5
outres,erase
```

```
outres,all,none
outres,nsol,all
outres,rsol,all
outres,strs,all
outres,epel,all
outres,eppl,all
outres,epcr,all
stabilize,off               ! Stabilization turned OFF by user
RATE,ON                                         ! Creep is turned On by the user
CUTCONTROL,CRPLIMIT, 1 ,1
solve
/com,*************************************************
/com,************** FINISHED SOLVE FOR LS 2 *************
/com,*************************************************
/com,******************* SOLVE FOR LS 3 ***************
/nopr
/gopr
autots,on               ! User turned on automatic time stepping
nsub,30,300,30,OFF
time,24.5
outres,erase
outres,all,none
outres,nsol,all
outres,rsol,all
outres,strs,all
outres,epel,all
outres,eppl,all
outres,epcr,all
stabilize,off               ! Stabilization turned OFF by user
RATE,ON                                         ! Creep is turned On by the user
CUTCONTROL,CRPLIMIT, 1 ,1
solve
/com,*************************************************
/com,************** FINISHED SOLVE FOR LS 3 *************
/com,*************************************************
/com,******************* SOLVE FOR LS 4 ***************
/nopr
/gopr
autots,on               ! User turned on automatic time stepping
nsub,30,300,30,OFF
time,35.5
outres,erase
outres,all,none
outres,nsol,all
outres,rsol,all
```

```
outres,strs,all
outres,epel,all
outres,eppl,all
outres,epcr,all
stabilize,off                ! Stabilization turned OFF by user
RATE,ON                                    ! Creep is turned On by the user
CUTCONTROL,CRPLIMIT, 1 ,1
solve
/com,*************************************************
/com,************** FINISHED SOLVE FOR LS 4 *************
/com,*************************************************
/com,******************* SOLVE FOR LS 5 ***************
/nopr
/gopr
autots,on                ! User turned on automatic time stepping
nsub,30,300,30,OFF
time,46.5
outres,erase
outres,all,none
outres,nsol,all
outres,rsol,all
outres,strs,all
outres,epel,all
outres,eppl,all
outres,epcr,all
stabilize,off                ! Stabilization turned OFF by user
RATE,ON                                    ! Creep is turned On by the user
CUTCONTROL,CRPLIMIT, 1 ,1
solve
/com,*************************************************
/com,************** FINISHED SOLVE FOR LS 5 *************
/com,*************************************************
/com,******************* SOLVE FOR LS 6 ***************
/nopr
/gopr
autots,on                ! User turned on automatic time stepping
nsub,30,300,30,OFF
time,57.5
outres,erase
outres,all,none
outres,nsol,all
outres,rsol,all
outres,strs,all
outres,epel,all
outres,eppl,all
```

```
outres,epcr,all
stabilize,off               ! Stabilization turned OFF by user
RATE,ON                                     ! Creep is turned On by the user
CUTCONTROL,CRPLIMIT, 1 ,1
solve
/com,*****************************************************
/com,************** FINISHED SOLVE FOR LS 6 *************
/com,*****************************************************
/com,******************* SOLVE FOR LS 7 ***************
/nopr
/gopr
autots,on               ! User turned on automatic time stepping
nsub,30,300,30,OFF
time,68.5
outres,erase
outres,all,none
outres,nsol,all
outres,rsol,all
outres,strs,all
outres,epel,all
outres,eppl,all
outres,epcr,all
stabilize,off               ! Stabilization turned OFF by user
RATE,ON                                     ! Creep is turned On by the user
CUTCONTROL,CRPLIMIT, 1 ,1
solve
/com,*****************************************************
/com,************** FINISHED SOLVE FOR LS 7 *************
/com,*****************************************************
/com,******************* SOLVE FOR LS 8 ***************
/nopr
/gopr
autots,on               ! User turned on automatic time stepping
nsub,30,300,30,OFF
time,79.5
outres,erase
outres,all,none
outres,nsol,all
outres,rsol,all
outres,strs,all
outres,epel,all
outres,eppl,all
outres,epcr,all
stabilize,off               ! Stabilization turned OFF by user
RATE,ON                                     ! Creep is turned On by the user
```

```
CUTCONTROL,CRPLIMIT, 1 ,1
solve
/com,*************************************************
/com,************** FINISHED SOLVE FOR LS 8 *************
/com,*************************************************
/com,******************* SOLVE FOR LS 9 ***************
/nopr
/gopr
autots,on               ! User turned on automatic time stepping
nsub,30,300,30,OFF
time,90.5
outres,erase
outres,all,none
outres,nsol,all
outres,rsol,all
outres,strs,all
outres,epel,all
outres,eppl,all
outres,epcr,all
stabilize,off               ! Stabilization turned OFF by user
RATE,ON                                 ! Creep is turned On by the user
CUTCONTROL,CRPLIMIT, 1 ,1
solve
/com,*************************************************
/com,************** FINISHED SOLVE FOR LS 9 *************
/com,*************************************************
/com,******************* SOLVE FOR LS 10 ***************
/nopr
/gopr
autots,on               ! User turned on automatic time stepping
nsub,30,300,30,OFF
time,101.5
outres,erase
outres,all,none
outres,nsol,all
outres,rsol,all
outres,strs,all
outres,epel,all
outres,eppl,all
outres,epcr,all
stabilize,off               ! Stabilization turned OFF by user
RATE,ON                                 ! Creep is turned On by the user
CUTCONTROL,CRPLIMIT, 1 ,1
solve
/com,*************************************************
```

```
/com,************** FINISHED SOLVE FOR LS 10 *************
/com,************************************************
/com,****************** SOLVE FOR LS 11 ***************
/nopr
/gopr
autots,on               ! User turned on automatic time stepping
nsub,30,300,30,OFF
time,112.5
outres,erase
outres,all,none
outres,nsol,all
outres,rsol,all
outres,strs,all
outres,epel,all
outres,eppl,all
outres,epcr,all
stabilize,off               ! Stabilization turned OFF by user
RATE,ON                                     ! Creep is turned On by the user
CUTCONTROL,CRPLIMIT, 1 ,1
solve
/com,************************************************
/com,************** FINISHED SOLVE FOR LS 11 *************
/com,************************************************
/com,****************** SOLVE FOR LS 12 ***************
/nopr
/gopr
autots,on               ! User turned on automatic time stepping
nsub,30,300,30,OFF
time,123.5
outres,erase
outres,all,none
outres,nsol,all
outres,rsol,all
outres,strs,all
outres,epel,all
outres,eppl,all
outres,epcr,all
stabilize,off               ! Stabilization turned OFF by user
RATE,ON                                     ! Creep is turned On by the user
CUTCONTROL,CRPLIMIT, 1 ,1
solve
/com,************************************************
/com,************** FINISHED SOLVE FOR LS 12 *************
/com,************************************************
/com,****************** SOLVE FOR LS 13 ***************
```

```
/nopr
/gopr
autots,on               ! User turned on automatic time stepping
nsub,30,300,30,OFF
time,134.5
outres,erase
outres,all,none
outres,nsol,all
outres,rsol,all
outres,strs,all
outres,epel,all
outres,eppl,all
outres,epcr,all
stabilize,off               ! Stabilization turned OFF by user
RATE,ON                                 ! Creep is turned On by the user
CUTCONTROL,CRPLIMIT, 1 ,1
solve
/com,*************************************************
/com,************** FINISHED SOLVE FOR LS 13 *************
/com,*************************************************
/com,******************* SOLVE FOR LS 14 ****************
/nopr
/gopr
autots,on               ! User turned on automatic time stepping
nsub,30,300,30,OFF
time,145.5
outres,erase
outres,all,none
outres,nsol,all
outres,rsol,all
outres,strs,all
outres,epel,all
outres,eppl,all
outres,epcr,all
stabilize,off               ! Stabilization turned OFF by user
RATE,ON                                 ! Creep is turned On by the user
CUTCONTROL,CRPLIMIT, 1 ,1
solve
/com,*************************************************
/com,************** FINISHED SOLVE FOR LS 14 *************
/com,*************************************************
/com,******************* SOLVE FOR LS 15 ****************
/nopr
/gopr
autots,on               ! User turned on automatic time stepping
```

```
nsub,30,300,30,OFF
time,156.5
outres,erase
outres,all,none
outres,nsol,all
outres,rsol,all
outres,strs,all
outres,epel,all
outres,eppl,all
outres,epcr,all
stabilize,off               ! Stabilization turned OFF by user
RATE,ON                                    ! Creep is turned On by the user
CUTCONTROL,CRPLIMIT, 1 ,1
solve
/com,*****************************************************
/com,************** FINISHED SOLVE FOR LS 15 *************
/com,*****************************************************
/com,******************* SOLVE FOR LS 16 ****************
/nopr
/gopr
autots,on               ! User turned on automatic time stepping
nsub,30,300,30,OFF
time,167.5
outres,erase
outres,all,none
outres,nsol,all
outres,rsol,all
outres,strs,all
outres,epel,all
outres,eppl,all
outres,epcr,all
stabilize,off               ! Stabilization turned OFF by user
RATE,ON                                    ! Creep is turned On by the user
CUTCONTROL,CRPLIMIT, 1 ,1
solve
/com,*****************************************************
/com,************** FINISHED SOLVE FOR LS 16 *************
/com,*****************************************************
/com,******************* SOLVE FOR LS 17 ****************
/nopr
/gopr
autots,on               ! User turned on automatic time stepping
nsub,30,300,30,OFF
time,178.5
outres,erase
```

```
outres,all,none
outres,nsol,all
outres,rsol,all
outres,strs,all
outres,epel,all
outres,eppl,all
outres,epcr,all
stabilize,off               ! Stabilization turned OFF by user
RATE,ON                                         ! Creep is turned On by the user
CUTCONTROL,CRPLIMIT, 1 ,1
solve
/com,*****************************************************
/com,************** FINISHED SOLVE FOR LS 17 *************
/com,*****************************************************
/com,******************* SOLVE FOR LS 18 ****************
/nopr
/gopr
autots,on               ! User turned on automatic time stepping
nsub,30,300,30,OFF
time,189.5
outres,erase
outres,all,none
outres,nsol,all
outres,rsol,all
outres,strs,all
outres,epel,all
outres,eppl,all
outres,epcr,all
stabilize,off               ! Stabilization turned OFF by user
RATE,ON                                         ! Creep is turned On by the user
CUTCONTROL,CRPLIMIT, 1 ,1
solve
/com,*****************************************************
/com,************** FINISHED SOLVE FOR LS 18 *************
/com,*****************************************************
/com,******************* SOLVE FOR LS 19 ****************
/nopr
/gopr
autots,on               ! User turned on automatic time stepping
nsub,30,300,30,OFF
time,200.5
outres,erase
outres,all,none
outres,nsol,all
outres,rsol,all
```

```
outres,strs,all
outres,epel,all
outres,eppl,all
outres,epcr,all
stabilize,off                ! Stabilization turned OFF by user
RATE,ON                                          ! Creep is turned On by the user
CUTCONTROL,CRPLIMIT, 1 ,1
solve
/com,*************************************************
/com,************** FINISHED SOLVE FOR LS 19 *************
/com,*************************************************
/com,******************* SOLVE FOR LS 20 ***************
/nopr
/gopr
autots,on                ! User turned on automatic time stepping
nsub,30,300,30,OFF
time,211.5
outres,erase
outres,all,none
outres,nsol,all
outres,rsol,all
outres,strs,all
outres,epel,all
outres,eppl,all
outres,epcr,all
stabilize,off                ! Stabilization turned OFF by user
RATE,ON                                          ! Creep is turned On by the user
CUTCONTROL,CRPLIMIT, 1 ,1
solve
/com,*************************************************
/com,************** FINISHED SOLVE FOR LS 20 *************
*set,_DS_PROGRESS          ! turn off progress updates to avoid virus scanning bug
*get,_wallasol,active,,time,wall
/nopr
*get,_numnode,node,0,count
*get,_numelem,elem,0,count
*get, _MAXELEMNUM, elem, 0, NUM, MAX
*get, _MAXNODENUM, node, 0, NUM, MAX,,,INTERNAL
*get, _MAXELEMTYPE, etyp, 0, NUM, MAX
*get, _MAXREALCONST, real, 0, NUM, MAX
/gopr
*get,_PCGITER,active,,solu,cgiter
/post1
! ****** Begin Command Snippet ******
*set,ARG1,200.
```

```
*set,ARG2,20.
*set,ARG3,15.7
*set,ARG4,175.105
/Post1
RSYS,0                  ! global
*GET,LSTSET, ACTIVE, 0, SET, NSET
TOTARRAYSTEPS=LSTSET
*dim,atime,array,TOTARRAYSTEPS
*dim,acurlo,array,TOTARRAYSTEPS
*dim,acursb,array,TOTARRAYSTEPS
*dim,TEMPERATUREVALUE,array,TOTARRAYSTEPS
*dim,EFFECTIVESTRESS,array,TOTARRAYSTEPS
*dim,YYSTRESS,array,TOTARRAYSTEPS
*dim,XYSTRESS,array,TOTARRAYSTEPS
*dim,EFFECTIVESTRAIN,array,TOTARRAYSTEPS
*dim,YYSTRAIN,array,TOTARRAYSTEPS
*dim,XYSTRAIN,array,TOTARRAYSTEPS
*dim,EYYSTRAIN,array,TOTARRAYSTEPS
*dim,EXYSTRAIN,array,TOTARRAYSTEPS
*dim,PYYSTRAIN,array,TOTARRAYSTEPS
*dim,PXYSTRAIN,array,TOTARRAYSTEPS
*dim,CYYSTRAIN,array,TOTARRAYSTEPS
*dim,CXYSTRAIN,array,TOTARRAYSTEPS

*DO,t,1,LSTSET,1
SET,,,,,,t

*GET,acurlo(t), ACTIVE, 0, SET, LSTP
*GET,acursb(t), ACTIVE, 0, SET, SBST                    !get the current sub step
*GET,atime(t), ACTIVE,0, SET, TIME

ETABLE, CSTRVALN, EPCR, Z                               ! Make an element table for
other stresses and strains
ETABLE, TEMPVAL, BFE, TEMP
ETABLE, ESTRESS, S, EQV
ETABLE, STRESSX, S, X
ETABLE, STRESSY, S, Y
ETABLE, STRESSZ, S, Z
ETABLE, STRESSXY, S, XY
ETABLE, STRESSYZ, S, YZ
ETABLE, STRESSXZ, S, XZ
ETABLE, ESTRAIN, EPTO, EQV
ETABLE, STRAINX, EPTO, X
ETABLE, ESTRINY, EPEL, Y
ETABLE, PSTRINY, EPPL, Y
```

```
ETABLE, CSTRINY, EPCR, Y
ETABLE, STRAINY, EPTO, Y
ETABLE, STRAINZ, EPTO, Z
ETABLE, ESTRINXY, EPEL, XY
ETABLE, PSTRINXY, EPPL, XY
ETABLE, CSTRINXY, EPCR, XY
ETABLE, STRAINXY, EPTO, XY
ETABLE, STRAINYZ, EPTO, YZ
ETABLE, STRAINXZ, EPTO, XZ

ELEMENTNUM=765
*GET,TEMPERATUREVALUE(t),ELEM,ELEMENTNUM,ETAB,TEMPVAL
*GET,EFFECTIVESTRESS(t),ELEM,ELEMENTNUM,ETAB,ESTRESS
*GET,YYSTRESS(t),ELEM,ELEMENTNUM,ETAB,STRESSY
*GET,XYSTRESS(t),ELEM,ELEMENTNUM,ETAB,STRESSXY
*GET,EFFECTIVESTRAIN(t),ELEM,ELEMENTNUM,ETAB, ESTRAIN
*GET,YYSTRAIN(t),ELEM,ELEMENTNUM,ETAB, STRAINY
*GET,XYSTRAIN(t),ELEM,ELEMENTNUM,ETAB, STRAINXY
*GET,EYYSTRAIN(t),ELEM,ELEMENTNUM,ETAB, ESTRINY
*GET,EXYSTRAIN(t),ELEM,ELEMENTNUM,ETAB, ESTRINXY
*GET,PYYSTRAIN(t),ELEM,ELEMENTNUM,ETAB, PSTRINY
*GET,PXYSTRAIN(t),ELEM,ELEMENTNUM,ETAB, PSTRINXY
*GET,CYYSTRAIN(t),ELEM,ELEMENTNUM,ETAB, CSTRINY
*GET,CXYSTRAIN(t),ELEM,ELEMENTNUM,ETAB, CSTRINXY

*ENDDO
! Hysteresis File
*CFOPEN, C:\FEA\FEA_N_%ARG1%_%ARG2%_%ARG3%_%ARG4%,data,,
*VWRITE, atime(1),acurlo(1), acursb(1),
TEMPERATUREVALUE(1),EFFECTIVESTRESS(1),YYSTRESS(1),XYSTRESS(1),EFFECT
IVESTRAIN(1),EYYSTRAIN(1),EXYSTRAIN(1),PYYSTRAIN(1),PXYSTRAIN(1),CYYSTR
AIN(1),CXYSTRAIN(1),YYSTRAIN(1),XYSTRAIN(1)
(E11.5,6X F10.2,6X F10.2,6X E11.5,6X E11.5,6X E11.5,6X E11.5,6X E11.5,6X E11.5,6X
E11.5,6X E11.5,6X E11.5,6X E11.5,6X E11.5,6X E11.5,6X E11.5)
*CFCLOS
! ****** End   Command Snippet ******
xmlo,ENCODING,ISO-8859-1
xmlo,parm
/xml,parm,xml
fini
/gopr
*get,_walldone,active,,time,wall
_preptime=(_wallbsol-_wallstrt)*3600
_solvtime=(_wallasol-_wallbsol)*3600
_posttime=(_walldone-_wallasol)*3600
```

```
_totaltim=(_walldone-_wallstrt)*3600
/wb,file,end                ! done with WB generated input
```

REFERENCES

American Iron and Steel Institute. (2012). *American Iron and Steel Institute, High-Temperature Characteristics of Stainless Steels- A Designers Series Handbook*. No. 9004, Nickel Development Institute, Toronto, Ontario.

Armstrong, P. J., and Frederick, C. O. (1966). A mathematical representation of the multiaxial Bauschinger effect. *Berkeley Nuclear Laboratories, Berkeley, UK*.

ASTM. (2015). Standard Practice for Strain-Controlled Axial-Torsional Fatigue Testing with Thin-Walled Tubular Specimens. *ASTM International, West Conshohocken, PA, 2015, https://doi.org/10.1520/E2207-15*.

Bari, S., and Hassan, T. (2000). Anatomy of coupled constitutive models for ratcheting simulation. *International Journal of Plasticity, 16*(3), 381-409. doi:10.1016/S0749-6419(99)00059-5

Barrett, R. A., Farragher, T. P., O'Dowd, N. P., O'Donoghue, P. E., and Leen, S. B. (2014). Multiaxial cyclic viscoplasticity model for high temperature fatigue of P91 steel. *MATERIALS SCIENCE AND TECHNOLOGY, 30*(1), 67-74.

Belyakov, A., Miura, H., and Sakai, T. (1998). Dynamic recrystallization under warm deformation of a 304 type austenitic stainless steel. *Materials Science & Engineering A, 255*, 139-147. doi:10.1016/S0921-5093(98)00784-9

Bhaduri, A. K., Gill, T. P. S., Albert, S. K., Shanmugam, K., and Iyer, D. R. (2001). Repair welding of cracked steam turbine blades using austenitic and martensitic stainless-steel consumables. *Nuclear Engineering and Design, 206*, 249-259. doi:10.1016/S0029-5493(00)00439-8

Blass, J. (1990). *Multiaxial fatigue criterion for 2-1/4 Cr-1 Mo steel for use in high-temperature structural design*. Paper presented at the ASME/IEEE joint power generation conference, Boston, MA (USA), 21-25 Oct 1990.

Booker, M. (1978). Use of generalized regression models for the analysis of stress-rupture data.

Bouchenot, T., Felemban, B., Mejia, C., and Gordon, A. (2016a). Development of Noninteraction Material Models With Cyclic Hardening. *Journal of Engineering Materials & Technology, 138*(4), 1-15. doi:10.1115/1.4033488

Bouchenot, T., Felemban, B., Mejia, C., and Gordon, A. P. (2016b). *Application of Ramberg-Osgood Plasticity To Determine Cyclic Hardening Parameters*. Paper presented at the *ASME 2016 Power Conference*, Charlotte, North Carolina, June 26-30, 2016.

Boyer, H., and Gall, T. (1985). *Metals HandBook*. American Society for Metal, OH.

Bree, J. (1967). Elastic-plastic behaviour of thin tubes subjected to internal pressure and intermittent high-heat fluxes with application to fast-nuclear-reactor fuel elements. *Journal of Strain Analysis for Engineering Design, 2*(3), 226-238.

Budahazy, V., and Dunai, L. (2013). Parameter-refreshed Chaboche model for mild steel cyclic plasticity behaviour. *PERIODICA POLYTECHNICA-CIVIL ENGINEERING, 57*(2), 139-155.

Bynum, J. E., Ellis, F. V., and Roberts, B. W. (1976). Tensile and Creep Properties for an Annealed Versus Tensile and Creep Properties for an Annealed Versus Temperature. *American Society of Mechanical Engineers, 97*(4), 1-28.

Chaboche, J. L. (1983). On the Constitutive Equation of Material Under Monotonic or Cyclic Loadings. *La Recherche Aerospatiale, 5*, 363-375.

Chaboche, J. L. (1986). Time-independent constitutive theories for cyclic plasticity. *International Journal of Plasticity, 2*, 149-188. doi:10.1016/0749-6419(86)90010-0

Chaboche, J. L. (1989). Constitutive Equations for Cyclic Plasticity abd Cyclic Viscoplasticity. *International Journal of Plasticity, 5*(3), 247-302.

Chaboche, J. L. (1997). Thermodynamic formulation of constitutive equations and application to the viscoplasticity and viscoelasticity of metals and polymers. *International Journals of Solids and Structures, 34*(18), 2239-2254.

Chaboche, J. L. (2008). A review of some plasticity and viscoplasticity constitutive theories. *International Journal of Plasticity, 24*(10), 1642-1693. doi:10.1016/j.ijplas.2008.03.009

Cheruvu, N. S. (1989). Degradation of Mechanical-Properties of Cr-Mo-V and 2.25Cr-1Mo Steel-Components After Long-Term Service at Elevated-Temperatures. *METALLURGICAL TRANSACTIONS A-PHYSICAL METALLURGY AND MATERIALS SCIENCE, 20*(1), 87-97.

Chopra, O. K., and Natesan, K. (1977). Interpretation of high-temperature creep of Type 304 stainless steel.

Davis, J. R. (1994). *Stainless steels*: Materials Park, Ohio : ASM International, c1994.

DeMarco, J., Karl, J., Sohn, Y., and Gordon, A. P. (2013). High-temperature mechanical response of A359–SiCp–30%: torsional loading (II). *MATERIALS AT HIGH TEMPERATURES, 30*(3), 224-235. doi:10.3184/096034013X13757116460599

Di Schino, A., Kenny, J. M., Mecozzi, M. G., and Barteri, M. (2000). Development of high nitrogen, low nickel, 18%Cr austenitic stainless steels. *Journal of Materials Science, 35*(19), 4803-4808.

Garofalo, F. (1965). *Fundamentals of creep and creep-rupture in metals*: New York, Macmillan.

Garud, Y. S. (1981). A New Approach to the Evaluation of Fatigue Under Multiaxial Loadings. *Journal of Engineering Materials and Technology, 103*(2), 118-125.

Geist, R. (1998). Four-stage model for predicting creep behavior. *Journal of Engineering Mechanics, 124*(1), 118-120.

Golan, O., Arbel, A., Eliezer, D., and Moreno, D. (1996). The applicability of Norton's creep power law and its modified version to a single-crystal superalloy type CMSX-2. *Material Science and Engineering A-Structural Materials Properties Microstructure and Processing, 216*(1-2), 125-130.

Halford, G. R., Lerch, B. A., Saltsman, J. F., and Arya, V. K. (1993). Proposed framework for thermomechanical life modeling of metal matrix composites.

Harvey, P. D., editor. (1982). Engineering Properties of Steel. *ASTM International, Metals Park, OH*.

Hongna, Q., Zhimin, Z., Jianmin, Y., Xueyan, Y., and Zhiyuan, D. (2017). Dynamic Recrystallization of Mg-8Gd-3Y-1Nd-0.5Zr Alloy during Hot Deformation. *Materials Science Forum, 898*, 311-322. doi:10.4028/www.scientific.net/MSF.898.311

Huang, J., Shi, D., Yang, X., and Hu, X. (2014). Effect of multi-axial stress state on creep behavior and stress rupture life of a Ni-based DS superalloy. *Computational Materials Science, 85*, 20-31. doi:10.1016/j.commatsci.2013.12.026

INCO Databook. (1968). Austenitic chromium-nickel stainless steels Engineering properties at elevated temperatures. *International Nickel Company Inc.*

Inoue, T., Yoshida, F., Niitsu, Y., Ohno, N., Uno, T., and Suzuki, A. (1989). Plasticity-Creep Behavior of 2-1/4Cr-1Mo Steel At 600°C In Multiaxial Stress State: Benchmark (A) By Ialips. *New York, N.Y.: American Society of Mec, 163*, 101-107.

Inoue, T., Yoshida, F., Niitsu, Y., Ohno, N., Uno, T., and Suzuki, A. (1994). Inelastic Stress-Strain Response of 2-1/4Cr-1Mo Steel Under Combined Tension-Torsion At 600-Degrees-C. *Nuclear Engineering and Design, 150*(1), 107-118.

Jin, S., Harmuth, H., and Gruber, D. (2014). Compressive creep testing of refractories at elevated loads—Device, material law and evaluation techniques. *Journal of the European Ceramic Society, 34*(15), 4037-4042. doi:10.1016/j.jeurceramsoc.2014.05.034

Jonsson, T., Folkeson, N., Svensson, J. E., Johansson, L. G., and Halvarsson, M. (2011). An ESEM in situ investigation of initial stages of the KCl induced high temperature corrosion of a Fe–2.25Cr–1Mo steel at 400°C. *Corrosion Science, 53*(6), 2233-2246. doi:10.1016/j.corsci.2011.03.007

Karl, J. O. (2013). *Thermomechanical fatigue life prediction of notched 304 stainless steel. [electronic resource]*: Orlando, Fla. : University of Central Florida, 2013.

Kim, S.-I., and Yoo, Y.-C. (2001). Dynamic recrystallization behavior of AISI 304 stainless steel. *Materials Science & Engineering A, 311*, 108-113. doi:10.1016/S0921-5093(01)00917-0

Lampman, S., Zorc, T., and Editors. (2007). *ASM Handbook- Properties and Selection: Irons, Steels, and High-Performance Alloys*. ASM International, Metals Park, OH.

Li, B., Reis, L., and de Freitas, M. (2006). Simulation of cyclic stress/strain evolutions for multiaxial fatigue life prediction. *International Journal of Fatigue, 28*(5), 451-458. doi:10.1016/j.ijfatigue.2005.07.038

Liang, T., Chen, X., Cheng, H., Chen, G., and Ling, X. (2015). Thermal aging effect on the ratcheting-fatigue behavior of Z2CND18.12N stainless steel. *International Journal of Fatigue, 72*, 19-26. doi:10.1016/j.ijfatigue.2014.10.014

Mattos, H. S. D. C., Peres, J. M. A., and Melo, M. A. C. (2015). Ratcheting behaviour of elasto-plastic thin-walled pipes under internal pressure and subjected to cyclic axial loading. *Thin-Walled Structures, 93*, 102-111. doi:10.1016/j.tws.2015.03.011

Maziasz, P. J., Swindeman, R. W., Montague, J. P., Fitzpatrick, M., Browning, P. F., Grubb, J. F., and Klug, R. C. (1999). Improved creep-resistance of austenitic stainless steel for compact gas turbine recuperators. *MATERIALS AT HIGH TEMPERATURES, 16*(4), 207-212.

McQueen, J. C., Ryan, N. D., and Evangelsta, E. (1993). Processes and materials Innovation. *Materials Science Forum, 435*, 113-115.

Messner, C., Messner, B., and Werner, E. A. (2006). On the ratchetting limit of forged duplex steels under combined thermal and mechanical loads. *Materials Science & Engineering A, 424*(1-2), 154-162. doi:10.1016/j.msea.2006.03.001

Metals, N. R. I. F. (1989a). Data Sheets on the Elevated-Temperature, Time-Dependent Low-Cycle Fatigue Properties of SCMV 4 (2.25Cr-1Mo) Steel Plates for Pressure Vessels #62. *NRIM Fatigue Data Sheet, NRIM, Tokyo, Japan*.

Metals, N. R. I. F. (1989b). "Data Sheets on the Elevated-Temperature, Time-Dependent Low-Cycle Fatigue Properties of SCMV 4 (2.25Cr-1Mo) Steel Plates for Pressure Vessels #62,. *NRIM Fatigue Data Sheet, NRIM, Tokyo,*.

Mills, W. J. (1988). Heat-to-heat variations in the fracture toughness of austenitic stainless steels. *ENGINEERING FRACTURE MECHANICS, 30*, 469-492. doi:10.1016/0013-7944(88)90058-6

Parker, J. D. (1985). Prediction of Creep Deformation and Failure for 1/2 Cr-1/2 Mo-1/4 V and 2-1/4 Cr-1 Mo Steels. *Journal of Pressure Vessel Technology, 107*(3), 279-284. doi:10.1115/1.3264451

Peckner, D., and Bernstein, I. M. (1977). *Handbook of stainless steels*: New York : McGraw-Hill, c1977.

Penkalla, H. J., Schubert, F., and Nickel, H. (1989). Multiaxial Creep of Tube of Ally 800 and Alloy 617 High Temperature. *Federal Republic of Germany, 105*, 105-114.

Pineda-León, E., Flores-Méndez, E., Rodríguez-Castellanos, A., Basaldúa-Sánchez, J. E., and Aliabadi, M. H. (2015). Plastic, viscoplastic and creep fracture problems with the boundary element method. *Fatigue & Fracture of Engineering Materials & Structures, 38*(1), 40-55. doi:10.1111/ffe.12207

Polák, J., Helešic, J., and Klesnil, M. (1988). Effect of Elevated Temperatures on the Low Cycle Fatigue of 2.25Cr1Mo Steel—Part I: Constant Amplitude Straining. *Low Cycle Fatigue: A Symposium, ASTM Special Technical Publication 942, Sept. 30, 1987, ASTM Bolton Landing, NY*, 43-57.

Pun, C. L., Kan, Q., Mutton, P. J., Kang, G., and Yan, W. (2014). Ratcheting behaviour of high strength rail steels under bi-axial compression–torsion loadings: Experiment and simulation. *International Journal of Fatigue, 66*, 138-154. doi:10.1016/j.ijfatigue.2014.03.021

Ramberg, W., and Osgood, W. R. (1943). Description of stress-strain curves by three parameters. *1943*(902).

Rieiro, I., Carsi, M., and Penalba, F. (1996). *Computational Methods and Testing for Engineering Integrity*. Book Review

Brief Article retrieved from https://login.ezproxy.net.ucf.edu/login?auth=shibb&url=http://search.ebscohost.com/login.aspx?direct=true&db=edsgao&AN=edsgcl.34576696&site=eds-live&scope=site

Rieiro, I., Ruano, O. A., Eddahbi, M., and Carsí, M. (1998). Integral method from initial values to obtain the best fit of the Garofalo's creep equation. *Journal of Materials Processing Technology, 78*(1-3), 177-183.

Science, N. I. F. M. (2004). Data Sheets on Long-Term, High-Temperature Low-Cycle Fatigue Properties of SCMV 4 (2.25Cr-1Mo) Steel Plate for Boilers and Pressure Vessels #94. *NIMS Fatigue Data Sheet, NIMS, Tsukuba, Japan.*

Shaban, M., and Eghbali, B. (2010). Determination of critical conditions for dynamic recrystallization of a microalloyed steel. *Materials Science & Engineering A, 527*, 4320-4325. doi:10.1016/j.msea.2010.03.086

Shang, D.-G., Sun, G.-Q., Deng, J., and Yan, C.-L. (2007). Multiaxial fatigue damage parameter and life prediction for medium-carbon steel based on the critical plane approach. *International Journal of Fatigue, 29*, 2200-2207. doi:10.1016/j.ijfatigue.2006.12.005

Simoneau, R., and Roberge, R. (1981). Cavitation-Corrosion Damage Mechanisms in Hydraulic Turbine Materials. *Materials to Supply the Energy Demand*, 467-486.

Sireteanu, T., Mitu, A.-M., Giuclea, M., and Solomon, O. (2014). A comparative study of the dynamic behavior of Ramberg-Osgood and Bouc-Wen hysteresis models with application to seismic protection devices. *Engineering Structures, 76*, 255-269. doi:10.1016/j.engstruct.2014.07.002

Sireteanu, T., Mitu, A. M., Giuclea, M., Solomon, O., and Stefanov, D. (2014). Analytical Method For Fitting The Ramberg-Osgood Model to Given Hysteresis Loops. *Proceedings of The*

Romanian Academy Series A-Mathematicals Physics Technical Sciences Information Science, 15(1), 35-42.

Smith, C. A. (1984). Stainless steel in the food processing industry. *Anti-Corrosion Methods and Materials*(4), 7. doi:10.1108/eb060851

Song, S. H., Wu, J., Wei, X. J., Kumar, D., Liu, S. J., and Weng, L. Q. (2010). Creep property evaluation of a 2.25Cr–1Mo low alloy steel. *Materials Science & Engineering A, 527*(9), 2398-2403. doi:10.1016/j.msea.2010.01.007

Tahami, F. V., Daei-Sorkhabi, A. H., and Biglari, F. R. (2010). Creep constitutive equations for cold-drawn 304L stainless steel. *Materials Science & Engineering: A, 527*(18/19), 4993-4999. doi:10.1016/j.msea.2010.04.055

Tsai, M. C., and Yang, J. R. (2003). Microstructural degeneration of simulated heat-affected zone in 2.25Cr–1Mo steel during high-temperature exposure. *Materials Science & Engineering A, 340*(1), 15-32. doi:10.1016/S0921-5093(02)00081-3

Tsuji, N., Matsubara, Y., and Saito, Y. (1997). Dynamic recrystallization of ferrite in interstitial free steel. *Scripta Materialia, 37*(4), 477.

Vicente Braz, T., Rodrigo, B., Behzad Zandi, H., Songlan, Y., Ulrich, K., and Hans-Jürgen, C. (2005). High-temperature oxidation of pure Fe and the ferritic steel 2.25Cr1Mo. *Materials Research, 8*(4), 365-369. doi:10.1590/S1516-14392005000400002

Wang, W., Zhao, W., and Qu, J. (2013). Effect of Heat Treatment on Microstructure and Mechanical Properties of 2.25Cr-1Mo Steel. *Steel Research International, 84*(2), 178-183.

Wert, D. E., and DiSabella, R. P. (2006). Strong, corrosion-resistant stainless steel: this strong, tough, corrosion-resistant stainless steel improves performance of equipment in aerospace,

medical instruments, oil drilling, firearms, and marine applications. *Advanced Materials & Processes*(8), 34.

Xu, J. F., and Li, B. (2012). Discussion on the Sustainability of Stainless Steel Applied in Architecture. *Advanced Materials Research, 476*(1), 1553.

Yang, H., and Kim, S. (2001). A study on the mechanical strength change of 2.25Cr–1Mo steel by thermal aging. *Materials Science & Engineering A, 319*, 316-320. doi:10.1016/S0921-5093(01)01008-5

Yeganeh, M., and Naghdabadi, R. (2006). Axial effects investigation in fixed-end circular bars under torsion with a finite deformation model based on logarithmic strain. *International Journal of Mechanical Sciences, 48*(1), 75-84. doi:10.1016/j.ijmecsci.2005.09.008

Yoon, K. J., Wiederhorn, S. M., Luecke, W. E., and Becher, P. F. (2000). Comparison of Tensile and Compressive Creep Behavior in Silicon Nitride. *Journal of the American Ceramic Society, 83*(8), 201.